Evaluation of Intranasal Particulate Strategies to Enhance the Delivery of Anti-Seizure Therapeutics to the Brain

Richard Neil Prentice

A thesis submitted for the degree of
Doctor of Philosophy
University of Otago,
Dunedin, New Zealand

March 2020

Abstract

Epilepsy is a common and serious neurological disorder to which a high proportion of patients continue to be considered "drug-resistant" despite the availability of a host of anti-seizure drugs. Investigation into new treatment strategies is therefore of great importance, one such strategy being the use of the nose to deliver drugs directly to the brain with the help of pharmaceutical formulation to overcome the physical challenges presented by this route. The overall aim of this thesis was to establish and apply a seizure model to the investigation of two types of particulate intranasal delivery systems; microparticles and cubosomes.

Chapter One introduces the topic of intranasal delivery of anti-seizure drugs, covering the link between the nose and seizures, pathways from the nose to the brain, current rudimentary formulations in clinical use, animal seizure models and their proposed application in studying intranasal treatments, and a critical discussion of relevant pre-clinical studies in the literature. Upon this, Chapter Two begins by validating a seizure model based on the Maximal Electroshock Seizure Threshold (MEST) test with the intention of using it to detect the effects of intranasally administered therapeutics. The design attempts to address previously scarcely acknowledged issues of sensitivity in the MEST model and confounding by anaesthetics which are currently necessary to reliably and ethically perform intranasal administration to the olfactory region in rats. The results show that the model was able to clearly detect a change in seizure threshold after administration of the positive control, intravenous phenytoin, which was supported by therapeutic brain and plasma concentrations of the drug as determined using an internally developed Liquid Chromatography Mass Spectrometry (LC-MS) assay. Importantly, this effect was able to be detected despite the use of the inhaled anaesthetic, isoflurane, to briefly sedate the animals 60 minutes prior to stimulation.

In Chapter Three, the seizure model is applied to the evaluation of tamarind seed polysaccharide (TSP) microparticles as a proposed intranasal delivery system for the pharmacokinetically troublesome anti-seizure drug phenytoin. In this first pharmacodynamic study, to the author's knowledge, of a dry powder mucoadhesive microparticle formulation for seizure treatment, the model identified a peak anti-seizure effect time of 120 minutes after administration, which coincided with peak brain concentrations and supported its utilisation in intranasal delivery screening. Furthermore, the complementary demonstration of a histologically intact nasal

epithelium and simultaneous measurement of phenytoin's major metabolite, 5-(4-Hydroxyphenyl)-5-phenylhydantoin (4-HPPH) in brain tissue and plasma, supported the hypothesis of a direct intranasal delivery to the brain and the suitability of the microparticles for further trials.

In Chapter Four, the seizure model is applied to explore a potential new type of anti-seizure therapeutic, the endogenous endocannabinoid-like molecule, oleoylethanolamide (OEA), which has not yet had an effect on seizures documented. A cubosome dispersion was selected as the delivery vehicle, presenting one of the few pharmacodynamic *in vivo* studies conducted with this class of formulation to date. Given the unknown effects of oleoylethanolamide, it was firstly administered intravenously as a control, but no effect on seizure threshold was evident. Considering the complex nature of the hydrolysis-susceptible oleoylethanolamide and the self-assembling cubosome dispersion, complementary *in vivo* pharmacokinetic studies (utilising an internally developed LC-MS assay) and *in vitro* structural stability studies (utilising Small-angle X-ray Scattering (SAXS)) were conducted to further explore confounding factors. Despite presenting with complexities of their own, they overall supported the lack of pharmacodynamic effect seen after systemic administration. Intranasal studies were conducted in an attempt to bypass the challenges of systemic administration, but also demonstrated no measurable change in seizure threshold. Histological studies to determine a safe dose uncovered a toxicity of cubosomes to the nasal epithelium at the highest dose, independent of lipid type, which has not yet been described in any *in vivo* liquid crystalline nanoparticle studies to date and should be considered in future related work.

In summary, this thesis presents a tailored seizure model for screening intranasal delivery systems, a practical template for studying these systems *in vivo*, and a pre-clinical evaluation of two such systems. Notwithstanding the discussed limitations, it concludes that dry-powder mucoadhesive microparticles appear to be a promising platform for future study of intranasal anti-seizure drug delivery, while cubosomes and oleoylethanolamide may be better suited to other applications until a more thorough *in vivo* exploration of their respective fields exists.

Acknowledgements & Foreword

Completing a PhD was always intended to be an experience for me, rather than a means to an end. I came to Shakila's lab as a curious young pharmacist eager to find out what academic research was all about and I feel I will leave having achieved that. I've seen a lot in my time; stuff I've really enjoyed and stuff I really haven't, but stuff that's left me with a solid understanding of the world of academia as well as a range of skills which I continue to find applications for in the world outside of it. For that I am grateful to Shakila for giving me the freedom and encouragement to explore, make my own mistakes and find my own successes.

The purpose of a PhD, as I understand it, is to become capable of independent research. I've often found myself reflecting on what this means, as although I feel I've become very independent during the course of mine, completing a multi-faceted project of this scale has been largely *de*-pendent on successfully working with others. On that note, I wish to acknowledge the following people and organisations for all they have generously done for me and/or my project: Dr Shakila Rizwan, Associate Professor Nigel Jones, Dr Andrew Clarkson, Professor Benjamin Boyd, Dr Andrew Clulow, Dr Mohammad Younus, Dr Sasi Yarragudi, Dr Anita Barzegar-Fallah, Dr Woravimol (Pummy) Krittaphol, Dr Mohammed Rizwan, Janika Welzel, Gabriella Dezsi, Amanda Fisher, Jo Preston, Kevin Crump, Len Stevenson, Dr Mark Vallarta, Dr Sam Cockerill, Martin Dalefield, Kristina Eiffert, Sonja Bimler, Alan Mitchell, Richard Easingwood, Katie Young, Helen Thacker, School of Pharmacy, University of Otago, Brain Health Research Centre, Health Research Council of New Zealand, Callaghan Innovation and the Australian Synchrotron. From offering advice or assistance, being generous with your time and resources, providing financial support, fixing machines for me, or things you said that stuck with me and sent me in the right direction, this PhD (and its side projects) wouldn't have been possible if you weren't there to help me out when you were. Thank you. Thank you also to my examiners Professor John Reynolds, Associate Professor Darren Svirskis and Dr Sarah Gordon and my exam convenor Associate Professor Grant Butt for your input into the final version of this thesis.

To conclude, I would like to dedicate this thesis to science. It aims to be as critical as possible of the data of others, as well as its own, in order to lessen the load on the middleman. The submission of this thesis, on the other hand, is dedicated to my wife and four month old son who have been so very patient. Daddy's had his fun; my time is yours now.

Publications arising from this thesis

Richard N Prentice, Younus Mohammad, Anita Barzegar-Fallah, Sasi B. Yarragudi & Shakila B Rizwan. A sensitive LC-MS/MS method for quantification of phenytoin and its major metabolite with application to in vivo investigations of intravenous and intranasal phenytoin deliver. *Journal of Pharmaceutical and Biomedical Analysis* (Manuscript under review).

Richard N Prentice, Younus Mohammad, Woravimol Krittaphol & Shakila B Rizwan. A sensitive LC-MS/MS method for the study of exogenously administered ^{13}C-oleoylethanolamide in rat plasma and brain tissue. *Journal of Chromatography B* (Manuscript under review).

Richard N Prentice & Shakila B Rizwan. A critical review of intranasal treatments for epilepsy. *Advanced Drug Delivery Reviews* (Manuscript in preparation).

Richard N Prentice, Nigel C Jones & Shakila B Rizwan. A modified Maximal Electroshock Seizure Threshold test for intranasal anti-seizure drug delivery screening. *Journal of Pharmacological and Toxicological Methods* (Manuscript in preparation).

Richard N Prentice, Younus Mohammad, Andrew J Clulow, Benjamin J Boyd & Shakila Rizwan. Influence of stabiliser and lipid type on the internal structure of cubosomes and hexosomes after incubation in rat plasma. *Journal of Colloid and Interface Science* (Manuscript in preparation).

Sasi B Yarragudi, Richard N Prentice & Shakila B Rizwan. In vivo brain uptake and anti-seizure effect of phenytoin delivered using size-tailored intranasal mucoadhesive microparticles. *Journal of Controlled Release* (Manuscript in preparation).

Table of Contents

Chapter One.: Intranasal Treatments for Epilepsy……...1

1.1 Epilepsy and its Treatment 1

1.2 Relationships between the Nose and Epilepsy 4

1.2.1 Historical and Epidemiological 4

1.2.2 Neurological 5

1.2.2.1 The Olfactory System 5

1.2.2.2 Epilepsy and the Olfactory System 6

1.2.3 Clinical and Social 8

1.3 The Anatomy and Physiology of Intranasal Administration to the Brain 11

1.3.1 The Nasal Passage and Epithelia 11

1.3.2 Respiratory Epithelium 12

1.3.3 Olfactory Epithelium 12

1.4 Nasal Routes of Absorption for Therapeutics 13

1.4.1 Systemic Transport 14

1.4.2 Intracellular Transport 15

1.4.3 Extracellular Transport 15

1.5 Animal Models for Intranasal Delivery 17

1.6 Animals as Seizure and Epilepsy Models for the Evaluation of Anti-Seizure Therapeutics 19

1.6.1 Overview of Key Models 19

1.6.1.1 Maximal Electroshock Seizure Test 21

1.6.1.2 Maximal Electroshock Seizure Threshold Test 22

1.6.1.3 Pentylenetetrazole Test 25

1.6.1.4 6-Hz “Psychomotor” Seizure Test 26

1.6.1.5 Kindling....29
1.6.2 Relevance to the Evaluation of Intranasal Delivery Pathways....30
1.7 Pharmaceutical Formulation of Anti-Seizure Therapeutics....33
1.7.1 Role of Pharmaceutical Formulation....33
1.7.2 Studies of Pharmaceutical Formulation for Anti-Seizure Therapeutic Delivery 34
1.7.2.1 Administration Technique....36
1.7.2.2 Adverse Effects and Toxicity....37
1.7.2.3 Quantification of Drug in Tissues....38
1.7.2.4 Qualitative Distribution in Tissue....43
1.7.2.5 Efficacy....44
1.7.2.6 In the Pipeline....46
1.7.2.7 Conclusions....47
Chapter Two: The Validation of a Seizure Model....55
2.1 Introduction....55
2.2 Aims....58
2.3 Hypotheses....58
2.4 Materials & Methods....59
2.4.1 Materials....59
2.4.2 Animals....59
2.4.3 Drug Administration....59
2.4.3.1 Isoflurane Anaesthesia....59
2.4.3.2 Intravenous Administration of Phenytoin Solution and Saline....60
2.4.4 Maximal Electroshock Stimulation Threshold Test....60
2.4.4.1 Auricular Electrode Habituation....60
2.4.4.2 Electrical Stimulation....60
2.4.4.3 Cross-Over Study Design....61
2.4.5 Tissue collection for pharmacokinetic analysis....62
2.4.6 LC-MS Method for Analysis of Phenytoin in Plasma and Brain Tissue....63

2.4.6.1 Extraction and Sample Preparation 63
2.4.6.2 Standard Preparation 64
2.4.6.3 LC-MS Analysis 64
2.4.6.4 Data analysis 66
2.5 Results 67
2.5.1 Pharmacodynamic Validation of the MEST Seizure Model with Intravenous Phenytoin 67
2.5.1.1 Pharmacodynamics I: Determination of the CC_{50} of the Group and Baseline Response 67
2.5.1.2 Pharmacodynamics II: Determination of the Response to Intravenous Phenytoin at the CC_{50} 68
2.5.2 Validation of LC-MS Method for Measuring Tissue Phenytoin and 4-HPPH Concentrations 69
2.5.2.1 Specificity 69
2.5.2.2 Sensitivity 70
2.5.2.3 Accuracy and Precision 71
2.5.3 Validation of Pharmacodynamic Responses with Tissue Drug Concentrations. 74
2.5.3.1 Pharmacokinetics 74
2.5.4 Validation of Animal Welfare 75
2.6 Discussion 77
2.7 Conclusions 82
Chapter Three: On the Intranasal Delivery of Phenytoin 83
3.1 Introduction 83
3.2 Aims 88
3.3 Hypotheses 89
3.4 Materials & Methods 90
3.4.1 Materials 90
3.4.2 Animals 90

3.4.3 Isolation of TSP and Preparation of Microparticles 90
3.4.4 Preparation of Phenytoin Control Solution 91
3.4.5 Drug Administration 91
3.4.5.1 Isoflurane Anaesthesia 91
3.4.5.2 Intranasal Microparticle Administration using an Intranasal Insufflator 92
3.4.5.3 Intranasal Phenytoin Solution Administration using a Rat Intranasal Catheter Device (RICD) 93
3.4.6 Maximal Electroshock Stimulation Threshold Test 93
3.4.7 Tissue Collection and Histological Processing 94
3.4.8 LC-MS Method for Analysis of Phenytoin and 4-HPPH in Plasma and Brain Tissue 95
3.5 Results 96
3.5.1 Pharmacodynamic Evaluation at 60 Minutes After Intranasal Treatment 96
3.5.2 Pharmacokinetic Analysis of Tested Animals' Brains and Plasma at 60 Minutes 98
3.5.2.1 Pharmacokinetics of Phenytoin in Tested Animals at 60 Minutes 98
3.5.3 Histological Evaluation of Tested Animals' Nasal Epithelium 99
3.5.4 Pharmacodynamic Evaluation at 120 and 180 Minutes 101
3.5.5 Pharmacodynamic Evaluation: The Big Picture 103
3.5.6 Pharmacokinetic Evaluation: The Big Picture 104
3.5.6.1 Standard Curve Validation of Brainstem and Olfactory Bulb Homogenates 104
3.5.6.2 Pharmacokinetic Analysis of Phenytoin and 4-HPPH in Tested Animals 105
3.5.7 Pharmacodynamic Evaluation of Microparticles Without Phenytoin 111
3.6 Discussion 113
3.7 Conclusions 125
Chapter Four: On the Intravenous and Intranasal Delivery of Oleoylethanolamide and its Effect on Seizures 127

4.1 Introduction 127
4.2 Aims 134
4.3 Hypotheses 135
4.4 Materials & Methods 136
4.4.1 Materials 136
4.4.2 Animals 136
4.4.3 Preparation of OEA Treatments 136
4.4.3.1 Preparation of OEA Cubosomes, Dispersion and Solution 136
4.4.3.2 Dynamic Light Scattering 137
4.4.4 Drug Administration 138
4.4.5 Behavioural Analysis in Intranasal Dose Determination Studies 138
4.4.6 Tissue Collection and Histological Processing 138
4.4.7 Maximal Electroshock Stimulation Threshold Test 139
4.4.8 Small-Angle X-ray Scattering 140
4.4.9 Liquid Chromatography Mass Spectrometry (LC-MS) Method for Analysis of ^{13}C-OEA in Plasma, Brain and Liver 141
4.4.9.1 Extraction and Sample Preparation 141
4.4.9.2 Standard Preparation 142
4.4.9.3 LC-MS Analysis 143
4.4.9.4 Data analysis 144
4.5 Results 146
4.5.1 Pharmacodynamic Evaluation of Intravenous OEA cubosomes 146
4.5.2 Validation of an LC-MS Method for Measuring Tissue ^{13}C-OEA Concentrations in Plasma, Brain and Liver Tissue 148
4.5.2.1 Specificity 148
4.5.2.2 Sensitivity 149
4.5.2.3 Accuracy and Precision 151
4.5.3 Pharmacokinetic Evaluation of OEA Biodistribution and *In Vivo* Stability 153

4.5.3.1 ^{13}C-OEA Cubosome Dispersion Characterisation 153

4.5.3.2 Pharmacokinetic Analysis 153

4.5.4 Small Angle X-ray Scattering (SAXS) Evaluation of Structural Kinetics in Plasma 156

4.5.5 Cubosome Nasal Toxicity Evaluation: Preliminary Histological Screening 159

4.5.6 Evaluation of Pharmacodynamics of OEA Cubosomes After Intranasal Administration..... 161

4.5.7 Evaluation of the Histological Effects of OEA Cubosomes on the Nasal Mucosa of Tested Animals 163

4.6 Discussion 165

4.7 Conclusions 175

Chapter Five : Summary & Future Directions……...177

References…..... 186

Appendices…..... 217

List of Figures

Figure 1.1. Basic organisation of the olfactory system. 6
Figure 1.2. Basic anatomy of the olfactory (A) and respiratory (B) epithelia of the nasal passages. 11
Figure 1.3. Possible transport pathways through the (A) respiratory and (B) olfactory epithelia of the nasal passage to the brain. (C) Cross-sectional diagram of the arrangement of olfactory nerve bundles into the fila olfactoria as they travel towards the brain. 13
Figure 1.4. (A) Pathways by which intranasally-administered therapeutics may be cleared or transported to the brain. (B) Diagram of rat brain highlighting the olfactory and trigeminal pathways to the brain. (C) Distribution of labelled insulin-like growth factor 30 minutes after intranasal administration to the respiratory and olfactory epithelia of an anaesthetised rat, showing transport to the olfactory bulbs and brainstem. 14
Figure 1.5. General classification of seizure models (A) and pharmacological profiles of clinically validated models (B). 20
Figure 1.6. Typical stages of MES seizures. 21
Figure 1.7. Characteristics of brainstem and forebrain seizures. 22
Figure 2.1. Crossover method design of the MEST test used in this study. 61
Figure 2.2. Principles of the "up and down" method to determine the threshold for tonic hindlimb extension by serial stimulation of a group of rats. 62
Figure 2.3. Molecular structures of (A) Phenytoin (Mw = 252.3 g/mol), (B) 4-HPPH (Mw = 268.3 g/mol) and (C) d_{10}-phenytoin (Mw = 262.3 g/mol). 65
Figure 2.4. (A) Tonic-clonic seizure with hind limb extension (HLE) and (B) Tonic-clonic seizure with fore limb extension (FLE) only. 67
Figure 2.5. Determination of the CC_{50} (A) and baseline response to stimulation at the CC_{50} (B) in the batch of rats that participated in the study of intravenous phenytoin at 60 minutes. 68
Figure 2.6. Effect of intravenous phenytoin solution (25 mg/kg) on HLE (black; n=8) and FLE (grey; n=14) at the group CC50 current (40 mA) 60 minutes after treatment administration. 69

Figure 2.7. Representative chromatograms of phenytoin (blue), d10-phenytoin (red) and 4-HPPH (green) extracted from rat brain homogenate (left) and rat plasma (right). 70
Figure 2.8. Standard curves of phenytoin (blue) and 4-HPPH (green) in plasma (left) and rat brain homogenate (right). 71
Figure 2.9. Plasma concentrations (A), brain concentrations (B) and brain/plasma ratio (C) of phenytoin (blue) and 4-HPPH (green) in rats stimulated at 60 minutes after intravenous phenytoin administration (25 mg/kg). 74
Figure 2.10. Weight progression of the rats over the course of the experiment..... 76
Figure 3.1. Illustration of the effect of non-linear pharmacokinetics on phenytoin dosing in five different human patients. 84
Figure 3.2. Efflux of phenytoin at the blood brain barrier by P-glycoprotein (P-gp). 85
Figure 3.3. Scanning electron micrographs of phenytoin-containing TSP microparticles, as presented by Yarragudi et al. 86
Figure 3.4. Intranasal pharmacokinetics of phenytoin after in vivo administration of phenytoin microparticles, as presented by Yarragudi et al. 87
Figure 3.5. Intranasal microparticle insufflator (constructed in-house, based on the design of the Penncentury^{TM} dry powder insufflator) used for microparticle administration in this study (left). 92
Figure 3.6. Apparatus used for the intranasal administration technique. 93
Figure 3.7. Histological processing method for nasal tissue. 95
Figure 3.8. Determination of the CC_{50} and baseline response to stimulation at the CC_{50} in the batches of rats that participated in the study of intranasal phenytoin microparticles (A and B) and phenytoin control solution (C and D) at 60 minutes. 97
Figure 3.9. Effect of intranasal phenytoin microparticles and phenytoin control solution on HLE (black; n=6 for MPs; n=11 for solution) and FLE (grey; n=10 for MPs; n=18 for solution) at the group CC50 currents 60 minutes after treatment administration. 98
Figure 3.10. Phenytoin tissue concentrations and brain/plasma ratio of rats stimulated at 60 minutes after intranasal administration of phenytoin microparticles (circles) or phenytoin control solution (squares). 99
Figure 3.11. Representative histological images of the olfactory epithelium of rats which participated in the 60 minute MEST studies with phenytoin microparticles and phenytoin control solution. 100

Figure 3.12. Determination of the CC50 and baseline response to stimulation at the CC50 in the batches of rats that participated in the study of intranasal phenytoin microparticles at 120 minutes (A and B) and 180 minutes (C and D). 102
Figure 3.13. Effect of intranasal phenytoin microparticles on HLE (black) and FLE (grey) at the group CC_{50} currents 60 minutes (n=6 and n=10 respectively), 120 minutes (n=6 and n=18 respectively) and 180 minutes (n=6 and n=16 respectively) after treatment administration.. 103
Figure 3.14. Comparison between standard curves prepared with olfactory bulbs (blue; n=3; R^2 = 0.9999 (Phenytoin); R^2 = 1 (4-HPPH)), brainstem (red; n=3; R^2 = 1 (Phenytoin); R^2 = 0.9998 (4-HPPH)) and remainder of brain tissue (grey; n=9; R^2 = 1 (Phenytoin); R^2 = 1 (4-HPPH)). 104
Figure 3.15. Phenytoin (top) and 4-HPPH (bottom) concentrations in plasma (purple), main brain (blue), brainstem (green) and olfactory bulbs (red) of rats administered phenytoin microparticles (60, 120 and 180 minutes) and phenytoin control solution (60 minutes). 107
Figure 3.16. Phenytoin (top) and 4-HPPH (bottom) brain region/plasma ratios. 109
Figure 3.17. Ratios of Phenytoin (left) and 4-HPPH (right) in the brainstem (green) and olfactory bulbs (red) compared to the main brain. 110
Figure 3.18. Determination of the CC_{50} and baseline response to stimulation at the CC_{50} in the batch of rats that participated in the study of intranasal drug-free microparticles at 120 minutes (n=18). 111
Figure 3.19. Effect of intranasal drug-free microparticles (n=5) on HLE (black; n=5) and FLE (grey; n=18) at the group CC_{50} current 120 minutes after treatment administration (i.e. the time of peak effect of phenytoin microparticles). 112
Figure 4.1. OEA and structurally related molecules AEA and PEA. 128
Figure 4.2. Schematic diagram of the mechanism of PPARa activation by OEA leading to non-genomic (rapid) and genomic (slow) effects. 130
Figure 4.3. The internal structure of cubosomes. 131
Figure 4.4. Relationship between cubosomes and other commonly studied self-assembling lyotropic liquid crystalline structures, liposomes and hexosomes. 132
Figure 4.5. Study design for intravenous OEA cubosome experiments. 140
Figure 4.6. Molecular structures of (A) OEA (M_w = 325.3 g/mol) and (B) OEA-d4 (M_w = 329.3 g/mol). 143

Figure 4.7. CC_{50} calculation (A) and baseline (B and C) data for the intravenous OEA cubosome MEST experiment.. 146
Figure 4.8. Effect of intravenous OEA cubosomes (7.5 mg/kg OEA) on HLE (black) and FLE (grey) at the group CC_{50} current 15 minutes (n=4 and 8 respectively; p = 0.32), 30 minutes (n=5 and 10 respectively; p = 0.56) and 60 minutes (n=4 and 7 respectively; p = 0.32) after treatment administration. 147
Figure 4.9. Blank tissue samples of rat plasma (left), liver homogenate (centre) and brain homogenate (right) spiked with the same concentration of internal standard (d4-OEA) (red)..... 148
Figure 4.10. Representative chromatograms of ^{13}C-OEA (green) and OEA-d_4 (red) in rat plasma (left), rat liver homogenate (centre) and rat brain homogenate (right). 149
Figure 4.11. Standard curves of ^{13}C-OEA in rat plasma, brain homogenate and liver homogenate.. 150
Figure 4.12. Pharmacokinetics of ^{13}C-OEA up to 90 minutes after intravenous administration to rats in cubosomes (^{13}C-OEA 10% w/w with phytantriol) (blue) or control solution (orange) at a concentration of 2 mg/mL.. 155
Figure 4.13. SAXS studies of OEA cubosomes in 50% Milli Q water incubated at 37 ºC for 420 minutes. 157
Figure 4.14. SAXS studies of OEA cubosomes in 50% rat plasma incubated at 37 ºC for 420 minutes. 158
Figure 4.15. Representative histological images of the olfactory epithelium of rats 60 minutes after intranasal administration saline (D), OEA cubosome dispersion at the maximum concentration of 20 mg/mL total lipid (E), or equivalent concentration of free OEA suspension (F)..... 160
Figure 4.16. Representative histological images of the olfactory epithelium of rats 60 minutes after intranasal administration of OEA cubosome dispersions at concentrations of 10 mg/mL and 5 mg/mL total lipid. 161
Figure 4.17. Determination of the CC50 and baseline response to stimulation at the CC50 in the batches of rats that participated in the study of intranasal OEA cubosomes (x mg/mL OEA)..... 162
Figure 4.18. Effect of intranasal OEA cubosomes on HLE (black) and FLE (grey) at the group CC_{50} currents 30 minutes (n=4 and n=17 respectively) and 60 minutes (n=9 and n=17 respectively) after treatment administration. 163

Figure 4.19. Representative histological images of the olfactory epithelium of rats which participated in the 60 minute MEST studies with OEA cubosomes. 164

List of Tables

Table 1.1. Comparison between key aspects of the rat and human nasal passages. 18
Table 1.2. Seizure behaviours observed in the MEST model with varying current intensity and relevant regions of brain activation. 24
Table 1.3. Pharmacological characterisation of the 6-Hz seizure model in mice. 26
Table 1.4. The Racine scale of the stages of seizure behaviour. 29
Table 1.5. Summary of studies using pharmaceutical formulation to investigate a direct nose-to-brain pathway for ASDs. 35
Table 1.6. Summary of intranasal doses and administration methods used in studies investigating intranasally-delivered ASDs. 49
Table 1.7. Summary of methodology used in studies analysing pharmacokinetics and anti-seizure efficacy of intranasally-delivered ASDs. 51
Table 1.8. Half-lives and times to peak effect of ASDs used in the reviewed formulation studies. 54
Table 2.1. Optimised parameters for phenytoin and 4-HPPH analysis. 64
Table 2.2. MRM optimised parameters for ions monitored. 65
Table 2.3. Inter-day accuracy and precision of phenytoin and 4-HPPH quantification in rat brain homogenate and plasma based on quality control samples. 72
Table 2.4. Intra-day accuracy and precision of phenytoin and 4-HPPH quantification in rat plasma and brain homogenate based on quality control samples. 73
Table 2.5. Plasma, brain and CSF concentrations reported at 60 minutes after intravenous phenytoin administration to male rats at comparable doses to those used in the present study. 79
Table 3.1. Intra-day accuracy and precision of phenytoin and 4-HPPH quantification in rat brainstem and olfactory bulb homogenates based on quality control samples. 105
Table 4.1. Optimised parameters for compound analysis. 143
Table 4.2. MRM optimised parameters for ions monitored. 144
Table 4.3. Inter-day accuracy and precision of ^{13}C-OEA quantification in rat plasma, brain and liver tissue based on quality control samples. 151
Table 4.4. Intra-day accuracy and precision of ^{13}C-OEA quantification in rat plasma, brain and liver tissue based on quality control samples. 152

Table 4.5. Particle characteristics of the cubosomes dispersion used for the experiments (10% ^{13}C-OEA-phytantriol cubosomes stabilised with Tween 80). 153

List of Equations

Equation 1.1. Calculation of Drug Targeting Efficiency (%DTE). 38
Equation 1.2. Calculation of Direct Transport Percentage (%DTP). 39
Equation 4.1. Calculation of corrected ^{13}C-OEA intensity. 145
Equation 4.2. Calculation of corrected analyte/IS ratio..... 145

List of Abbreviations

^{12}C-OEA	12-Carbon oleoylethanolamide
^{13}C	13-Carbon
^{13}C-OEA	13-Carbon-labelled oleoylethanolamide
4-HPPH	5-(4-Hydroxyphenyl)-5-phenylhydantoin
A.U	Arbitrary Units
ACN	Acetonitrile
ADT	After Discharge Threshold
AEA	Anandamide
ASD	Anti-seizure drug
ASP	Anticonvulsant Screening Programme
AUC	Area Under the Curve
BBB	Blood-Brain Barrier
CC_{50}	Convulsive current (50% of animals)
CC_{97}	Convulsive current (97% of animals)
C_{max}	Maximum concentration
CNS	Central nervous system
Conc	Concentration
cryo-TEM	Cryogenic Transmission Electron Microscopy
CSF	Cerebrospinal Fluid
CV%	Coefficient of Variation (percentage)
CYP	Cytochrome P450 enzyme
d_{10}-phenytoin	Deuterated phenytoin
d_4-OEA	Deuterated oleoylethanolamide
Da	Daltons
DLS	Dynamic Light Scattering
DMSO	Dimethylsulfoxide
DPX	Dibutylphthalate Polystyrene Xylene
DTE	Drug Targeting Efficiency
DTP	Direct Transport Percentage
ECT	Electroconvulsive Therapy
ED_{50}	Effective dose (50% of animals)
EDTA	Ethylenediaminetetraacetic acid
EEG-fMRI	Electroencephalogram-Informed Functional Magnetic Resonance Imaging
EPR	Enhance Permeability and Retention
ETSP	Epilepsy Therapy Screening Programme
F/E	Flexion/Extension
FAAH	Fatty Acid Amide Hydrolase
FLE	Forelimb Extension
GABA	Gamma Aminobutyric Acid
GMO	Glyceryl Monooleate
HLE	Hindlimb Extension
HPLC	High Performance Liquid Chromatography
Hz	Hertz

i.n	Intranasal
i.p.	Intraperitoneal
i.v	Intravenous
ILAE	International League Against Epilepsy
kDa	Kilodaltons
keV	Kilo Electron Volts
LC-MS	Liquid Chromatography Mass Spectrometry
LEA	Linoleoylethanolamide
LLOQ	Lower Limit of Quantification
LOT	Lateral olfactory tract
m/z	Mass to Charge Ratio
MDT	Multi-Drug Transporter
MeOH	Methanol
MES	Maximal Electroshock Seizure
MEST	Maximal Electroshock Seizure Threshold
min-EST	Minimal Electroshock Seizure Threshold
MPs	Microparticles
MRM	Multiple Reaction Monitoring
Mw	Molecular weight
nAChR	Nicotinic acetylcholine receptor
NAEs	N-acylethanolamides
NBF	Neutral buffered formalin
NMRI	Naval Medical Research Institute
OEA	Oleoylethanolamide
PBS	Phosphate-buffered saline
PDI	Polydispersity index
PE	Polyethylene
PEA	Palmitoylethanolamide
PG	Propylene glycol
P-gp	P-glycoprotein
PLA	Polylactide
PLGA	Poly(D,L-lactide-co-glycolide
PPARα	Peroxisome Proliferator-Activated Receptor α
PTZ	Pentylenetetrazole
q	Scattering vector
QC	Quality control
R^2	Coefficient of determination
RICD	Rat Intranasal Catheter Device
rpm	Revolutions per minute
RSD	Relative Standard Deviation
s.c.	Subcutaneous
SAXS	Small Angle X-ray Scattering
TBME	Tert-Butyl Methyl Ether
TSP	Tamarind Seed Polysaccharide
Tyr Kin	Tyrosine Kinase

VAC	Volts of Alternating Current
WAXS	Wide Angle X-ray Scattering

Chapter One

Intranasal Treatments for Epilepsy

1.1 Epilepsy and its Treatment

Epilepsy has been defined as a disorder of the brain characterised by an enduring predisposition to generate epileptic seizures and by the neurobiologic, cognitive, psychological, and social consequences of this condition. The condition therefore requires the occurrence of more than one epileptic seizure, an event that is defined as a transient occurrence of signs and/or symptoms due to abnormal excessive or synchronous neuronal activity in the brain[1]. A seizure may be generalised, as is the most commonly recognised presentation by the layman involving convulsions, but in a lot of cases may be, at least initially, focal (or partial) in nature[2]. In this case, the seizure develops in a localised area of the brain (at which point a patient may experience an aura associated with that region – e.g. déjà vu or sensory hallucinations) and may or may not progress to a generalised seizure affecting the whole brain. Individuals may remain conscious and alert during this focal experience, in which case it is classified as a simple partial seizure. Alternatively, they may experience altered consciousness or lose it all together, in which case it is classified as a complex partial seizure.

Epilepsy is the most common serious neurological disorder[3]. It is a disease of all ages, affecting up to 50 million people worldwide[4] and comes with the huge burdens of reduced quality of life, high unemployment rates, reduced life expectancy and comorbidities such as depression[5]. Despite decades of international research towards developing pharmacological treatments and the current availability of over 22 anti-seizure drugs (ASDs)[6], it is somewhat disconcerting to

reflect on the statistic that approximately 30% of patients still fall under the classification of "drug-resistant", with temporal lobe epilepsy (i.e. focal epilepsy arising from the temporal lobe) thought to be the most susceptible to becoming drug resistant[7]. Drug resistance is defined by the International League Against Epilepsy (ILAE) as the failure of adequate trials of two tolerated and appropriately chosen and used ASD schedules (whether as monotherapies or in combination) to achieve sustained seizure freedom[8]. Proposed mechanisms of drug resistance have been discussed in detail elsewhere[9,10] but in general, may involve genetic variation, disease-related mechanisms (seizure etiology, progression of disease, neural network changes, alterations in drug target(s), alterations in drug uptake into the brain) or drug-related mechanisms (tolerance or ineffective mechanism of action).

Two phrases are important to consider in this definition of drug resistance in the context of developing future pharmaceutical treatments for it. The first is the endpoint of "sustained seizure freedom", as quality of life does not correlate particularly well with seizure frequency and the constant threat of randomly having a seizure is usually more destructive than the actual seizure itself[11]. The second is "tolerated", as side effects have a strong inverse correlation with quality of life[12] and will often lead to discontinuation or non-compliance, resulting in a longer time period before resistance is recognised. The "appropriately chosen and used" and "adequate trials" aspects can be addressed by clinicians and patients themselves. There has been much discussion in recent years on how to move forward to address what appear to be the two clear needs as far as pharmaceuticals are concerned; increased efficacy in drug-resistant individuals and improved tolerability. While the latter has been significantly improved, it still remains an issue[13]. Pharmaceutical companies, however, have pulled back from the expensive process of developing new ASDs, as the market for them would appear to be saturated[6].

Several strategies have been suggested in order to develop better treatments. The most widely recognised is the need to develop and utilise more broad and goal-oriented models in screening protocols, given that most ASDs on the market were initially selected for development based on successful performance in the Maximal Electroshock Seizure (MES) and/or the subcutaneous pentylenetetrazole (s.c. PTZ) tests, thereby sending ASD discovery down a multi-decade road of unearthing similar compounds to those which were already used and disregarding compounds that may have been effective through unique mechanisms and might have been of benefit to the large "drug-resistant" population[14,15]. As well as developing screening models relevant to drug resistance, there is also a focus on establishing models with which to identify and test disease-modifying anti-epileptogenic drugs.

Hitting a target pharmacologically with a rational or serendipitous therapeutic molecule is the simplest and most high throughput method of screening and developing new ASDs and will no doubt remain extremely important as the focus moves towards disease-modifying agents and treatments for specific types of epilepsy. However, there exists a potentially very useful supplementary approach that pharmacology alone cannot address and which appears to have therefore remained largely confined to the literature; the utilisation of pharmaceutical formulation. Perhaps the most interesting aspect of this is the potential it offers to exploit endogenous molecules[16,17], which are normally subject to rapid *in vivo* degradation, but may exert important therapeutic effects where synthetic molecules fail. From another perspective, pharmaceutical formulation might be used to achieve more efficient targeting of drug to the brain to improve tolerability and efficacy (e.g. through the use of nanoparticles), or for simply incorporating a difficult molecule into a physiologically-friendly solution or suspension[18–22]. Finally, and perhaps most obviously, it provides a pathway to optimally deliver molecules by nonconventional routes and orifices.

The following review explores the nose, a somewhat alternative approach to ASD treatment for which pharmaceutical formulation is intimately relevant, and while investigated from some angles, has not yet had its full potential explored. The nose has had longstanding and interesting relationships with both epilepsy and the brain and this Chapter will discuss these, along with the potential value of delivering ASDs to the brain through the nose as a therapeutic strategy for the treatment of seizures and epilepsy.

1.2 Relationships between the Nose and Epilepsy

1.2.1 Historical and Epidemiological

Historical examples of treating epilepsy through the nose can be drawn from all corners of the world. In Eastern countries, the smell of a shoe has been, and apparently still is, used as a first aid measure to arrest seizures[23]. In the Western world, the burning of the ammonia-based hartshorn under the nose as a first aid measure for treating seizures was reported in the 17th century[24]. In later times, it was suggested that the use of ammonia or amyl nitrate may arrest the course of a seizure[25] and later still that such a stimulus may be used to condition a patient to inhibit seizures psychologically by thinking of it during the prodromal phase[26,27]. The commonality between these "treatments" is obviously the potent and disenchanting nature of the aroma. More recently, and in contrast to these reports, Betts[28] proposed conditioning with aromatherapy as a means of controlling seizures. However, while pleasant olfactory sensations may have played a role in this, they could not be distinguished from effects of transdermal oil absorption or simply the relaxation associated with the sessions. The relationship between the nose and epilepsy is therefore something which science has sought to make progress on for centuries and explain through the apparent link between olfactory sensation networks and the networks involved in the generation and propagation of seizures.

Evidence of the involvement of the olfactory sensory network with some types of epilepsies can be found in the symptoms experienced by some patients, namely olfactory auras and impaired olfactory function. An aura is the subjective experience of a simple partial seizure[29], related to activation of a specific area (or areas) of the brain. It is usually a hallucination, but may also possibly be an illusion or a vaguer episode with a quality of reminiscence (e.g. déjà vu). The usual occurrence in an olfactory aura is the experience of an unpleasant odour, with the earliest influential description of an olfactory case dating back to 1889, describing a woman with a horrible smell of "dirty burning stuff" prior to a seizure[30]. It has been estimated that 19-30% of epileptic auras are olfactory, but these occur in only 0.6-16% of people with temporal lobe epilepsy and 0.9-8.1% of all people with focal epilepsy[30]. Of note, it appears that such auras may be more prevalent in patients with temporal lobe epilepsy, and the involvement of the olfactory network in this particular condition is further supported by the occurrence of many abnormalities in olfactory function in these patients. These include impairment of odour discrimination, memory and identification, as well as temporarily altered detection thresholds, with an increased sensitivity before a seizure and decreased sensitivity for hours or days

afterwards[30]. The fact that temporal lobe epilepsy represents most cases of drug-resistant epilepsy (at least those managed surgically)[31] suggests a potentially significant role for the nose in the treatment of this phenomenon.

1.2.2 Neurological

1.2.2.1 The Olfactory System

The olfactory system is remarkably similar between different species[32] and is presented diagrammatically in Figure 1.1. The olfactory epithelium is located in the dorsal or dorsoposterior nasal passage and contains bipolar sensory neurons with an axon in the olfactory bulb and a dendrite in the epithelium capped with numerous cilia which extend into a surface mucous layer and can interact with dissolved odourant molecules. The axonal synapses of the olfactory neurons converge onto mitral or tufted cells in the glomeruli of the olfactory bulbs[33], with stimulation of different classes of receptor neurons leading to the formation of a map of excited glomeruli[34]. Unlike all other sensory inputs which are primarily relayed through the thalamus, the olfactory bulbs first transmit signals along the myelinated lateral olfactory tract (LOT) to project diffusely into the largest region of the primary olfactory cortex called the piriform cortex, which is only two synapses removed from the external environment[34]. The piriform cortex is made up of three layers, a sparsely populated superficial layer, a main input layer containing densely packed somata of glutamate-releasing principal neurons and finally, a deep layer containing principal neurons at a lower density[34]. Gamma aminobutyric acid (GABA)-releasing interneurons are scattered across all layers and provide feedforward and feedback inhibition of principal cells[34]. From the primary olfactory cortex, information is projected widely to secondary olfactory areas such as the orbitofrontal cortex via the mediodorsal thalamic nucleus[35].

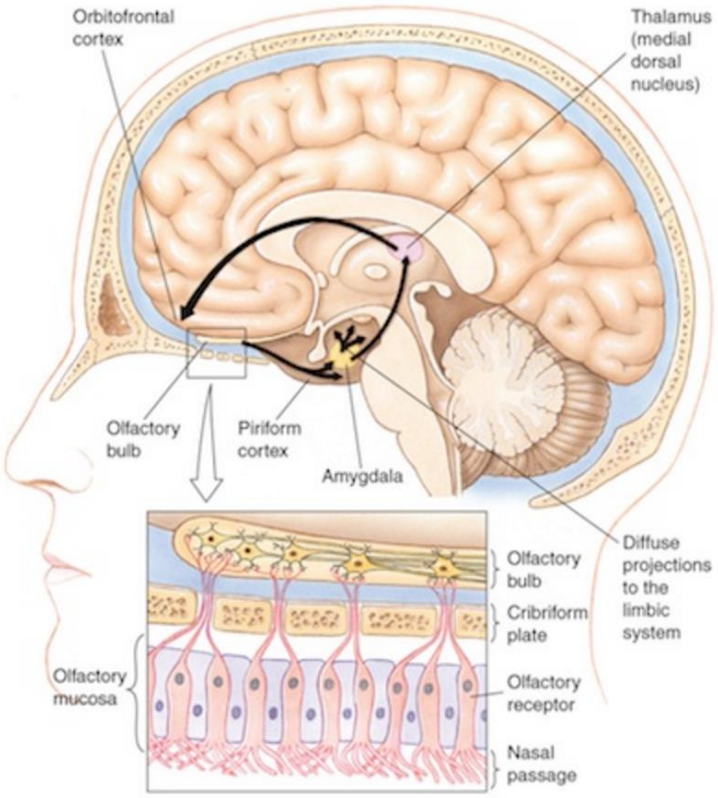

Figure 1.1. Basic organisation of the olfactory system. Adapted from Nicola-Antoniu.[36]

1.2.2.2 Epilepsy and the Olfactory System

The olfactory system, in particular the piriform cortex, has been suggested to have an important role in epilepsy, as suggested by the historical and epidemiological links described above, which science has since illuminated. Olfactory impairment in some focal epilepsies, especially of the temporal lobe, has been shown by neuroimaging to be associated with changes in the piriform cortex that parallel the odour discrimination, memory and identification impairment reported[30]. Furthermore, atrophy and reduced olfactory bulb volume have been described[37,38]. Seizures that produce olfactory hallucinations typically show widespread orbitofrontal and anterior temporal lobe activity. Olfactory auras have been suggested to correspond to epileptic activity that causes an intense activation of the piriform cortex and amygdala, as is seen when an unpleasant odour is smelt in the environment, however it is worth noting that human seizures have been noted to arise from the piriform cortex without an olfactory aura[30,39]. Interestingly, a similar intense activation of the olfactory cortex is also a hypothesis behind the success of strong odours in prevention of some seizures by disrupting the synchronised progression of

epileptic discharges between regions[40 30]. Alternative explanations include a change in alertness due to a smell which may interrupt seizure progression or a pharmacological effect of the odourants[30].

The many neurological connections between the olfactory system and seizures have been reviewed in detail by Vaughan and Jackson[30] and Vismer et al.[41], with both attesting to the great therapeutic potential that may be achieved by targeting the piriform cortex. The links between the two systems are numerous, with implications of a role for the piriform cortex in seizure generation and distribution, epileptogenesis and pharmacoresistance[30]. As highlighted by Vismer et al[41], the propagation of seizures through the brain is not a random process and they instead exploit existing circuits that normally support highly controlled recurrent activity. In this respect, the anatomical arrangement of neural networks in the piriform cortex make it inherently susceptible to seizure activity[30]. Each glomerulus in the olfactory bulb has over 1000 broad projections (mainly mitral cells) across the piriform cortex to random pyramidal cells[30]. This is necessary to allow complex odour mixtures to be detected, but also forms a large, highly interconnected, excitatory network which needs to be carefully regulated by interneurons[30]. If local inhibitory circuits are modified or removed, it is extremely prone to forming hyper-excitable local networks[30]. Furthermore, strong reciprocal connections of the piriform cortex to nearby structures (e.g. olfactory bulbs, amygdala, hippocampus) normally provide an additional means of modulating olfactory inputs, but run the risk of becoming circuits that could sustain seizure activity[30,42].

Vaughan and Jackson[30] reviewed the roles of the piriform cortex in generation and distribution of seizures. In terms of generation, the most obvious connection can be found in the deep anterior piriform cortex which contains a well-known chemoconvulsant trigger zone called the 'area tempestas'[41], which is crucial for seizure initiation within the limbic network. In addition to chemical stimulation, the piriform cortex can be electrically kindled to generate seizures which follow the same progression of motor features as kindling from other sites such as the amygdala[30]. With regards to the distribution of seizure activity, they noted a number of elements. Firstly, the role of the piriform cortex in the process of amygdala kindling[42–44] (as well as the loss of GABA-ergic interneurons in it during this process[45]). Secondly, its role as a common target of discharge spread in frontal and temporal lobe epilepsies (indicated by the sites of lesions that can produce an olfactory aura[46]. Thirdly, the impact of these epilepsies on olfactory function[47] and detection of piriform cortex activity by electroencephalogram-informed functional magnetic resonance imaging (EEG-fMRI)[48]). Fourthly, its relationship to

clinical descriptions of aura progression, and finally, its broad outputs to cortical and subcortical regions. Both this distributive ability, combined with the potential for sustained hyper-excitability, form the basis of hypotheses for a role of the piriform cortex in epileptogenesis (through recruitment as a secondary hyper-excitable node) and drug resistance (through alterations in neural networks)[30]. Though these processes fall outside the scope of this review and project, it is interesting to consider the effect piriform cortex-targeted therapeutics may have on them in light of these theories.

1.2.3 Clinical and Social

The clinical application of intranasal (i.n) treatments for seizures have been investigated for almost two decades. Despite the extensive aforementioned neurological links between the olfactory sensory network and seizures, the current clinical treatments have emerged to exploit an entirely different opportunity; the rich vascular bed present in the lower nasal passage[49]. This presents itself as an obvious candidate for rapid absorption of lipophilic therapeutics, namely the benzodiazepines, which have so far been used for this purpose. The administration method has proven a valuable asset in addressing the need for a practical, effective and socially acceptable treatment for seizure emergencies outside of hospital (including prolonged single seizures, acute repetitive seizures, and status epilepticus). Due to a lack of registered formulation development, this has been used as an off-license management strategy, but pharmaceutical companies have taken an interest in optimising nasal spray composition and devices[21]. Importantly, trials are being conducted in human subjects, supporting the potential clinical translatability of other such intranasal approaches that are being developed in basic science models. The subject has recently been reviewed by Kälviänen[50] and Kapoor et al.[21], to which the reader is referred for a detailed discussion, but the key information will be briefly discussed below.

It has been shown that prompt initiation of medical treatment for seizure emergencies occurring outside of hospital can reduce the risks associated with progression to status epilepticus[51]. To make this possible, intranasal, rectal and buccal benzodiazepines have all been used given that they are able to be administered quickly and safely by non-clinical caregivers, who will most commonly be the first people available to act in such situations. While each achieves rapid access to the systemic circulation through blood vessel-rich areas, from a social perspective, the intranasal route has gained a lot of favour. Firstly, it avoids the social embarrassment and legal liability concerns associated with rectal administration[52,53], and secondly, it avoids the risk

of aspiration of buccal doses, and inconsistent absorption due to ictal hypersalivation[54,55]. Furthermore, from a clinical perspective, the onset of action and effectiveness of intranasal benzodiazepines has been shown to be superior to rectal administration[56].

The most studied benzodiazepine for intranasal administration is midazolam, which was first reported to treat acute seizures in 1996[57] and was followed by a number of other studies testifying to its efficacy and safety[58–62]. It achieves 67-100% bioavailability and peaks within 10 minutes, leading to seizure control within 2-5 minutes after administration[50]. It is classified as a "water soluble benzodiazepine" as good solubility can be achieved in aqueous solutions below a pH of 4[63], however this is likely responsible for the commonly reported burning or irritation sensation in the nose, and bitter taste lasting for 30-45 seconds, after administration[64,65]. With increasing pH, midazolam reverts to a lipophilic form, affording it high systemic absorption and bioavailability. Notably, intranasal administration of midazolam up to doses of 10 mg has been repeatedly shown to be more effective than rectal diazepam, including in a home-administration setting[66–69], supplementing the social benefits of this route described above. Furthermore, despite having a slightly slower onset than i.v. diazepam (2-5 minutes vs 2-3 minutes[50]), it has been suggested to also have applications in an emergency room setting, in that the total time until seizure cessation after arriving at hospital is reduced by avoiding the delay associated with establishment of an i.v. line[70–73].

Diazepam, the i.v. benzodiazepine of choice (half-life around 50 hours) and the rectal alternative to i.n. midazolam, has also been tested by the i.n. route. Peak plasma concentrations are reached significantly later than with i.n. midazolam (45 minutes vs 10 minutes[74]), but time to onset of seizure cessation has not yet been reported, let alone in a head to head trial with midazolam. Nasopharyngeal adverse effects studied with one formulation were reported to resolve within 12 hours[74], but would seem to be more extensive and long lasting, or perhaps just more meticulously reported, than those of midazolam. Side effects listed included headache, dysgeusia, nasal discomfort, lacrimation, nausea, rhinorrhea, somnolence, oropharyngeal pain, paranasal sinus hypersecretion, tongue injury, dizziness, nasal congestion, parosmia, cough, fatigue, myalgia and throat irritation[74]. Additionally, it is possible that the co-solvents required to formulate the lipophilic diazepam may explain the apparent increase in adverse effects compared with low pH midazolam solution, which was likely buffered quickly in the nasal passage. Furthermore, different formulation compositions of diazepam may also influence i.n. bioavailability[75].

Finally, lorazepam is reported to be four to six times less lipid soluble than midazolam and diazepam, and has been found to have a peak effect time of 30 minutes and half-life of 18.5 hours after intranasal administration[76,77]. It has been evaluated in a study in children up to doses of 4 mg and found to be non-inferior to i.v. lorazepam with the same median onset time of 3 minutes (range 1-25 minutes)[78]. Evaluation of adverse effects and pharmacokinetics after i.n. administration has also been performed in healthy volunteers in comparison to the i.v. route[76], however, the formulation used was likely different. Thus, it is uncertain whether any benefit is obtained from lorazepam compared with the more extensively studied midazolam, other than perhaps an extended duration of action and being easier to formulate than diazepam.

Overall, it would appear that intranasal administration of anti-seizure medication is a rapid, effective and socially acceptable practice with industry engagement in product development both in terms of formulation and administration devices. However, the scope is currently limited to benzodiazepines, which are really only an emergency treatment of severe prolonged or cluster seizures due to issues such as side effects, tolerance and dependence, as well as reliance on a systemic absorption mechanism. It should also be noted that because systemic absorption is the main proposed route of entry into the brain, high doses are still required, so it does not currently offer any benefit in terms of decreasing systemic exposure. The more exploratory pharmaceutical science field has been developing an increased interest in taking this further and exploring the potential of the nose as a route for addressing other challenges in the clinical treatment of seizures and epilepsy, primarily focusing on bypassing the systemic circulation and exploiting direct nose-to-brain transport pathways.

1.3 The Anatomy and Physiology of Intranasal Administration to the Brain

1.3.1 The Nasal Passage and Epithelia

The nasal septum divides the nasal cavity longitudinally into two passages, each having three key regions: the nasal vestibule (a slight dilatation just inside the nares and before the main chamber), the respiratory region and the olfactory region[33,79]. The latter two comprise the main chamber of the nasal passage and essentially consist of an epithelial layer covered by a continuous layer of mucous. Bony structures (turbinates) lined with mucosal tissue project into the lumen to increase the surface area of the nasal passage and facilitate filtering, humidification and warming of inspired air[79]. Four types of epithelia exist in the nasal passages and help distinguish the different regions. The nasal vestibule primarily contains a squamous epithelium, which becomes a non-ciliated, cuboidal/columnar (transitional) epithelium, then a ciliated, pseudostratified cuboidal/columnar (respiratory) epithelium in the anterior main chamber and finally the olfactory epithelium in the dorsal or dorsoposterior main chamber[79]. The respiratory and olfactory epithelia (Figure 1.2) will be the focus of the following discussion as they are considered to be the most relevant to therapeutic delivery to the brain[33]. For detailed reviews of nasal anatomy to supplement the following text, the reader is referred to more extensive reviews[33,79–82].

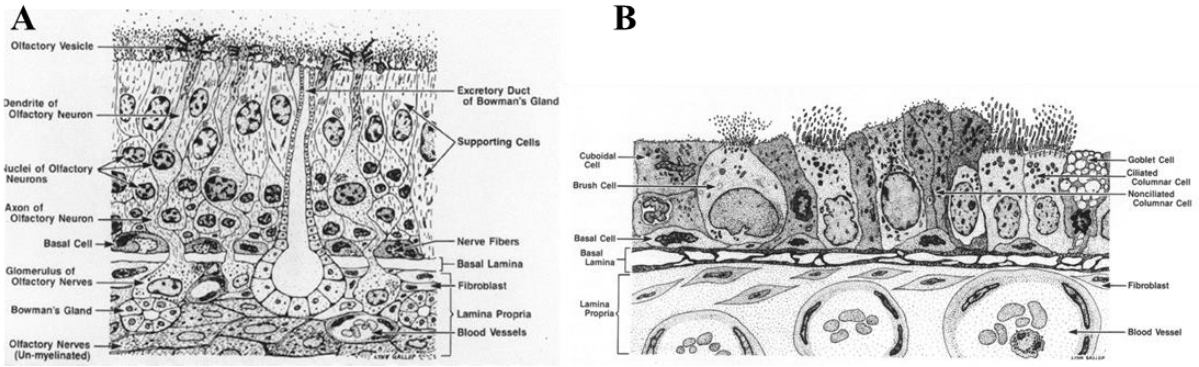

Figure 1.2. Basic anatomy of the olfactory (A) and respiratory (B) epithelia of the nasal passages. Figures adapted from Uriah & Maronpot.[83]

1.3.2 Respiratory Epithelium

The respiratory epithelium (Figure 1.2B and Figure 1.3A) consists of goblet cells, cuboidal cells, brush cells, basal cells and ciliated and non-ciliated columnar cells[33,83]. It also contains various glands for producing nasal secretions in addition to the mucous secreted by goblet cells[33]. The mucous layer consists of a low viscosity layer, which bathes the cilia, and a more viscous layer on top[84]. Deposited substances are generally subject to rapid mucociliary clearance by the motile cilia of the brush cells, which results in removal from this region in approximately 15-20 minutes[81]. The respiratory epithelium has a far richer supply of blood vessels and lymphatics in comparison to the olfactory epithelium[82]. Interestingly, it is innervated by branches of the trigeminal nerve, many fibres of which extend through the epithelium so that their free nerve endings lie just beneath tight junctions (i.e. very close to the surface)[33]. The trigeminal nerve has a predominantly sensory function whereby information, in the case of the nasal epithelium fibres, is relayed back to both the brainstem at the level of the pons and a small portion to the olfactory bulbs[33,82] (Figure 1.4B). It should be noted that while most significant to the respiratory epithelium, the extension of free trigeminal nerve endings to near the surface is also a feature of the olfactory epithelium[33].

1.3.3 Olfactory Epithelium

The key feature of the olfactory epithelium is the many dendrites of bipolar sensory (olfactory) neurons extending out from the central nervous system (CNS) to make direct contact with the external environment[84] (Figure 1.2A and Figure 1.3B). Each dendritic process ends in a small swelling, known as the olfactory knob, which projects 10-23 cilia into the overlying mucous layer[84]. It is important to note that in contrast to the respiratory epithelium, these cilia are non-motile, so dynamic mucociliary clearance does not occur in this area[33,79,84]. Rather, mucous slowly drains into the respiratory region when it is over-produced. The axons of each olfactory neuron are collected into nerve bundles surrounded by interlocking olfactory ensheathing cells (the fila olfactoria), which are subsequently collected into a bunch of nerve bundles and further enclosed by fibroblasts to form a peri-neural sheath[80,82] (Figure 1.3C). These channels extend back through small gaps in the cribriform plate (separating the nose and the cranial cavity) to enter the cranial cavity, pass through the subarachnoid space containing cerebrospinal fluid (CSF), and synapse (along with around 1500 other olfactory neuron axons) with a single mitral of tufted cell in the olfactory bulb[84]. Other features of the olfactory epithelium include microvillus sustentacular cells (which act as adjacent supporting cells for the olfactory

neurons[33]), Bowman's gland cells (which form ducts originating in the lamina propria and produce a serous fluid to aid dissolution of odourant molecules[33]) and horizontal basal cells which lie along the basal lamina and act as progenitors to olfactory neuron progenitor basal cells, sustentacular cells and cells of the Bowman's gland and duct. As in the respiratory epithelium, blood and lymphatic vessels also exist in the lamina propria[33], but to a lesser extent[82].

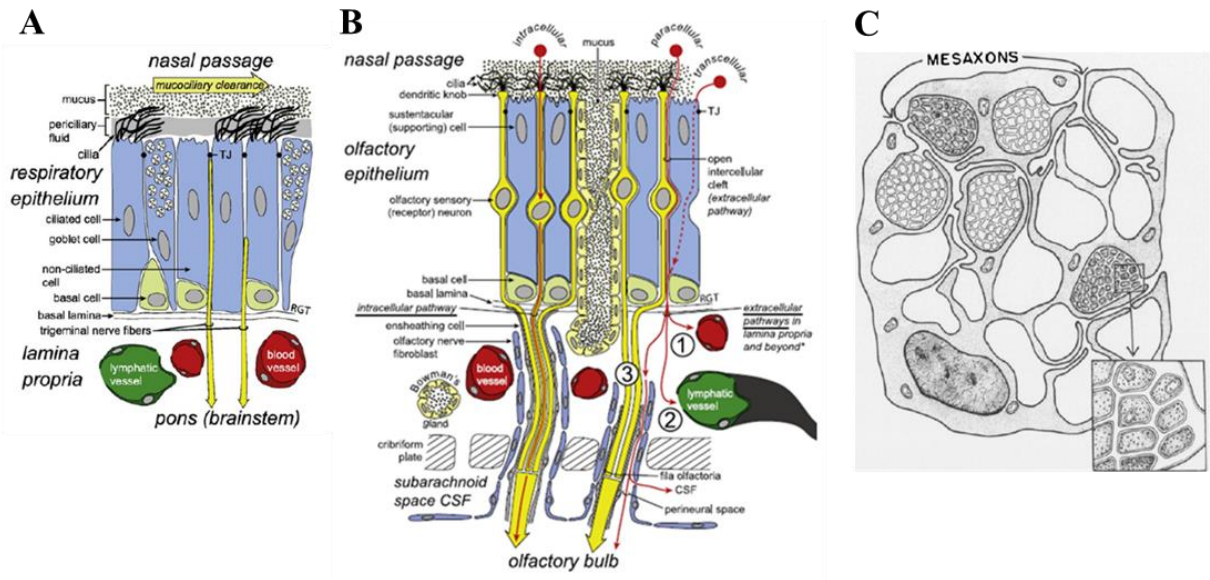

Figure 1.3. Possible transport pathways through the (A) respiratory and (B) olfactory epithelia of the nasal passage to the brain. (C) Cross-sectional diagram of the arrangement of olfactory nerve bundles into the fila olfactoria as they travel towards the brain. Figures adapted with permission from Lochhead & Thorne[33] and Mistry et al.[80] TJ = Tight junction; CSF = cerebrospinal fluid.

1.4 Nasal Routes of Absorption for Therapeutics

The features of the abovementioned epithelia provide a number of potential delivery routes to the CNS (Figure 1.3 and Figure 1.4), collectively divided into the olfactory and respiratory pathways. These have been reviewed in detail elsewhere[33,82], but will be summarised below. As implied by Figure 1.4, the different pathways are most easily classified as systemic, intracellular or extracellular and a prerequisite for all pathways, other than intracellular transport via olfactory neurons, is an initial transport into the lamina propria. Depending on the properties of the molecule, macromolecule or particle concerned, it may achieve this via paracellular transport through tight junctions or alternatively, passive diffusion or transcytosis through

epithelial cells. Alternatively, it will be trapped in the nasal mucous and eventually cleared from the surface.

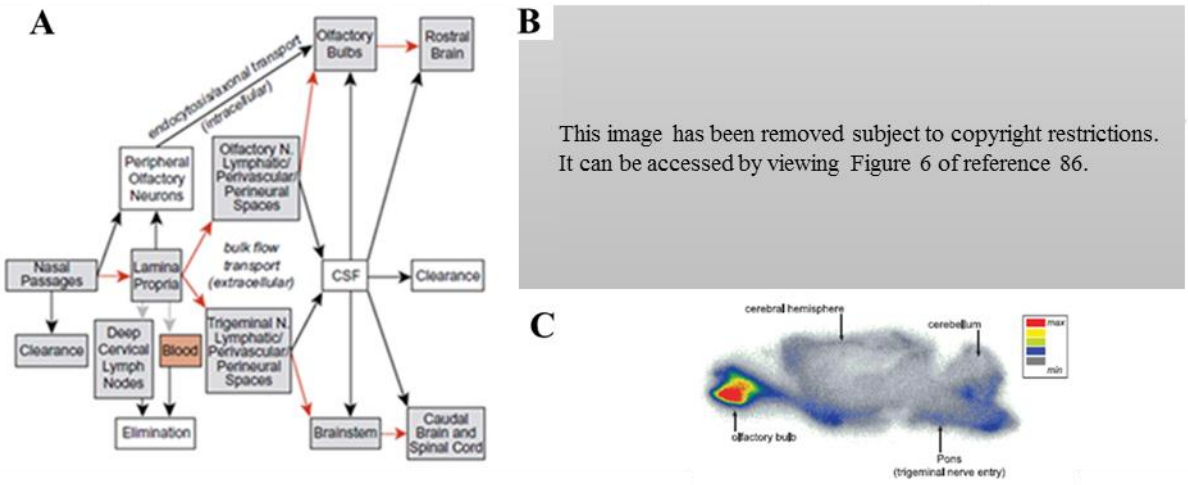

Figure 1.4. (A) Pathways by which intranasally-administered therapeutics may be cleared or transported to the brain. (B) Diagram of rat brain highlighting the olfactory and trigeminal pathways to the brain. (C) Distribution of labelled insulin-like growth factor 30 minutes after intranasal administration to the respiratory and olfactory epithelia of an anaesthetised rat, showing transport to the olfactory bulbs and brainstem. Figure adapted from Thorne et al.[85](with permission), Lochhead et al.[86] and Lochhead & Thorne.[33] (with permission). AICA = anterior inferior cerebellar artery; SCA = superior cerebellar artery; MCA = middle cerebral artery; OFA = olfactofrontal artery; CSF = cerebrospinal fluid.

1.4.1 Systemic Transport

As indicated in previous sections, the nasal mucosa is highly vascular, which may lead to extensive, and possibly undesired, systemic absorption of therapeutics, especially via the more endowed respiratory epithelium. Vasculature in this region has of a mixture of continuous and fenestrated endothelia, permitting transport of both small and large molecules into the systemic circulation[82]. A proposed advantage of systemic intranasal delivery into the bloodstream may be the potential for 'counter-current transfer' whereby drug may enter the venous blood supply in the nasal passages, but then be rapidly transferred to carotid arterial blood, thereby reaching the brain rapidly and in higher concentrations compared to if it underwent an initial distribution throughout the systemic circulation[82]. Alternatively, if substances are not absorbed into the

bloodstream, they may drain into the lymphatic vessels in the lamina propria and ultimately to the cervical lymph nodes[33].

1.4.2 Intracellular Transport

The most desirable of the brain delivery pathways to exploit is the intracellular transport of therapeutic molecules directly through the olfactory neurons. Given that these neurons extend numerous cilia directly into the mucous covering the surface of the epithelium, providing a large surface area for odourant detection, the hope has been that they may also provide a large surface area for therapeutic absorption by passive diffusion, or in the case of larger macromolecules or nanoparticles, a receptor-mediated or adsorptive endocytosis. Therapeutics might then diffuse or be transported as cargo through these neurons directly to their axonal synapses within the CNS[80]. Studies have shown that large molecules such as horseradish peroxidase, wheat germ agglutinin-horseradish peroxidase and albumin, as well as some viruses may be transported intracellularly along the olfactory neuron axons towards the brain[33,87]. A similar route has been proposed for intracellular transport through trigeminal nerve fibres[33], however, this would first require transport of the molecules into the lamina propria via other pathways, as discussed earlier. Given that the trigeminal nerve transmits information to both the brainstem and olfactory bulbs, albeit to varying degrees, it can be difficult to infer from experimental data the route(s) (trigeminal or olfactory) by which intranasally-administered molecules reach the olfactory bulbs if they appear in both regions[82]. Despite the apparent potential for intracellular delivery through these neurons, the current consensus seems to be that this pathway is too slow to be mediating the rapid direct uptake of the various molecules reported in literature, which is instead attributed to extracellular pathways[33,81,82]. It may therefore have limited relevance in acute nasal delivery applications.

1.4.3 Extracellular Transport

Extracellular pathways from the nose to the brain are presently believed to play the most significant role in rapid and direct transport of molecules into the CNS[33]. They primarily involve bulk flow by extracellular diffusion or convection in perineural or perivascular spaces associated with nerve bundles or blood vessels passing through the cribriform plate to the olfactory bulbs or the anterior lacerated foramen to the brainstem[33]. The perineural spaces surrounding the olfactory and trigeminal nerves appear to allow transport of some molecules into the subarachnoid space[82,88]. It has been suggested that this may be facilitated by the

propulsion of molecules by structural changes occurring during depolarisation and propagation of action potentials in adjacent axons in the fila olfactoria[82,89]. Similarly, between the outermost layer of blood vessels and the basement membrane of surrounding tissue exist perivascular spaces, through which bulk flow is thought to be facilitated by arterial pulsations. Interestingly, it has been suggested that if molecules can exploit such a pathway to travel into the CNS, movement deeper into the brain via a cerebral perivascular network or CSF flow pathways could result in rapid and widespread distribution[33,86,90].

Lochhead and Thorne[33] proposed that in order to exploit bulk flow pathways, a molecule would need to reach the lamina propria (e.g. via paracellular transport) and escape absorption into blood vessels and drainage into lymphatic vessels. However, they also noted the interesting possibility that molecules might be able to move more easily into such bulk flow pathways on the basis that olfactory neurons are constantly regenerating (about every three to four weeks[82]) and olfactory ensheathing cells maintain continuous open spaces for the regrowth of new fibres during this process. It should be noted that the key role of perivascular and perineural channels is to drain neuronal waste from interstitial fluid, so net flow is believed to be away from the CNS[82]. However, it has been proposed that flow could be bidirectional depending on such factors as posture and local vessel architecture[33,86] and the existing literature would seem to agree, given the data suggesting intranasally administered molecules are able to rapidly move into the CNS via this route.

1.5 Animal Models for Intranasal Delivery

The rat is the most commonly used model for studying direct nose-to-brain delivery routes[91]. Rats have a similar nasal epithelium, submucosa and olfactory sensation network to humans[34,79,92], and are a relatively cost-effective and easy-to-handle model[92]. They do, however, exhibit some important anatomical and physiological differences which must be kept in mind when considering the potential for extrapolation of experimental results to humans. These parameters have been reviewed by others[82,84,92] and are presented in Table 1.1, but the two most significant, in this author's opinion, will be briefly discussed below for the purposes of this review.

Most commonly referenced is the relatively small proportion of the total nasal epithelium that constitutes the olfactory region in humans compared to rats. This may be expected to have a large impact on the percentage of drug transport via direct olfactory pathways (as opposed to respiratory epithelium-associated systemic pathways) between rats and humans. Selective deposition of drug on the olfactory epithelium may act as the first step towards addressing this issue, but the actual surface area available for absorption and the size of the olfactory bulbs that drug may be transported to must also be considered. On an absolute scale, the olfactory bulbs of humans are larger than those of rats[93]. Traditionally quoted values of olfactory epithelium surface area in humans (e.g. 5 cm^2 vs 6.75 cm^2 in rats)[84,94] have therefore implied that a higher percentage of drug delivery might be required from a smaller olfactory surface area to achieve comparable olfactory bulb concentrations. More recent reviews, however, have suggested that the olfactory epithelium of humans constitutes a larger area (e.g. 12.5 cm^2)[21,33,94], which puts the absolute surface area at almost double that of rats and favours the theoretical translatability of drug delivery through this region, should it be convincingly demonstrated in a rat model.

The second important factor to consider concerns cerebrospinal fluid (CSF). As indicated earlier, current literature suggests that the most rapid and significant direct route from the nose to the brain may be in the CSF through perineural or perivascular channels. Given that the volume of CSF in humans is much greater than that of rats[84], a drug may undergo significant dilution if it is widely dispersed by this pathway in the brain, suggesting that brain concentrations detected in rat models may significantly overestimate those which would be expected in humans. In saying that, drug in the CSF would be expected to come into contact with the olfactory bulbs first, and preferential transport (e.g. diffusion) into the parenchyma here due to the high concentration gradient may still permit a sufficient targeted delivery.

Furthermore, CSF turnover rate of rats (hourly) is higher than in humans (5 hourly)[84], suggesting that if drug reaches the brain via the CSF in humans, it would have a longer period to cross into the parenchyma than in the rat.

Table 1.1. Comparison between key aspects of the rat and human nasal passages. Based on Kapoor et al.[21], Lochhead & Thorne[33] and Illum[84,92] with reference to a 70 kg human and a 250 g rat.

	Human	**Rat**
Nasal cavity volume	25 cm^3	0.26-0.4 cm^3
Nasal cavity surface area	150-160 cm^2	13.4-14 cm^2
Surface area per unit volume	6.4	51.5
Olfactory epithelium area (area, %)	12.5 cm^2 , 8%	6.75 cm^2 , 50%
CSF volume	160 mL	150 µL
CSF volume replacement frequency	5 hourly	Hourly
Shape of upper airways	L-shaped	Linear
Type of breathing at rest	Oronasal	Obligate nose
Connection between nasal cavity and oral cavity	No (incisive canal is not patent)	Yes (nasopalatine canal is patent)
Vascular swell bodies in septum	No	Yes
Turbinates (number and shape)	3; comma shaped	3; t-shaped with elaborate scrolls
Presence of ethmoid sinuses (air cells) and spheroid sinuses	Yes	No
Maxillary sinuses	Large; open	Small; closed
Nasal secretion movement	Mostly posteriorly (to nasopharynx)	Mostly anteriorly (towards nostril)
Inspiratory airflow route	Close to floor of nasal passage	Upward and laterally

1.6 Animals as Seizure and Epilepsy Models for the Evaluation of Anti-Seizure Therapeutics

1.6.1 Overview of Key Models

In order to screen for antiseizure activity of a compound, simple, high throughput models are preferred to avoid investing extensive time and resources in inactive compounds[6]. Many models of seizures and epilepsy have been described (Figure 1.5A)[14,95], however, the problem with most is that they haven't been clinically validated[95], i.e. shown the ability to correctly predict the effectiveness of a drug in humans. Traditionally, the Anticonvulsant Screening Programme (ASP), recently rebranded the Epilepsy Therapy Screening Programme (ETSP), has used the Maximal Electroshock Seizure (MES) test and the s.c. pentylenetetrazole (PTZ) test for this purpose, due to their simplicity and good predictive value for clinical efficacy in humans[14] (Figure 1.5B). Another simple test, the 6-Hz test, has made its way into the acute screening protocol in more recent times in an attempt to identify therapies that may be effective against "drug-resistant" seizures. Kindling has also been used as a validated chronic model to secondarily differentiate effectiveness in partial epilepsy.

A

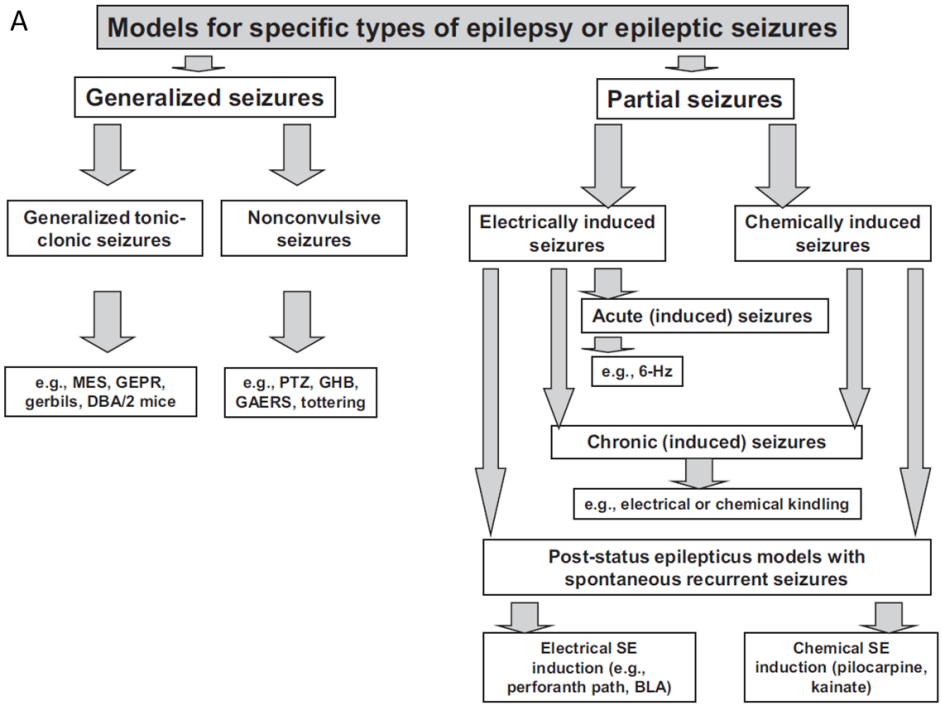

B

Drug	Anticonvulsant effect in rodent models			Clinical efficacy (seizure suppression)		
	MES (mice/rats)	s.c. PTZ (mice/rats)	Amygdala kindling (rats, focal seizures)	Partial seizures	Generalised seizures	
					Convulsive	Non-convulsive
Predominant Na^+ (and Ca^{2+}) channel activity						
Phenytoin	+	NE	+	+	+	NE
Carbamazepine	+	NE	+	+	+	NE
Oxcarbazepine	+	NE	+	+	+	NE
Lamotrigine	+	±	+	+	+	+
Zonisamide	+	±	+	+	+	+
Predominant Ca^{2+} channel activity						
Ethosuximide	NE	+	NE	NE	NE	+
GABA systems						
Benzodiazepines	+	+	+	+	+	+
Vigabatrin	NE	+	+	+	+	NE
Tiagabine	NE	+	+	+	+	NE
Mixed						
Valproate	+	+	+	+	+	+
Felbamate	+	+	+	+	+	+
Topiramate	+	NE	+	+	+	+
Phenobarbital	+	+	+	+	+	±
Novel targets						
Gabapentin	±	±	+	+	+	NE
Pregabalin	+	NE	+	+	+	NE
Levetiracetam	NE	NE	+	+	+	±
Lacosamide	+	NE	+			
Retigabine	+	+	+			

Figure 1.5. General classification of seizure models (A) and pharmacological profiles of clinically validated models (B). Figures adapted with permission from Löscher.[14] MES = Maximal electroshock seizure test; s.c. PTZ = subcutaneous pentylenetetrazole test; NE = no effect; 6-Hz = 6-Hertz test; SE = Status epilepticus; BLA = basolateral amygdala; GAERS = genetic absence epilepsy rat from Strasbourg; GEPR = genetic epilepsy prone rat.

For any seizure experiment, it is essential to consider the hypothesis that is being tested when selecting a model[95]. In the context of this review, it is the hypothesis that intranasal delivery of anti-seizure therapeutics will elicit anti-seizure effects by way of one or more of the pathways discussed earlier. Therefore, as the most validated and commonly used models of primary ASD testing, the above-mentioned four models (as well as a variation of MES, the MEST) will be described below, followed by a discussion of their usefulness in the context of assessing intranasal therapies.

1.6.1.1 Maximal Electroshock Seizure Test

The Maximal Electroshock Seizure (MES) test was the first model to be used to systematically screen compounds for anti-seizure efficacy, leading to the discovery of phenytoin in 1937[96]. The test is considered to be a measure of the effect of a drug to prevent seizure spread through neural tissue and thereby prevent generalised tonic-clonic seizures[95]. The classic procedure entails the application of a suprathreshold electrical stimulus to mice (50 mA) or rats (150 mA) using a constant current stimulator with a sinusoidal alternating current waveform for 0.2 seconds at a frequency of 50-60 Hz[95,97]. The endpoint is usually tonic hind limb extension (HLE), the most severe seizure behaviour resulting from this type of stimulation (Figure 1.6). Naïve animals are pre-tested to ensure they exhibit this behaviour and failure to demonstrate tonic HLE on a subsequent stimulation after treatment implies anti-seizure drug action. The stimulus is most commonly applied through corneal electrodes, but auricular electrodes may also be used. While initially thought to be equivalent, studies have shown differences in the characteristics of seizures elicited by each of these mechanisms (Figure 1.7). For instance, transauricular seizures have been shown to more reliably produce tonic HLE at maximal currents, as well as to decrease latency to, and increase duration of, HLE[98,99].

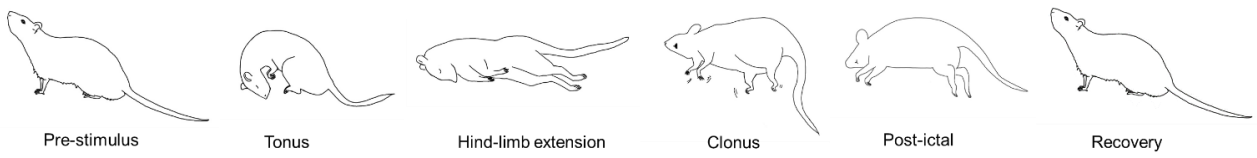

Figure 1.6. Typical stages of MES seizures (adapted from unknown source).

It is a simple procedure in that the outcome is binary and the suprathreshold nature of the stimulus reduces variability in response, but it does run the risk of failing to detect more subtle

anti-seizure effects, such as is the case for primidone and clonazepam, which are known to be clinically effective in humans, but which produce a negative result[99]. For this reason, we will also consider a slightly more technical, but more sensitive variation of this test, the Maximal Electroshock Seizure Threshold (MEST) test which, although not a conventional model used by the ETSP, will be discussed next due to its ability to detect effects on seizure threshold.

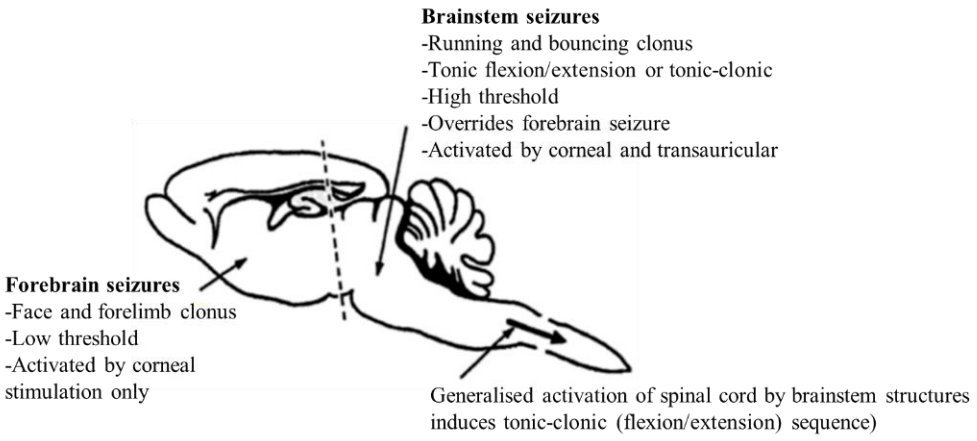

Figure 1.7. Characteristics of brainstem and forebrain seizures. Figure reprinted with permission from Peterson & Albertson.[97]

1.6.1.2 Maximal Electroshock Seizure Threshold Test

In contrast to the MES test, the MEST test is considered to be a measure of the effect of a compound on anticonvulsant threshold, rather than spread and is therefore more sensitive to detect anti-seizure hits. For example, as mentioned above, primidone and clonazepam do not show anticonvulsant activity in MES, however a dose-dependent anticonvulsant effect is detected by MEST, which translates to humans[99].

The aim of this test is to determine the current that elicits tonic hind limb extension in 50% of a group of animals (i.e. CC_{50} - the convulsive current in 50% of rats)[99]. This is most commonly determined using the "up and down" method of Kimball et al.[15,99,100] which involves stimulation of a group of animals in series, where the current used for stimulation of a given animal depends on the response of the preceding animal. If the preceding animal displays tonic HLE after stimulation, the current for stimulation of the next animal is lowered, usually by 0.06 log units

in rats and 0.01 log units in mice[99]. If the preceding animal did not display HLE, the stimulation current is elevated by the same log interval. The current used for the first animal is determined by the researcher, but must approximate the CC_{50} of the group[100], which can pose some technical difficulty with the use of this model. The complete data set of responses is used to calculate the CC_{50} for the group. One advantage of this model is that animals can be subjected to multiple stimulations as threshold does not significantly change provided at least 48 hours is left between sessions[101]. In this way, control and treated thresholds can be assessed in the same group of animals to lessen variability. In contrast to MES, this test will also yield information on proconvulsant effects if these are present[101].

The lower stimulation currents employed in this test result in a wider range of responses depending on the brain regions activated (Table 1.2). This is turn leads to more pronounced differences becoming evident between transcorneal and transauricular stimulation, the most obvious being the clonic phase. With corneal stimulation, facial (vibrissae, jaw and ears) and forelimb clonus can be observed, while with transauricular, a behaviour referred to as "running-bouncing" clonus is seen[102], which has parallels to the behaviour seen in audiogenic seizures induced in genetically-susceptible rats[97,103] and involves a more symmetrical clonus in all four limbs interspersed with periods of running and possibly bouncing due to jerks of the hindlimbs. The mechanisms behind these behaviours can be linked to the pathways of seizure propagation in each (Table 1.2); simply, a seizure initiated in the forebrain through the corneas, compared to one initiated in the hindbrain by way of the ears. Ultimately, both types of seizure must engage the brainstem to elicit the tonic HLE component of maximal seizures, but the corneally-induced seizure must spread further to get there and has been proposed to better represent seizure spread and better detect drugs which block this[99]. In support of this, phenobarbital and primidone demonstrate lower potency in auricular compared to corneal MEST testing[99]. It has also been found, however, that seizure threshold determined by transauricular stimulation is lower and less variable than thresholds determined by transcorneal stimulation, consistent with the more severe seizures and more consistent induction of seizures performed in MES, which possibly supports increased reliability of the model using this stimulation route.

Table 1.2. Seizure behaviours observed in the MEST model with varying current intensity and relevant regions of brain activation. Table reprinted with permission from Peterson & Albertson.[97] Note: The currents indicated are approximate only and may vary greatly between laboratories.

Response to corneal electroshock	Alternative names	Stimulus current (mA)		Quantified convulsion components	Brain region activated
		Rats	Mice		
Subconvulsive response	Stun, rage	<18	<5	No convulsive response	No epileptiform activity
Face and forelimb clonus	Minimal clonic seizure, minimal electroshock	18-20	5	Amygdala kindling scale, clonic spasm	Forebrain, limbic seizures
Running-bouncing	Wild running	20-21	10	Occurrence of running episode	Minimal activation of brainstem
Tonic flexion	Flexion, opisthotonus	20-21	10	Occurrence of tonic flexion	Minimal activation of brainstem
Threshold tonic-clonic	Threshold tonic extension, threshold for maximal seizures (MEST)	22-50	12-30	Occurrence of tonic hindlimb extension, duration of tonic extension, flexion/extension (F/E) ratio (maximal)	Submaximal activation of brainstem
Maximal tonic-clonic	Maximal electroshock (MES)	150	50	Occurrence of tonic hindlimb extension, duration of tonic extension, F/E ratio (minimal)	Maximal activation of brainstem

Despite the potential usefulness of the MEST test in more sensitively screening for antiseizure (or proseizure) effects[99], it has not been adapted by the ETSP. This is most likely due to a combination of reasons which make it more technically complex and variable and therefore decrease throughput and increase cost. Aside from these drawbacks, the other major limitation is that it gives no insight into the mechanism of action of the compound – i.e. whether it elevates threshold or prevents seizure spread or both[104]. Ethosuximide, phenytoin and valproic acid have been used as key drugs to illustrate this concept previously in that valproic acid (which increases seizure threshold and prevents spread) is active in MES (seizure spread measure), MEST

(maximal threshold measure) and PTZ (minimal threshold measure) tests, while phenytoin (prevents seizure spread) is active in MES and MEST and ethosuximide (increases minimal threshold) is only active against PTZ[104]. This supported the use of the MES and PTZ models for routine evaluation of potential ASDs, as they could distinguish potential usefulness against different types of seizures. It does not however, underscore the use of the MEST test in basic research which clearly still has value. It is worth noting in this respect that minimal threshold seizures may also be induced with electroshock, thereby overcoming some of the limitations that will be discussed next with the PTZ model, but the endpoint of the minimal electroshock seizure threshold test (min-EST) has been reported to be highly variable and therefore not suitable for routine evaluation of ASDs[104].

1.6.1.3 Pentylenetetrazole Test

For years, the s.c. PTZ test has been used as a first line screening model by the ASP in order to detect drugs that block generalised non-convulsive seizures, such as absence and myoclonic seizures, which are not detected by the MES test (e.g. ethosuximide). It has recently been demoted to the end of the screening pipeline in the revitalised ETSP where a failure marks a drug with a cautionary red flag, but does not necessarily halt development[6]. This change is the result of its clinical predictive ability being questioned after failing to correctly predict the effect of lamotrigine and levetiracetam in suppression of absence seizures and giving false positive data for vigabatrin and tiagabine[95]. This is possibly a result of its predictive value being restricted to certain chemical categories of compounds – i.e. those acting on GABA pathways – as PTZ elicits its actions by antagonism of the $GABA_A$ receptor[105].

The aim of this test has classically been to find the convulsive dose of subcutaneously injected PTZ inducing a clonic threshold seizure of at least five seconds duration in 97% of animals (CD_{97}) by observing animals for a post-injection period of 30 minutes for such a "threshold" seizure, after which they are euthanased[95]. Part of the problem with the PTZ test has most likely been its dependence on pharmacological actions to produce acute seizure behaviours. This requires consideration of route, doses, metabolism, time of measurement and pharmacokinetics and pharmacodynamics of the test drug, as well as interspecies variation in all these things and has led to conflicting data for some drugs between labs, a subject which has been discussed in detail elsewhere[105]. Traditionally, it has been an s.c. injection, but i.v. administration has been suggested as an alternative to overcome some of the limitations associated with PTZ delivery by the s.c. (or even the i.p.) route. Key issues with the model include interspecies variation in

metabolism of PTZ and use of the model for the analysis of drugs with a short duration of action that peaks early in the 30 minute observation period and has necessitated the use of 'time to seizure onset' as the measure of effectiveness in a lot of studies[105]. Time to the first threshold seizure (after s.c. injection) or initial myoclonic twitch (during i.v. infusion) therefore appear to be the most reliable endpoints to differentiate ASDs[105]. Being a threshold test, seizure behaviour as a whole may also be assessed, in order to provide a more sensitive measure of anti-seizure effect and enrich the prediction of possible clinical potency against different seizure types[105]. Finally, U-shaped dose curves have been reported to contribute to variability with some drugs (e.g. phenytoin and carbamazepine) due to possible proconvulsant effects induced at high doses in rodents and humans, so testing at a single high dose is not recommended

1.6.1.4 6-Hz "Psychomotor" Seizure Test

The 6-Hz test was first developed in the 1950s, but at the time was largely disregarded due to a lack of response to phenytoin, which was interpreted as a poor utility to predict efficacy in humans[106]. More recent times have seen its resurrection[107,108] and ultimately elevation to the ETSP testing pathway as an acute model of "drug-resistant" partial seizures[6]. This ascension has for the most part stemmed from two things; (1) the ineffectiveness and therefore "resistance" of this model to phenytoin and other commonly used ASDs[107,109] (Table 1.3) and (2) the remarkable effectiveness of levetiracetam against the 6-Hz seizure, which correlates with clinical activity in human refractory partial epilepsies[110], while it is ineffective in the traditional screening tests, MES and s.c. PTZ[111,112].

Table 1.3. Pharmacological characterisation of the 6-Hz seizure model in mice. Adapted with permission from Potschka.[109] R = Resistant; S = Sensitive, efficacy demonstrated; ? = Unknown.

ASD	**6-Hz**	
	32 mA	**44 mA**
Carbamazepine	R	R
Phenytoin	R	R
Valproate	S	S
Ethosuximide	S	R
Lamotrigine	R	R
Topiramate	R	R
Felbamate	S	R
Tiagabine	S	R
Levetiracetam	S	S
Lacosamide	S	?
Retigabine	S	S

The endpoint of the test, the 6-Hz seizure, is described as immobility or stun, awkward but upright posture, Straub (elevated) tail, facial automatisms (head nodding, jaw movement, twitching of the vibrissae) and forelimb clonus[107,113,114]. It is induced by means of corneal electrodes, through which a rectangular pulse train with a frequency of 6 Hz and pulse width of 0.2 ms is passed for 3 seconds[107]. Two currents are conventionally used, 32 mA and 44 mA, corresponding to the 1.5 x CC_{97} (current at which 97% of animals demonstrate the endpoint) and 2 x CC_{97} reported by Barton et al. in their characterisation of the model[107]. At 44 mA, only two ASDs, levetiracetam and valproic acid, completely protected against the 6-Hz seizure, however, their efficacy was reduced compared to 32 mA stimulation[107].

The proposed partial nature of the seizures has been supported by immunohistochemistry of c-fos expression as a marker of seizure-induced neuronal activation. Barton et al.[107] showed an intense c-fos staining to be induced by the 32 mA stimulus, which was localised to the amygdala and piriform cortex. Increasing to 44 mA, resulted in additional intense staining of the dentate gyrus, the recruitment of which was a hypothesised cause for the decrease in potency of ASDs at 44 mA, leading them to suggest that levetiracetam may exert its major effects via the amygdala, supporting its effectiveness in the kindling model of partial epilepsy[115]. They proposed that a lack of recruitment of the hippocampus (specifically, the dentate gyrus) at 32 mA suggests a different pattern of limbic seizure activation compared with MES and PTZ.

As stated earlier, the most unique purported feature of the 6-Hz test was being the "only acute electrically-induced seizure model in which levetiracetam was effective"[108], however this was not entirely true. Despite criticisms of the MES test for failing to respond to levetiracetam, it should be noted that levetiracetam has been reported to show similar effectiveness to valproic acid in the corneal MEST test[111]. Furthermore, it is also interesting to consider that behaviour in the minimal electroshock seizure threshold test (min-EST) mentioned earlier presents similarly to the 6-Hz seizure and is also, per se, "resistant" to phenytoin and any other ASD that affects seizure spread, but not minimal threshold[104]. Nonetheless, the 6-Hz test clearly has some technical advantages over MEST (or min-EST) as an acute seizure screening test which have propagated its use; these being the suprathreshold, one fits all, nature of its stimulation currents and the relatively large difference in current required to elicit a simple stun versus a clonic or tonic seizure response, providing clearer and less variable outcomes[114]. Furthermore, the relatively very short pulse width and reduced frequency of the electrical stimulus may be expected to decrease the volume of directly stimulated neural tissue[116] causing perhaps a much more focal discharge than min-EST or MEST, which is consistent with data reported above.

The 6-Hz model had previously only been characterised in mice[107,108], however, its very recent pharmacological characterisation in rats[113] stands to expand its potential scope as an acute screening model for activity in "drug resistant" seizures. Metcalf et al.[113] concluded that the 6-Hz test could be conducted in rats in a similar way to mice, but did find some differences between the two species. Interestingly, they found phenytoin to be effective in their CF-1 mice and suggested that either genetics or a different time point of testing after drug administration may have contributed to this finding. In contrast, they found rats to be resistant to phenytoin, as well as a number of other compounds, while response to levetiracetam was maintained. They speculated that different toxicity assessments between species (as efficacy is determined on the basis of the ratio between effective and toxic doses) or different pharmacological profiles of some compounds between species may at least partially explain their results. They also noted the possibility that 6-Hz may induce a different pattern of neuronal or brain-region activation in rats, which could explain the apparently more widespread lower sensitivity to drugs spanning different mechanisms (i.e. compounds acting on sodium channels, $GABA_A$ receptors or GABA uptake in comparison to the mouse 6-Hz model), possibly implying a greater usefulness in detecting compounds with novel mechanisms compared to the mouse. They noted that a significant limitation of the key studies that have pharmacologically characterised the 6-Hz model to date, including their one, is that they did not quantify blood or brain drug concentrations in their animals, so pharmacokinetic variability or inaccurate dosing was not accounted for. This factor was addressed by Leclercq and Kaminski[117] in a study of phenytoin and levetiracetam with different mouse strains, from which they concluded that pharmacokinetics could not explain the differences in drug responses seen (e.g. Naval Medical Research Institute (NMRI) mice are not resistant to phenytoin and are more responsive to levetiracetam than other strains), so genetic differences were the most likely cause. It should be noted that they used 'duration of immobility' as their endpoint, which appears to differ from previous studies employing 6-Hz. It is also unclear whether their findings would also apply to rats, given that the use of a different species is a much bigger genetic leap.

So while the 6-Hz test is a relatively simple model of great interest for the modern screening of compounds for activity in pharmacoresistant epilepsy, the model would seem to require further characterisation and possibly development to realise its full potential. It should be noted that demonstration of the efficacy of levetiracetam in the 6-Hz model was performed retrospectively and despite currently being used by the ETSP to differentiate compounds, it has also yet to demonstrate clinical translatability. For example, several investigational ASDs (brivaracetam,

carisbmate and retigabine) have potently suppressed 6-Hz seizures at 44 mA, but have not shown evidence of effectiveness in humans with drug-resistant partial seizures[118].

1.6.1.5 Kindling

Kindling traditionally involves repeated excitatory electrical stimuli via a depth electrode surgically implanted into a region of the limbic system (for example, the amygdala, which will be discussed in this review given its relevance to temporal lobe epilepsy). This is used to induce partial, and later secondarily generalised, seizures that increase in length and severity with continued stimulations, ultimately creating an animal with a permanently increased susceptibility to seizures. Seizure severity is classified according to the Racine scale (Table 1.4).

Table 1.4. The Racine scale of the stages of seizure behaviour. Adapted from Töllner et al.[119] and Racine.[120]

Stage	Behaviour
1	Immobility, slight facial clonus (eye closure, twitching of vibrissae, sniffing)
2	Head nodding associated with more severe facial clonus
3	Clonus of one forelimb
4	Rearing, often accompanied by bilateral forelimb clonus
5	Tonic-clonic seizure accompanied by loss of balance and falling

Initially, the threshold for inducing after discharges (the after-discharge threshold (ADT)) is determined by a stepwise procedure, then constant current stimulations are delivered once daily through the electrode until this induces reproducible (e.g. at least 10) fully kindled secondarily generalised seizures (i.e. Stage 5 on the Racine scale)[119]. The ADT is then determined again in the kindled animal on multiple occasions until this too is reproducible[119]. Recorded parameters include seizure severity, seizure duration, afterdischarge duration and generalised seizure threshold (where this differs from ADT), which are defined elsewhere[119]. The effect of treatments or other variables on kindling development can also be evaluated by comparing the number of days until the first stage 5 seizure, the number of days until the fully kindled state is reached, the cumulative seizure duration and the cumulative afterdischarge duration[119].

In contrast to models of acute seizures, kindling is a model of chronic epilepsy and therefore is thought to represent the epileptic brain much better when testing antiseizure interventions[95]. The changes that occur in the brain as a result of limbic kindling have been linked to those which occur in human temporal lobe epilepsy[121] and it is the only model that has successfully predicted (i.e. not retrospectively) the clinical usefulness of novel ASDs, such as levetiracetam, against partial seizures in humans with epilepsy[14]. Furthermore, models of pharmacological resistance have been developed from it[119,122,123], such as the phenytoin-resistant rat, which provide scope for assessing the ability of new treatments to overcome certain mechanisms of resistance (e.g. the multi-drug transporter (MDT) hypothesis)[124]. Despite its usefulness, limbic kindling is a very labour-intensive and time consuming process, making it unsuitable as an initial screening model. Potential replacements (e.g. corneal kindling), however, have so far been unsuccessful as their predictive ability is not clear[14,95].

1.6.2 Relevance to the Evaluation of Intranasal Delivery Pathways

As discussed earlier, there are three main pathways that intranasal therapeutics are thought to be able to exploit in order to reach the brain; the direct olfactory, direct trigeminal and indirect systemic pathways. Based on previous reports and theoretical considerations, these may target drugs to the olfactory bulbs and piriform cortex, the brainstem, or the whole brain via blood vessels, respectively.

Considering the olfactory pathway first, an ideal model would exhibit focal seizures generated or propagating through the piriform cortex or closely associated areas, such as the amygdala. The most obvious therefore would be the very well-characterised amygdala kindling model of epilepsy in which seizures secondarily generalise from this region. Though the nose-to-brain field is still, as Kozlovskaya[91] puts it, immature, perhaps the most well thought out publications (in terms of marrying hypothesis to method selection) in the current intranasal ASD delivery literature[21,22] have employed this technique somewhat successfully, as will be discussed in the next section. In contrast, a model described above which does not appear to have been used before, but reportedly represents acute focal seizures in the relevant regions[107] is the 6-Hz seizure test. As discussed, while it appears to still be a model in need of more reproducible and thorough characterisation, its recent expansion to the rat arena makes it an intriguing potential platform for assessment of olfactory delivery, particularly in light of its technical simplicity relative to the kindling model.

In the MES model of generalised seizures, the olfactory targeting pathway would seem to have minimal relevance, given that it functions in the forebrain, whereas it has been shown, by way of precollicular lesions, that the tonic components of corneal MES seizures do not depend on the forebrain for their initiation or progression[102]. In further support of this, the "area tempestas" (part of the piriform cortex that is very sensitive to induction of seizures by GABA antagonists and is thought to function as a broadcasting system by triggering generalised seizures in response to stimulation of limbic circuits) cannot exert control over tonic seizures induced by corneal MES, again supporting that generation of these seizures does not depend on the forebrain[125]. Therefore, any selective forebrain delivery of drug to areas like the piriform cortex would be expected to be ineffective in stopping the spread of corneal MES seizures, however a potential effect on the clonic components, despite not being the endpoint of this test, cannot be ruled out. As MEST similarly uses tonic endpoints, it would also likely be of little use. Minimal electroshock threshold could be considered, but is not a preferred test for reasons discussed above. Likewise, one might also consider the use of minimal seizures observed in the PTZ model, but given its systemic, pharmacological nature, it would be expected to have widespread effects throughout the brain, suggesting that it would lack the specificity required to assess intranasal delivery in targeting a focus and the spread of seizure activity. Transauricular MES (and MEST) seizures would seem to have even less involvement than transcorneal MES with the forebrain and given that lesions of the amygdala have no effect on transauricular electroshock seizures (or tonic audiogenic seizures for that matter)[125], a drug effect targeted to this region is unlikely to be detected by this model. A clonic phase is reportedly not reliably seen after the tonic phase resulting from transauricular stimulation[97], so may not be a suitable alternative for assessment. Despite the predicted failure of this test to model olfactory pathway delivery to the limbic regions, its role in detecting trigeminal pathway delivery to the brainstem would seem a lot more promising, as will be discussed shortly.

In order to speculate about the possible effects of inhibitory drugs being focally delivered to olfactory networks, it is interesting to consider a study which reported the effects of olfactory bulb ablation in mice on response to seizure tests[126]. In corneal MES, olfactory bulb ablation was reported to decrease the duration of clonic convulsions and postictal coma, however, it did not affect the tonic component, which is consistent with the above discussion. In contrast to the predictions above, they found a marked increase in corneal electroshock seizure threshold after ablation of the olfactory bulbs. It should be noted that although the authors reported using a minimal electroshock threshold test (defined by Swinyard[114] as clonic activity of the vibrissae, lower jaw, or forelimbs, without loss of posture), they seem to have classified a "minimal full

seizure" as including running movements, clonic convulsion, tonic flexion and tonic extension. This would suggest that their measure was closer to the definition of the threshold for a maximal electroshock seizure, although it was not specified whether the flexion and extension involved the hindlimbs. The CC_{50} reported for their controls, is similar to the maximal electroshock seizure threshold reported elsewhere for CF-1 mice (8.85 mA)[104], which suggests this was the likely measure reported. Finally, in the s.c. PTZ test, total incidence of convulsion was not different from control, but in contrast to the MES model, clonus was more marked and long-lasting in mice without olfactory bulbs, suggesting perhaps a decreased inhibition of seizures by the olfactory bulbs. Such a theory may be consistent with the ability of strong olfactory stimuli to interfere with kindled seizures[40], but introduces uncertainty as to the effect inhibitory ASDs would be expected to have in the PTZ model. To add to the complexity, tonic convulsion incidence was decreased, indicating an apparently opposite effect of olfactory bulb ablation on this component. Overall, the effects of olfactory bulb ablation are most definitely a lot more complex and far-reaching than might be expected from acute drug administration, but offer insight into the role of the olfactory networks in these seizure models.

The trigeminal pathway primarily offers a potential route from the respiratory mucosa through the rear of the brain via the brainstem and assessment of drug delivery by this route calls for a different approach from a model. As stated earlier, the MES and MEST tests present as the most obvious candidates, given their unquestionable relationship with the brainstem. Transauricular stimulation may possibly have advantages over transcorneal in that it would appear to generate seizures directly through the brainstem, rather than initially spreading through the frontal brain, providing a more specific assessment of focal drug delivery. Of note, it has been used in a few studies on this topic[127–129] which will be discussed in the next section. In this author's opinion, MEST presents itself as a more appropriate initial candidate for assessment of intranasal delivery to the brainstem in order to detect an effect on seizure threshold, rather than setting the benchmark as the ability to interfere with a superthreshold stimulus which runs the risk of masking more subtle information. Recalling the earlier discussion, the kindling and 6-Hz models would likely be of little use in assessing delivery by this pathway, while the PTZ model again may suffer from eliciting a pharmacological effect on the whole brain.

Finally, for assessment of drug delivery by a systemic pathway (or an alternative widespread brain delivery pathway, such as a direct transport in the CSF), any model may feasibly detect an anti-seizure effect of intranasally delivered drug. This will, however, be largely dependent on the usual ability of the model to detect a specific compound after systemic administration

(e.g. phenytoin is reported to be effective in MES, MEST and kindling, but generally not in the PTZ or 6-Hz models), as well as the dose of drug that is able to be delivered through the nose. In the context of the systemic circulation, this will be subject to the usual impeding factors (e.g. dilution, protein binding, metabolism, efflux transporters) and may mean that the relatively low doses attainable through the intranasal route could render them completely ineffective. Nonetheless, intranasal pharmaceutical studies with ASDs to date have generally reported a direct nose-to-brain delivery component co-existing with a significant systemic component, but still with some degree of anti-seizure efficacy where this was tested. The following section will discuss these studies and what can be learnt from them as a whole in order to move forward.

1.7 Pharmaceutical Formulation of Anti-Seizure Therapeutics

1.7.1 Role of Pharmaceutical Formulation

The potential advances that could come from exploiting a direct nose-to-brain delivery route to deliver anti-seizure therapeutics, as well as the essential role of pharmaceutical formulation in achieving this have been introduced thus far. The clearest advantage of this direct delivery would be the avoidance of the systemic circulation, at least prior to initial contact with the brain. The doses of ASDs required to achieve therapeutic plasma concentrations are much larger than the quantities of drug that are actually required in the brain[130,131], secondary to pharmacokinetic factors such as systemic metabolism, plasma protein-binding, clearance and widespread tissue distribution. A direct intranasal route may therefore allow the administration of much lower doses in order to increase tolerability, a modifiable contributor to the definition of drug-resistant epilepsy. Furthermore, while still speculative, a direct delivery by an olfactory pathway to seizure generating or propagating regions such as the piriform cortex, may also play a role in circumventing proposed mechanisms of resistance, such as inadequate drug levels reaching these regions due to overactive efflux transporters at the blood-brain barrier (BBB)[132,133]. Even in responsive epilepsy, such a pathway might conceivably be exploited as a means of controlling some types of focal epilepsy and not just reducing systemic exposure, but also exposure of unproblematic brain regions to the drug. To test all these exploratory visions, however, there are challenges to overcome, both in therapeutic formulation (reviewed elsewhere[21,22]) and the pre-clinical evaluation of the mechanisms by which direct nose-to-brain delivery may be an effective therapeutic tool. While research into the latter expands beyond

just anti-seizure treatment, the following section will be limited to discussing studies which explore this therapeutic use, in light of their relevance to this review and the PhD project it underlies.

1.7.2 Studies of Pharmaceutical Formulation for Anti-Seizure Therapeutic Delivery

Anti-seizure therapeutics have been formulated into a range of different pharmaceutical delivery systems to date in attempts to exploit a direct nose-to-brain delivery pathway (Table 1.5). The components of these formulations are listed for the reader's reference, given that administration vehicles can potentially confound the results of seizure tests[134], but the specific formulation methodology, ingredient rationale, stability and release properties fall outside the scope of this review. Instead it will discuss methodological aspects of in vivo testing of such formulations and what can be learnt from the imperfect endeavours to do so thus far. The discussion should be taken in the context of a recent review of intranasal pharmaceutical formulations in general that suggested that compounds reach the brain most efficiently by direct routes in the order of particles > gels > solutions, but in terms of total brain delivery, the order was gels > particles > solutions, suggesting a higher systemic contribution from gels[91]. It should be noted that they did not differentiate whether particles referred to nanoparticles, microparticles or both however, which is important as these systems, reviews of which can be found elsewhere[80,135,136], may act differently to deliver drugs.

Table 1.5. Summary of studies using pharmaceutical formulation to investigate a direct nose-to-brain pathway for ASDs.

ASD/therapeutic	Delivery system	Materials	Toxicity study	PK study	Efficacy study	
Carbamazepine	Gel	Carbopol 974P (mucoadhesive polymer, Hypromellose, pH 7.4	X	✓	X	[137]
Phenobarbital	Gel	Carbopol 974P (mucoadhesive polymer, Hypromellose, pH 9.5	X	✓	✓	[138]
Carbamazepine	Mucoadhesive o/w nanoemulgel	Oleic acid, Labrasol, xanthan gum (anionic mucoadhesive polymer)	X	X	✓	[139]
Carbamazepine	Thermo-reversible gel	Carbopol 974P (mucoadhesive polymer), Pluronic F127	X	✓	X	[140]
Lamotrigine	Thermo-reversible gel	Carbopol 974P (mucoadhesive polymer), Pluronic F127	X	✓	X	[141]
Carbamazepine	Microemulsion	Oleic acid, Tween 80, Propylene glycol	✓	X	✓	[129]
Carbamazepine	Microemulsion	Oleoyl polyoylglycerides, Polyoxyl 40 hydrogenated castor oil, Diethylene glycol monoethyl ether, Polycarbopil (mucoadhesive)	✓ (earlier paper[142])	✓	X	[143]
Lamotrigine	Microemulsion	Glyceryl monostearate, Oleic acid, Tween 80, Pluronic P188	X	✓	✓	[127]
Phenytoin	Microemulsion	Capmul MCM (glyceryl monocaprylate), Labrasol, PEG-8 caprylic/capric glycerides and Transcutol (diethylene glycol monoethyl ether)	✓	✓	✓	[128]
Diazepam	Polymeric nanoparticles	PLGA (Poly(D,L-lactide-co-glycolide), Pluronic F127	X	✓	X	[144]
Thyrotropin releasing hormone	Polymeric nanoparticles	PLA (Polylactide)	X	X	✓	[16,17]
Valproic acid	Lipid nanoparticles	Cetyl palmitate, soy lecithin, octyldodecanol	X	✓	✓	[145]
Lamotrigine	Microspheres (as suspension)	Chitosan, glutaraldehyde	✓	X	✓	[146]

1.7.2.1 Administration Technique

A number of techniques have been used for intranasal administration to rats over the years. Most studies have been carried out in anaesthetised rats in a supine position to facilitate deposition and retention on the olfactory epithelium, which comprises the upper third of the nasal cavity[82]. Most researchers position animals with their head horizontal to the bench to prevent drainage to the oesophagus and trachea when supine[82]. Historical techniques have involved cannulation of the trachea to aid breathing, then circulation of drug solution in the nasal cavity by a peristaltic pump under anaesthesia or alternatively, sealing the oesophagus with adhesive before administration (and possibly the nares after administration) of a small volume with a micropipette[92]. In contrast, more modern approaches involve administration of a small volume through the nares to the conscious or lightly sedated (e.g. halothane) rat[92]. This may be a single dose administered to one nostril via insertion of polyethylene (PE) tubing[147], or smaller aliquots gradually sniffed in over a period of time after placement on the nares[85]. The former offers the advantage of being able to direct the dose to the posterior nasal cavity where the olfactory epithelium lies, in contrast to the latter which will have significant initial contact with the respiratory epithelium and consequently be subject to rapid mucociliary clearance and higher systemic absorption. Tubing-mediated delivery may also be used simply to ensure adequate coverage of the nasal mucosa via a deep delivery point. In line with these advantages, Table 1.6 (at end of Chapter on page 49) shows that the majority of studies investigating intranasal delivery of ASD formulations employed a similar tubing administration method. Interestingly, Czapp et al.[138] reported alternating between delivery at the opening of the nares and tubing-mediated delivery into the deep nasal cavity, which may have had implications for their pharmacokinetic and efficacy results, which did not differentiate between the two administration techniques.

The volume of an administered dose may affect deposition within the nasal cavity and is a key challenge to the intranasal delivery of lipophilic therapeutics, such as most ASDs, in general. There is a balance between adequately covering the epithelia through which absorption is intended (olfactory and/or respiratory) and avoiding so large a volume that it overflows out of the nasal passage, causing a lower dose to be delivered and running the risk of deposition in the nasopharynx and subsequent inhalation causing respiratory distress in an experimental animal[82]. Rats generally receive a volume of 40-100 µL if given as a series of drops applied to the nares, whereas with administration to the posterior nasal passage via tubing, lower volumes of 20-40 µL are used, as there is less surface area to cover[82]. Considering this, the rationale for

the volumes used in a number of the studies in Table 1.6 is unclear given that doses were administered mostly via tubing, suggesting a targeted delivery to the upper nasal passage was desired. Rats commonly received between 100-200 µL of fluid in their nasal passages, with a mouse also receiving a 100 µL dose, suggesting that the nasal passages would have been saturated with formulation and inhalation or swallowing would have been extremely likely. Others, usually purely pharmacokinetic studies utilising mice or rats, used total volumes of 14-27 µL which are more in line with the above guidelines and may be more likely to detect direct olfactory delivery to the brain.

While light sedation is necessary to perform most intranasal administration procedures on rodents[82], it should be noted that anaesthesia (mainly long-acting anaesthesia) has been suggested to increase nasal absorption of therapeutics in rats, most likely due to impairment of mucociliary clearance and decreased losses due to drainage and mechanical removal (e.g. sneezing/snorting) in the conscious state[147]. For this reason, results may overestimate the true absorption that would be expected in a conscious animal. Nonetheless, such studies are still a valuable screening tool with which to assess nasal absorption of different therapeutics. Almost all of the studies in Table 1.6 utilised anaesthesia in the dose administration process. Two did not report either way, but considering the volumes administered, almost certainly would have required it, while another claimed to have administered a gel via tubing to conscious rats. In addition to the effect on anaesthesia on mucociliary clearance, efficacy studies of intranasal antiseizure therapeutics must also control for another potential confounder, the effect of anaesthetics on seizure threshold, which will return in the later discussion.

1.7.2.2 Adverse Effects and Toxicity

Intranasal delivery studies in general seem to give poor attention to adverse effects or toxicity of administered formulations to the nasal mucosa[148]. While this is an aspect that seems to be brushed over in preclinical trials, it is important to consider, especially in terms of exploiting a direct nose-to-brain pathway. Kozlovskaya et al[91] suggested that the fractions of drug reported to have been delivered to the brain intranasally in a number of studies were so substantial that they implied a breach of physiological barriers by formulation constituents (e.g. permeation enhancers and co-solvents). Furthermore, they speculated about the toxicity that could potentially result from chronic exposure of olfactory or trigeminal neurons to drugs or particles transported via intracellular routes. To consider adverse effects as a whole, one must evaluate both behavioural and histological aspects. While the former receives a lot of attention in human

trials[74], preclinical studies offer an excellent opportunity to screen histologically and optimise dosage and formulation, given the great similarities between rodent and human nasal epithelia[79] and the extensive guidelines on nasal tissue processing and evaluation[79,83,149,150]. Most of the studies reviewed in Table 1.5 did not report any data on either behavioural or histological adverse effects and those that did presented low quality images of sheep nasal mucosa exposed in vitro without any indication as to what type of epithelium or anatomical structures were shown[128,129,142,146]. Given that all studies performed in vivo experiments in rodents, be they pharmacokinetic, pharmacodynamic or both, there seems no reason why the nasal passages of those rats could not have been dissected after the experiment and histologically processed to provide a substantially more meaningful evaluation of epithelial integrity.

Behavioural assessment is also important in rodents as, aside from ethical considerations and determining how much formulation an animal can feasibly tolerate in its nasal passage, it may draw attention to a highly irritant formulation. It also has implications for follow on studies, such as evaluation of antiseizure effects, given that susceptibility to these might be altered by stress or pain secondary to a nasal administration. Therefore, this appears to be an area which deserves more attention in intranasal studies.

1.7.2.3 Quantification of Drug in Tissues

The efficiency of intranasal delivery is most adequately assessed by calculation of two parameters (Equation 1.1 and Equation 1.2)[91]. The first is Drug Targeting Efficiency percentage (%DTE), which is the relative exposure of the brain to the drug following IN and systemic administration. The second is the Nose-to-brain Direct Transport Percentage (%DTP) - the percentage of the dose that is estimated to reach the brain via direct routes compared with the overall delivery to the brain. A %DTE > 100% indicates better overall brain delivery via the intranasal route compared the parenteral route, while a %DTP > 0% indicates an increased efficiency of brain delivery by direct routes (e.g. olfactory and trigeminal pathways)[91].

Equation 1.1. Calculation of Drug Targeting Efficiency (%DTE). AUC_{brain} = AUC (concentration vs time) for brain; AUC_{blood} = AUC (concentration vs time) for blood.

$$\%\mathrm{DTE} = \frac{(\mathrm{AUC_{brain}}/\mathrm{AUC_{blood}})_{\mathrm{in}}}{(\mathrm{AUC_{brain}}/\mathrm{AUC_{blood}})_{\mathrm{iv}}} \cdot 100\%$$

Equation 1.2. Calculation of Direct Transport Percentage (%DTP).B_{IN} = Brain AUC over time after i.n. administration; B_{IV} = Brain AUC over time after i.v. administration; B_X = Brain AUC fraction contributed by systemic circulation through blood-brain barrier after i.n. administration; P_{in} = Blood AUC over time following i.n. administration; P_{iv} = Blood AUC over time following i.v. administration.

$$\%DTP = \frac{B_{in} - B_X}{B_{in}} \cdot 100\% \qquad B_X = \frac{B_{iv}}{P_{iv}} \cdot P_{in}$$

Calculation of these parameters is based on the following assumptions[91]:

- Drug pharmacokinetics are assumed to be linear (no saturation of individual absorption, distribution, metabolism or elimination processes).

- AUC_{brain} and AUC_{blood} are assumed to reflect pharmacologically relevant drug concentrations in the brain and blood despite (1) that drug can exist in several forms in these sites (e.g particle-based formulations may exist as free, protein-bound or encapsulated drug) and (2) differences in intra-brain disposition of the drug, as a result of reaching the brain via different routes. The latter, may obviously be remedied by microdissection of different brain regions and the former may possibly be addressed with analytical methods.

Kozlovskaya et al.[91] reviewed all nose-to-brain delivery studies available in February 2014 and found that only 3.1% contained the pharmacokinetic information required to calculate *in vivo* AUC of concentration vs time for both brain and systemic circulation after i.n. and parenteral routes respectively. They noted that drug was in most cases not completely eliminated at the last sampling point (8-24 hours), introducing error into drug exposure calculations derived from partial curves. With this is mind, we turn to the studies involving anti-seizure therapeutics that presented pharmacokinetic data, a number of which have been published since that time.

There have been some remarkable claims made about the intranasal delivery of anti-seizure therapeutics in recent years, but unfortunately the designs of the studies (Table 1.7, at end of Chapter on page 51) and the non-standardised reporting of results make the pharmacokinetic data difficult to interpret. Eskandari et al.[145] reported a brain:plasma ratio of around 8 for valproic acid delivered in intranasal lipid nanoparticles (4 mg/kg), compared to a ratio of less than one from an intraperitoneal control (150 mg/kg) at 60 minutes after administration. The different doses used, the single time point evaluation and the use of intraperitoneal

administration as a control impede assessment of contribution from the direct pathway that the authors claim was demonstrated in these results. Though it is likely that sustained release from the lipidic formulation and nasal absorption played a role in the differences seen, one may speculate that the control was disadvantaged at 60 minutes, considering that this time point equates to the lower limit of the half-life of valproic acid in rats[151] (Table 1.8). Acharya et al.[128] assessed an intranasally administered microemulsion containing phenytoin. They reported higher levels of phenytoin in the brain after the i.n. microemulsion compared to i.p. phenytoin solution at 15 and 30 minutes following administration. Again, this study suffered from an i.p control and insufficient time points to calculate any pharmacokinetic parameters. There was also no data provided on plasma concentrations. Alam et al.[127] also assessed a type of lipid nanoparticle, this time with lamotrigine. Once again, there was no i.v. (or even i.p) control and measurements were performed at only one time point, 24 hours after administration with the intent of demonstrating a sustained effect of drug delivered with the intranasal formulation. Plasma concentration was higher than brain concentration at this time. Two of these studies also employed intranasal solutions of their respective ASDs, which performed better than the systemic controls, suggesting that intranasal delivery of the free drug solution did occur, but that the formulations appeared to enhance drug delivery in some way, at least at the time point tested.

Two further studies assessed intranasal particle delivery in more detail, however still with setbacks. Patel et al.[143] studied an intranasal microemulsion containing carbamazepine both with and without a mucoadhesive agent to aid retention in the nasal passage. They studied time points from 30-480 minutes after administration and reported a carbamazepine %DTE of 241, 188 and 110 for their mucoadhesive microemulsion, microemulsion and carbamazepine solution respectively. Similarly, %DTP values were reported as 59, 47 and 9. The catch here was that the i.v. control values from which these values were calculated was based on i.v. administration of the microemulsion, rather than free drug solution which likely had significant effects on the pharmacokinetic profile. Evidence of this is implied in their supporting gamma scintigraphy images which to this author, suggest both an extravasation in the tail vein where they were injected and an extensive accumulation of the emulsion particles in the liver. Sharma et al[144] studied the delivery of diazepam with polymeric nanoparticles with reported mucoadhesive properties, also covering a time range of 30-480 minutes. They reported a %DTE of 258 for the i.n. nanoparticles and 125 for the i.n. drug solution, while %DTP values were 61.3 and 1. The i.n. nanoparticles resulted in brain levels higher than i.v. and i.n solutions from 30 minutes onwards. Despite this more encouraging indication of direct delivery, it should be

noted that both studies derived their "drug quantification" data indirectly from scintillation measurements of Technetium-99m in tissues, so the values do not unequivocally represent actual quantities of the drugs concerned.

The most extensive studies in this area have been reported with intranasal gels comprising the mucoadhesive polymer Carbopol 974P. Barakat et al.[137] began by testing such a gel loaded with carbamazepine over 5-120 minutes after administration. They reported a peak in i.n. concentrations in the brain at 5 minutes after administration (brain:plasma ratio of around 10), which significantly exceeded plasma concentrations for up to 20 minutes after administration. The i.v. control was administered at a 40 times higher dose (8 mg/kg vs 0.2 mg/kg), but brain levels did not peak until 20 minutes and maximum concentration (C_{max}) was 4.5 fold lower than i.n. Despite these intriguing results, an i.v. comparison with an equivalent dose to that administered i.n. would have been useful for direct comparison, especially considering that higher doses of carbamazepine can lead to induction of its own metabolism[152], which could have potential to alter the systemic pharmacokinetic profile. Czapp et al.[138] followed with a study of a gel containing phenobarbital, recording two types of pharmacokinetic data. The first was microdialysis in the frontal cortex extracellular space from 15-240 minutes. The gel provided a higher drug concentration in the dialysate than i.n. or i.v. control solutions, which was significantly different from 30 minutes onwards, but the plasma:dialysate ratio was not significantly different after this. The second method was the classic brain homogenisation from 2-240 minutes, although they microdissected and analysed different regions to provide more detailed information at 10 minutes. They found that whole brain concentrations rapidly increased during the first 10 minutes after gel administration, but so too did plasma concentrations. Ultimately, they found no difference in whole brain penetration rates between i.n. and i.v. administration. Upon microdissection at 10 minutes, however, they found the olfactory bulbs to have 3-fold higher concentration after i.n. gel administration. Concentrations in other brain regions, however, including those implicated in trigeminal nerve delivery routes (e.g. pons), remained similar or even decreased compared with i.v. Despite this, it is interesting to consider their finding of respiratory centre depression at high doses of the i.n. gel that was not seen after i.v. administration which might imply selective delivery to this area. However, brains of these animals were not analysed and they instead attributed this to increased toxic metabolites reaching the brain due to shorter systemic exposure.

More recently, Serraheiro et al.[140,141] investigated intranasal gels containing carbamazepine or lamotrigine administered to mice. They calculated the %DTE in both experiments to be 96%

and 98% respectively, which implied equivalent overall drug delivery to the brain by both i.n. and i.v. routes. Their concentration vs time plots for lamotrigine show the i.v. administration resulted in a shorter T_{max} (5 minutes vs 45 minutes) and greater C_{max} in the brain, however, upon microdissection into olfactory bulbs, frontal cortex and remaining brain, the i.n. profile revealed significant heterogeneity between the regions. In line with the observations of Czapp et al.[138], they observed markedly elevated concentrations (25 to 67 fold) in the olfactory bulbs at 5 and 10 min relative to the other brain regions. Importantly, this remained elevated above plasma levels, suggesting an alternative source of penetration. Concentrations in the rest of the brain appeared to steadily increase over the time period, but did not reach the magnitude of that seen in the olfactory bulbs. Had other regions of the brain been dissected and analysed separately, it may have revealed further differences, although the results of Czapp et al. would suggest otherwise[138]. In the case of carbamazepine, the results were not so profound. They claimed to have shown higher values in the olfactory bulbs and frontal cortex up to 15 minutes after administration, but unlike lamotrigine, these were barely above plasma levels and very similar to concentrations seen after intravenous administration. Given that these two experiments were performed by the same lab, it would suggest different behaviour of the drug molecule, perhaps highlighting different absorption routes and brain distribution patterns. While the study of Barakat et al.[137] discussed earlier would appear to contest this, the fact that it was performed in rats may suggest an interspecies difference. Alternatively, the differences may be an indication that, from a pharmaceutical perspective, one thermo-reversible gel does not fit all and the interactions of different therapeutics with a delivery system may significantly affect their *in vivo* performance.

From the above-discussed data, it is evident that the pharmacokinetics of intranasal anti-seizure therapeutics has a foundation, but there are clearly improvements and further discoveries to be made. Firstly, it is interesting to note that the claims of superior brain delivery from the particle-based studies are all based on the analysis of whole brains, rather than microdissected ones, which the gel studies insisted were required to identify significantly elevated concentrations compared to plasma. Whether this is because of the proposed benefit of particles over gels by Kozlovskaya et al.[91] or simply the methodological shortcomings of the particle studies is unclear and further, more comprehensive and objective, studies with these systems are clearly needed to begin answering these questions. Furthermore, routine pharmacokinetic analysis of different brain regions, particularly those of relevance to olfactory and trigeminal pathways (e.g. olfactory bulbs and brainstem) will further elucidate the roles of different pathways in nose-to-brain transport and how they might be best utilised to treat neurological diseases such

as epilepsy. Another factor to consider is the therapeutic relevance of the concentrations reported to reach the brain. While not detailed in this review, ASDs have been studied for many decades and a deeper literature search will reveal what is considered as a therapeutic brain concentration in a given animal model. Intranasal delivery systems that hope to be translated for human use one day for the delivery of existing ASDs would do well to consider whether the doses they are delivering via direct pathways are relevant to the treatment of seizures when reporting their results. However, in the case of heterogeneous delivery this may be difficult, so will require efficacy studies and validated positive controls, which they will ultimately encounter on the pathway to translation anyway. Finally, putting the direct-pathway-only mentality aside, a realist may speculate that if you can successfully exploit a direct nose-to-brain route through administration of a lower overall dose than is required systemically (i.e. achieve a %DTP above 0) and deliver sufficient therapeutic concentrations directly to key brain regions (e.g. olfactory bulbs), then perhaps it does not matter if some is absorbed systemically, provided that the systemic exposure is low enough that it will not have any significant adverse effects.

1.7.2.4 Qualitative Distribution in Tissue

To supplement (or replace in some cases) tissue quantification data, a few of the listed studies performed gamma scintigraphy using formulations labelled with Technetium-99m[127,128,143,144], which was reportedly associated with the drug. Acharya et al[128] provided images of rats after i.n phenytoin microemulsion and i.p phenytoin solution. They reported accumulation of i.v. phenytoin in the liver and spleen, while the i.n. microemulsion was associated with the brain and respiratory tract. Similarly, Patel et al[143] presented images after administration of i.v. microemulsion, i.n. microemulsion, i.n. mucodhesive microemulsion and i.n. carbamazepine solution. They claimed that brain distribution was higher with i.n. compared with i.v. administrations, particularly for the mucoadhesive formulation, but the image quality obscures the shape of the animal and possibly even exhibits different scales. Finally, Alam et al.[127] presented images of a rat at different time points after i.n. lipid nanoparticle administration describing an initial deposition in the nostrils which moves to the brain. They also noted a significant portion in the oesophagus and abdominal region. While this data complements their pharmacokinetic studies to an extent, it is very difficult to discern objectively where the drug is depositing, especially given that the brain sits directly above where the liquid formulation is initially deposited. In particular, this renders comparisons of relative i.v. and i.n. brain distribution rather useless.

Kubek et al.[16], on the other hand, used fluorescent illumination (exact procedure not specified) to examine the brains of animals after administration of polymeric nanoparticles containing Nile Red. This was necessary as due to the endogenous nature of their therapeutic molecule, TRH, the exogenously administered peptide could not be directly quantified and distinguished from the endogenous peptide in the brain tissue. Based on the Nile Red fluorescence, they claimed widespread distribution and sustained presence of nanoparticles within the brain for up to 96 hours, however, the control presented was a rat exposed to larger-sized nanoparticles at 24 hours, rather than Nile Red alone. Given that free Nile Red will emit a red wavelength on contact with polar membrane lipids[153] such as the extensive array found in the brain, the claim that this represented the presence of nanoparticles would seem unconvincing. Furthermore, they developed an immunohistochemistry assay to detect their nanoparticle polymer in the brain, but only showed a validation of the assay after intra-amygdala injection of the nanoparticles, rather than their detection in the brain of an intranasally-treated animal.

Thus, while qualitative data may provide a supplement to quantified drug distribution patterns, it would seem to be inadequate, at least in the ways it was used in the reviewed studies, to convincingly demonstrate the existence of a direct nose to brain pathway. The gamma-scintigraphy studies did, however, provide an interesting insight into distribution of the formulation into other body regions after the intranasal administration (e.g. possible swallowing or inhalation) indicating that the administration and volume could be optimised further. In saying that, it should be noted that the animals were anaesthetised so that they could be imaged, which likely changed the distribution compared to when they were conscious, especially in terms of clearance from the nasal cavity which may explain partially why the label appears to remain in the head area.

1.7.2.5 Efficacy

The other important consideration in any drug delivery study is demonstrating pharmacodynamic efficacy in an animal model. As discussed in the previous section, a number of clinically-predictive seizure models have been designed to provide a platform for high throughput and cost effective screening of anti-seizure therapeutics. In Table 1.5, it can be seen that the intranasal formulation literature to date has largely focused on the recapitulation of well-characterised anti-seizure drugs and this provides an advantage as far as efficacy testing is concerned in that it can be predicted which seizure models will be most useful for testing whether these molecules are reaching the brain in sufficient concentrations to elicit an effect.

The discussion in the previous section also highlights how it might be predicted, based on the theory of direct nose-to-brain pathways, which models may be most useful for detecting these specific effects from direct nasal delivery routes and thereby fit a model to the question.

Of the studies in Table 1.7, eight employed a seizure model. Most performed the Maximal Electroshock Seizure (MES) test or unvalidated variations thereof, while two performed a pentylenetetrazole (PTZ) test and two used an amygdala kindling model. Aside from the kindling studies, no rationale was provided for why a specific model or seizure endpoint was chosen. In most cases, the model chosen was at least relevant to the drug being tested, but in the case of carbamazepine and lamotrigine-based formulation testing in the PTZ model this is questionable[14]. While most reported anti-seizure effects, in a lot of cases this could not be reliably attributed to anything other than an enhancement of systemic absorption, especially in the cases where efficacy claims were not accompanied by pharmacokinetic data[129,139,146]. Furthermore, considering the lack of adverse effect and toxicity data provided, as discussed above, it is possible that damage to physiological barriers could have been a major contributor to any enhanced delivery. Nonetheless, like the pharmacokinetics data, and despite their limitations, they would seem to support the use of the nose as a rapid and sustained method of drug delivery.

The end points used were fairly standard in most studies, except in the case of MES variations, which in this author's opinion, were not justified. Assuming the reported values were not a typing error, Samia et al.[139] employed extremely lengthy stimulations and used stimulations until death as an endpoint, which would seem to have no scientific basis. Eskandari et al.[145] used parameters of 110 mA, 100 Hz, 1 ms pulse width and 0.2 s shock duration, validating their method with a seemingly excessive dose of i.p. phenytoin (90 mg/kg), on the basis that more than 50% of rats displayed extension when untreated, but none did when treated. Given that less than 100% of untreated rats displayed extension, it is unclear firstly how they used a decrease in extension:flexion ratio compared to control as an endpoint, secondly why they did not simply report it as flexion:extension ratio and furthermore, why the decrease in this parameter appeared to be almost as high as the drug-treated rats in those given blank nanoparticles. Although not commented on by the authors, this might suggest that the components of the formulation itself may have played a role in eliciting the apparent anti-seizure effects, as has been reported elsewhere[134]. Alternatively, it is also possible this may have been related to the anaesthesia (reported as 'light ether') used during administration that the untreated controls may not have received.

In fact, most studies who reported using anaesthesia did not comment on whether this was also applied to untreated controls to which efficacy data was compared or normalised to account for a potential confounding effect on seizure threshold[127,139,145,146]. For short-acting inhaled anaesthesia, this was likely less influential, but certainly with systemically-administered longer-acting anaesthetics, ketamine[154,155] and propofol[156], this may have been an important confounder in tests performed 60 minutes or less after administration. Czapp et al.[138], was an exception, in that they specifically stated that the administration of propofol alone in preliminary experiments did not affect kindling parameters and also administered anaesthesia to all i.v. controls. They did, however, require increased doses of propofol to administer increased doses of nasal gel (containing more phenobarbital) and considering the synergistic interaction previously reported between propofol and phenobarbital[157], it should be noted that this may have contributed somewhat to the significant anti-seizure effects noted at the higher, but not the lower, dose after i.n. administration.

The most commonly used time point for testing, regardless of the ASD studied, was 60 minutes. Given that a key aim of intranasal delivery is to exploit direct and rapid routes to the brain, which the pharmacokinetic data discussed in the previous section suggest the existence of, the rationale for the popularity of this time point was unclear. In some cases, such as that of Czapp et al.[138], where kindling parameters were measured 60 minutes after administration, it may have been related to the fact that substantial anaesthesia was used during the administration (in that case, i.v. propofol), necessitating a significant time delay to allow the animals to regain consciousness before stimulations. Alternatively, it may have been based on the time to peak effect of systemic phenobarbital[99], but given that relatively high concentrations were found in the olfactory bulbs at 10 minutes after i.n. compared with i.v. administration, an earlier time point would have been interesting if it were possible. Only one study performed stimulations at a range of time points (15-120 minutes) to determine a time of peak effect[145], which would have been useful in other studies given that nasal administration may change the pharmacokinetics of an ASD. The parenteral half-lives and times to peak effect of the ASDs used in the reviewed studies are included for the reader's reference in Table 1.8.

1.7.2.6 In the Pipeline

Outside of the published literature, pharmaceutical formulation for the intranasal treatment of seizures is also gaining traction in the patent and pharmaceutical company scene, particularly in the arena of cannabinoids. The potential role of these molecules in the treatment of

pharmacoresistant epilepsy is an area of much current interest[158], but their inherent lipophilicity and low bioavailability makes delivery an issue. It would appear that intranasal pharmaceuticals are being explored to address this challenge, albeit not specifically for seizures, but neurological conditions in general. One such recent example, which is aiming to exploit a direct nose-to-brain pathway, or at least a rapid systemic absorption for cannabinoids, is a contract between a Canadian health company and the University of Queensland Pharmacy department to formulate sol gels for this purpose[159]. Another example is found in a patent for the development of phospholipid nanoparticles containing cannabinoids, with intranasal delivery listed as a potential application[160]. Hence, while this area is still young, formulation is increasingly being recognised as a requirement to exploit intranasal delivery, and innovative therapeutics, to their fullest.

1.7.2.7 Conclusions

The above discussion highlights some important considerations that should be addressed in order to further the exploration of the field of intranasal treatment of seizures with the development of pharmaceutical formulations. All but one of the formulation publications discussed have come from the past decade, suggesting why this area still appears to be establishing a solid foundation. Gels would seem to be the most well-characterised pharmacokinetically for the delivery of ASDs, but a review of the wider intranasal formulation literature suggests that particulate delivery systems may be an important contributor once they are more rigourously studied[91]. A number of other attempts to formulate, with similar drugs (lamotrigine[161,162], valproic acid[163,164], carbamazepine[165], midazolam[166]) and approaches (microspheres, microemulsions and gels) have been published, but without biological testing to follow up pharmacokinetic and pharmacodynamic efficacy at present. With all its shortcomings, the existing literature would suggest that there are quite likely advantages to delivering anti-seizure drugs through the nose, but which direct pathways (if any) are able to be exploited and whether this can be achieved without damaging the nasal mucosa, as well as whether it is a feasible chronic treatment, is yet to be determined. More attention to obtaining quality and hypothesis-driven pharmacokinetic and pharmacodynamic data with suitable controls, as well as more detailed and standardised reporting of methodology should contribute a lot towards answering these questions.

With all this in mind, the following Chapters aim to establish and apply an intranasal screening model to the investigation of two types of particulate delivery systems for delivering ASDs

intranasally to the brain. **Chapter Two** begins by validating a screening model based on the MEST test to measure changes in seizure threshold using a known ASD, phenytoin. **Chapter Three** follows by evaluating the ability of the model to measure the effects of phenytoin delivered intranasally using a previously characterised microparticle formulation. **Chapter Four** then concludes by applying the model to the investigation of oleoylethanolamide, an endogenous molecule with hypothesised, but unknown anti-seizure activity, where delivery is mediated by a cubosome dispersion. All experimental Chapters aim to provide as holistic an assessment as possible, with histological and pharmacokinetic data to accompany the pharmacodynamic data as appropriate, exemplifying an improved standard for future studies of intranasal ASD delivery that follow on from those discussed in the above review.

Table 1.6. Summary of intranasal doses and administration methods used in studies investigating intranasally-delivered ASDs.

Drug/therapeutic	Animal model	Dose	Volume	Anaesthesia	Method	Reference
Carbamazepine	Mouse	12-16 µg	12-16 µL in one nostril	Ketamine and xylazine (i.p)	Tubing	[140]
Carbamazepine	Mouse	0.625 mg	100 µL in one nostril	Diethyl ether	Cannula strengthened by jacketed non-protruding needle	[139]
Carbamazepine	Rat	35-40 µg	10 µL in each nostril	Ketamine (i.m)	Tubing	[143]
Carbamazepine	Rat	50 µg (administered) 40 µg (accepted)	50 mg gel into one nostril. Estimated that 80% was accepted.	None	Tubing	[137]
Carbamazepine	Rat	1.6-2 mg	55 µL in each nostril	None mentioned	Tubing	[129]
Lamotrigine	Mouse	0.11-0.125 mg	Not stated. Both nostrils.	Ketamine and xylazine (route not stated)	Tubing	[146]
Lamotrigine	Mouse	120-160 µg	12-16 µL in one nostril	Ketamine and xylazine (i.p)	Tubing	[141]
Lamotrigine	Rat	0.72-0.97 mg	100 µL in each nostril	Ketamine (i.m)	Not stated	[127]
Phenytoin	Rat	3.52 mg	88 µL in each nostril	None mentioned	Tubing	[128]

Phenobarbital	Rat	1.1-1.2 mg 2-2.2 mg 6-6.6 mg	7-40 µL in each nostril	Propofol (i.v)	Deposited at opening of nares or using tubing	[138]
Valproic acid	Rat	0.72-0.84 mg	100 µL in each nostril over a few minutes	Light ether	Tubing	[145]
Diazepam	Rat	40-50 µg	10 µL each nostril	Ketamine (i.p)	Tubing	[144]
Thyrotropin releasing hormone (TRH)	Rat	20 µg	25 µL in each nostril (chronic administration)	Isoflurane	Surgically inserted cannulae	[16,17]

Table 1.7. Summary of methodology used in studies analysing pharmacokinetics and anti-seizure efficacy of intranasally-delivered ASDs.

ASD/molecule	Tissues analysed	Pharmacokinetic parameters reported	Time points after administration	Routes/formulations compared	Test	Endpoint	Time of test	Anaesthesia	Reference
Diazepam	Brain, plasma	%DTE, Brain concentration, Plasma concentration, C_{max}, T_{max}, AUC	30, 60, 120, 240, 480 min	i.n. (drug solution) i.n. (drug formulation) i.v. (drug solution)	-	-	-	Ketamine (i.p)	[144]
Lamotrigine	Brain – olfactory bulbs, frontal cortex, remainder. Plasma. Liver.	DTE, Brain concentration, Plasma concentration, Liver concentration, Brain:Plasma ratio, T_{max}, C_{max},, AUC, k_{el} (terminal elimination rate constant), k (tissue elimination rate constant), $t_{1/2}$, Mean residence time (MRT), Absolute i.n. bioavailability (F), AUC ratio (liver:plasma)	5, 10, 15, 30, 60, 120, 240 min	i.n (drug formulation) i.v. (drug formulation)	-	-	-	Ketamine and xylazine (i.p)	[141]
Carbamazepine	Brain – olfactory bulbs, frontal cortex, remainder. Plasma. Liver.	DTE, Brain concentration Plasma concentration, Brain:Plasma ratio, Liver concentration, T_{max}, C_{max}, AUC, k_{el}, $t_{1/2}$, MRT, F.	5, 10, 15, 30, 60 min	i.n (drug formulation) i.v. (drug formulation)	-	-	-	Ketamine and xylazine (i.p)	[140]
Carbamazepine	Brain Plasma	Brain concentration, Plasma concentration, AUC, T_{max}, C_{max}, K_{el}, $t_{1/2}$, %DTE, %DTP.	30, 60, 120, 240, 480 min	i.n. (drug formulation x 2) i.n (drug solution) i.v. (drug formulation)	-	-	-	Ketamine (i.m)	[143]

Carbamazepine	Brain Plasma	Brain concentration, Plasma concentration, Brain:Plasma ratio, AUC, C_{max}, T_{max}, MRT, AUC ratio (brain:plasma).	5, 10, 15, 20, 30, 45, 60, 90, 120 min	No treatment i.n. (drug solution) i.n. (drug formulation) p.o. (drug solution)	-	-	-	None	[137]
Lamotrigine	Brain Plasma	Brain concentration, Plasma concentration.	24 hours	IN (solution) vs IN (formulation) vs PO	MES (auricular)	HLE incidence Latency to HLE Duration of HLE	60 min 24 hours	Ketamine (i.m)	[127]
Phenobarbital	Whole brain. OB, frontal cortex, piriform cortex, amygdala, hippocampus, parahippocampal cortex, caudal cortex, cerebellum, pons. Frontal cortex dialysate. Plasma.	Dialysate:Plasma ratio (microdialysis in frontal cortex) Brain concentration (homogenate) Plasma concentration (homogenate) Brain:Plasma ratio (homogenate)	10 min (microdissected regions) 2, 5, 10, 20, 30, 60, 200, 240 min (whole brain and plasma) 15, 30, 60, 90, 120, 180, 240 min (dialysate)	i.n. (formulation without drug) i.n. (formulation with drug) i.v. (formulation without drug) i.v. (formulation with drug)	Amygdala kindling	ADT Seizure severity Seizure duration Afterdischarge duration GST	60 min	Propofol (i.v)	[138]
Valproic acid	Brain Plasma	Brain concentration, Plasma concentration, Brain:Plasma ratio.	60 min	i.n. (formulation without drug) i.n. (formulation with drug) i.n. (drug solution) i.p. (formulation without drug) i.p. (formulation with drug) i.p. (drug solution)	MES variation (auricular)	E:F ratio of hindlimbs	15, 30, 60, 90, 120	Light ether	[145]

Phenytoin	Brain	Brain concentration.	15 and 30 min	No treatment i.n. (drug formulation) p.o. (drug formulation) i.p. (drug solution)	MES (auricular)	Duration of HLE	60 min	None mentioned	[128]
Carbamazepine	-	-	-	i.n. (solution) i.n. (formulation) p.o. (formulation) i.n. (solution) No treatment	MES (auricular)	Duration of HLE	60 min	None mentioned	[129]
Carbamazepine	-	-	-	i.n. (drug formulation) i.n. (drug solution) No treatment	MES variant (auricular) PTZ (i.p)	MES variant: number of trials until death PTZ: onset to convulsion, time until death	5 min (MES variant) 15 min (PTZ)	Diethyl ether	[139]
Lamotrigine	-	-	-	Saline (route not reported) i.n. (drug formulation) i.p. (drug formulation)	PTZ (s.c.)	Onset to clonic convulsion Protection against mortality	30 min	Ketamine and xylazine (route not reported)	[146]
Thyrotropin releasing hormone	-	-	-	i.n. (drug formulation) i.n. (formulation without drug)	Amygdala kindling	ADD Number of seizures until first stage 5 Number of seizures until fully kindled	Daily stimulations until fully kindled Doses administered at both 60 and 30 min before stimulation.	Isoflurane	[16,17]

Table 1.8. Half-lives and times to peak effect of ASDs used in the reviewed formulation studies.

ASD/therapeutic	**Plasma half-life (h)** [141,151,167,168]			**Time to peak effect after single parenteral dose** [99,169]	
	Rats	**Mice**	**Human**	**Rats**	**Mice**
Carbamazepine	1.2-3.5	30-60	25-50	30 min	15 min
Phenobarbital	9-20	7.5	70-100	60 min	30 min
Lamotrigine	12-30	8*	21-50	60 min	120 min
Phenytoin	1-8	16	15-20	30 min	120 min
Valproic acid	1-5	0.8	8-15	15 min	5 min
Diazepam	1.4	7.7	24-72	15 min	15 min

*Estimated from plasma concentration graph in Serralheiro et al[141]

Chapter Two

The Validation of a Seizure Model

2.1 Introduction

The first step towards testing intranasal drug delivery systems in this thesis was to establish a suitable model with which to measure their effects on seizure threshold. The suitability and previously reported use of a range of models was discussed in **Chapter One**. Based on this discussion, it was decided that the Maximal Electroshock Seizure Threshold (MEST) test was most suited to perform these early investigations. The test has several key benefits, as touched on in **Chapter One**, including an increased sensitivity to detect anti-seizure effects (compared to an "all or nothing" suprathreshold effect as in the MES test), the ability to simultaneously test for pro-seizure effects that may be caused by previously un-investigated therapeutics or different doses of known anti-seizure drugs[170], and the lack of assumption of a pharmacological mechanism of drug action (as opposed to chemically induced seizures)[171].

As discussed in **Chapter One**, the typical MEST test is based on the "up and down" method of Kimball et al[99,100] and compares the threshold for hind-limb extension (HLE) with and without anti-seizure drug treatment by stimulating each rat on two occasions: once after control treatment administration, then again >48 hours later after drug treatment administration. The

mean current inducing HLE in 50% of rats (CC_{50}) in each group is calculated and compared between the groups. An increase in CC_{50} (i.e. seizure threshold) after test drug treatment suggests an anti-seizure effect of the drug treatment in the animals.

Despite its common use in the literature, this typical design has a few limitations which may have presented as obstacles for the proposed study of intranasal delivery in this thesis. Firstly, in the traditional MEST experiment, interday variability and the possibility of sequence effect are not accounted for. Generally, the control trial is performed first, followed by the drug trial on the assumption that the order of the treatments and the effect of multiple stimulations has no effect on the seizure threshold. Although it has been reported that the CC_{50} does not significantly vary for HLE or fore limb extension (FLE) provided 48 hours is left between stimulations[101], a host of factors may influence seizure threshold[99] and inter-lab (and even inter-batch) variability can be considered a very real possibility. Secondly, the traditional MEST experiment analyses a batch of rats as a group on the basis of seizure threshold for a single parameter; usually HLE. This means that the responses of individual rats cannot be assessed at baseline and after treatment to reduce intra-subject variability as they are likely to be stimulated at different currents in each trial. Furthermore, only one response (e.g. HLE or FLE) can be assessed per round of the "up and down" method, limiting the information obtained from each stimulation and potentially missing more subtle variations in responses. Finally, the success of the "up and down" method is dependent on quickly reaching a value close to the true population CC_{50} in the serial stimulations[100]. If this is not achieved by correctly estimating the starting current for a particular group of animals, which can be a particular issue after they have received drug treatment with an unknown effect, then the confidence interval will be large. This may be further complicated by the administration of potentially confounding anaesthetic prior to drug administration as was a requirement for intranasal delivery studies in the following Chapters.

With the expectation that the effects of drugs delivered intranasally may be localised in the brain and could be more subtle than those seen after systemic administration, it was necessary to aim for the highest sensitivity and lowest variability possible while still maintaining a fairly simple screening procedure. This Chapter therefore establishes and validates a new study design based on the MEST procedure where baseline threshold for a group of animals is determined initially, then used to stimulate each group with and without drug treatment in a cross-over fashion. The anti-seizure drug chosen to validate this new study design was phenytoin. The rationale for its use over other drugs was primarily due to its use as a model drug for intranasal delivery in **Chapter Three**, the subsequent reasoning for which is discussed in that Chapter.

Also of critical importance was that phenytoin, unlike certain other drugs discussed in **Chapter One**, has been shown to be highly effective at increasing the threshold against MEST seizures in rodents[172–174] and could therefore be administered as a positive control to validate the ability of the test to show statistically significant effects in our lab. To complement the pharmacodynamic experiments in this Chapter and the one that follows, a highly sensitive analytical liquid chromatography mass spectrometry (LC-MS) method was also validated and used to quantify the concentrations of phenytoin and its major hepatic metabolite 5-(4-Hydroxyphenyl)-5-phenylhydantoin (4-HPPH) in the brain tissue and plasma of the tested animals in order to evaluate the pharmacokinetics of the drug in this study. Finally, the effect of the procedure on animal welfare is evaluated to justify the use of the model in future Chapters from an ethical standpoint.

2.2 Aims

The overall aim of this Chapter was to validate a modified version of the MEST seizure model using a known anti-seizure drug, so that it could be applied to intranasal delivery studies in the succeeding Chapters. To achieve this, the following objectives were set:

- Validate the ability of a modified MEST study design to detect the anti-seizure effect of phenytoin.
- Develop and validate an LC-MS method to detect phenytoin and its major metabolite (4-HPPH) in rat plasma and brain tissue.
- Evaluate phenytoin concentrations in brain and plasma after intravenous administration in the seizure-tested rats to correlate with pharmacodynamic effects.
- Assess the impact of multiple stimulations of individual animals on their welfare during the course of the experiment.

2.3 Hypotheses

- The primary hypothesis on which this Chapter is based was that a therapeutic intravenous dose of the established anti-seizure drug phenytoin would show an anti-seizure effect in the MEST test under the conditions used in our laboratory and with the crossover study design proposed.
- It was also hypothesised that therapeutic brain and plasma levels would accompany the pharmacodynamic effects, thereby validating the ability of the model to detect anti-seizure effects in the experiments constituting the subsequent Chapters. The hypothesis was based on the abundance of previous literature which documents the ability of phenytoin to increase the threshold for seizures elicited by the Maximal Electroshock Stimulation method.
- Finally, it was also hypothesised that individual animals could receive three independent stimulations at 48 hour intervals without significant adverse effects on their wellbeing, an aspect which has not been specifically reported on in previous literature employing the MEST test.

2.4 Materials & Methods

2.4.1 Materials

Phenytoin (5,5-diphenylhydantoin) sodium injection (250 mg/5 mL) (DBL™ Phenytoin injection BP) was purchased from hameln pharmaceuticals GmbH (Germany). Isotonic (0.9 %) saline was purchased from Baxter (Australia). Isoflurane was provided by the Hercus-Taieri Resource Unit, University of Otago. Phenytoin sodium, 4-HPPH (5-(4-Hydroxyphenyl)-5-phenylhydantoin), propylene glycol (PG), formic acid (for mass spectrometry, ~98%) and phosphate-buffered saline (PBS) sachets (pH 7.4) were purchased from Sigma Aldrich (New Zealand). Deuterated phenytoin (d_{10}-phenytoin; (5,5-(diphenyl-d_{10}) hydantoin)) was purchased from Toronto Research Chemicals (Canada). All water used in this study was ion exchanged, distilled and passed through a Milli-Q water purification system (Millipore, USA). Acetonitrile (ACN) (LiChrosolv®), Methanol (MeOH) (LiChrosolv®), tert-Butyl Methyl Ether (TBME) (LiChrosolv®) and Ethanol (EMSURE®) were purchased from Lab Supply (New Zealand). All of these solvents were liquid chromatography grade. Male Wistar rat plasma and brain tissue for LC-MS method validation and standard preparation was obtained in-house from control rats administered saline treatments.

2.4.2 Animals

All procedures involving animals were approved by the University of Otago Animal Ethics Committee pursuant to Animal Use Protocol 08/16. Male Wistar rats (260-320 g, 7-8 weeks old) sourced from the Hercus Taieri Resource Unit were used in this experiment. Specific weights and ages of animals over the course of the experiments can be found in the Results section of this Chapter and **Appendix A and B**, respectively. Animals were housed under laboratory conditions in the Hercus Taieri Resource Unit for the duration of the experiment.

2.4.3 Drug Administration

2.4.3.1 Isoflurane Anaesthesia

Preliminary experiments determined that a short inhaled anaesthesia would be required in order to perform intranasal administration for MEST experiments in **Chapters Three and Four**. Therefore, in the interests of consistency, this anaesthesia was also administered in this validation experiment to ensure that the anti-seizure effect of phenytoin could be detected compared to control despite any potential contribution from the anaesthetic. Animals were

anaesthetised with 5 % isoflurane and an oxygen flow rate of 1 mL/minute for three and a half minutes immediately prior to drug administration, as described in **Chapters Three and Four**.

2.4.3.2 Intravenous Administration of Phenytoin Solution and Saline

While the animals were unconscious, phenytoin sodium solution (25 mg/kg ≈ 150-180 µL) or equivalent volume of saline (0.5 mL/kg) was administered via a lateral tail vein using a 0.3 mL Lo-dose U-100 insulin syringe with 29 G x 12.7 mm needle (BD Biosciences, New Zealand). The phenytoin dose used was reported elsewhere to achieve therapeutic and non-toxic plasma concentrations that persisted up to 60 minutes[175–177] and previous studies indicated it would be sufficient to raise the threshold for hind-limb extension in the MEST test up to this time point[99,172,174]. Considering this and the initial planned time point for the intranasal MEST trial in **Chapter Three**, the treatment was administered 60 minutes before stimulation in this validation experiment.

2.4.4 Maximal Electroshock Stimulation Threshold Test

2.4.4.1 Auricular Electrode Habituation

In order for the animals to feel more comfortable with the stimulation procedure and minimise technical errors due to uncooperative behaviour, rats were habituated to the application of auricular (ear clip) electrodes (Harvard Apparatus, USA) over a period of four days prior to the first stimulation, as well as between successive stimulation days. This was achieved through once daily application of the electrodes and placement into the custom-made transparent acrylic container (420 x 420 x 210 mm) in which the stimulations would occur, for up to 30 seconds. Following this, the electrodes were removed and the animal returned to their home cage.

2.4.4.2 Electrical Stimulation

Preliminary experiments with an Electoconvulsive therapy (ECT) unit (Ugo Basile, Italy) demonstrated the importance of using a sinusoidal rather than rectangular pulse current stimulator (as had been reported by some studies in the literature[145,178,179]) for this procedure in order to observe the necessary maximal seizure response. The constant current stimulator used in these experiments was therefore a Rodent Shocker Sine-Wave Shock Generator with Foot Switch (230 Volts of alternating current (VAC), 50 Hertz (Hz)) (Harvard Apparatus, USA). Auricular electrodes smeared with a conductive gel were applied to each animal's ears immediately prior to stimulation. The animal was placed in the container described above and

a stimulus of 0.2 seconds duration was delivered through the electrodes to initiate a seizure. The current used for the stimulation varied, as described below. Each test was recorded on video for later reference and blinded evaluation of the seizure response observed.

2.4.4.3 Cross-Over Study Design

To account for variability in seizure thresholds and observed seizure behaviours in our animals, we modified the typical design of the MEST test as discussed in the introduction to this Chapter. This involved using a cross-over method, as outlined in Figure 2.1, where a total of three stimulations were delivered to each rat, no less than 48 hours apart.

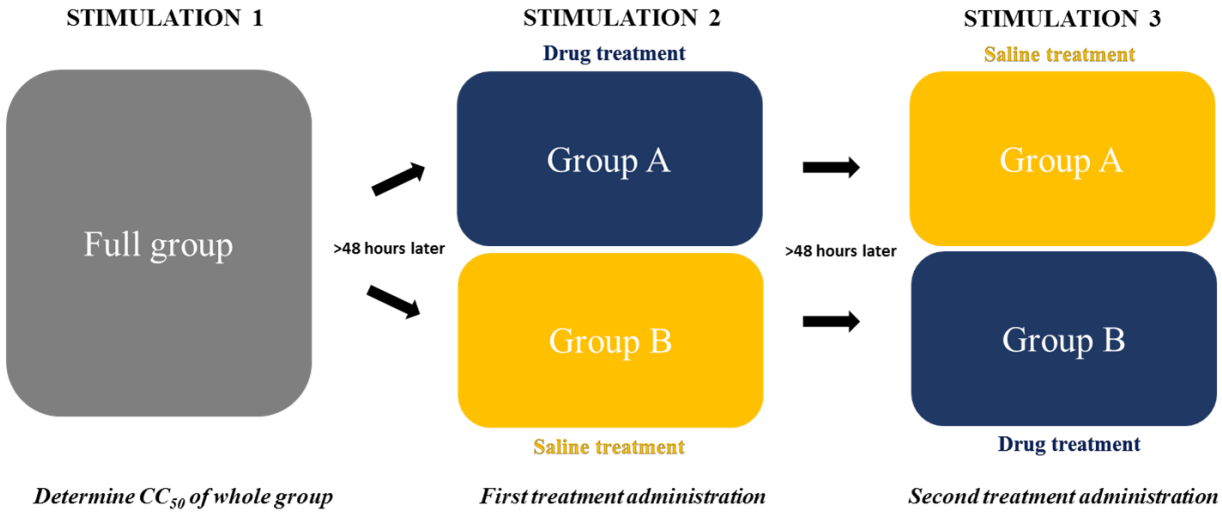

Figure 2.1. Crossover method design of the MEST test used in this study.

For the first stimulation, the "up and down" method was used to estimate the convulsive current inducing the maximal seizure endpoint of hind-limb extension in 50% of animals (CC_{50}) in the group (Figure 2.2). Isoflurane anaesthesia was performed 60 minutes before each stimulation so as to determine the CC_{50} under the influence of any potential confounding effects from the anaesthesia and to therefore determine a reasonable estimate of it for the subsequent treatment trials that would also need to employ it. The initial current of stimulation was 50 mA, based on the CC_{50} threshold of male Wistar rats reported in the literature[15,101,172]. Each animal was stimulated in series, altering the current of stimulation by 0.06 log units down or up, depending on whether the previous animal did or did not display the endpoint, respectively. The CC_{50} calculated for the group of rats (using the method of Kimball et al.[100]) was used as the

stimulation current for all of the animals in the subsequent two stimulations. All stimulations for a given rat were performed at least 48 hours apart. Exact relative timings of all the stimulations are presented in **Appendix A**.

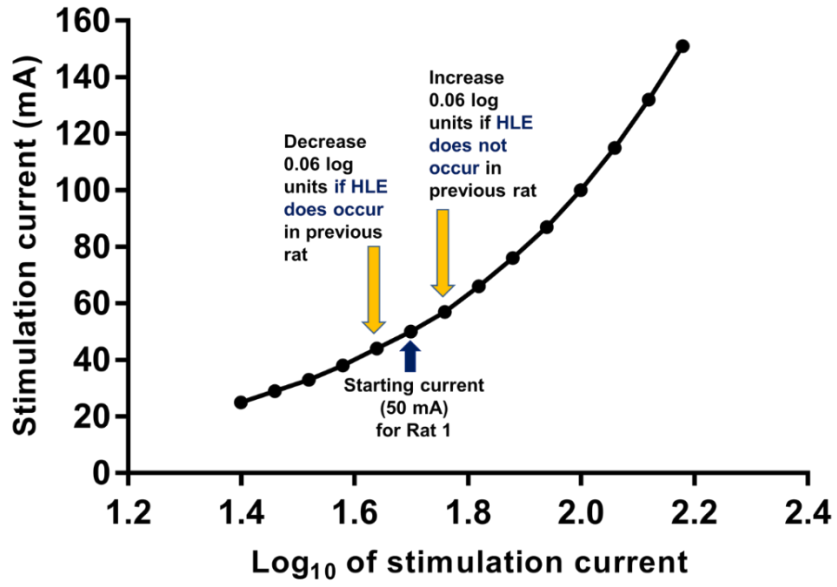

Figure 2.2. Principles of the "up and down" method to determine the threshold for tonic hindlimb extension by serial stimulation of a group of rats.

Prior to the second stimulation, rats were randomly divided into two groups. All were briefly sedated with isoflurane anaesthesia as outlined above, then intravenously administered phenytoin sodium solution (25 mg/kg) or an equivalent volume of isotonic saline (0.5 mL/kg). After 60 minutes, they were stimulated at the CC_{50} and their response recorded. The third stimulation followed the same protocol, except that the treatments were switched so that the response of each rat was measured after both saline and phenytoin treatment. Outcomes were compared statistically with Prescott's test[180], with $p < 0.05$ considered statistically significant.

2.4.5 Tissue collection for pharmacokinetic analysis

Tissues were collected and processed in order to study brain concentrations of phenytoin and 4-HPPH in rats that had participated in the pharmacodynamic MEST experiments. Rats were euthanased by guillotine decapitation within 10 minutes of the third and final MEST stimulation. Trunk blood was collected in a 6 mL tube coated with sodium heparin (BD Biosciences, New Zealand) at the time of euthanasia and centrifuged at the conclusion of the

experiment (2000 G for 10 minutes at ambient temperature (Heraeus Multifuge X3FR, Thermo Fisher Scientific, New Zealand). The brain was also dissected and kept on ice until the conclusion of the experiment, after which they were frozen and kept at -80 ºC until required for LC-MS analysis.

2.4.6 LC-MS Method for Analysis of Phenytoin in Plasma and Brain Tissue

2.4.6.1 Extraction and Sample Preparation

Thawed brains were homogenised after adding 2 mL/g (based on wet weight determined after rinsing in PBS at time of dissection and blotting with filter paper after thawing) of Milli Q water prior to homogenisation on ice with a tip sonicator for periods of up to 5 seconds at a time until sufficiently homogenous (UP50H Ultrasonic Processor, hielscher Ultrasound Technology, Germany) (1 cycle, 100% amplitude). The homogenate was aliquoted into 1.7 mL ultra clear microtubes (Axygen, USA) in aliquots of 100 µL. Plasma was able to be thawed and extracted without dilution with water as it could be accurately pipetted due to low viscosity. A pilot run was conducted before the main study to estimate phenytoin concentrations in the tissues and where appropriate, samples for the main study were diluted with blank plasma or brain homogenate in order to be quantifiable within the standard range.

Each 100 µL sample aliquot had 5 µL internal standard (d_{10}-phenytoin) and 5 µL methanol (standard solvent) added (in the case of standards, the latter contained a standard concentration of phenytoin and 4-HPPH). This was vortexed, then 200 µL chilled ACN was added. This mixture was sonicated briefly in a water bath (Elmasonic S 60 (H), Elma Ultrasonics, New Zealand), then 800 µL chilled TBME was added and it was sonicated briefly again, then vortexed briefly. It was then centrifuged at 17,200 G for 20 minutes at 4 °C (Prism™ R Microcentrifuge, Labnet International, Inc., USA).

The samples were taken into a precooled tray, then 800 µL of the supernatant was taken and transferred to a new tube. These tubes containing the supernatant were then evaporated to dryness in a centrifugal evaporator (Thermo Savant Speed Vac®, Thermo Fisher Scientific, New Zealand) until dry (8-12 hours). A 200 µL volume of methanol was then added to each tube and it was briefly sonicated and vortexed to reconstitute. A brief centrifugation (10,000 rpm for 1 second) followed to ensure all liquid was moved to the bottom of each tube. Samples were then pipetted into the top of a 1 mL syringe (BD Biosciences, New Zealand) and filtered

through a 13 mm Nylon 0.22 µm syringe filter (Microanalytix, New Zealand) into a 250 µL insert (PP BM insert with bottom spring case (Phenomenex, USA)) in a 2 mL clear glass vial (Thermo Fisher Scientific, New Zealand). Samples were stored at ambient temperature until analysis.

2.4.6.2 Standard Preparation

Stock solutions for standard preparation were produced by dissolving analyte powders (phenytoin sodium, 4-HPPH and d_{10}-phenytoin) in methanol at a concentration of 1 mg/mL. Serial dilution of these solutions in methanol was performed to achieve the desired standard concentrations. To prepare standard samples for analysis, aliquots of standard solutions (5 µL) were mixed with blank plasma or brain homogenate aliquots (100 µL) in place of the 5 µL of blank methanol added to the unknown samples, as described above. The extraction procedure was the same from that point forward. Standards covered a range of 7.81 to 250 ng/mL for plasma and 23.4 to 750 ng/g for brain tissue. Quality control (QC) samples were prepared alongside standards at concentrations within the relevant ranges.

2.4.6.3 LC-MS Analysis

Samples were analysed using an Agilent 1290 High Performance Liquid Chromatography (HPLC) system (G4226A autosampler, LC binary SL pump, TCC SL (Agilent, USA)) connected to an AB Sciex QTRAP 5500 mass spectrometer with Turbo Spray ion source (Sciex, USA). Parameters were optimised to detect the analytes of interest as shown in Table 2.1.

Table 2.1. Optimised parameters for phenytoin and 4-HPPH analysis.

Entrance potential (V)	10.0
Curtain gas (psi)	15.0
Collision gas	Medium
Ionspray voltage (V)	5500.0
Temperature (ºC)	600.0
Ion source gas 1 (psi)	40.0
Ion source gas 2 (psi)	40.0

Figure 2.3 shows the molecular structures and molecular masses of the compounds analysed (A-C) as well as the predicted fragmentation in positive ion mode (arrows).

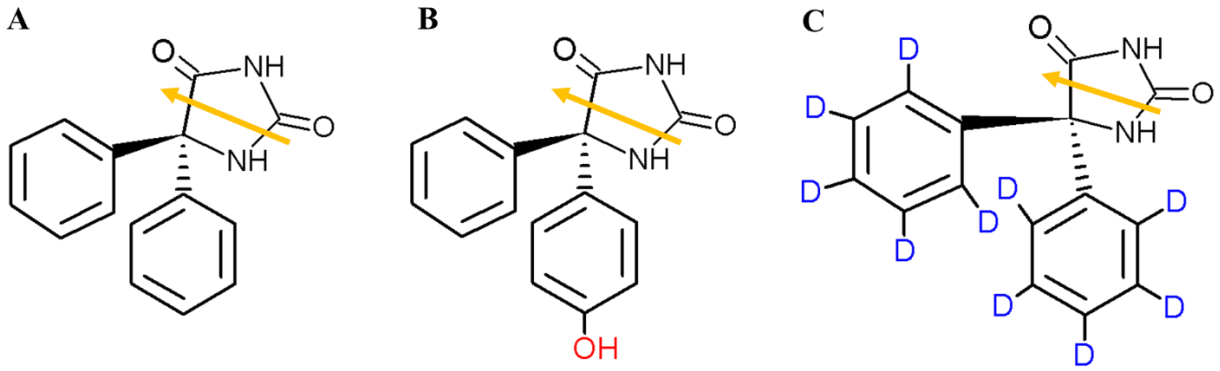

Figure 2.3. Molecular structures of (A) Phenytoin (Mw = 252.3 g/mol), (B) 4-HPPH (Mw = 268.3 g/mol) and (C) d_{10}-phenytoin (Mw = 262.3 g/mol). The expected fragmentation point which produces the predominant daughter ion of each ($[M+H]^+$) is shown with a yellow arrow.

As predicted from the fragmentation shown in Figure 2.3 and previous literature[181], the precursor/product ion pairs found to produce the highest intensity in positive ion mode were 253.011/182.100 for phenytoin, 263.152/192.088 for d_{10}-phenytoin and 269.051/198.100 for 4-HPPH. These were monitored in multiple reaction monitoring (MRM) mode (positive ionisation) using the optimised parameters shown in Table 2.2.

Table 2.2. MRM optimised parameters for ions monitored.

Q1	Q3	Time (msec)	ID	DP (volts)	CE (volts)	CXP (volts)
253.011	182.100	150.0	Phenytoin	71	27	10
263.152	192.088	150.0	d_{10}-Phenytoin	31	37	12
269.051	198.100	150.0	4-HPPH	71	25	6

Mobile phase A consisted of 0.1% formic acid in Milli Q water. Mobile phase B was 0.1% formic acid in 2:1 Acetonitrile:Methanol. Analysis was performed at a flow rate of 0.25 mL/min by injecting 5 µL of sample into a Kinetex EVO 5 µ 100 Å C18 (150 x 2.1 mm) column (fitted with a 4 x 2.0 Gemini-NX C18 SecurityGuard Cartridge) (Phenomenex, USA) maintained at 40 °C. Starting pressure was approximately 1700 psi. The gradient was started at 80% A, 20% B, where it was held for 30 seconds before shifting to 5% A, 95% B over 7 minutes to elute the

analytes. It was then held at this ratio for 5 minutes to clean out matrix components, then returned to 80% A, 20% B over 30 seconds and allowed to re-equilibrate for 6 minutes, giving a total run time of 19 minutes. Eluent was allowed to flow to the MS detector for the first 6.9 minutes for compound elution, then was diverted to waste until 13.0 minutes, then allowed to flow to the detector again until 19.0 minutes to re-equilibrate. A mixture of 90% methanol in Milli Q water was used for needle cleaning between samples (10 seconds). Draw speed and eject speed were 200 µL/min. 4-HPPH eluted first at 4.06 minutes, followed by d_{10}-phenytoin at 5.12 minutes and phenytoin at 5.16 minutes. The auto-sampler was maintained at a temperature of 20 °C during analysis.

2.4.6.4 Data analysis

Data was collected in Analyst® software (Sciex, USA) and analyte/internal standard ratio was used to construct calibration curves and analyse the data in Microsoft Excel (Microsoft, USA). The assays were validated using triplicate samples on three separate days. The lower and upper limits of quantification of each of the assays was determined experimentally by analysis of accuracy and precision, with limits of ±15% considered acceptable. Intra- and inter-day variability was assessed using quality control samples for which accuracy and precision limits of ±15% were considered acceptable. Accuracy was calculated by taking the values of the standards as quantified by the assay and presenting them as percentages of the nominal standard concentrations that were expected. Precision was calculated as the ratio of the standard deviation to the mean of a set of measurements and is presented as the coefficient of variation as a percentage (CV%), also known as the relative standard deviation (RSD). Standard curves were plotted in GraphPad Prism® (GraphPad, USA) for presentation in this thesis. Tissue concentration data was compared statistically with two-sided t-tests (unpaired or ratio paired) as appropriate, with $p < 0.05$ considered statistically significant.

2.5 Results

2.5.1 Pharmacodynamic Validation of the MEST Seizure Model with Intravenous Phenytoin

2.5.1.1 Pharmacodynamics I: Determination of the CC_{50} of the Group and Baseline Response

The CC_{50} of the group of rats that participated in this study was estimated using the up and down method in order to determine a suitable stimulation current for the subsequent experiments. The primary endpoint used to determine the CC_{50} was tonic hind limb extension (HLE). All rats displayed tonic-clonic seizures during this first stage of the experiment, either with or without hind limb extension (Figure 2.4).

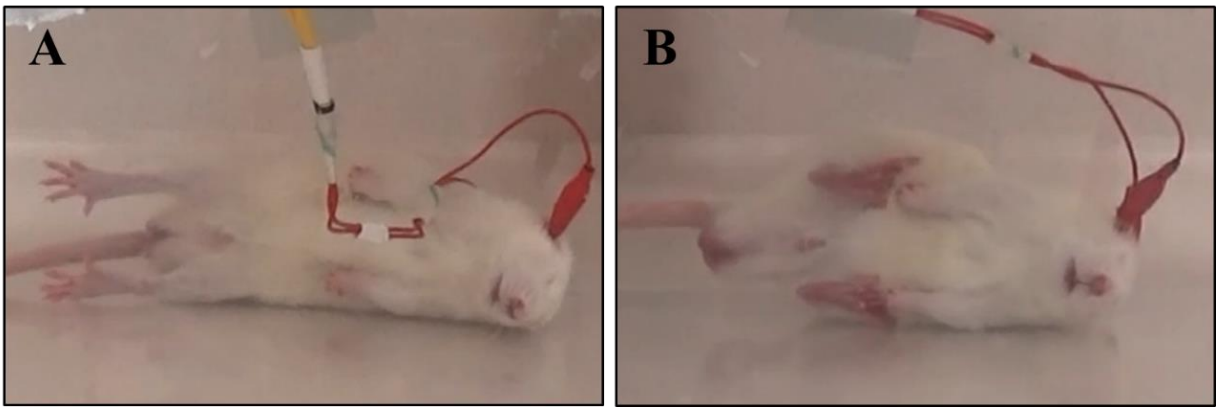

Figure 2.4. (A) Tonic-clonic seizure with hind limb extension (HLE) and (B) Tonic-clonic seizure with fore limb extension (FLE) only.

Figure 2.5 shows the course of the serial stimulations during the experiment and the data from which the CC_{50} of the population was calculated to be 40 mA (95% CI: 35-45 mA) (Panel A). Also shown is the subsequent experimental data of rats stimulated at this batch-specific CC_{50} of 40 mA after being administered intravenous saline (Panel B) to represent the baseline control response, from which it can be seen that 57% showed HLE.

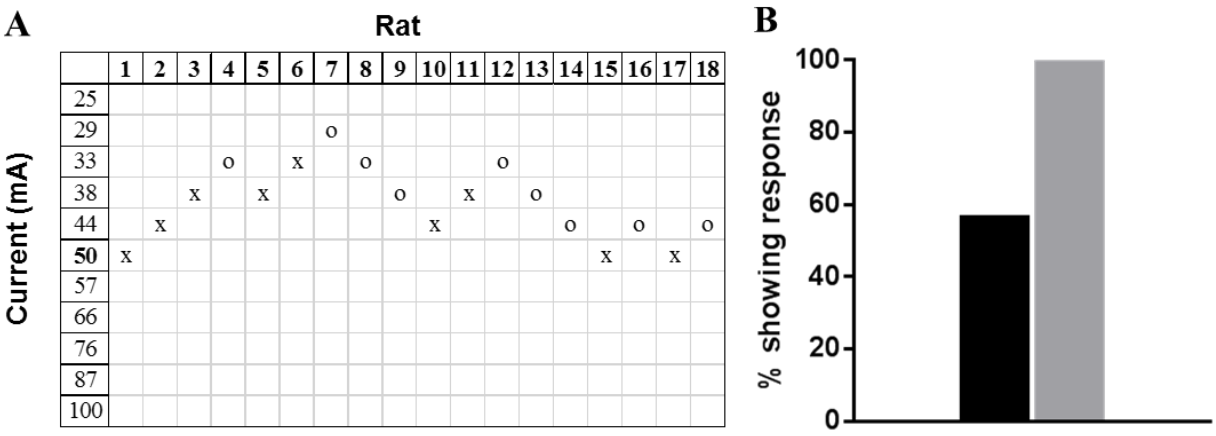

Figure 2.5. Determination of the CC_{50} (A) and baseline response to stimulation at the CC_{50} (B) in the batch of rats that participated in the study of intravenous phenytoin at 60 minutes. (A) Shows the experimental data from the up and down method which was used to estimate the CC_{50}, where "X" represents HLE and "O" represents no HLE. (B) Shows the baseline responses of the rats when stimulated at the calculated CC_{50} 60 minutes after intravenous saline administration and serves as an indication of the accuracy of the statistically estimated CC_{50} and the resolution for detecting anti-seizure drug effects. The black bar represents the percentage of rats which exhibited HLE at the calculated CC_{50} and the grey bar represents those which exhibited FLE (with or without HLE).

2.5.1.2 Pharmacodynamics II: Determination of the Response to Intravenous Phenytoin at the CC_{50}

As can be seen in Figure 2.6, 100% of HLE was prevented by intravenous phenytoin and 93 % of FLE. In addition, no pro-seizure effect (i.e. HLE occurring in rats which previously did not show HLE) was observed. The anti-seizure effect of phenytoin was statistically significant for HLE ($p = 0.0035$) and FLE ($p = 0.0006$) according to Prescott's test and is presented as the percentage change in the response – i.e. the percentage of rats which displayed the response after saline treatment, but not after phenytoin treatment (anti-seizure effect) and vice versa (pro-seizure effect).

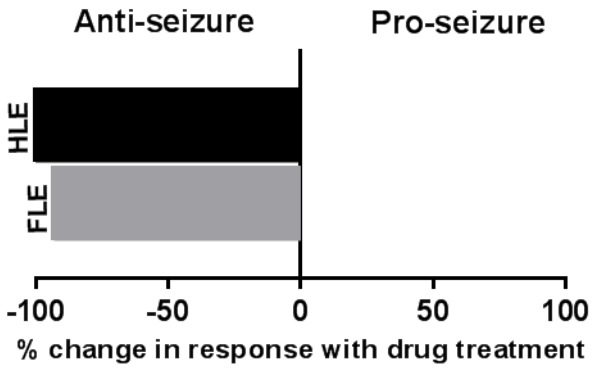

Figure 2.6. Effect of intravenous phenytoin solution (25 mg/kg) on HLE (black; n=8) and FLE (grey; n=14) at the group CC_{50} current (40 mA) 60 minutes after treatment administration. Data is presented as percent change in response with respect to intravenous saline treatment in the same rats. Animal numbers and the method used to calculate the percentage difference are shown in Appendix C. Note that two rats were excluded due to a technical error rendering their results invalid.

Rats that did not display FLE (i.e. all but one which was given phenytoin in this study) did not have a tonic phase as part of their seizure. All of these non-tonic responses began with a clonus of all four limbs and ended with a mild post-ictal period. In most cases, the clonus was characteristic of that seen in rats which are genetically-prone to audiogenic (sound-induced) seizures which originate at a similar location, as described in **Chapter One**. This highlights the lower threshold seizure activity that was being expressed phenotypically as the seizure struggled to spread and induce a tonic convulsion as it did in saline-treated rats. In the cases where the drug was most effective, this initial clonus was only short (one to three seconds), while in others it was longer (up to ten seconds). Between the initial clonus and post-ictal period, other behaviours indicating activation of low-threshold seizure circuits in regions of the forebrain were observed in a number of rats, manifestations of which included rearing, forelimb clonus, facial clonus, myoclonic jerks and vocalisation.

2.5.2 Validation of LC-MS Method for Measuring Tissue Phenytoin and 4-HPPH Concentrations

2.5.2.1 Specificity

The optimised method parameters allowed resolution of three clear peaks representing the two analytes and internal standard in rat plasma and brain tissue (Figure 2.7). Phenytoin eluted

consistently at 5.16 minutes, 4-HPPH at 4.06 minutes and the internal standard d_{10}-phenytoin at 5.12 minutes in samples from both matrices. Blank samples, containing neither of the analytes, confirmed the specificity of the signal (**Appendix D**). A small peak was noted in the blanks around the phenytoin elution time, but further experiments determined this was not attributable to phenytoin and the signal was well below the limit of quantification (<20% of the lower limit of quantification (LLOQ)) making it insignificant.

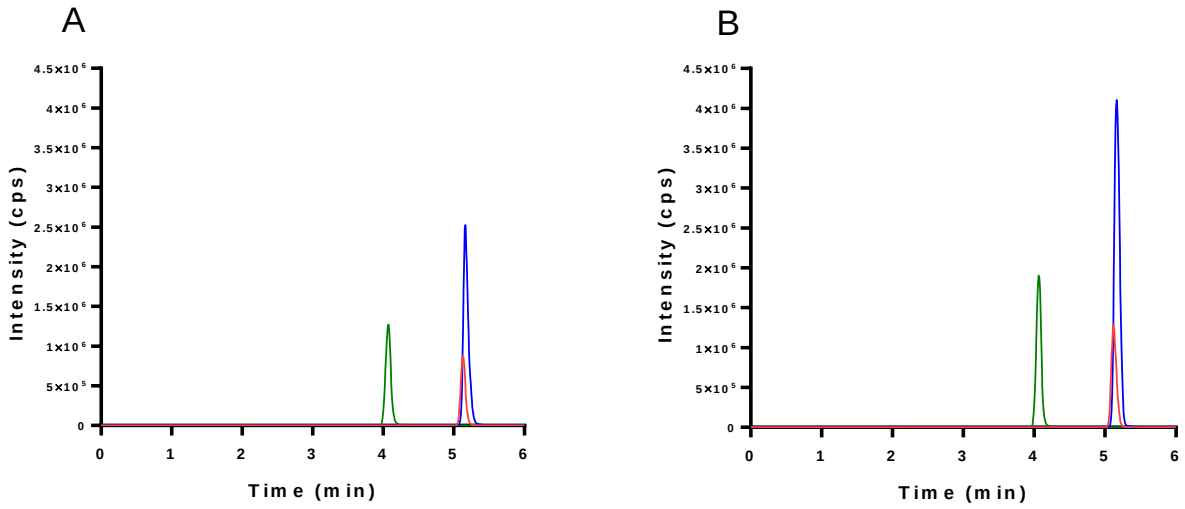

Figure 2.7. Representative chromatograms of phenytoin (blue), d10-phenytoin (red) and 4-HPPH (green) extracted from rat plasma (A) and rat brain homogenate (B). Note that original data has been plotted using GraphPad Prism® to enhance clarity. The phenytoin and 4-HPPH concentrations of the analytes in the samples used to produce these chromatograms were 125 ng/mL in plasma and 375 ng/g in brain tissue (equivalent to 125 ng/mL in brain homogenate). The internal standard (d_{10}-phenytoin) concentration was equivalent to 90 ng/mL in plasma and 270 ng/g in brain tissue (equivalent to 90 ng/mL in the diluted brain homogenate).

2.5.2.2 Sensitivity

To determine the sensitivity of the assay, standard curves were produced by plotting mean analyte/internal standard ratio values against concentration and fitting to second order polynomial (quadratic) equations. The standard curve was validated in triplicate on three separate days (Figure 2.8). Accuracy and precision for all concentration values was within an

acceptable range of ± 15% and the fit of the curve maintained a coefficient of variation (R^2) value of greater than 0.99 (**Appendix E**).

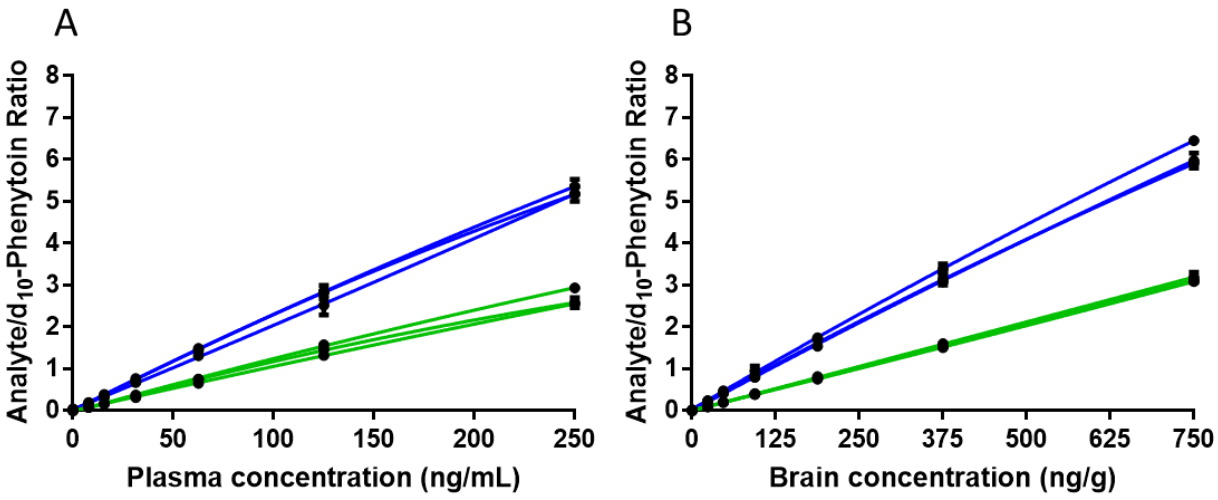

Figure 2.8. Standard curves of phenytoin (blue) and 4-HPPH (green) in plasma (A) and rat brain homogenate (B). Data shown are the mean values (± standard deviation) of the standards prepared and measured in triplicate on three different days. The relationship between analyte concentration and analyte/internal standard ratio was best modelled by fitting second order polynomial (quadratic) curves to the data as shown in the Figure. R^2 values are provided in Appendix E.

2.5.2.3 Accuracy and Precision

The inter-day and intra-day accuracy and precision of the assays, based on quality control samples, are shown in Table 2.3 and Table 2.4, respectively. Variability was within an acceptable range of ± 15% for all assays.

Table 2.3. Inter-day accuracy and precision of phenytoin and 4-HPPH quantification in rat brain homogenate and plasma based on quality control samples.

		Plasma		
Analyte	**Nominal conc (ng/mL)**	**Inter-day (n=3)**		
		Mean (ng/mL)	**Accuracy (%)**	**Precision (CV%)**
Phenytoin	15.6	15.3	98.1	4.0
	62.5	62.2	99.6	3.1
	250	255.2	102.1	4.5
4-HPPH	15.6	16.8	107.6	4.3
	62.5	65.0	104.0	3.2
	250	272.2	108.9	3.6
		Brain		
Analyte	**Nominal conc (ng/g)**	**Inter-day (n=3)**		
		Mean (ng/g)	**Accuracy (%)**	**Precision (CV%)**
Phenytoin	46.9	49.8	106.	2.8
	187.5	192.4	102.6	2.4
	750	768.8	102.5	1.6
4-HPPH	46.9	49.1	104.7	3.5
	187.5	185.9	99.2	2.1
	750	750.5	100.1	1.7

Table 2.4. Intra-day accuracy and precision of phenytoin and 4-HPPH quantification in rat plasma and brain homogenate based on quality control samples.

Plasma

Analyte	Nominal conc (ng/mL)	Intraday 1 (n=3)			Intraday 2 (n=3)			Intraday 3 (n=3)		
		Mean (ng/mL)	Accuracy (%)	Precision (%CV)	Mean (ng/mL)	Accuracy (%)	Precision (%CV)	Mean (ng/mL)	Accuracy (%)	Precision (%CV)
Phenytoin	15.6	15.8	92.6	5.1	14.5	92.6	5.1	15.75	100.8	3.0
	62.5	59.6	102.7	5.9	64.2	102.7	5.9	62.9	100.7	1.2
	250	243.8	100.4	2.9	250.9	100.4	2.9	270.9	108.4	1.1
4-HPPH	15.6	17.1	109.1	1.9	17.5	112.3	5.5	15.8	101.4	4.0
	62.5	65.2	104.4	4.5	67.4	107.8	7.3	62.3	99.7	3.5
	250	266.9	106.8	4.8	285.8	114.3	2.7	263.9	105.6	1.4

Brain

Analyte	Nominal conc (ng/g)	Intraday 1 (n=3)			Intraday 2 (n=3)			Intraday 3 (n=3)		
		Mean (ng/g)	Accuracy (%)	Precision (%CV)	Mean (ng/g)	Accuracy (%)	Precision (%CV)	Mean (ng/g)	Accuracy (%)	Precision (%CV)
Phenytoin	46.9	51.7	110.2	5.0	49.3	105.2	3.6	48.4	103.2	4.6
	187.5	193.1	103.0	4.5	197.8	105.5	2.0	186.3	99.4	4.9
	750	777.8	103.7	3.8	777.6	103.7	4.5	751.1	100.1	1.4
4-HPPH	46.9	48.9	104.4	4.9	47.0	100.3	6.1	51.2	109.2	6.3
	187.5	180.9	96.5	4.0	186.7	99.6	5.7	190.2	101.5	1.8
	750	733.3	97.8	4.4	755.8	100.8	2.5	762.5	101.7	1.8

2.5.3 Validation of Pharmacodynamic Responses with Tissue Drug Concentrations

2.5.3.1 Pharmacokinetics

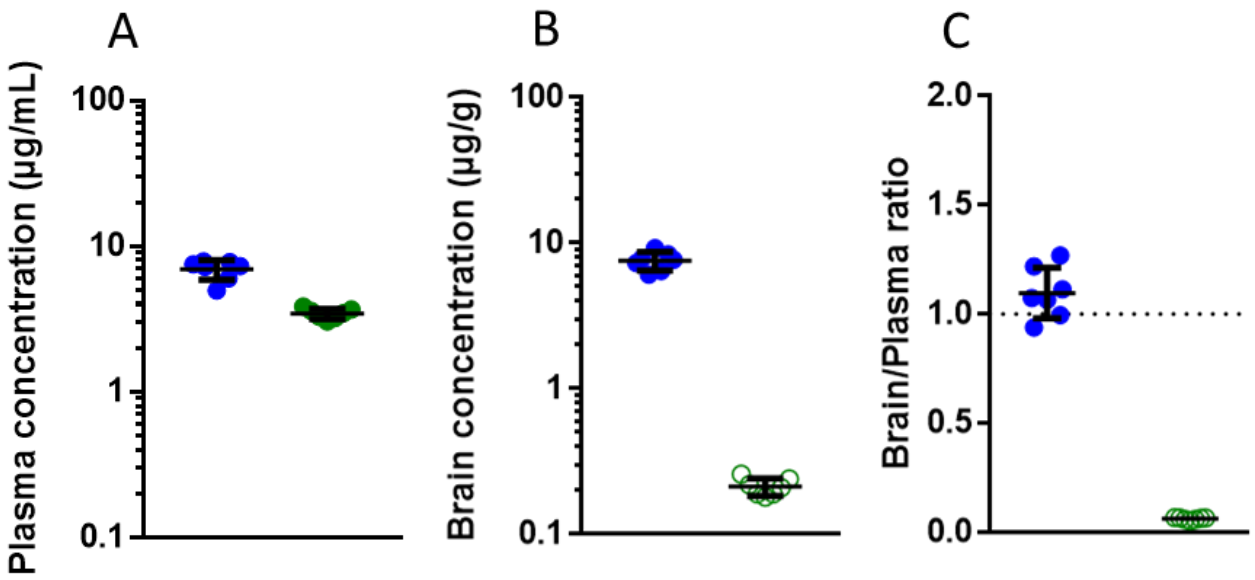

Figure 2.9. Plasma concentrations (A), brain concentrations (B) and brain/plasma ratio (C) of phenytoin (blue) and 4-HPPH (green) in rats stimulated at 60 minutes after intravenous phenytoin administration (25 mg/kg). Unfilled symbols represent data that was below the lower limit of quntification of the assay (or partially derived from such data in the case of the brain/plasma ratio). Note that the data is more accurately representative of tissue concentrations around 70 minutes due to the delay between seizure cessation and euthanasia, but is presented as 60 minutes for ease of comparison with the pharmacodynamic data.

The plasma and brain concentrations of phenytoin are presented in Figure 2.9. The mean plasma concentration (Figure 2.9A) was found to be 6.96 µg/mL (± 1.07 µg/mL), which is just below the lower limit of the textbook therapeutic range of 10-20 µg/mL[151]. One rat exhibited a lower plasma concentration than the rest which was attributed to an administration error resulting in a lower dose being given. This rat also exhibited FLE in the pharmacodynamic study (**Appendix F**). The mean concentration of 4-HPPH in plasma (Figure 2.9A) was found to be 3.45 µg/mL (± 0.28 µg/mL), which was to be expected given that 60 minutes has passed in which phenytoin would have begun to be metabolised. Plasma was also analysed for the rats which received intravenous saline for the final stimulation in order to confirm the successful washout of phenytoin after three days. Neither phenytoin nor 4-HPPH was detected within the quantifiable range in the plasma of these rats and was therefore considered to be absent.

The mean brain concentration of phenytoin (Figure 2.9B) was found to be 7.57 µg/g (± 1.09 µg/g), but this was not statistically different to the plasma concentration ($p = 0.3064$). On the contrary, the concentration of 4-HPPH (Figure 2.9B) was 0.21 µg/g (±0.03 µg/g) which was significantly lower than that found in plasma ($p < 0.0001$). The analysis of brain tissue of the saline-treated rats was not considered necessary given the absence in plasma, as stated above.

The brain/plasma ratio is also presented in Figure 2.9C, as this represents the average ratio of phenytoin and 4-HPPH in these compartments in individual rats which is not evident from the graphs of brain and plasma concentrations of the group. The Figure suggests a predominance of phenytoin in the brain compared to plasma (average ratio = 1.10 ± 0.12), which is consistent with the expected distribution of the drug and the pharmacodynamic effects observed, but this did not reach statistical significance ($p = 0.071$). Also shown is the marked lack of 4-HPPH in the brain compared with that in plasma (average ratio = 0.06 ± 0.01, which is consistent with the increased polarity and water solubility of the metabolite and was highly significant ($p < 0.0001$).

2.5.4 Validation of Animal Welfare

Based on the author's experience in researching the MEST procedure to establish this model, animal welfare considerations are an important element that is usually omitted from scientific literature. This study was a crossover trial involving multiple stimulations of the same animals, so it was scientifically, as well as ethically important to assess animal welfare over the course of the experiment to minimise confounding variables such as stress, which can impact seizure threshold[182,183]. The final results of this Chapter will therefore be a brief description of the animal experience during this introductory study as a reference for future users and to present the final validating evidence for its continued use in the following Chapters.

During the seizures, two adverse effects were noted in some rats within the group. Firstly, porphyrin discharge from the eyes and secondly tongue-biting, both of which were attributable to the intense muscle contractions that occur during a generalised seizure. After each stimulation, discharge was wiped from around the eyes if appropriate and a finger was wiped under the animal's mouth to sample the saliva for blood. In cases where tongue-biting was suspected, animals were given special attention during post-stimulation monitoring and none were noted to display signs of pain or have difficulty eating. All rats began behaving normally again within 30 minutes of a stimulation, but were less active than usual. Phenytoin-treated rats displayed less severe seizure behaviours and subsequently recovered much more quickly on the

day of the stimulation. By the following day, behaviour of all animals had returned to normal and they showed no evidence of residual effects.

Ear clips were reapplied without stimulation prior to the second and third stimulations to check for aversive responses that could suggest a fearful memory of the previous stimulation. No evidence was apparent to suggest that the animals remembered the previous stimulations. All rats behaved normally when the clips were reapplied and they were placed into the container, supporting the fact that they were unconscious throughout the seizures and the stimulation procedure had no noticeable impact on their psychological wellbeing. This was particularly important to consider for the phenytoin-treated rats which exhibited less severe and shorted duration seizure behaviours after stimulation, but were still unconscious during them and did not appear to have any negative memory of the procedure.

Finally, weight was monitored at least once daily over the duration of the experiment (Figure 2.10). A small decrease in weight appeared to occur in the 24 hours following each stimulation, but weight began increasing again within 36 hours (in all but one rat, whose weight continued to decrease very slightly until 48 hours post-stimulation) and all rats were gaining weight again by the time of the subsequent stimulation.

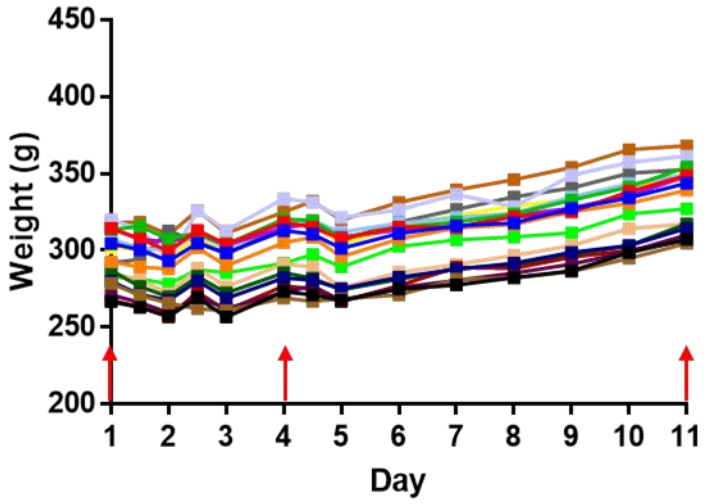

Figure 2.10. Weight progression of the rats over the course of the experiment. Days of the three stimulations are indicated by red arrows.

2.6 Discussion

This Chapter aimed to use intravenous phenytoin as a positive control to validate a suitable seizure model for testing the efficacy of intranasal drug delivery systems in the subsequent Chapters this thesis. While the proposed model was more complex compared with MES or traditional MEST experiments, the increased sensitivity and reduction in sources of variability was proposed to maximise its ability to detect anti-seizure effects after intranasal administration. Even at a glance, it was clear the model was successfully validated in this Chapter in that the intravenous dose of phenytoin prevented HLE in 100% of rats and FLE in 93 %, the latter incomplete protection being attributable to an incomplete dose delivered to one rat. While this result was expected based on the previous literature[99,172,174], it served as a demonstration of technical competency to perform the seizure induction procedure and the validity of the original crossover study design to detect it.

In order to statistically compare the pharmacodynamic data, Prescott's test was chosen[180]. This method presents an advantage over other tests of paired binomial data sets such as McNemar's test and the Mainland-Gart test in that it acknowledges both the possibility of a sequence effect (i.e. order that treatments were given in the crossover study) and the "no preference" group in the study which showed the same response regardless of treatment. Obviously in the present experiment the latter group was non-existent given the dose of the drug, but for intranasal experiments, where effects were expected to be more subtle, this was considered important to minimise error due to chance. As indicated above, Prescott's test confirmed the significance of the anti-seizure effect observed in this validation trial with p values of 0.003 and 0.0006 for HLE and FLE respectively.

As discussed earlier, the "up and down" method of Kimball et al.[100] is usually used to estimate the CC_{50} with 95% confidence limits with and without drug treatment in order to compare between the two[99,101]. Usually, the drug vehicle is used as a control treatment, but saline was used in the present study as the altered design of the present study presented a unique opportunity to actually test the accuracy of the estimated CC_{50} experimentally by examining the results from the saline treated rats, and therefore determine the resolution for detecting drug effects in the individual experiment. As shown in Figure 2.5, the CC_{50} was calculated to be 40 mA with a narrow confidence interval of 35-45 mA which ultimately translated to an appropriate 57% of rats displaying HLE experimentally upon stimulation at 40 mA. The

stimulation current was therefore shown to be an accurate estimation of the CC_{50} for HLE and supported the credibility of the "up and down" method to determine it in the subsequent studies.

As discussed in **Chapter One**, the need to administer an anaesthetic prior to intranasal dose delivery in the succeeding Chapters was an anticipated challenge given the potential for anaesthetics to affect seizure threshold and confound the effect of the test drug[157,184]. The anaesthetic chosen for use in this study was isoflurane given its short duration of action and rapid recovery profile (return of righting reflex within 7.5 ± 5.7 minutes and successful rotarod test within around 11.6 ± 4.7 minutes after half an hour of anaesthesia)[185] and recommendation for use by Impel Neuropharma (the manufacturers of the Rat Intranasal Catheter Device (RICD) used in **Chapter Three and Four**). It was administered prior to intravenous dosing in this Chapter in order to evaluate its influence, if any, on the experiment and the implications this might have for the intranasal experiments. The design of this study was proposed as a strategy to mitigate any effect of the anaesthetic by estimating the initial CC_{50} in rats after exposure to isoflurane without drug treatment and then stimulating treated rats at this CC_{50}. If the seizure threshold were altered by the isoflurane in any way, this should have been reflected in the CC_{50} and therefore still result in 50% of saline-treated rats showing HLE when stimulated at it, provided the threshold was not so high that the CC_{50} could not be calculated, in which case drug effects would most likely be concealed by the isoflurane anyway.

The results of the experiment in this Chapter were interesting in that the estimated CC_{50} at 60 minutes after isoflurane administration was actually lower than the estimate of 50 mA provided for untreated male Wistar rats in the literature[101]. This was considered to represent one of two things; either isoflurane unexpectedly had a pro-seizure rather than anti-seizure effect as suggested by one study[184] or it did not significantly affect seizure threshold at 60 minutes after administration. Previous studies have suggested that transauricular MEST stimulation, as used in this study, requires lower stimulus currents than transcorneal stimulation to achieve the same response[98]. Given that the 50 mA estimate in the literature was based on transcorneal stimulation, it is quite possible this, along with general variability in animal genetics within the Wistar species, resulted in the lower than expected CC_{50} rather than confounding from isoflurane. It was therefore considered most likely that after 60 minutes, the effect of isoflurane on seizure threshold was insignificant which supported the likelihood of the model being able to detect anti-seizure effects after intranasal administration, at least at studies proposed for this time point and beyond, in **Chapters Three and Four**. Regardless of any isoflurane contribution in any direction, the effects of phenytoin were clearly observed compared to the saline-treated

trial of each rat in this study. The subsequent question posed in **Chapter Three** would be whether the dose of phenytoin delivered in those intranasal experiments could achieve the same.

The above pharmacodynamic evidence all supported proceeding to studies of intranasal delivery using this model. As an additional means of validation, concentrations of phenytoin were quantified in plasma and brain tissue to support the attribution of the pharmacodynamic effect seen to phenytoin and the credibility of the tissue quantification method. Due to the obvious impracticalities associated with measuring brain concentrations in human patients, the therapeutic range of phenytoin is defined in humans and rodents by plasma concentrations. The dose of phenytoin chosen for this validation study was therefore based on other studies where a single dose of phenytoin was administered and reported to achieve therapeutic plasma concentrations in rodents (10-20 µg/mL total phenytoin[151]) that persisted for up to 60 minutes[175–177], as estimated from the provided figures and summarised in Table 2.5. Some studies also provided information on brain concentrations. The most closely relevant to this study is the data of Ogiso et al.[175] who provided phenytoin concentrations in brain and CSF, although it should be noted that they administered an in-house solution consisting of saline and propylene glycol (20:80 v/v) rather than the commercial formulation which might have influenced drug behaviour[134]. Walton et al.[186] also provided data on brain concentrations, but only up to 30 minutes. Nonetheless, the concentrations during this time frame appeared more or less consistent with the former study suggesting extrapolation would have supported the above data at 60 minutes. Wang and Patsalos[176] provided CSF concentrations only, but given that these were consistent with those reported by Ogiso et al.[175] at 60 minutes, it is likely that brain concentrations would have been too.

Table 2.5. Plasma, brain and CSF concentrations reported at 60 minutes after intravenous phenytoin administration to male rats at comparable doses to those used in the present study.

Study	**Rat gender and strain**	**Phenytoin dose**	**Average concentration after 60 minutes**		
			Plasma (µg/mL)	Brain (µg/g)	CSF (µg/mL)
Ogiso et al.[175]	Male Wistar	20 mg/kg	10	12	1.5
Gerber et al.[177]	Male Sprague-Dawley	25 mg/kg	12	-	-
Wang & Patsalos[176]	Male Sprague-Dawley	30 mg/kg	10	-	2

The average plasma concentration in the present study (6.96 ± 1.07 µg/mL) appeared to be similar, but lower than that reported elsewhere. The same was noted for the average brain concentration (7.57 ± 1.09 µg/g) compared with Ogiso et al.[175]. The difference may have been due to variations in the methodology of the studies described above (e.g. differences in dose, administration site, rat strain, rat age/weight or analytical method sensitivity) but to some extent may also have reflected the delay between stimulation and euthanasia of each rat which in a number of cases was up to ten minutes. However, additional studies by Kim et al.[187] and Kim et al.[188], found retrospectively, in which male Sprague-Dawley rats were given a 25 mg/kg intravenous dose of phenytoin reported average plasma concentrations of ~7.5 µg/mL, which support that the concentration found in the present study was reasonable at 60 minutes after administration.

Despite plasma concentration being slightly below the lower limit of the textbook therapeutic range of 10-20 µg/mL at 60 minutes in this study, the plasma concentration was still clearly adequate to elicit a significant anti-seizure effect at this time point. This might be seen as a reflection of the sensitivity of the model used due to stimulation at the CC_{50} threshold. As an illustration of this, Loscher et al.[174] reported a significant anti-seizure effect (~35 mA increase in seizure threshold) of phenytoin in the MEST test at 60 minutes after a 15 mg/kg dose, while after a supramaximal stimulus in the MES test by Loscher et al.[99] after the same dose and at the same time point, the anti-seizure effect was poor (~10% protection from HLE). No phenytoin could be quantified in the plasma of saline-treated rats in the present study which confirmed adequate washout of phenytoin from the previous experiment and that the pharmacodynamic results in these rats reflected responses to stimulation in the absence of phenytoin. It is not possible to comment on whether the average brain concentration found in phenytoin rats in this study was technically inside or outside the brain therapeutic range, as this is not defined in the literature and is a complex concept given the potential for regional distribution, however clearly it was also adequate to elicit the anti-seizure effect despite being lower than might have been expected from the data of Ogiso et al.[175].

In addition to presenting the average brain and plasma concentrations of phenytoin, the present study also calculated the brain to plasma ratio of phenytoin for individual rats. As shown in Figure 2.9, this yields a more accurate result than just comparing the averages of brain and plasma concentrations as was done in the other mentioned studies. As can be seen in the Figure (Panel C), the average brain/plasma ratio was 1.10 ± 0.12 suggesting an accumulation of phenytoin in the brain compared to plasma which is consistent with the other reports described

above[175,186]. Walton et al.[186] noted a retention of phenytoin in the brain while average plasma concentration started to decrease which they attributed to phenytoin binding to sites in the brain parenchyma and therefore delaying its diffusion back out into the plasma. As noted earlier, they only measured up to 30 minutes, but the same elevation of average brain concentration above plasma is reflected in the data of Ogiso et al.[175] up to 60 minutes as is evident in the data from the present study. This weighting towards the brain appeared to subsequently disappear between 60 minutes and the next time point they measured at 120 minutes suggesting a shift towards elimination of phenytoin from the brain after 60 minutes at this dose. Interestingly, the results of Kim et al.[188] disagreed with this pattern, reporting a brain to plasma ratio of around 0.45 at their measured time point of 30 minutes after administration, but given the anomalous nature of this finding it is suspected that this may have been a result of the analytical method used for brain tissue for which few details were disclosed regarding the validation of analyte detection.

The major metabolite of phenytoin, 4-HPPH, is less commonly measured in the literature, but was measured in conjunction with phenytoin in the present study in order to more accurately evaluate its pharmacokinetics. The most comparable study found in the literature was that of Kim et al.[187] who, as mentioned earlier, injected a commercial solution of phenytoin intravenously into male Sprague-Dawley rats at a dose of 25 mg/kg and found both phenytoin and 4-HPPH plasma concentrations very similar to those in the present study. No data was provided on 4-HPPH brain concentrations in this study, but the omission of brain tissue data from the figure presenting 4-HPPH tissue to plasma ratios at 30 minutes while this was shown in an equivalent figure for phenytoin suggests that it was not detectable in the brain. This is consistent with the very low brain to plasma ratio of 4-HPPH shown in Figure 2.9B of the present study, showing the poor penetration of the metabolite into the brain from plasma. The fact that some was able to be detected in the brain could be a combination of the increased sensitivity of the analytical method used here and the later time point (60 minutes vs 30 minutes) at which the sample was collected. Further support of the low brain permeability of 4-HPPH is provided by DeVane et al.[189] who were unable to detect any brain 4-HPPH, in this case in the maternal rat brain, over 16 hours after a 30 mg/kg intraperitoneal dose of phenytoin. The peak 4-HPPH plasma concentration was relatively low (~1 µg/mL) in this study, possibly due to slower metabolism in female rats[99], especially in pregnancy[190].

2.7 Conclusions

The results of this Chapter demonstrated the validity of a new study design based on the MEST test for assessing the effects of drug therapy on seizure threshold with increased sensitivity and reduced variability. It was demonstrated experimentally that the CC_{50} could be accurately estimated using the "up and down" method in a group of rats, that the known anti-seizure effect of phenytoin could be clearly detected and that isoflurane administration 60 minutes prior to stimulation did not appear to influence the ability for the effects of phenytoin on seizure threshold to be detected. Phenytoin and its major metabolite 4-HPPH behaved as expected in terms of pharmacokinetics, not only supporting the pharmacodynamic data, but also the validity of the quantification method developed to measure them. These findings combined with the ability to perform this procedure with minimal impact on animal welfare provided a solid foundation on which to proceed to the next Chapter which aimed to evaluate an intranasal drug delivery system and test the capabilities of the model in detecting anti-seizure effects following the intranasal delivery of phenytoin.

Chapter Three

On the Intranasal Delivery of Phenytoin

3.1 Introduction

Phenytoin was the first non-sedating anti-seizure drug to be discovered, emerging in the early 1900s near the dawn of the pharmacological ASD age following the serendipitous discovery of the anti-seizure effects of phenobarbital[191]. It is thought to act by modifying ion transport to reduce post-tetanic potentiation in seizure foci and pathways and by selectively decreasing high frequency action potentials while having few CNS side effects at therapeutic doses[192,193]. Its primary mode of action is to prevent or reduce propagation of a seizure from its area of origin[192]. It is a powerful, fast-acting, long-acting and useful anti-seizure drug for generalised and partial seizures that is widely used, but has fallen out of favour in some circles over time due to a perception of an increased likelihood and severity of adverse effects compared to newer ASDs[194,195]. While conclusive evidence appears to be lacking to support this perception, as well as whether it is any more or less effective at controlling seizures than its alternative first line counterparts such as sodium valproate[194,196,197], its relative pharmacokinetic complexity after systemic administration cannot be denied and lends to the clinical attractiveness of its successors.

Phenytoin is a poorly water soluble drug, available in oral and intravenous formulations as a sodium salt. Upon systemic administration it is highly bound by plasma proteins (90%) necessitating elevated doses to maintain free plasma concentrations within its narrow therapeutic range and allow sufficient phenytoin to cross into the brain. It undergoes hepatic metabolism primarily by the cytochrome P450 (CYP) enzymes CYP2C9 and CYP2C19 to produce the pharmacologically inactive and slightly water soluble major metabolite 5-(4-

hydroxyphenyl)-5-phenylhydantoin (4-HPPH), which is subsequently metabolised to the very water soluble 4-HPPH-O-glucuronide and excreted in the urine[198]. Complexity arises because the conversion to 4-HPPH is saturable within the narrow therapeutic range, imparting a non-linear and dose-dependent pharmacokinetic elimination profile to the drug which also exhibits significant interpatient variability[198,199]. The consequences of this are illustrated in Figure 3.1.

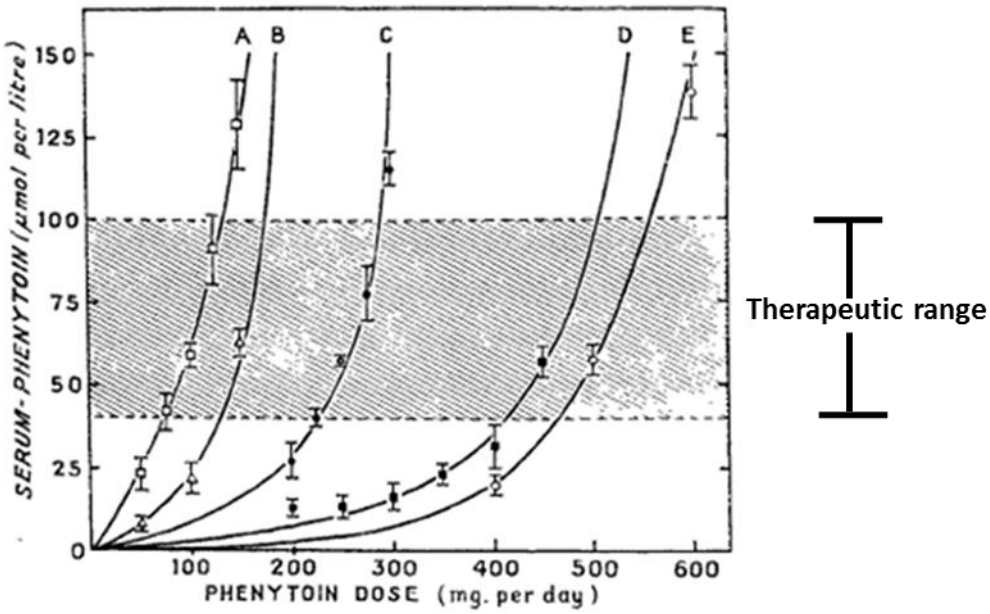

Figure 3.1. Illustration of the effect of non-linear pharmacokinetics on phenytoin dosing in five different human patients. Figure adapted with permission from Richens & Dunlop[199]. The grey shaded area indicates the therapeutic range of phenytoin.

The final contributor to the unpopularity of phenytoin has been that it is a substrate for the multi-drug transporter P-glycoprotein (P-gp)[200]. P-gp is highly expressed in brain capillary endothelial cells and functions as a protective efflux transporter, ejecting molecules back out into the blood plasma rather than permitting them passage into the brain parenchyma (Figure 3.2)[9]. It is this transporter that links phenytoin to the multi-drug transporter (MDT) hypothesis of drug-resistant epilepsy. The hypothesis proposes that the high rates of ASD treatment failure discussed in **Chapter One** may be, at least in part, due to an upregulation of P-gp (and other efflux transporters) in the epileptic focus of the brain and subsequent reduction in drug levels to sub-therapeutic concentrations[9,201,202]. It has been the subject of extensive study over the past few decades and has spawned new animal models; of particular interest, the phenytoin-resistant kindled rat[122,174,203], which supported the idea that humans with epilepsy could also develop resistance to phenytoin and other ASD substrates as a result of transporter upregulation[9,133].

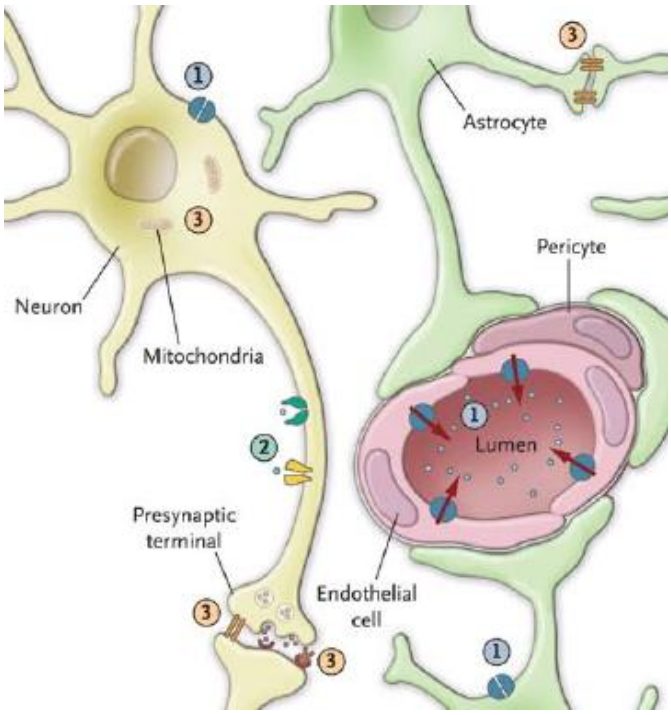

Figure 3.2. Efflux of phenytoin at the blood brain barrier by P-glycoprotein (P-gp). Efflux transporters are indicated by the number 1. Figure reprinted with permission from Kwan et al.[9]*. Copyright Massachusetts Medical Society. The other numbers indicate alternative proposed resistance mechanisms, namely, altered expression or function of voltage-gated ion channels (2) and mechanisms not currently targeted by marketed ASDs such as mitochondrial dysfunction, autoantibodies to neurotransmitter receptors and gap junctions (3).*

The systemic challenges of phenytoin clearly leave a lot to be desired. The concept of delivering it via a direct intranasal route to the brain, without the need to navigate the systemic circulation, is therefore an enticing possibility. Such a delivery route could theoretically reduce dosage requirements and variability by bypassing pre-CNS plasma protein binding, metabolism and P-gp efflux while also providing improved targeting of phenytoin to key regions involved in seizure spread, as discussed in **Chapter One**, where it is likely to exert its greatest effect. Also based on the discussions in that Chapter, the poor aqueous solubility of phenytoin dictates that formulation into a suitable drug delivery vehicle is a necessary prerequisite to successful administration via an intranasal route.

The idea has been lightly explored in the literature outside the present author's lab group. Firstly, the reader may recall the intranasal phenytoin microemulsion study of Acharya et al.[128] referenced in **Chapter One**, but if so, also the associated discussion of its shortcomings. Secondly, Kapoor et al.[21] recently reported formulation of a supersaturated phenytoin solution, but abandoned the idea of further testing in favour of an intranasal benzodiazepine, on their presumption that phenytoin would not be sufficiently potent for intranasal administration

because it requires grams as an intravenous loading dose for seizure emergencies. This logic would seem to overlook the complex pharmacokinetics discussed above which contribute to this requirement for large systemic doses and their potential to be bypassed by exploiting a direct nasal route.

By far, the most extensive study of a phenytoin intranasal delivery system is that performed within this author's lab group by Yarragudi et al.[204] who developed spray-dried muco-adhesive tamarind seed polysaccharide (TSP)-based phenytoin microparticles (MPs), tailored to a 10 µm size to maximise deposition in the olfactory region of the nasal passage (Figure 3.3). The formulation of phenytoin with the polymer was optimised so that it existed in an amorphous (i.e. non-crystalline) state in order to facilitate solubility and release and encapsulated the drug with an efficiency of 96%.

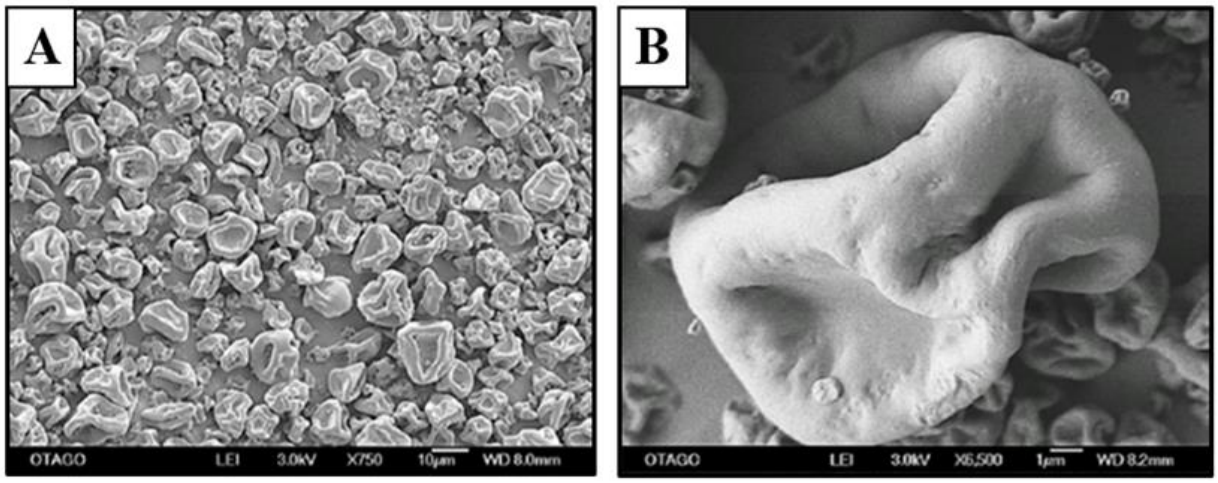

Figure 3.3. Scanning electron micrographs of phenytoin-containing TSP microparticles, as presented by Yarragudi et al.[204]

While two other studies have pitched the concept of phenytoin microparticles (formulated with alginate-chitosan and Poly(ε-Caprolactone respectively), their experiments did not go further than fundamental physical characterisation[205,206]. Yarragudi et al.[204] performed physical, *in vitro* and *ex vivo* characterisation, as well as preliminary investigations on histopathology and *in vivo* pharmacokinetics which suggested a sustained release and direct nose-to-brain delivery of phenytoin (Figure 3.4), as well as decreased systemic exposure with regards to other major organs.

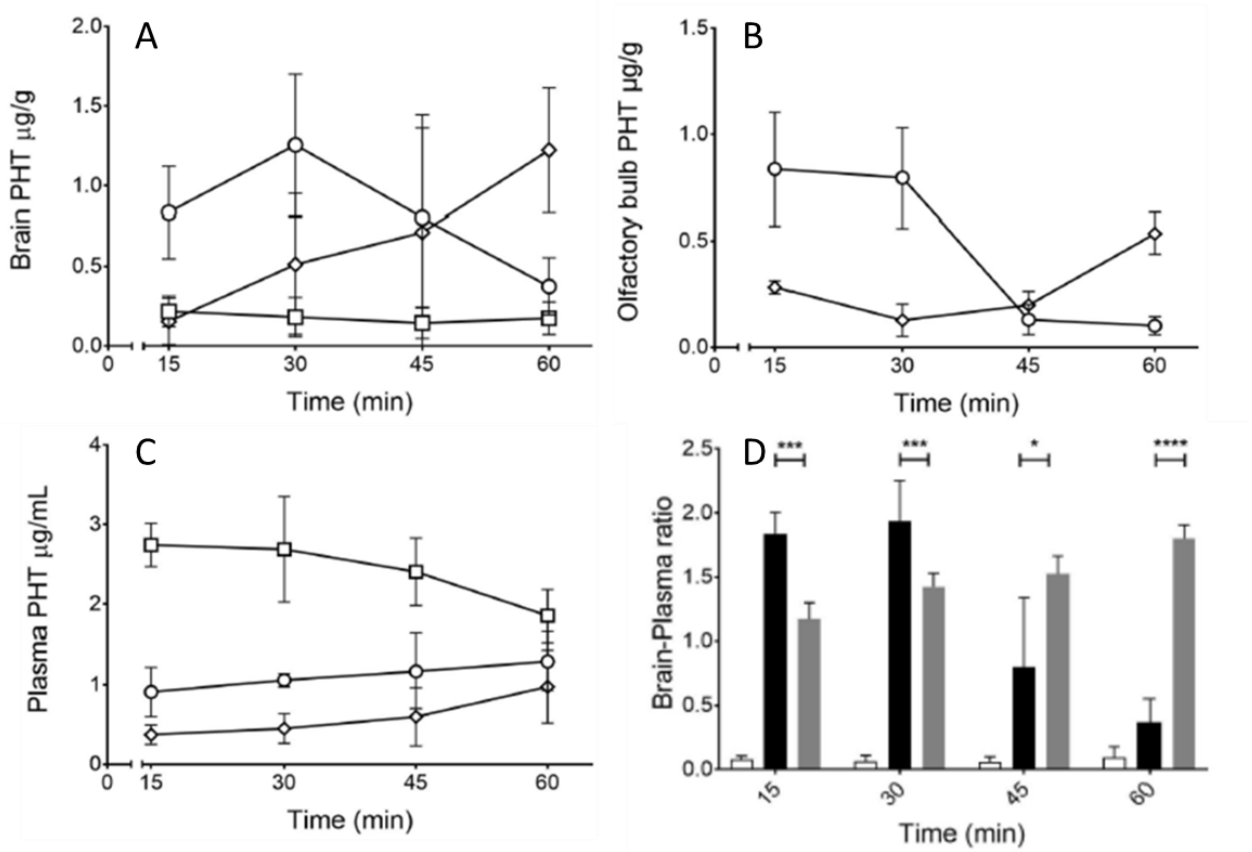

Figure 3.4. Intranasal pharmacokinetics of phenytoin (PHT) after in vivo administration of phenytoin microparticles, as presented by Yarragudi et al.[204] Phenytoin concentrations in the brain (A), olfactory bulbs (B) and plasma (C) are shown, along with the brain to plasma ratio (D). Intravenous solution (square/white bars), intranasal solution (circles/black bars), intranasal microparticles (diamonds/grey bars).

The results of that study set the premise for this **Chapter** which explores whether the previously reported pharmacokinetics translate to any biological effect in the seizure model established in **Chapter Two** and offers further insight into histological effects on the nasal epithelium and regional brain distribution (in this case, after an actual seizure).

3.2 Aims

The overarching aim of this Chapter was to apply the MEST model established in **Chapter Two** to the study of an intranasal delivery system, namely, phenytoin microparticles. To evaluate this application and therefore the ability of the model to detect an intranasally-mediated effect, the following objectives were set:

- Determine the anti-seizure effect of phenytoin microparticles compared to a phenytoin control solution after intranasal administration.
- Determine the plasma and brain tissue levels of phenytoin and its major metabolite (4-HPPH) after intranasal administration of phenytoin in microparticles and control solution in the seizure-tested rats.
- Determine the effects of phenytoin microparticles and control solution on the integrity of the nasal epithelium of the seizure-tested rats over the course of the study.
- Determine the anti-seizure effect of blank microparticles without phenytoin at the determined time of peak effect of phenytoin microparticles to exclude a vehicle contribution.

3.3 Hypotheses

The hypotheses for this Chapter were founded on the *in vivo* studies of Yarragudi et al.[204] with phenytoin microparticles as outlined in Figure 3.4. It was hypothesised that:

- The MEST model established in **Chapter Two** will be able to detect anti-seizure effects after intranasal administration.
- Intranasal microparticles will facilitate a direct nose-to-brain delivery of the anti-seizure drug phenytoin to a sufficient level to demonstrate an anti-seizure effect in the seizure model.
- The anti-seizure effect of intranasal phenytoin microparticles will be greater than that observed after administration of intranasal phenytoin control solution.
- Tissue levels of phenytoin and its major metabolite, 4-HPPH, will complement the anti-seizure effects observed.
- Increased levels of phenytoin will be found in the olfactory bulbs and/or brainstem compared to the rest of the brain due to the drug reaching the CNS via a direct route associated with neuronal pathways that exist in the nasal mucosa.
- Phenytoin microparticles will not disrupt the integrity of the olfactory mucosa to achieve their drug delivery while phenytoin control solution will cause some disruption due to the solvents required to solubilise the drug.
- Blank microparticles which do not contain phenytoin will not have any effect in the seizure model after intranasal administration.

3.4 Materials & Methods

3.4.1 Materials

Tamarind gum powder was purchased from Xi'an Jiatian Biotechnology (China). Phenytoin (5,5-diphenylhydantoin) sodium injection (250 mg/5 mL) (DBL™ Phenytoin injection BP) was purchased from hameln pharmaceuticals GmbH (Germany). Isotonic (0.9 %) saline was purchased from Baxter (Australia). Isoflurane was provided by the Hercus-Taieri Resource Unit, University of Otago. Phenytoin sodium, 4-HPPH (5-(4-Hydroxyphenyl)-5-phenylhydantoin), propylene glycol (PG), formic acid (for mass spectrometry, ~98%) and phosphate-buffered saline sachets (pH 7.4) were purchased from Sigma Aldrich (New Zealand). Deuterated phenytoin (d_{10}-phenytoin; (5,5-(diphenyl-d_{10}) hydantoin)) was purchased from Toronto Research Chemicals (Canada). All water used in this study was ion exchanged, distilled and passed through a Milli-Q water purification system (Millipore, USA). Acetonitrile (ACN) (LiChrosolv®), Methanol (MeOH) (LiChrosolv®), tert-Butyl Methyl Ether (TBME) (LiChrosolv®) and Ethanol (EMSURE®) were purchased from Lab Supply (New Zealand). All of these solvents were liquid chromatography grade. Male Wistar rat plasma and brain tissue for LC-MS method validation and standard preparation was obtained in-house from control rats administered saline treatments.

3.4.2 Animals

All procedures involving animals were approved by the University of Otago Animal Ethics Committee pursuant to Animal Use Protocol 72/16. Male Wistar rats sourced from the Hercus Taieri Resource Unit were used in all experiments. Specific weights and ages of animals over the course of the experiments can be found in **Appendix A and B**. Animals were housed under laboratory conditions in the Hercus Taieri Resource Unit for the duration of the experiment.

3.4.3 Isolation of TSP and Preparation of Microparticles

Tamarind seed polysaccharide was isolated from tamarind gum powder as described by Yarragudi et al.[207] A 20 g quantity of tamarind gum powder was dispersed in 1 L of Milli Q water and brought to a boil for 20 minutes under constant stirring (800 rpm). Following this, the dispersion was left overnight at ambient temperature to allow protein and fibre sedimentation to occur. The following day, it was centrifuged at 4700 G for 25 minutes (Heraeus Multifuge X3FR, Thermo Fisher Scientific, New Zealand) before the supernatant was separated and mixed with twice the volume of absolute ethanol to form a TSP precipitate. The

precipitate was separated and washed with Milli Q water before being placed in a 60 ºC oven for 12 hours. The dried film of purified TSP was then crushed into flakes and stored in a dessicator until required.

Microparticles were prepared using a Mini Spray Dyer **(**Büchi B-290, Büchi Labortechnik AG, Switzerland) as described by Yarragudi et al.[204,207]. The feed solution for blank microparticles was prepared by adding 4 g of purified TSP to 200 mL of Milli Q water which was constant stirred for at least 2 hours at a temperature of 60 ºC before cooling to ambient temperature. The feed solution for phenytoin microparticles was prepared by the same method, except that 50 mL of Milli Q water was replaced by 50 mL of a phenytoin dispersion. The latter was prepared by dispersing 1 g of phenytoin sodium in 2 mL of propylene glycol by sonication then adding 48 mL of Milli Q water and constantly stirring at 60 ºC for one hour before addition to the TSP dispersion (3 g of TSP and 150 mL of Milli Q water) which was then stirred for at least a further two hours at 60 ºC before allowing to cool to ambient temperature. Feed solutions were spray-dried using a standard nozzle cap with an orifice diameter of 0.7 mm. Spray drying parameters were as described by Yarragudi et al.[204]: feed solution flow rate = 2 mL/min, inlet temperature = 120 ºC, outlet temperature = 75 ºC, atomising airflow = 574 L/h and aspiration = 55%. Dried microparticles were collected and stored in a desiccator until required.

3.4.4 Preparation of Phenytoin Control Solution

The phenytoin control solution was based on that used by Yarragudi et al.[204] and was prepared by dissolving phenytoin sodium in a mixture of ethanol (50%), propylene glycol (10%) and water (40%) with a brief sonication. The solution was kept at 37 ºC immediately prior to administration in order to maintain a solution of phenytoin with no visible precipitate.

3.4.5 Drug Administration

3.4.5.1 Isoflurane Anaesthesia

Preliminary experiments determined that it was necessary to anaesthetise the animals briefly in order to successfully administer the intranasal dose to the olfactory region and avoid causing stress and reflexive sneezing. Animals were therefore anaesthetised by placing in a chamber with 5 % isoflurane and an oxygen flow rate of 1 mL/minute for three and a half minutes. The duration was determined in preliminary experiments to be sufficient to prevent the sneeze reflex in most animals for around one minute after removal from the chamber in order to permit intranasal administration.

3.4.5.2 Intranasal Microparticle Administration using an Intranasal Insufflator

Microparticles were loaded into the needle chamber and weighed before attachment to the rest of the insufflator apparatus. Each rat was anaesthetised with isoflurane for three and a half minutes as described above. The unconscious rat was then removed from the chamber and laid on the bench in a supine position. The blunt needle at the tip of the insufflator was promptly and gently positioned inside one nostril so it was directed downwards towards the olfactory region (Figure 3.5). Rotation of the stopcock handle of the insufflator enabled the syringe to be filled with compressed air by applying pressure to the plunger. The stopcock was then opened to spray the powder out through the needle tip. After administration, the needle was carefully withdrawn and removed so that it could be weighed again to enable estimation of the dose delivered. Average weights of phenytoin microparticles administered are given in **Appendix G**. The rat was moved to a recovery cage and returned to an upright position while regaining consciousness. Where animals received two intranasal doses over the course of the experiment, the alternate nostril was used in the second experiment (i.e. each nostril was only used once).

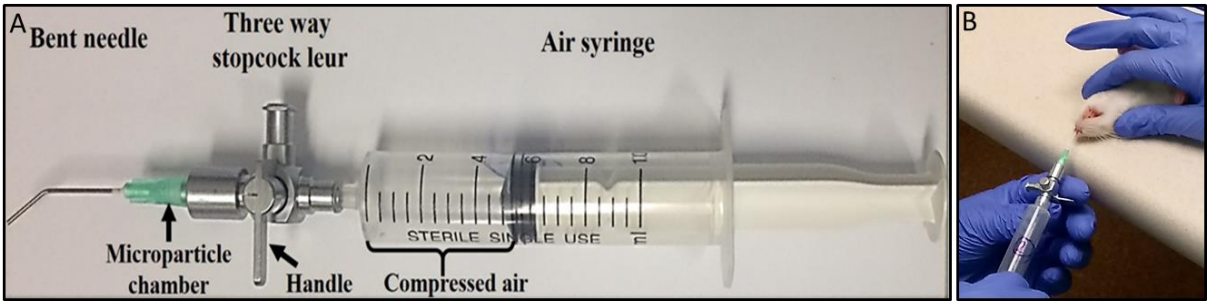

Figure 3.5. Intranasal microparticle insufflator (constructed in-house, based on the design of the Penncentury™ dry powder insufflator) used for microparticle administration in this study (A). It consisted of a 10 mL Luer Lock syringe, three way stopcock a 21 G needle bent at a 45 º angle 1 cm from the tip to direct the dose to the olfactory region. Intranasal microparticle administration technique (B). Figure adapted from Yarragudi et al.[204].

3.4.5.3 Intranasal Phenytoin Solution Administration using a Rat Intranasal Catheter Device (RICD)

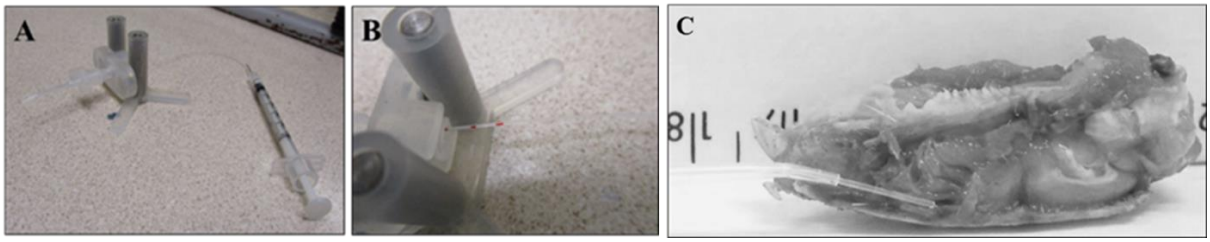

Figure 3.6. Apparatus used for the intranasal administration technique. (A) PE tubing attached to a syringe and threaded through the rat intranasal catheter device (RICD), ready for administration (B) Markings on the tubing to guide insertion distance (C) Demonstration of how the RICD targets the olfactory region in a sagittally-dissected rat nasal passage.

A 15 cm long piece of PE 10 tubing (Fort Richard Laboratories, New Zealand) was threaded onto the 29 G needle of a 0.3 mL BD® Ultrafine Lo-dose insulin syringe (BD Biosciences, New Zealand). Drug solution was drawn into the syringe through the tubing and adjusted to a volume of 20 µL. The tubing was then threaded into a Rat Intranasal Catheter Device (RICD) (Impel Neuropharma, USA) in preparation for administration (Figure 3.6). Each rat was anaesthetised with isoflurane for three and a half minutes as described above. The unconscious rat was then removed from the chamber and laid on the bench in a supine position. The tip of the RICD was promptly and gently positioned inside one nostril and the tubing gently guided in until 1 cm had entered the nasal cavity. At this point, the syringe was gently depressed to administer the dose. The apparatus was held in position for 5 seconds following administration, then was gently pulled out of the nasal cavity. The rat was then moved to a recovery cage and returned to an upright position before regaining consciousness. As described above, where animals received two intranasal doses over the course of the experiment, the alternate nostril was used in the second experiment (i.e. each nostril was only used once).

3.4.6 Maximal Electroshock Stimulation Threshold Test

The MEST experiments were performed in accordance with the stimulation procedure and cross-over study design outlined in **Chapter Two**.

3.4.7 Tissue Collection and Histological Processing

Tissues were collected and processed in order to quantify brain concentrations of phenytoin and 4-HPPH (as in **Chapter Two**) and to study the effects of phenytoin microparticles and solution on the olfactory epithelium in rats that had participated in the pharmacodynamic MEST experiments. Rats were euthanised by guillotine decapitation within 10 minutes of the final MEST stimulation. Trunk blood was collected in a 6 mL blood tube coated with sodium heparin (BD Biosciences, New Zealand) at the time of euthanasia and centrifuged at the conclusion of the experiment (2000 G for 10 minutes at ambient temperature (Heraeus Multifuge X3FR, Thermo Fisher Scientific, New Zealand). The brain, brainstem and olfactory bulbs were also dissected and kept on ice until the conclusion of the experiment, after which they were frozen and kept at -80 ºC until required for LC-MS analysis.

In the 60 minute phenytoin microparticles and phenytoin solution MEST studies, the nasal cavity was dissected and preserved for histological analysis at the conclusion of the experiment as outlined in Figure 3.7. The eyes, lower jaw and excess skin and tissue around the nasal passage were removed from the skull after dissection of the brain. A blunt needle was inserted 0.5 cm into the posterior nasopharyngeal duct and used to flush the nasal passage with 10 mL of 10% neutral buffered formalin (NBF). Subsequently, the nasal passage was fixed in 50 mL of NBF for 48-72 hours. The fixed nasal passage was then decalcified in 10% ethylenediaminetetraacetic acid (EDTA) (pH 7.2) for two to three weeks, sliced coronally into blocks, as per published methods[83,150] and embedded in paraffin wax. A microtome (Leica Jung RM 2025, Leica Biosystems, Australia) was used to cut 5 µm sections from region III which were subsequently deparaffinised, stained with haemotoxylin and eosin, and cover-slipped with dibutylphthalate polystyrene xylene (DPX) mounting medium. Sections were imaged on an Aperio ScanScope (Leica Biosystems, Australia). Images were analysed using Aperio ImageScope v12.2.2.5015 software (Leica Biosystems, Australia).

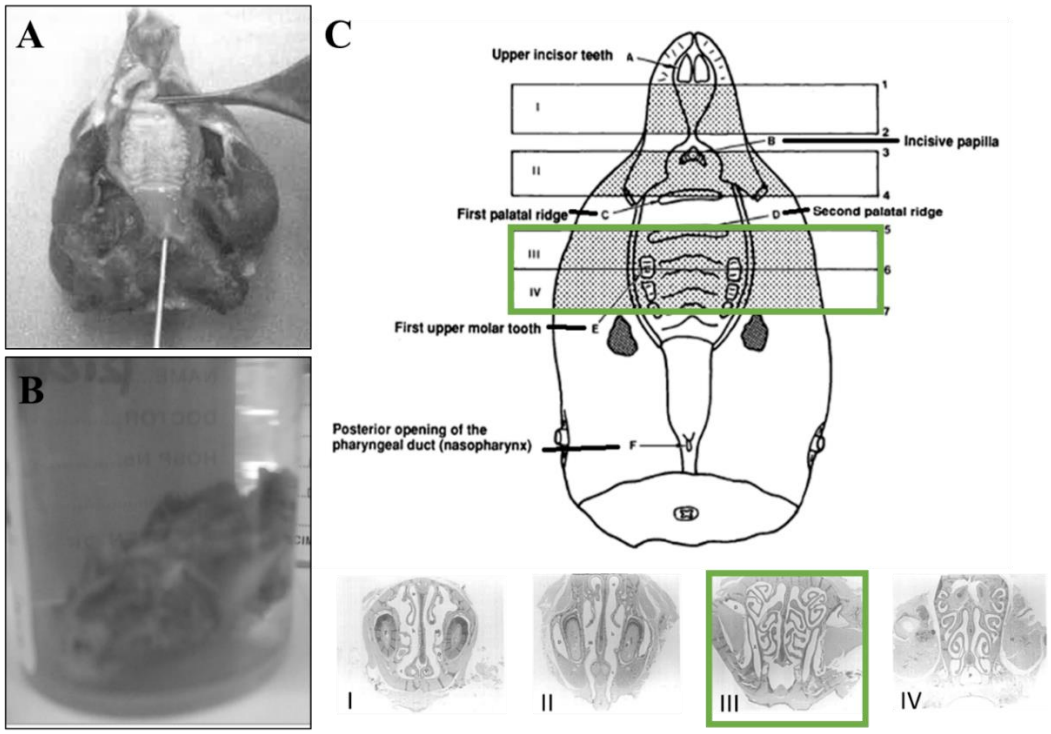

Figure 3.7. Histological processing method for nasal tissue. (A) Demonstration of the procedure for flushing the nasal cavity with 10% NBF. Image reprinted with permission from Everitt & Gross.[208] (B) Dissected rat skull undergoing fixation in 10% NBF. (C) Recommended sectioning sites for assessment of toxicity to different regions of the nasal passage. Sections from the faces of Regions I, II, III and IV are shown below the main diagram. The green box indicates the region that is used in this study. Figure adapted with permission from Young.[150]

3.4.8 LC-MS Method for Analysis of Phenytoin and 4-HPPH in Plasma and Brain Tissue

LC-MS quantification of phenytoin and 4-HPPH concentrations in plasma and brain tissue of rats from all MEST studies was performed and analysed in accordance with the validated method outlined in **Chapter Two**. The brain was dissected into three regions (olfactory bulbs, brainstem and main brain) for these studies in order to compare relative levels and their possible relationship to hypothesised routes of intranasal delivery. Standard curves were prepared using homogenates from each of these brain regions and compared to assess for any variation which could affect the relative quantification.

3.5 Results

3.5.1 Pharmacodynamic Evaluation at 60 Minutes After Intranasal Treatment

The first trial to detect an anti-seizure effect was performed at 60 minutes after treatment, based on the pharmacokinetic study of Yarragudi et al.[204] (Figure 3.4) which reported the highest phenytoin concentrations after intranasal phenytoin microparticles at this time point. Phenytoin control solution, as used by Yarragudi et al.[204], was also tested at this time point for comparison as levels in the brain were expected to be low compared to those after phenytoin microparticle administration by this stage.

The CC_{50} and control responses to stimulation for these studies are shown in Figure 3.8. The rats in the phenytoin microparticles group had a calculated CC_{50} of 63 mA (95% CI: 47-83 mA) (Figure 3.8A), which translated to 55 % of rats exhibiting HLE after intranasal saline administration in the experimental control data (Figure 3.8B). In the phenytoin control solution group, the calculated CC_{50} for the group was 47 mA (95% CI: 41-54 mA) (Figure 3.8C) and 61% of saline-treated rats subsequently exhibited HLE (Figure 3.8D). All saline-treated rats in both groups displayed FLE.

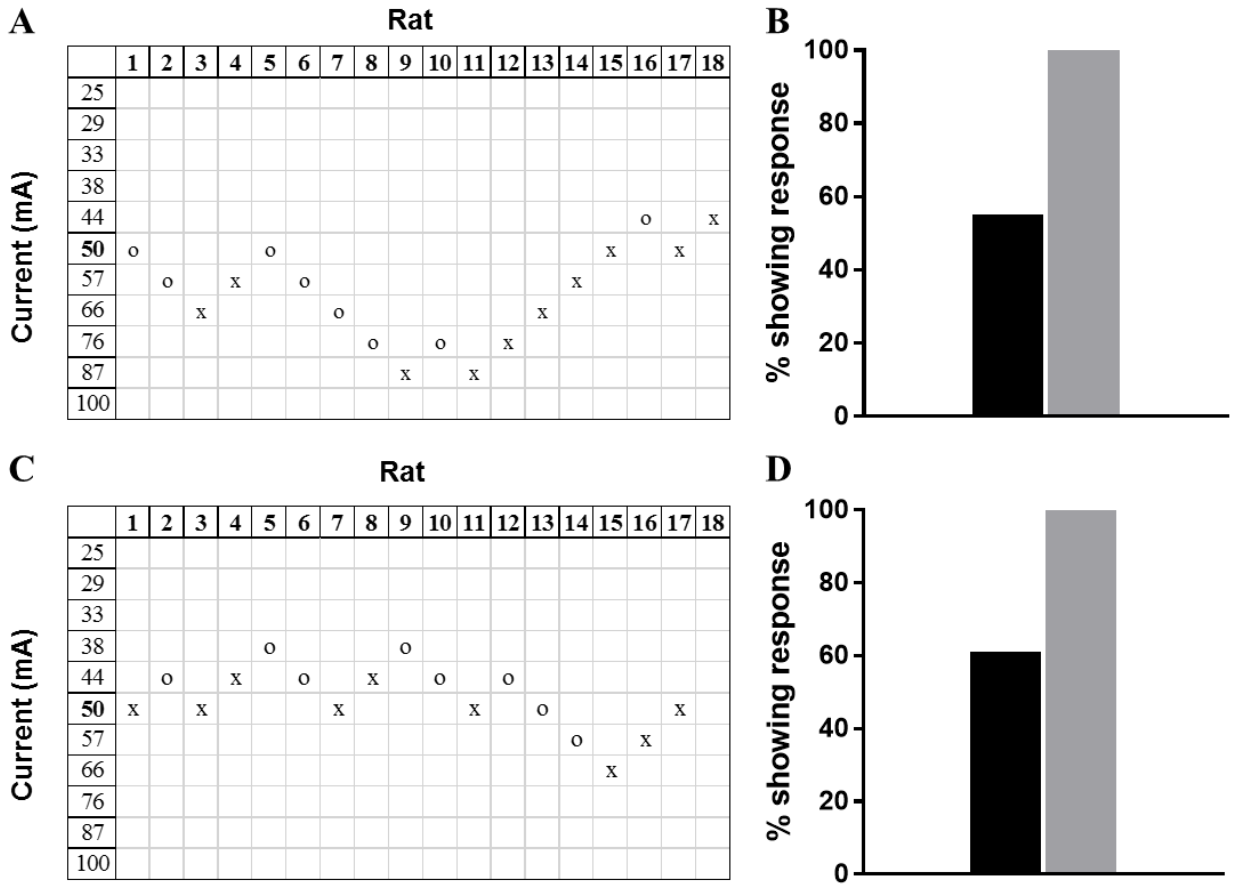

Figure 3.8. Determination of the CC_{50} and baseline response to stimulation at the CC_{50} in the batches of rats that participated in the study of intranasal phenytoin microparticles (A and B) and phenytoin control solution (C and D) at 60 minutes. The panels on the left (A and C) show the experimental data from the up and down method which was used to estimate the CC_{50}, where "X" represents HLE and "O" represents no HLE. The panels on the right (B and D) show the baseline responses of the rats when stimulated at the calculated CC_{50} 60 minutes after intranasal saline administration and serve as an indication of the accuracy of the estimated CC_{50} and the resolution for detecting anti-seizure drug effects. The black bar represents the percentage of rats which exhibited HLE at the calculated CC_{50} and the grey bar represents those which exhibited FLE (with or without HLE).

Figure 3.9 shows the effect of phenytoin microparticles and phenytoin control solution at 60 minutes after intranasal administration. No statistically significant decrease in HLE was associated with phenytoin microparticles at 60 minutes, despite the incidence of HLE being calculated to be 17% lower in the phenytoin microparticles group ($p = 0.8$) and they had no effect on FLE. Unexpectedly (recalling the data of Yarragudi et al.[204] in Figure 3.4), phenytoin solution at this time point was more effective, decreasing HLE by 64% ($p = 0.0136$). The incidence of FLE after phenytoin solution was still not statistically different however,

calculated as 6% less due to the response of a single rat (p = 1). To investigate this result further, pharmacokinetic and histological studies were performed.

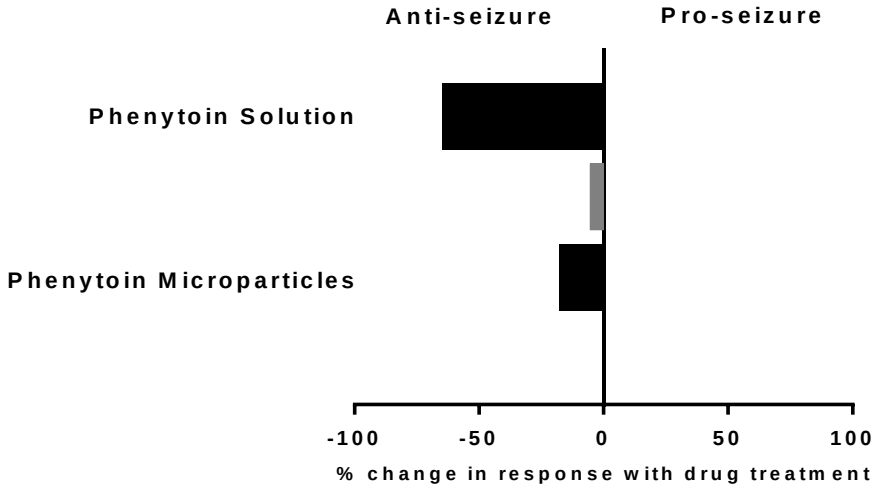

Figure 3.9. Effect of intranasal phenytoin microparticles and phenytoin control solution on HLE (black; n=6 for MPs; n=11 for solution) and FLE (grey; n=10 for MPs; n=18 for solution) at the group CC50 currents 60 minutes after treatment administration. Data is presented as percent change in response with respect to intranasal saline treatment in the same rats. Animal numbers and the method used to calculate the percentage difference are shown in Appendix C.

3.5.2 Pharmacokinetic Analysis of Tested Animals' Brains and Plasma at 60 Minutes

3.5.2.1 Pharmacokinetics of Phenytoin in Tested Animals at 60 Minutes

To address the immediate question that emerged from the pharmacodynamic data above, concentrations of phenytoin in plasma and the main brain (cerebrum and cerebellum) were analysed and are presented in Figure 3.10. Mean plasma (Figure 3.10A) and brain (Figure 3.10B) concentrations, as well as mean brain/plasma ratios (Figure 3.10C) all trended towards being higher in the phenytoin control solution group, which supported the pharmacodynamic results. While this was not statistically significant when comparing average brain (134 ng/g (microparticles), 307 ng/g (solution), p = 0.0567) and plasma (131 ng/mL (microparticles), 203 ng/mL (solution), p = 0.2833) concentrations, it became significant when comparing the brain/plasma ratios (p = 0.0147), the ratio for control solution being significantly greater than 1.0 (p < 0.0001) while the ratio for microparticles was not (p = 0.9541). The one particularly high concentration that can be seen in the phenytoin control solution data for plasma and brain was matched to the rat in which FLE was prevented in the MEST test.

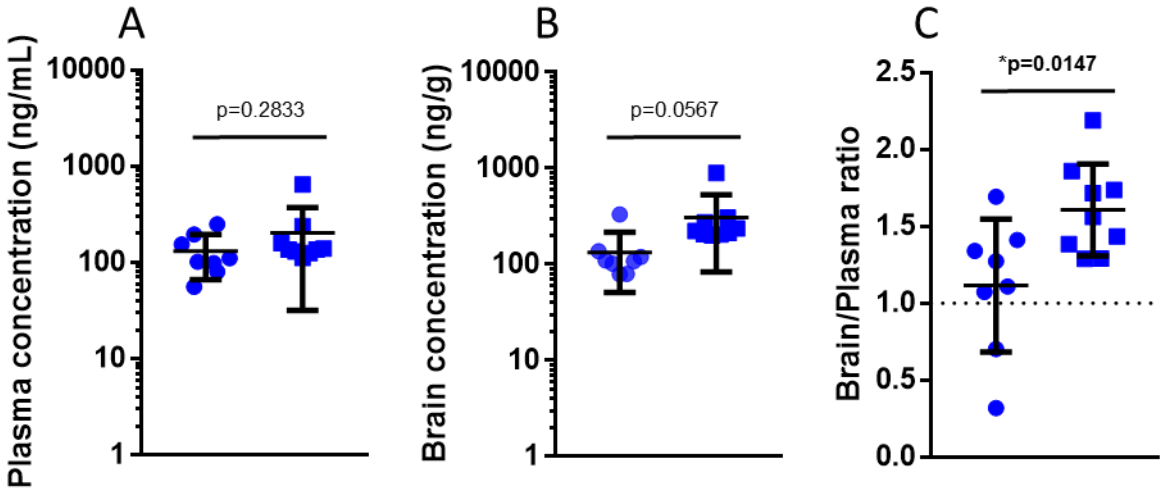

Figure 3.10. Phenytoin plasma concentrations (A), brain concentrations (B) and brain/plasma ratio (C) of rats stimulated at 60 minutes after intranasal administration of phenytoin microparticles (circles) or phenytoin control solution (squares).

3.5.3 Histological Evaluation of Tested Animals' Nasal Epithelium

To further speculate on the intranasal pathway each formulation used to get phenytoin to the brain, histology of the olfactory epithelium was examined in the tested rats (Figure 3.11) with reference to Renne et al.[149]. A clear destruction of the nasal epithelium was seen 60 minutes after administration of phenytoin control solution (Panel B) in which the olfactory epithelium appeared to have degenerated, fragmented and detached from the lamina propria. Three days later, the impact of this insult was still evident in the atrophic epithelium that remained, with obvious thinning and loss of the usual cellular architecture (Panel F). The olfactory epithelium of rats given phenytoin microparticles (Panel D and H), on the other hand, appeared no different to that after saline (Panel C and G) at either time point, maintaining an intact network of olfactory neurons and supporting cells atop a wholesome lamina propria.

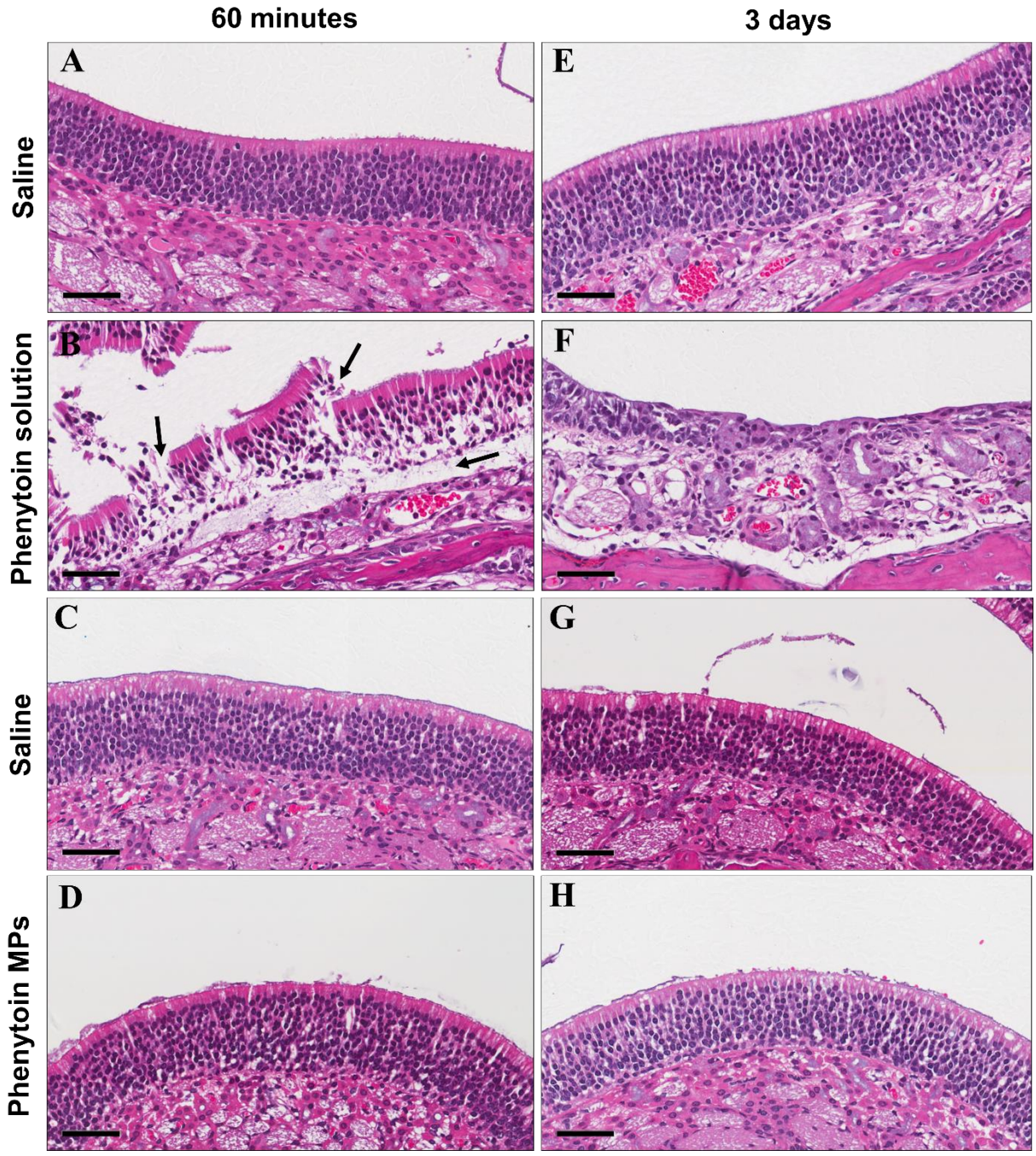

Figure 3.11. Representative histological images of the olfactory epithelium of rats which participated in the 60 minute MEST studies with phenytoin microparticles and phenytoin control solution. Images show short-term effects of the formulations on the olfactory epithelium in rats stimulated at 60 minutes after administration of saline (A and C), phenytoin control solution (B) and phenytoin microparticles (D) and longer-term effects at three days after administration of saline (E and G), phenytoin control solution (F) and phenytoin microparticles (H). Scale bars = 50 µm.

3.5.4 Pharmacodynamic Evaluation at 120 and 180 Minutes

Due to the lack of a statistically significant anti-seizure effect seen at 60 minutes with intranasal phenytoin microparticles, trials were conducted at time points later than 60 minutes with microparticles to find the time of peak effect which was suggested by Yarragudi et al.[204] to occur later than 60 minutes. The CC_{50} and control responses to stimulation for these studies are shown in Figure 3.12. The rats in the 120 minutes group had a calculated CC_{50} of 62 mA (95% CI: 45-85 mA) (Figure 3.12A), which translated to 28 % of rats exhibiting HLE after intranasal saline administration in the experimental control data (Figure 3.12B). In the 180 minutes group, the calculated CC_{50} for the group was 54 mA (95% CI: 34-84 mA) (Figure 3.12C) and 33 % of saline-treated rats subsequently exhibited HLE (Figure 3.12D). All saline-treated rats in both groups displayed FLE.

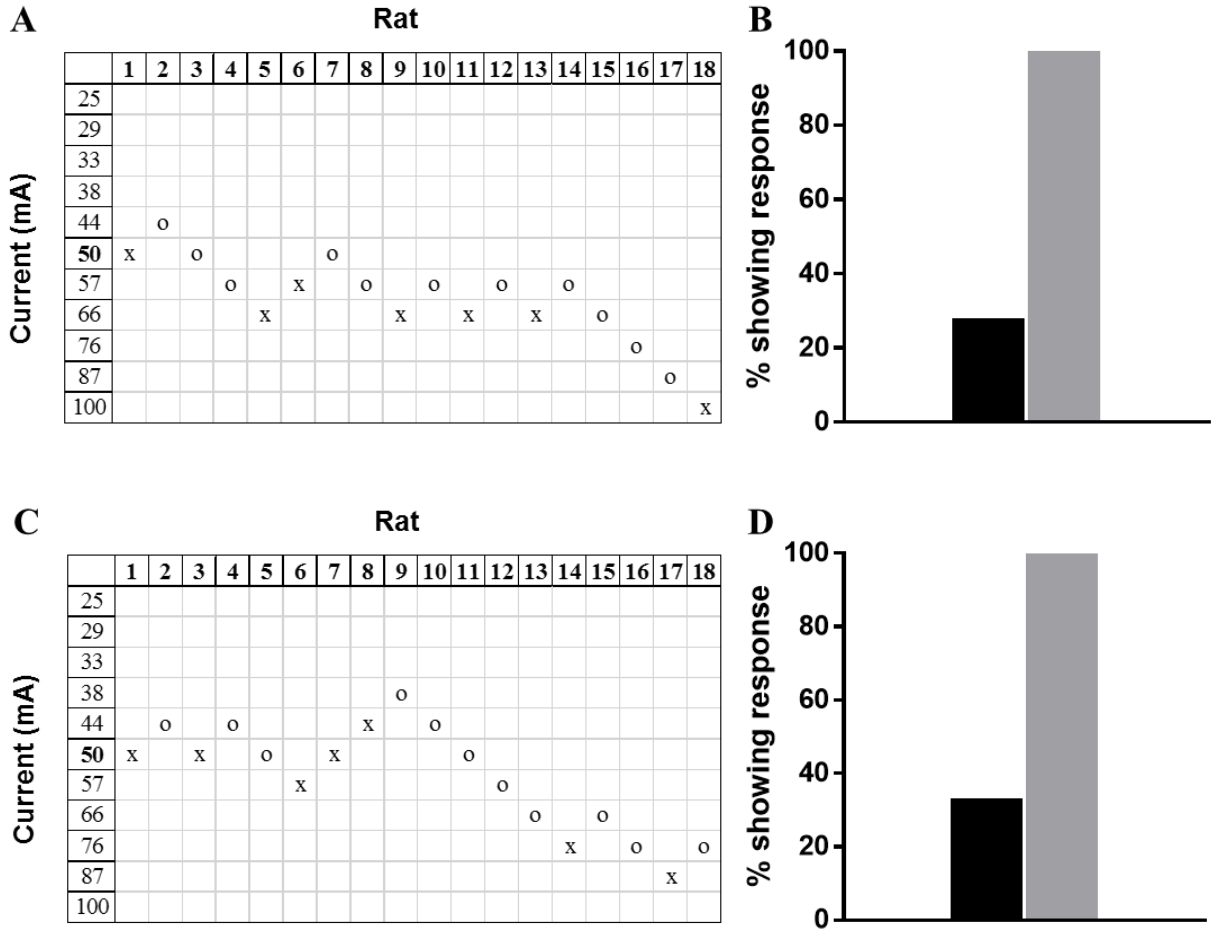

Figure 3.12. Determination of the CC50 and baseline response to stimulation at the CC50 in the batches of rats that participated in the study of intranasal phenytoin microparticles at 120 minutes (A and B) and 180 minutes (C and D). The panels on the left (A and C) show the experimental data from the up and down method which was used to estimate the CC_{50}, where "X" represents HLE and "O" represents no HLE. The panels on the right (B and D) show the baseline responses of the rats when stimulated at the calculated CC_{50} 60 minutes after intranasal saline administration and serve as an indication of the accuracy of the estimated CC_{50} and the resolution for detecting anti-seizure drug effects. The black bar represents the percentage of rats which exhibited HLE at the calculated CC_{50} and the grey bar represents those which exhibited FLE (with or without HLE).

3.5.5 Pharmacodynamic Evaluation: The Big Picture

Figure 3.13 shows the effect of intranasal phenytoin microparticles on seizure responses at 60, 120 and 180 minutes. No statistically significant differences were evident, despite the consistent trend of a reduction in incidence of HLE after phenytoin microparticles by 17% ($p = 0.8$), 80% ($p = 0.3647$) and 67% ($p = 0.1412$) respectively. No reduction in FLE was observed. A single rat in the 120 minutes group demonstrated HLE after phenytoin microparticles, but not after saline and is presented as a 7 % increase in the incidence of HLE, however this was deemed to be an anomaly as the overall effect was heavily weighted towards an anti-seizure effect, further supported by the exclusively anti-seizure effect at the other time points. When data from all three experiments was pooled before analysis the anti-seizure result was, however, significant ($p = 0.016$), showing the microparticles in fact did have an effect. In the case of the 120 and 180 minute groups, the lack of statistical difference according to Prescott's test was likely due to the decreased resolution for detection of an anti-seizure effect due to the lower than expected percentage or HLE seen in the control group at the statistically estimated CC_{50}. The trend in the data therefore suggested the time of peak anti-seizure effect of intranasal phenytoin microparticles to be 120 minutes after administration.

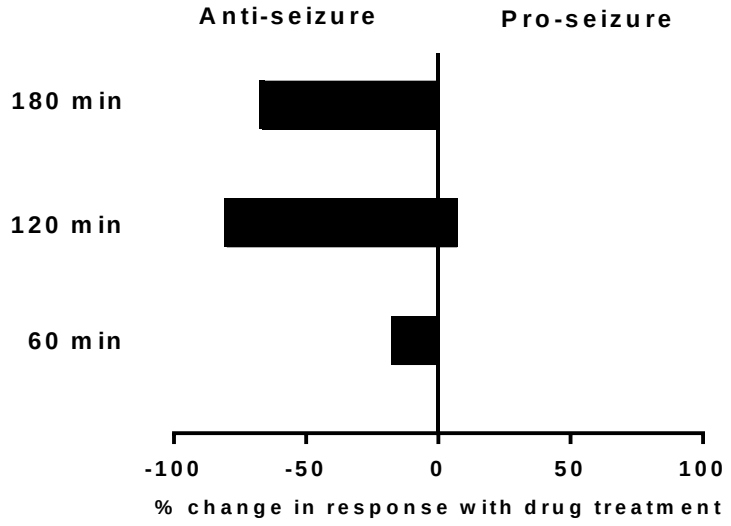

Figure 3.13. Effect of intranasal phenytoin microparticles on HLE (black) and FLE (grey) at the group CC_{50} currents 60 minutes (n=6 and n=10 respectively), 120 minutes (n=6 and n=18 respectively) and 180 minutes (n=6 and n=16 respectively) after treatment administration. Data is presented as percent change in response with respect to intranasal saline treatment in the same rats. Animal numbers and the method used to calculate the percentage difference are shown in Appendix C. Note that FLE is not visible in the above Figure as no change was found in this experiment.

3.5.6 Pharmacokinetic Evaluation: The Big Picture

To substantiate the pharmacodynamic findings, plasma and brain tissue levels of phenytoin and its major metabolite (4-HPPH) were measured in the seizure-tested rats.

3.5.6.1 Standard Curve Validation of Brainstem and Olfactory Bulb Homogenates

Standard curves were constructed in brainstem and olfactory bulb homogenates so that these brain regions could be analysed separately from the remainder of the brain (henceforth referred to as the main brain) to provide more insight into intranasal pathways of phenytoin delivery (Figure 3.14). The mean values were found to be within the precision and accuracy limits (±15%) stated for the validated brain method in **Chapter Two** (**Appendix H**), indicating that the standard curve of the analytes did not differ significantly between the different types of brain tissue and samples could be compared directly.

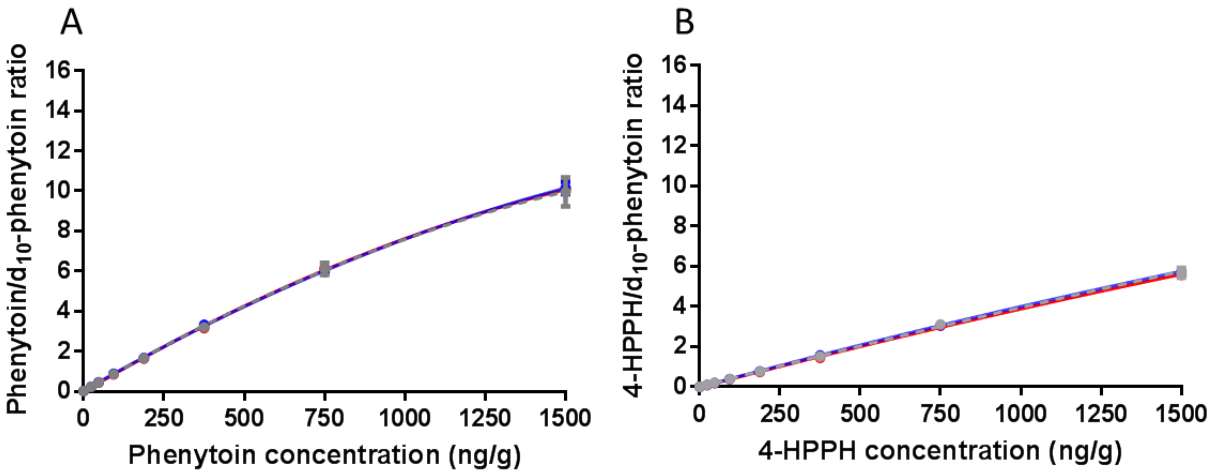

Figure 3.14. Comparison between phenytoin (A) and 4-HPPH (B) standard curves prepared with olfactory bulbs (blue; n=3; R^2 = 0.9999 (Phenytoin); R^2 = 1 (4-HPPH)), brainstem (red; n=3; R^2 = 1 (Phenytoin); R^2 = 0.9998 (4-HPPH)) and remainder of brain tissue (grey; n=9; R^2 = 1 (Phenytoin); R^2 = 1 (4-HPPH)). Variability between different regions was not significant and was within limits of the assay as validated in ***Chapter Two****.*

The intra-day accuracy and precision of the assays, based on quality control samples, are shown in Table 3.1. Variability was within the acceptable range of ±15% for both brainstem and olfactory bulb assays.

Table 3.1. Intra-day accuracy and precision of phenytoin and 4-HPPH quantification in rat brainstem and olfactory bulb homogenates based on quality control samples.

		Brainstem		
Analyte	**Nominal Conc. (ng/g)**	**Intraday (n=3)**		
		Mean (ng/g)	**Accuracy (%)**	**Precision (CV%)**
Phenytoin	46.9	48.9	104.3	6.0
	187.5	197.8	105.5	5.8
	750	739.5	98.6	1.6
4-HPPH	46.9	50.2	107.0	4.2
	187.5	200.8	107.1	4.6
	750	744.4	99.3	4.1
		Olfactory bulbs		
Analyte	**Nominal Conc. (ng/mL)**	**Intraday (n=3)**		
		Mean (ng/g)	**Accuracy (%)**	**Precision (CV%)**
Phenytoin	46.9	48.7	104.0	2.0
	187.5	187.7	100.1	3.1
	1000	758.4	101.1	0.4
4-HPPH	46.9	48.0	102.4	1.8
	187.5	187.8	100.1	2.1
	750	759.8	101.3	2.7

3.5.6.2 Pharmacokinetic Analysis of Phenytoin and 4-HPPH in Tested Animals

The concentrations of phenytoin and 4-HPPH in the plasma and various brain regions after intranasal administration of phenytoin microparticles and phenytoin control solution are presented in Figure 3.15. Phenytoin plasma concentrations (Figure 3.15A) were found to decrease significantly between 60 (131 ng/mL) and 180 minutes (44 ng/mL) after microparticle administration. In comparison to the phenytoin control solution group at 60 minutes (203 ng/mL), the only significant difference was with phenytoin concentrations 180 minutes (44 ng/mL) after microparticles. The only statistically significant difference in average brain phenytoin concentrations between the time points after microparticles was the decrease in olfactory bulb concentrations between 120 and 180 minutes. In agreement with the pharmacodynamic findings, however, brain concentrations in all regions (i.e. olfactory bulbs, main brain and brainstem) (Figure 3.15B) after microparticles consistently trended towards increasing between 60 minutes (134 ng/g) and 120 minutes (142 ng/g) then towards decreasing

by 180 minutes (68 ng/g), suggesting a scientific relevance to the data, despite not being statistically significant.

The plasma concentration of 4-HPPH (Figure 3.15C) was found to remain similar between 60 (230 ng/mL) and 180 (192 ng/mL) minutes after phenytoin microparticles and was not significantly different to that after control solution at 60 minutes ($p = 0.0556$). Brain concentrations (Figure 3.15D) generally followed the same trends described for phenytoin concentrations, although the 4-HPPH concentrations after phenytoin control solution were notably lower than expected, being on par with concentrations 120 to 180 minutes after microparticles instead of being higher. Consequently, no significant differences were found within or between groups for 4-HPPH concentrations in the brain. Due to this unexpected result, the plasma concentrations of phenytoin and 4-HPPH after phenytoin control solution were statistically compared to concentrations in all brain regions using ANOVA. No significant difference was found between plasma and brain concentrations of phenytoin, but the concentration of 4-HPPH was significantly lower in all brain regions compared to plasma (424 ng/mL) (ANOVA: $p < 0.0001$; Tukey's post-hoc: main brain (38 ng/g, $p = 0.0003$), brainstem (40 ng/g, $p = 0.0004$), olfactory bulbs (29 ng/g, $p = 0.0018$)).

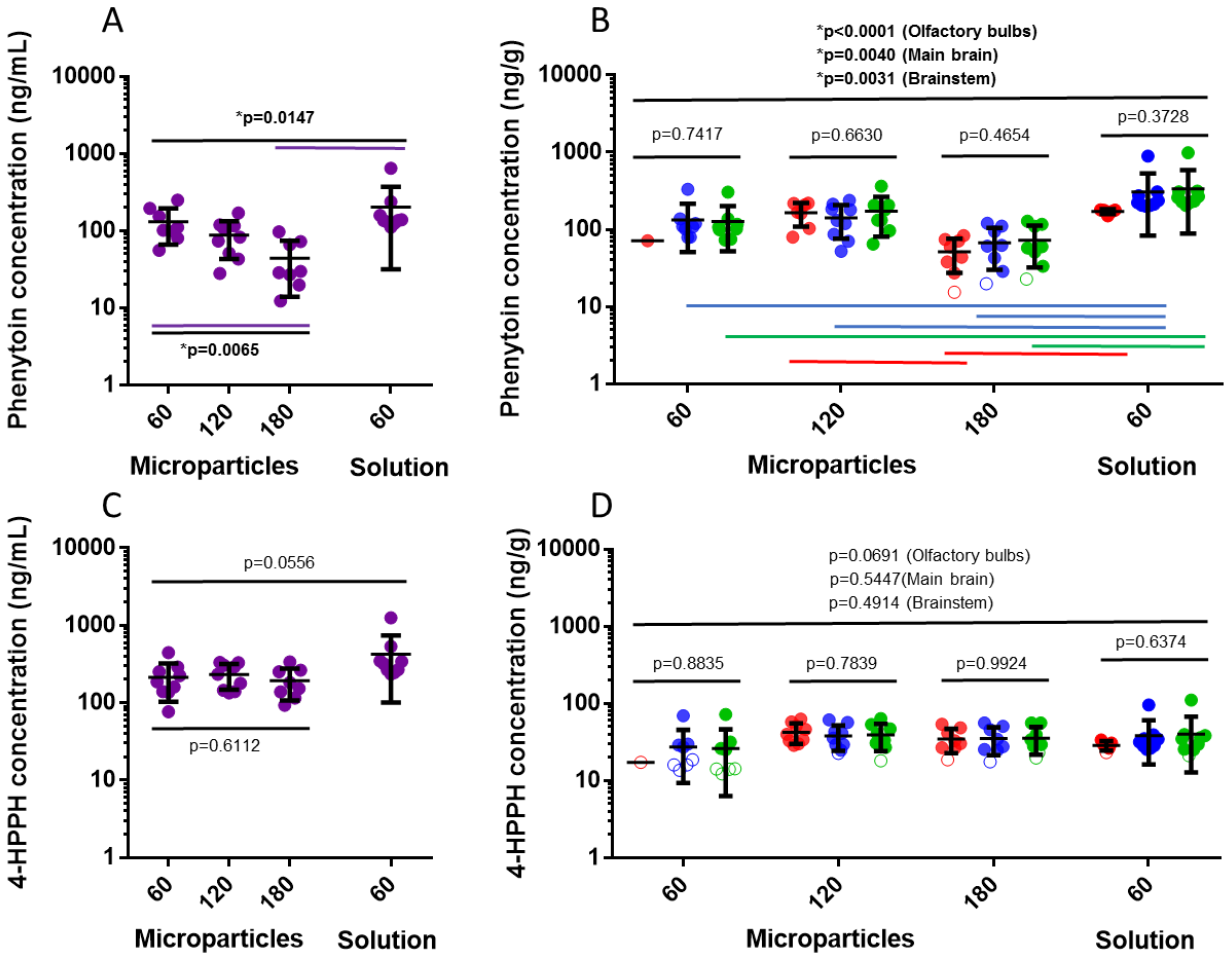

Figure 3.15. Phenytoin (A and B) and 4-HPPH (C and D) concentrations in plasma (purple), main brain (blue), brainstem (green) and olfactory bulbs (red) of rats administered phenytoin microparticles (60, 120 and 180 minutes) and phenytoin control solution (60 minutes). Concentrations are plotted on a log scale for clarity. Unfilled symbols indicated values that were below the LLOQ of the assay or calculated from at least one such value. P-values are shown for comparison between different brain regions at a given time point and between each brain region in different experiments using one-way ANOVA. With respect to the latter, the coloured bars (matched to the symbol colours) represent statistically significant differences determined by post-hoc analysis (Tukey's) of inter-study differences. Labels on the x axis reflect the time point at which stimulation occurred and it should be noted that tissue collection occurred up to ten minutes after this.

The brain region/plasma ratios of phenytoin and 4-HPPH calculated for individual rats are shown in Figure 3.16. For phenytoin (Figure 3.16A), the brain region/plasma ratios at 60 minutes after microparticles were not found to differ from 1.0, while in all other groups, the ratios were found to be significantly greater than 1.0 according to ratio paired t-tests and significantly greater than their 60 minute microparticle counterparts (noting that olfactory bulbs could not be compared to the 60 minute microparticle group due to limited data). All ratios in these latter groups showed a similar trend with olfactory bulbs being the lowest, main brain higher and brainstem the highest. The difference between olfactory bulbs and brainstem was statistically significant at 180 minutes after microparticles and 60 minutes after control solution. Interestingly, the ratios within each brain region in these groups (e.g. brainstem data at 120 and 180 minutes after microparticles and 60 minutes after control solution) were all of a similar magnitude, despite the different magnitudes of the concentrations described above. For 4-HPPH (Figure 3.16B), all brain region/plasma ratios were well below 1.0. As with the brain concentration data, no significant differences were found between brain regions within groups, but between groups, there were significant differences in that the brain/plasma ratio was consistently higher at 120 and 180 minutes after microparticles in all three brain regions compared to 60 minutes after microparticles (with the exception of the olfactory bulbs for which not enough data was available to test) as well as control solution.

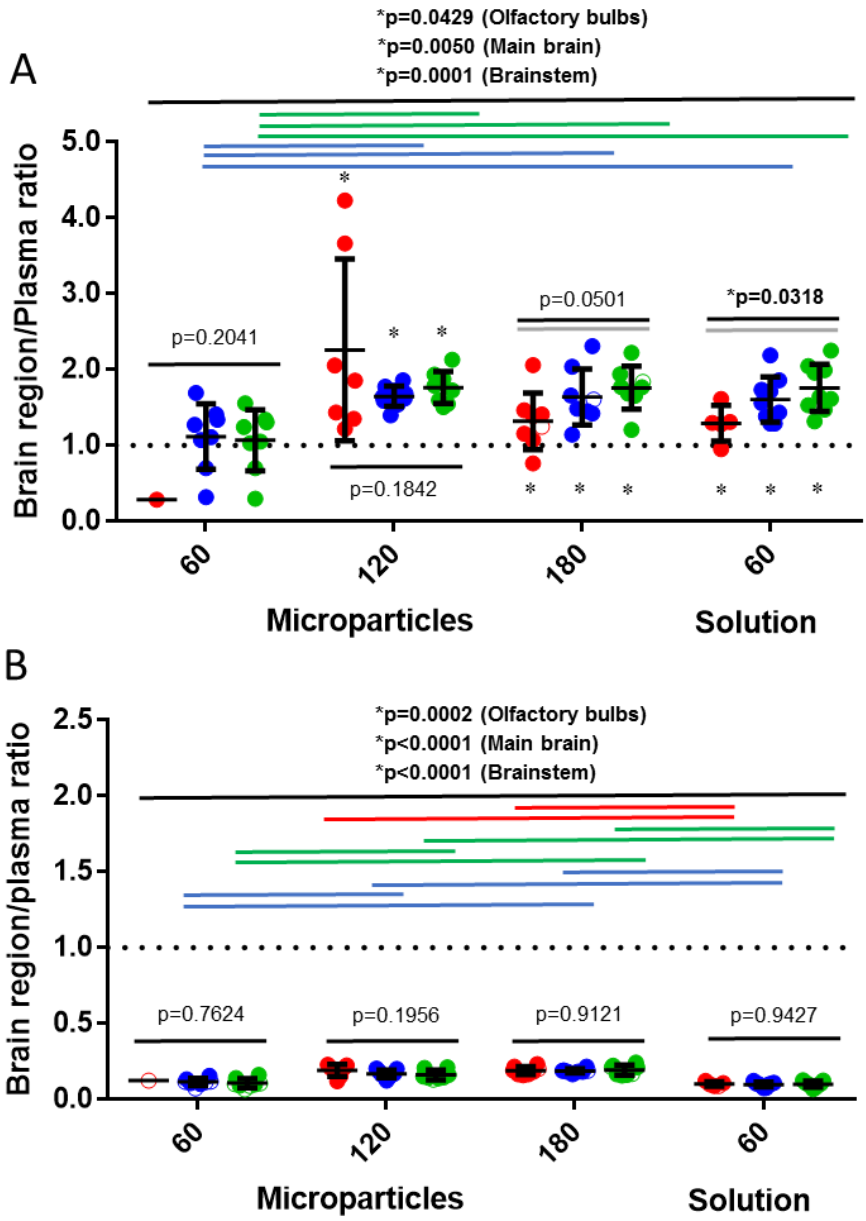

Figure 3.16. Phenytoin (A) and 4-HPPH (B) brain region/plasma ratios. The ratios of main brain (blue), brainstem (green) and olfactory bulbs (red) to plasma are shown for rats administered phenytoin microparticles (60, 120 and 180 minutes) and phenytoin control solution (60 minutes). Unfilled symbols indicated ratios that were derived from at least one concentration below the LLOQ of the assay. P-values are shown for comparison between different brain regions at a given time point and between each brain region in different experiments using one-way ANOVA. With respect to the latter, the coloured bars (matched to the symbol colours) represent statistically significant differences determined by post-hoc analysis (Tukey's) of inter-study differences. The post-hoc significant differences between OBs and brainstem after phenytoin microparticle administration at 180 minutes and after phenytoin control solution are each represented by a grey bar. Asterisks represent mean values that were significantly different to 1.0 according to a ratio-paired t-test. Labels on the x axis reflect the time point at which stimulation occurred and it should be noted that tissue collection occurred up to ten minutes after this.

Figure 3.17 presents the ratio of phenytoin and 4-HPPH in the brainstem and olfactory bulbs to that in the main brain. For phenytoin (Figure 3.17A), no significant differences were found within the brainstem or olfactory bulb groups at different time points and compared with the control solution. However, significant differences were found between the olfactory bulb and brainstem ratios at 180 minutes after microparticles ($p = 0.0233$) and 60 minutes after phenytoin control solution ($p = 0.0022$) which is consistent with those described above for the brain region/plasma ratios. Ratio-paired t-tests on these groups determined that the brainstem/main brain ratio was significantly higher than 1.0 at 180 minutes after microparticles and that the olfactory bulb/main brain ratio was significantly lower than 1.0 at 60 minutes after control solution. For 4-HPPH (Figure 3.17B), no significant differences were found within or between brain regions.

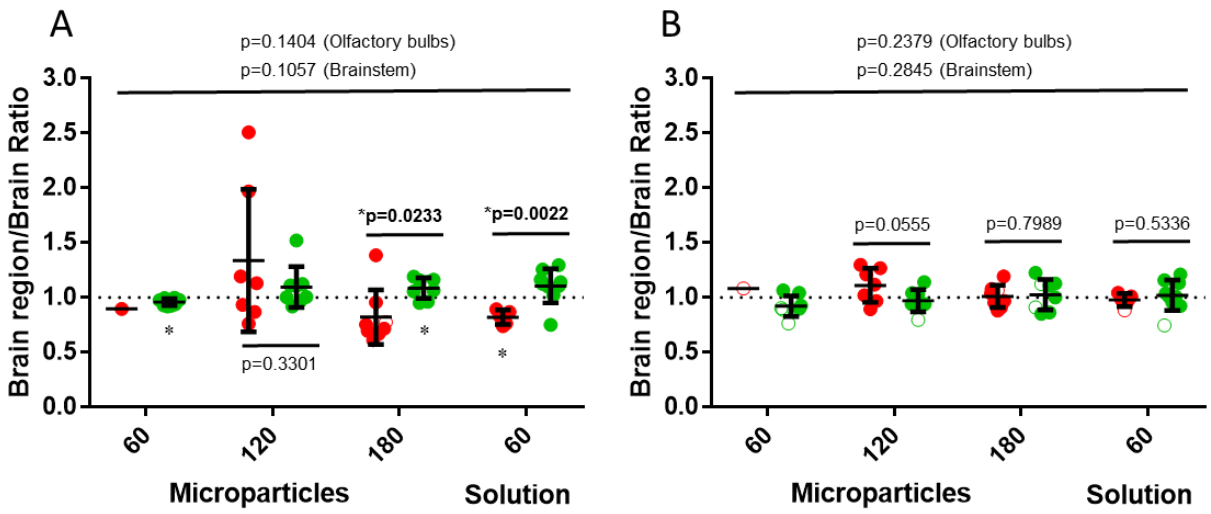

Figure 3.17. Ratios of Phenytoin (A) and 4-HPPH (B) in the brainstem (green) and olfactory bulbs (red) compared to the main brain. P-values are shown for comparison between different brain regions at a given time point using unpaired two-tailed t-tests and between each brain region in different experiments using one-way ANOVA. Asterisks represent mean values that were significantly different to 1.0 according to a ratio-paired t-test. Labels on the x axis reflect the time point at which stimulation occurred and it should be noted that tissue collection occurred up to 10 minutes after this.

3.5.7 Pharmacodynamic Evaluation of Microparticles Without Phenytoin

To exclude a contribution of the vehicle (i.e. the TSP polymer which formed the scaffold of the microparticles) to the results seen, blank microparticles without phenytoin were tested at the time of peak anti-seizure effect of phenytoin microparticles (120 minutes). The CC_{50} and control responses to stimulation for these studies are shown in Figure 3.18. The rats had a calculated CC_{50} of 56 mA (39-82 mA) (Figure 3.18A), which translated to 28 % of rats exhibiting HLE after intranasal saline administration in the experimental control data (Figure 3.18B).

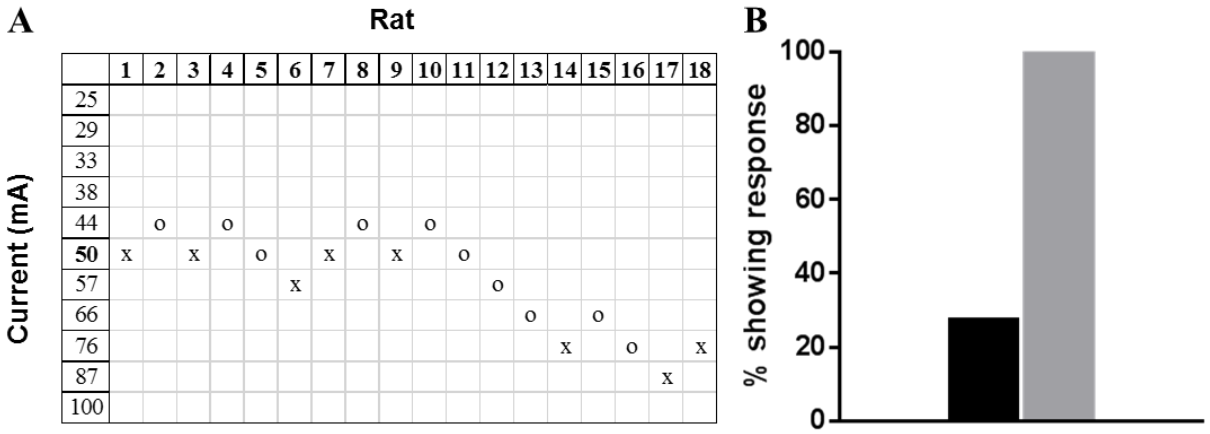

Figure 3.18. Determination of the CC_{50} and baseline response to stimulation at the CC_{50} in the batch of rats that participated in the study of intranasal drug-free microparticles at 120 minutes (n=18). (A) shows the experimental data from the up and down method which was used to estimate the CC50, where "X" represents HLE and "O" represents no HLE. (B) shows the baseline responses of the rats when stimulated at the calculated CC50 120 minutes after intranasal saline administration and serves as an indication of the accuracy of the estimated CC_{50} and the resolution for detecting anti-seizure drug effects. The black bar represents the percentage of rats which exhibited HLE at the calculated CC_{50} and the grey bar represents those which exhibited FLE (with or without HLE).

Figure 3.19 shows the effect of blank microparticles at 120 minutes after intranasal administration. No statistically significant effect on the incidence of HLE was seen ($p = 1$), however, a surprising amount of variability in responses in both directions were observed. The incidence of FLE was unchanged after blank microparticle administration.

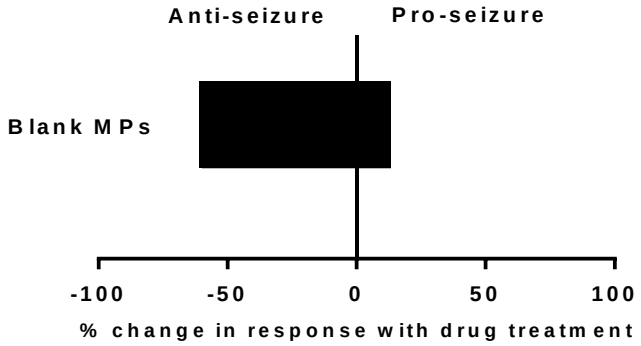

Figure 3.19. Effect of intranasal drug-free microparticles (n=5) on HLE (black; n=5) and FLE (grey; n=18) at the group CC_{50} current 120 minutes after treatment administration (i.e. the time of peak effect of phenytoin microparticles). Data is presented as percent change in response with respect to intranasal saline treatment in the same rats. Animal numbers and the method used to calculate the percentage difference are shown in Appendix C. Note that FLE is not visible in the above Figure as no change was found in this experiment.

3.6 Discussion

This Chapter applied the MEST model established in **Chapter Two** to the study of intranasal phenytoin microparticles, designed by Yarragudi et al.[204]. The pharmacokinetics of phenytoin release from the microparticles after intranasal delivery to rats was studied up to 60 minutes by that author (Figure 3.4) and found to be highest at this terminal time point, which therefore made it the starting point for the study of seizure prevention conducted in this Chapter. The results were surprising. The reduction in incidence of HLE was found to be significant with phenytoin solution, but not microparticles at 60 minutes. As shown in Figure 3.4, Yarragudi et al.[204] had found that while phenytoin from microparticles was highest in the brain at 60 minutes after administration, phenytoin from control solution peaked at 30 minutes after administration and dropped off to become significantly lower than that from microparticles by 60 minutes. This suggested a lesser anti-seizure effect would be observed with the latter, but this was not the case.

It was initially thought that this may be due to a confounding contribution from the ethanol in the control solution, which has been shown to decrease seizure threshold in the MES test after systemic administration[209]. A vehicle control was not run in this study (in order to allow for experimental evaluation of the statistically determined CC_{50} after saline, as discussed in **Chapter Two**), so a contribution cannot be excluded, but tissue phenytoin concentrations were measured to verify the discrepancy and were found to support the pharmacodynamic outcome (Figure 3.10). These therefore contrasted with the data of Yarragudi et al.[204] in that brain concentrations of phenytoin after delivery in control solution were significantly higher than after microparticles. Relative plasma concentrations were, however, similar to those of Yarragudi et al.[204] in that phenytoin from control solution appeared slightly higher than that from microparticles, but did not reach statistical significance. The reason for the relative brain concentration discrepancy between the two studies is unclear, but possible contributing factors are herein discussed in the context of formulation, animal and analytical method related factors.

The first difference to note between the studies is that the dose and composition of the phenytoin control solution varied slightly in this study compared to that which was reported by Yarragudi et al.[204]. Firstly, the dose of phenytoin solution administered by Yarragudi et al.[204] was 15 µL (equivalent to 1.5 mg of phenytoin) based on the average dose of phenytoin delivered in microparticles, as calculated by needle weight before and after administration. The average dose of phenytoin administered in microparticles at 60 minutes in the present study was calculated to be slightly higher at 1.7 ± 0.37 mg of phenytoin (**Appendix G**), so a control

solution volume of 20 µL (2 mg of phenytoin) was administered so as not to bias the experiment in favour of the microparticles. It was expected that this minor dose difference would not significantly affect the outcome given that Yarragudi et al. [204] had reported approximately three times lower brain concentrations after phenytoin control solution at 60 minutes compared with microparticles, but given the unanticipated result it warrants consideration, especially given the non-linear nature of the pharmacokinetics of phenytoin and the unreported characteristics of its potential metabolism by the nasal epithelium. In light of the remarkably different brain to plasma ratio compared to Yarragudi et al.'s study, the small dose increase seems unlikely to be the cause of the discrepancy as it would be reasonable to expect a corresponding relative increase in plasma concentration. Furthermore, the histological insult by the solution (Figure 3.11B) means metabolism by the nasal epithelium probably did not play a role due to the destruction of enzyme-bearing cells.

Secondly, the propylene glycol content of the phenytoin control solution was reported to be 1% by Yarragudi et al.[204], but it is uncertain if this was the actual concentration used or a reporting error as a 10% PG concentration was found to be necessary to keep the phenytoin in solution in the present study. If the concentrations were indeed different, it is thought unlikely that this could have had such a dramatic effect on the brain concentration given that the histological insult to the olfactory epithelium (Figure 3.11B) is the most likely cause for the success of the control solution and supplementary data investigating the effect of a dispersion containing 12.5% PG (**Appendix I**) showed no such insult. Furthermore, it was considered that if a 1% concentration was used and phenytoin was not dissolved fully, this may have led to a reduced brain concentration, but this would not explain the peak seen by Yarragudi et al.[204] at 30 minutes and the plasma concentrations which were on par with those of microparticles in both studies. As a final note regarding dose, it could be considered that the dose of microparticle powder might have been different between the studies, however Yarragudi et al.[204] reported an average weight of delivered powder of 1.5 mg (albeit with no standard deviation), which was very similar to the 1.7 mg average in the present study (**Appendix G**), so this is not likely to have caused the difference.

The next consideration to note is with regards to the animals which participated. The rats in the present study had undergone three generalised seizures, one immediately prior to the measurement of their brain concentrations, as opposed to the naïve rats used by Yarragudi et al.[204] Previous studies in rats and humans have suggested that seizures may affect the brain concentrations of ASDs due to changes in BBB function (i.e. transient leakiness and changes in multi-drug transporter expression) and cerebral blood perfusion[200,210–214], however, the

direction in which this effect occurs is still a matter of debate. Most studies having examined permeability on the basis of hydrophilic proteins, dyes or contrast media rather than lipophilic ASDs such as phenytoin, the former suggesting that increased ASD concentrations would be expected after seizures while the latter suggest a decrease or net lack of difference, at least at the epileptic focus[200,212,213,215]. The present study analysed whole brain concentrations of phenytoin and is therefore not directly comparable with any of the above, but the principle that seizures could have altered concentrations compared to naïve rats applies. How this might explain the opposite brain concentrations after each of the formulations compared with Yarragudi et al. is more perplexing. Seizures would have been expected to affect the distribution of phenytoin in the same way, if at all, as it was still delivered by an intranasal route in each case and showed similar regional distribution, at least in the regions analysed (Figure 3.15). It is therefore considered unlikely that this was the cause.

Next it should be considered that different analytical methods were used to analyse the results of each of the studies; i.e. HPLC by Yarragudi et al.[204] and LC-MS in the present study. While the accuracy and precision of each was validated, the procedures involved a less than simple series of dilutions, concentrations and calculations. The data above has so far been discussed in terms of relative concentrations for comparison to Yarragudi et al.[204] due to a final interesting discrepancy in that concentrations in the latter study, where comparable data was available, were generally about five times greater than those calculated in this Chapter. Given the acceptable limits of accuracy and precision reported, the most likely reason for this is deemed to be a calculation anomaly. The details of the calculation procedure used by Yarragudi et al.[204] were not available, but that used in the present study is provided in **Appendix J** for the reader's reference. The author is confident that this procedure provides accurate quantitative values of plasma and brain concentrations, an assertion which is verifiable by comparing the values quantified in **Chapter Two** with those in the literature 60 minutes after a similar single intravenous dose (20-30 mg/kg) of phenytoin as discussed in the previous Chapter[175–177,188]. In the absence of this evidence, one may have suspected that a difference in extraction efficiency of the phenytoin between the studies might have contributed to the different values quantified. However, this suspicion is countered by the fact that both studies quantified phenytoin using the analyte/internal standard ratio and standards prepared in the same matrix and with the same extraction procedure as the samples which would have rendered any such differences ineffectual. Considering all this, the low phenytoin brain concentration from control solution compared with microparticles reported by Yarragudi et al.[204] would seem to be somewhat of an

anomaly rather than a wide-ranging difference due to an inherent flaw in the method which would have been expected to equally affect all of the data including plasma concentrations.

In this respect, it is worth briefly commenting on the HPLC method used by Yarragudi et al.. The recommended concentration of a low quality control to assess intra-day and inter-day variability is within three times the concentration of the lower limit of quantification (LLOQ)[216] in order to assure accuracy and precision at low concentrations. The LLOQs for phenytoin in plasma and brain were reported to be 48 ng/mL and 84 ng/g respectively, however the low quality control standard concentration was 1000 ng/mL (or ng/g) in both cases, making it approximately twenty times the LLOQ of phenytoin in plasma and ten times that in the brain tissue. The concentrations reported from the plasma samples were close to the low QC concentration and therefore can generally be considered accurate, however, the same cannot be guaranteed for all the brain samples (in particular the anomalous 60 minutes control solution sample) which was outside the limits of the low QC and may therefore have been subject to a degree of unquantified intra-assay error.

Despite the unexplained differences in quantitative concentrations, the brain to plasma ratio offers a normalised comparison between the studies, with values above 1.0 indicating an accumulation of phenytoin in the brain above that in plasma. Due to the elevated brain concentration relative to plasma found in the present study, the average brain/plasma ratio was tipped in favour of the control solution (Figure 3.10C) in contrast to the study of Yarragudi et al.[204] at 60 minutes (Figure 3.4). The discrepancy in brain to plasma ratio is an interesting finding as phenytoin plasma levels continued to increase over time while brain levels decreased, whereas literature[175,186] and the trend in Figure 3.16 (discussed later) suggest that phenytoin accumulates in the brain due to its hydrophobic nature and concentrations only begin to reduce after plasma concentrations start to decline and shift the equilibrium. One might speculate on the possibility of extensive direct brain delivery leading to a peak, followed by equilibration and redistribution into plasma contributing to the steadily increasing plasma levels. Alternatively, extensive metabolism in the brain contributing to the rapid reduction in phenytoin concentration is possible, but the data available is inadequate to provide evidence for either of these suggestions.

Whatever the case, histology provided the illuminating data to explain how the control solution was likely so much more effective than the microparticles in the present study. The high brain to plasma ratio (reflecting increased brain concentrations with only marginally increased plasma concentrations compared with microparticles), suggested that phenytoin from the

control solution was exploiting a direct route to the brain, however, histology showed that this was not without massive insult to the olfactory epithelial barrier (Figure 3.11B), which is clinically unacceptable, especially in light of the lasting damage when examined three days later. For this reason and the suspected confounding of pharmacodynamic studies that could have been attributable to ethanol, no further control studies were conducted in this Chapter. Yarragudi et al.[204] did not provide any histology data for rats given intranasal control solution, but given that the same proportion of ethanol was used and the dose volume differed by only five microliters, it can be inferred that the effect would have been the same. Why this did not result in the elevated brain concentrations at 60 minutes that were observed here is unclear. While information is not freely available in the literature to evaluate commercially sensitive nasal formulations currently under development for seizure treatment, the data presented here raises questions about the long-term effects of those that contain irritating components such as ethanol in order to achieve dissolution.[74,217] It also highlights the importance of more study into physiologically friendly drug delivery systems such as TSP microparticles which may act in their place, delivering directly to the brain by mechanisms other than total obliteration.

After addressing the above comparisons with the data of Yarragudi et al.[204] at 60 minutes after administration, this discussion now proceeds to the extended data that was obtained in this Chapter to determine the time of peak effect of the phenytoin from MPs and offer further insight into the intranasal delivery pathway by examining pharmacokinetics. It is important to highlight before proceeding that the maximum intranasal anti-seizure effect of phenytoin in these experiments did not push the seizure threshold any higher than that necessary to prevent HLE, so all rats, except the one in the phenytoin control solution trial mentioned above, still exhibited FLE despite a reduction in HLE. As may have been expected, this contrasts with the much higher dose of intravenous phenytoin in **Chapter Two** which increased the threshold sufficiently to prevent HLE and FLE, eliminating the tonic component of the seizures altogether, except for one rat who likely received a lower dose due to administration difficulty as indicated by tissue phenytoin concentrations. This distinction is not commonly made in the literature, with studies reporting prevention of HLE, but not the relative magnitude of the effect, which in the above case would have led to phenytoin microparticles appearing to have a similar effect to the intravenous 25 mg/kg dose. The data of Bankstahl et al.[101] gives an indication of the change in threshold that might be expected to correspond to each of the cases with prevention of FLE requiring an approximately 20-30 mA increase in threshold above the increase required to prevent HLE.

The MEST experiments as a whole indicated 120 minutes to be the time of peak anti-seizure effect of the phenytoin microparticles (Figure 3.13). Importantly for the credibility of the seizure model for testing intranasal delivery systems, this finding was supported by the pharmacokinetic analysis which showed peak phenytoin levels in the main brain coinciding with this time point, despite the reducing concentrations of phenytoin in plasma after 60 minutes (Figure 3.15A). Furthermore, the average brain to plasma ratio also followed this trend with a peak at 120 minutes (Figure 3.16A). This data is in agreement with the predictions of Yarragudi et al.[204] who speculated, based on *ex vivo* release studies using porcine nasal mucosa, that brain levels of phenytoin from microparticles would continue to increase after 60 minutes, albeit not for the 4 hours that the *ex vivo* study predicted. With regards to the pharmacokinetics, it should be noted that the peak phenytoin concentration achieved in the brain at 120 minutes was still significantly lower than the concentration after phenytoin control solution at 60 minutes (Figure 3.15A and B). However, considering the confounding reasons discussed earlier (i.e. damage to the epithelial barrier by the control solution, along with a slight dose advantage) this is unimportant other than to suggest that if microparticles had been able to achieve this slightly higher concentration, a more significant (including statistically so) anti-seizure effect would likely have been observed, as was the case for the solution. Had control studies been performed at 120 and 180 minutes as well, it would have been interesting to see the trend in phenytoin levels compared with microparticles, but as discussed earlier, such trials were unjustifiable for the purposes of this study.

Phenytoin concentrations in the olfactory bulbs and brainstem were also analysed for comparison to the main brain results in order to speculate on which intranasal pathway phenytoin was using to reach the brain. It should be noted before proceeding that olfactory bulb sample numbers were limited in some cases due to technical difficulties in dissecting the tissue, so may not represent the entire group of rats studied. Nonetheless, within each brain region the same trend described above for the main brain was seen, with peak levels being reached at 120 minutes. Yarragudi et al.[204] reported concentrations in the olfactory bulbs to be elevated above control solution levels at 60 minutes after microparticle administration (Figure 3.4B), which in the same manner as the main brain concentration data discussed extensively above, is in disagreement with the present study which found the opposite. The two studies did agree, however, that olfactory bulb concentrations did not exceed those in the main brain at this time point (after microparticles or control solution) which is in contrast to studies such as that of Czapp et al.[138] and Serralheiro et al.[140,141] who reported higher concentrations of their respective

model anti-seizure drugs phenobarbital, lamotrigine and carbamazepine in the olfactory bulbs relative to the brain to suggest a direct delivery via them/targeted delivery to them.

This could be seen to support the review of direct intranasal pathway evidence in **Chapter One** by suggesting that accumulation in the olfactory bulbs may not be the case, contrary to what the aforementioned studies have suggested for other ASDs employing alternative delivery systems. Bulk transport pathways which lead to direct but widespread brain delivery seem more likely rather than a localised concentration that might be expected if intracellular pathways were being used. In saying that, Figure 3.17A (complemented by the brain region/plasma ratio data in Figure 3.16A) also reveals a trend towards elevation of brainstem concentrations of phenytoin relative to main brain after microparticles and the phenytoin control solution study at 60 minutes. While this was not statistically significant other than the brainstem/brain ratio at 180 minutes after microparticles (Figure 3.17A), is interesting in that it could suggest direct movement of phenytoin to the brain predominantly via a brainstem-related pathway (e.g. bulk flow peripheral to trigeminal neurons) rather than the olfactory bulbs. Also interesting, is that the brain region/plasma ratios at 120 and 180 minutes after microparticles and 60 minutes after control solution (Figure 3.16A) all had a similar magnitude, despite variations in concentration, which may suggest that phenytoin from microparticles and solution was following a common pathway to the brain. The difference seen in the 60 minute microparticle data, in this respect, might have reflected a delay in uptake compared with control solution due to the existence of an intact epithelium to traverse in the former, but not the latter.

To supplement the discussion of intranasal phenytoin delivery pathways, 4-HPPH (the inactive, major metabolite of phenytoin) was also quantified in plasma and brain regions of the tested rats (Figure 3.15C and D). The first important thing that can be taken from looking at the 4-HPPH concentrations is confirmation that phenytoin found in the brain was clearly not the result of tissue contamination by blood, which is a common criticism of studies such as this where complete tissue perfusion (with saline for example) is not possible before analysis. Yarragudi et al.[204] rebutted this criticism by pointing out that the volume of blood vessels in the rat brain amounts to approximately 48 µL of blood which represents an insignificant amount of drug compared to the total brain concentrations found[218], however, the rebuttal would have been stronger had 4-HPPH concentrations been presented. Despite not being a classical low-permeability reference compound, such as radiolabelled sucrose (1-2%[219]) which can be used as a co-administered marker of blood vessel volume in the brain[220], penetration was expected to be very low after systemic delivery, based on the results presented in **Chapter Two** which

suggested very limited brain penetration from the systemic circulation (~5%). This finding is consistent with other reports discussed in **Chapter Two**[189,221].

It is therefore interesting that in the intranasal studies performed in this Chapter, the 4-HPPH levels in the brain appeared to be higher than expected, suggesting that perhaps this molecule was also following a direct pathway to the brain. In order for this to be true, however, some of the phenytoin would have to have been metabolised in the nasal passage prior to reaching the brain. It is important to acknowledge that CYP enzymes are expressed in the nasal epithelium[222,223] and it could therefore be a site of metabolism of phenytoin to 4-HPPH other than the liver. Interestingly though, CYP2C9 and CYP2C19, the two enzymes reported to be responsible for metabolism to 4-HPPH[224], have not to this author's knowledge been reported to exist in the nasal epithelium[222,223]. Furthermore, Antunes-Viegas et al.[225] studied metabolism of phenytoin in an *ex vivo* nasal tissue model but found no metabolism to 4-HPPH occurred in the tissue. While one could look critically upon the reliability of the *ex vivo* methodology, the different species the tissue was derived from, and the LLOQ of 200 ng/mL of their detection method, the available literature would seem to refute the possibility that phenytoin could be metabolised to 4-HPPH in the nasal epithelium. In contrast, the data of the present study, as discussed below, supports the possibility. The truth may lie in a couple of manuscripts that describe extensive capacity of other enzymes in the CYP2C family, namely CYP2C6 and CYP2C18, to metabolise phenytoin to 4-HPPH, the latter exceeding the turnover of CYP2C9 and CYP2C19 by at least four times[226,227]. While hepatic expression is poor compared with CYP2C9 and CYP2C19[228], CYP2C18 also happens to be the only 2C isoform that is highly expressed in the rat nasal mucosa[223] which both explains the scarcity of pharmacokinetic documentation for the enzyme with respect to phenytoin and supports the existence of a metabolic pathway for local phenytoin hydroxylation in the nose. While seemingly counterproductive to the idea that intranasal phenytoin delivery completely bypasses the pharmacokinetic hurdles of the systemic circulation, the notion does support the direct delivery of molecules to the brain through the nose which is, in the broader picture, a core theme of this thesis which aims to be a stimulus for expansion of quality research in the area.

As with phenytoin, concentrations of 4-HPPH in the brain following microparticle administration trended towards increasing between 60 and 120 minutes (Figure 3.15D). Unlike phenytoin concentrations, however, they did not show any evidence of reducing at 180 minutes, instead remaining at a similar level at 180 minutes and maintaining a similar distribution between the brain regions. As discussed earlier, plasma concentrations of phenytoin trended towards reducing after 60 minutes (Figure 3.15A), but for 4-HPPH they remained essentially

the same at all three time points after microparticle administration suggesting that production rate from phenytoin metabolism was essentially balanced by 4-HPPH clearance. This meant that the brain to plasma ratios (Figure 3.16B) reflected the brain concentration trend with an elevation at 120 minutes that persisted to 180 minutes. The main brain to plasma ratio of 4-HPPH at 60 minutes after microparticles was already twice that seen after the aforementioned 25 mg/kg intravenous dose in **Chapter Two** (Figure 2.9C) (0.12 ± 0.02 vs 0.06 ± 0.01) and while that intravenous ratio would be expected to decrease over time with phenytoin and 4-HPPH plasma levels (recall **Chapter Two** discussion), the ratio at 120 and 180 minutes after microparticles was even higher, supporting a direct intranasal delivery of 4-HPPH to the brain after nasal metabolism.

A further interesting consideration which could be relevant to the above is that 4-HPPH has been reported to exert a long-lasting inhibition of the hydroxylation of phenytoin in rats that produced it, meaning that during repeated administration, reduced elimination of subsequent doses is observed[229]. Considering the sustained release of phenytoin from microparticles, it is possible that in the context of an intranasal metabolism to 4-HPPH, phenytoin metabolism in the nose could be inhibited over time, leading to higher local concentrations of phenytoin which could be delivered directly to the brain and may have contributed to the high brain to plasma ratio at 120 minutes. What is usually a challenge to systemic delivery due to the potential for overshooting the therapeutic window and causing toxicity might therefore be an aid to optimal intranasal delivery. It should be noted though that limited evidence suggests the inhibition of phenytoin metabolism by 4-HPPH may not be significant in humans after systemic administration[230], so the translatability of this potential advantage is unknown.

The brain concentrations of 4-HPPH after the phenytoin control solution (Figure 3.15D) were interesting in comparison to those after microparticles, as unlike phenytoin levels, 4-HPPH did not appear to be elevated above the peak levels of the molecule measured after microparticles in the study. This contrasted with the plasma level (Figure 3.15C) which trended towards being elevated above those after microparticles at all time points. While the raised plasma 4-HPPH levels could expectedly be a product of the raised phenytoin levels in plasma which would be proportionately metabolised by the liver, this finding was not replicated in the brain concentrations. Consequently, the 4-HPPH brain to plasma ratios for the phenytoin control solution (Figure 3.16B) at 60 minutes were similar to those after microparticles at the same point and significantly less than those after microparticles at 120 and 180 minutes. A possible explanation for this can be constructed by again considering the histological confounding discussed earlier. If phenytoin were metabolised in the nasal epithelium, the nasal epithelium

would be required to be intact in order for this to occur. If the cells were damaged and could not metabolise the phenytoin, 4-HPPH would not be produced in the nasal cavity and therefore would not travel directly to the brain in quantities proportional to the phenytoin dose, as was postulated in the case of microparticles. Instead, phenytoin might be expected to be absorbed more easily into the systemic circulation through the damaged epithelium and exposed blood vessels and metabolised in the liver to 4-HPPH, thereby appearing elevated in the plasma, but not the brain due to its poor permeability when delivered systemically.

As implied earlier, no data on 4-HPPH was presented by Yarragudi et al.[204], despite validating the method to detect it. The reason for this is not stated, but it prevents what otherwise would have been an interesting comparison between the studies and perhaps could have shed some light on the discrepancies by allowing metabolite concentrations and trends to be followed to support the phenytoin concentrations reported. One possibility is that concentrations of 4-HPPH were not quantifiable with the method used. The LLOQ reported for 4-HPPH in the brain was 441 ng/g, which is high compared with the 23.4 ng/g in the more sensitive method used in this study. Even when applying the approximately 5-fold multiplication factor mentioned earlier to the 4-HPPH concentrations found in this study, they would still fall below the brain LLOQ of Yarragudi et al.[204]. Despite this, the LLOQ of plasma in that study was reported to be 185 ng/mL and based on the same logic, should have been quantifiable, but perhaps a lack of brain concentrations led to a decision to omit an incomplete data set.

A final additional experiment which could have contributed to the discussion of intranasal phenytoin delivery would have been an equivalent dose administered systemically by intravenous injection to track the fate of systemically absorbed compound compared to that delivered directly to the brain and the effect on seizures compared with intranasal microparticle delivery. In other words, it must be considered that increased levels of phenytoin in the brain at 120 minutes could have been a reflection of accumulation over time following absorption into the systemic circulation rather than direct intranasal delivery. Given the suspected confounding effect of ethanol in the MEST test, however, and its significant presence in the commercial intravenous formulation, such a study was not performed in this Chapter. Yarragudi et al.[204], whose focus was purely pharmacokinetics, did perform this experiment at time points up to 60 minutes (Figure 3.4) which can be used as an indicator of what would have been expected in terms of tissue levels of phenytoin. It was reported that brain concentrations were significantly and consistently lower than intranasal after an intravenous dose at 60 minutes, despite plasma concentrations being significantly and consistently higher, and thus brain to plasma ratio being consistently low, therefore brain concentrations would not be expected to increase at 120

minutes to match those achieved by intranasal administration. The same can therefore be inferred for any phenytoin absorbed into the blood from the nasal passage. Furthermore, phenytoin was too low to be quantified in the olfactory bulbs after intravenous dose administration by Yarragudi et al.[204], further supporting a direct delivery pathway in the case of intranasal administration. As a final comment, concentrations of 4-HPPH in the brain from the intravenous study of Yarragudi et al.[204] would also have been useful to further interrogate the data discussed above suggesting that 4-HPPH may also have been directly delivered to the brain through an intranasal pathway by providing a direct dose comparison.

Despite all of the evidence above to support phenytoin delivery from microparticles eliciting a peak anti-seizure effect at 120 minutes, the blank microparticles (without phenytoin) experiment at this time point exhibited an interesting variability in responses in individual rats (Figure 3.19) which, while far from revealing a statistically significant effect on seizure threshold was unexpected and is worth discussing as the reasons for it were unclear. No data exists, to this author's knowledge, to suggest that the polymer would have an acute pharmacological effect on seizure threshold. Therefore, even though the amount of TSP administered was slightly higher than in the phenytoin microparticles study (given that the phenytoin mass was replaced with TSP), this is unlikely to have contributed to the outcome. Furthermore, considering the 1000 Dalton (Da) limit proposed for good nasal absorption[231–233], the size of the TSP molecules (720-880 kilodaltons (kDa))[207] seems to preclude the possibility that they could even be taken up through an intact nasal mucosa to reach the brain, as opposed to phenytoin which is well below this limit (252 Da). Any effect therefore would have to have been locally mediated and happen to coincide with the peak brain concentrations of phenytoin. All of this seems less and less likely when considering that phenytoin microparticles had no significant effect at 60 minutes, yet contained 75% of the TSP dose of the blank microparticles.

So if there was no effect from the microparticles, attention must be directed to the seizure model and the technical limitations that could have led to such a finding. While the validation in **Chapter Two** seemed promising, variability appears to have arisen and limited some of the subsequent studies in this Chapter. By looking at the data from a different perspective (i.e. comparing overall percentage of HLE in saline vs phenytoin groups as shown in **Appendix K**), it can be seen that the values for the blank microparticles trial are very similar (28 vs 22%) supporting a lack of real effect, whereas the trend towards a lower incidence of HLE is more evident in the phenytoin microparticles groups at 120 minutes (28% vs 11%) and 180 minutes (33% vs 12%) supporting a true effect which was supported by pharmacokinetic data. Furthermore, the p values derived from Prescott's test, while not endowing statistical

significance on any of the results, other than upon pooling, offer a far greater statistical probability of the phenytoin microparticles having a true effect ($p = 0.3647$ (120 minutes) and $p = 0.1412$ (180 minutes) compared with $p = 1$ for blank microparticles, the latter effectively suggesting there is no possibility that the apparent effect of TSP microparticles is real based on the data available. Furthermore, while the anti-seizure percentage difference in the blank microparticle study is numerically larger than the pro-seizure effect (60% vs 13%), the number of rats in each group only differed by one (**Appendix L**).

It is worth discussing a few general limitations of the MEST study design which became apparent here in its application to test an intranasal delivery system. Firstly, variability in batches of rats used for determining the CC_{50} threshold meant the threshold was calculated to have much wider confidence limits in the rats which participated in the later microparticle trials (120 and 180 minutes) and the resulting experimental response after saline reflected more of a CC_{30}, limiting the resolution for detecting drug effects compared with earlier experiments. It is possible that variation in ages and weights within studies (**Appendix A and B**) and mixtures of different genetic backgrounds may have led to the variability in this first stage and the difficulty in the estimating the CC_{50} in a number of groups. A future suggestion would be to employ rats that are as homogenous as possible, something which could not be strictly controlled in this study as the author was not able to personally breed the animals. Nonetheless, at least the study design allowed for the experiment to be continued with lower resolution rather than producing only CC_{50} thresholds with confidence intervals too large to meaningfully compare as may have occurred with the traditional design.

Another consideration is that because the CC_{50} was determined separately for each batch of rats, the stimulation current was different in each experiment which could possibly have led to variability in responses based on the current rather than the time point after treatment or the presence or absence of phenytoin. For instance, it could be argued that because the stimulation current was slightly lower for blank microparticles (56 mA) compared with phenytoin microparticles at 120 minutes (62 mA), that the blank microparticle rats could have been more susceptible to intra-subject variations in threshold due to extra-experimental variables (e.g. response to isoflurane, social cues, stress). This might have contributed to the changes seen in both pro- and anti-seizure directions while the overall difference in the groups was very small as discussed above. Overall, the statistically calculated CC_{50} values determined in all of the MEST experiments in this Chapter were not found to be statistically different from one another (**Appendix M**). The experimentally determined CC_{50} values after saline administration, on the contrary, showed that different batches did appear to have different CC_{50} values; the ones with

around 30% HLE after saline suggesting a higher stimulation current would have been optimal to achieve 50% HLE. In this context, and given that the saline trials for both blank and phenytoin microparticles showed approximately 30% HLE, the 8 mA difference in stimulation current between the experiments was probably not a significant contributor to variability. Perhaps the real orchestrator of variability was simply whether there was any anti-seizure drug present or not. In the cases where phenytoin was present, the effect on seizure threshold was decidedly anti-seizure regardless of the stimulation currents used (63, 62 and 54 mA for 60, 120 and 180 minutes respectively) the magnitude of which complemented brain drug concentrations, while when it was not, there seemed to be more room for extra-experimental variables to have a significant influence.

3.7 Conclusions

This Chapter used the seizure model established in the previous Chapter to evaluate tamarind seed polysaccharide microparticles as an intranasal delivery system for phenytoin. A peak anti-seizure effect of the drug was identified at 120 minutes after microparticle administration, suggesting the microparticles to be a fairly slow-acting, but sustained anti-seizure drug delivery system with potential for future application in the regular dosing of phenytoin. As well as this, these experiments were also an evaluation of the seizure model to detect the more subtle effects of phenytoin that were expected after delivery by the nasal route at much lower doses. In this respect, it succeeded in that pharmacodynamic data was obtained that complemented pharmacokinetic studies of phenytoin concentrations in the plasma and brain. In addition, the simultaneous monitoring of the drug's major metabolite, 4-HPPH, offered an interesting insight into intranasal trafficking of phenytoin and supported the argument that a direct route to the brain was being exploited. Interestingly, accumulation of phenytoin in the olfactory bulbs was not observed and, if anything, the brain distribution was weighted slightly towards the brainstem, suggesting an alternative pathway to the commonly referenced passage through the olfactory neurons. Lastly, the importance of histological studies as an essential component of intranasal drug delivery studies was emphasised by the comparison of the biocompatible phenytoin microparticles with an evidently incompatible ethanol-containing phenytoin control solution. Overall, the results supported the application of the seizure model as a screening tool to gauge the effects of intranasally delivered anti-seizure drugs, setting the necessary foundations for an investigation into a compound with untested activity.

Chapter Four

On the Intravenous and Intranasal Delivery of Oleoylethanolamide and its Effect on Seizures

4.1 Introduction

Having explored the delivery of an existing ASD through the nose in **Chapter Three** with some encouraging results, this Chapter now heads further towards the unknown in the investigation of oleoylethanolamide (OEA). OEA is an endogenous molecule which is hypothesised to have an anti-seizure effect[234], but this has not so far been tested or reported on in the literature. A likely reason for the lack of investigation into the effects of OEA is the rapid *in vivo* hydrolysis it is subject to after systemic administration by Fatty Acid Amide Hydrolase (FAAH), which limits its therapeutic utility[235]. Despite this, it has been reported to show neuroprotective effects in other conditions including stroke[236,237] and Parkinson's disease[238].

The hypothesis that OEA could have an anti-seizure effect is based primarily on the effects reported from structurally related molecules in the N-acylethanolamide (NAE) class, palmitoylethanolamide (PEA)[239,240] and anandamide (AEA)[241] (Figure 4.1). In the case of anandamide, the ED_{50} (effective dose in 50 % of animals) in the MES test was unable to be measured up to a dose of 300 mg/kg i.p., highlighting the significance of its short plasma half-life due to FAAH hydrolysis[235,242]. When combined with the FAAH inhibitor phenylmethylsulfonyl fluoride, anandamide still exhibited a fairly high ED_{50} of 50 mg/kg i.p.

(at a time of peak effect of 20 minutes)[241], but it was able to demonstrate an anti-seizure effect. As acknowledged by the authors, however, it is debatable whether the effect seen was entirely due to the exogenously administered anandamide or a generalised FAAH inhibition resulting in an increase in endogenous levels and effects of NAEs. Interestingly, the ED_{50} of palmitoylethanolamide (PEA) determined in the MES test in another study[239] was much lower (9.2 mg/kg i.p. with a time of peak effect of 2 hours). While the longer time to peak effect may be explained by poor absorption due to precipitation at the injection site (as noted by the authors), the reason for the lower ED_{50} is less clear. It could be related to an alternative site of anti-seizure action at which PEA is more potent or allosteric (as it does not act at cannabinoid receptors like anandamide[242,243]), a lower affinity for FAAH[244] or perhaps the so-called 'entourage effect' whereby it acts indirectly by decreasing FAAH metabolism of other NAEs such as anandamide[242]. Notably, it also did not induce any neurological impairment up to a dose of 250 mg/kg, highlighting a potentially significant benefit to the investigation of naturally biocompatible endogenous molecules as therapeutics when considering the marked role that intolerable adverse effects play in the failure of epilepsy treatments. PEA has also been tested in chemically-induced seizures (e.g. pentylenetetrazole test) and found to suppress the tonic, but not the clonic, components of the seizures[239,240]. Furthermore, one of these studies also showed PEA to be largely ineffective in amygdala-kindled animals and suggested a possible selective action on brainstem compared to forebrain circuits or that perhaps the molecular substrates of tonic and clonic seizures were differentially affected by NAEs[240].

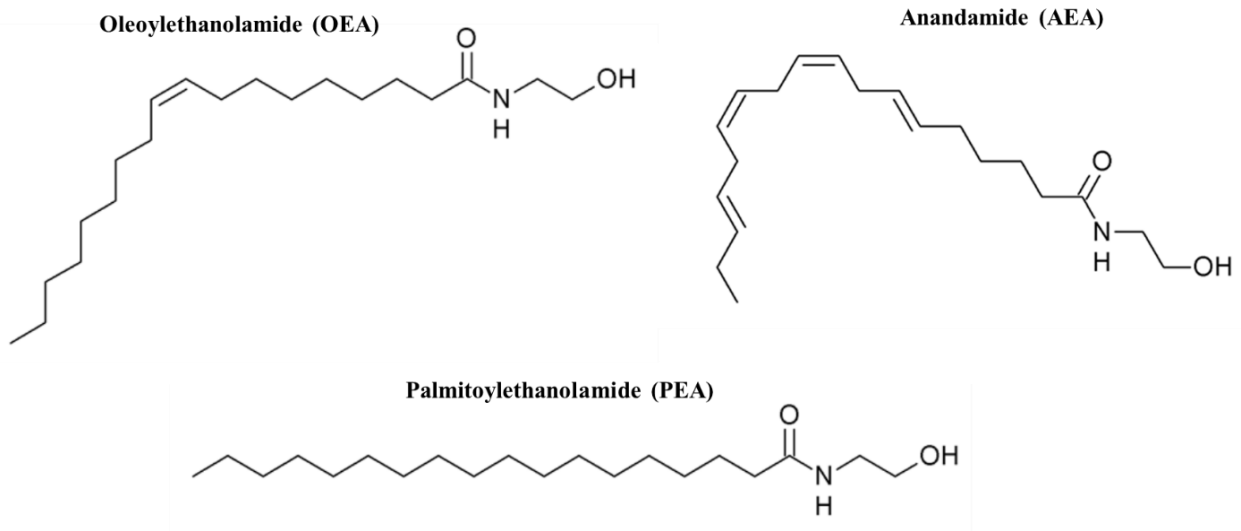

Figure 4.1. OEA and structurally related molecules AEA and PEA.

The main mechanism of action proposed for the neuroprotective effects of OEA is peroxisome proliferator-activated receptor alpha (PPARα) agonism, although it is thought to act at other receptors as well[242,245]. It should be noted that PEA also acts at the PPARα receptor, but is markedly less potent (EC_{50} = 3 μM vs 120 nM for OEA) and the activity of AEA at the receptor remains a matter of debate[242]. Interestingly, other drugs with reported PPARα agonist activity have demonstrated anti-seizure effects[246–248], including the clinically-used anti-seizure drug, valproic acid[249–253]. Furthermore, a consequence of the ketogenic diet, a commonly used adjunct for managing drug-resistant epilepsy, is increased levels of polyunsaturated fatty acids, which also act as PPARα agonists and it has been postulated that this may play a role towards its efficacy[254]. This has been further substantiated by a study which found no added benefit from combining fenofibrate, a PPARα agonist, and the ketogenic diet on increasing seizure threshold in the PTZ test, compared to each treatment alone, suggesting a possible common pathway (Figure 4.2). This phenomenon is, however, a chronic effect. While a change in gene transcription resulting from PPARα agonism is the most widely accepted hypothesis for the effects of OEA, it is inherently slow, meaning other non-genomic pathways are likely to elicit the rapid effects that have been reported with acute administration in other conditions[236–238,245,255]. Non-genomic actions have also been associated with PPARs, however, and it has been suggested that effects may be achieved through ligand-bound PPARα stimulating the activity of tyrosine kinases (Tyr Kin), which, in turn, phosphorylate surface-expressed nicotinic acetylcholine receptors (nAChR) and reduce their response to agonists[242,256] (Figure 4.2) thereby modulating excitation and potential seizure pathways[257].

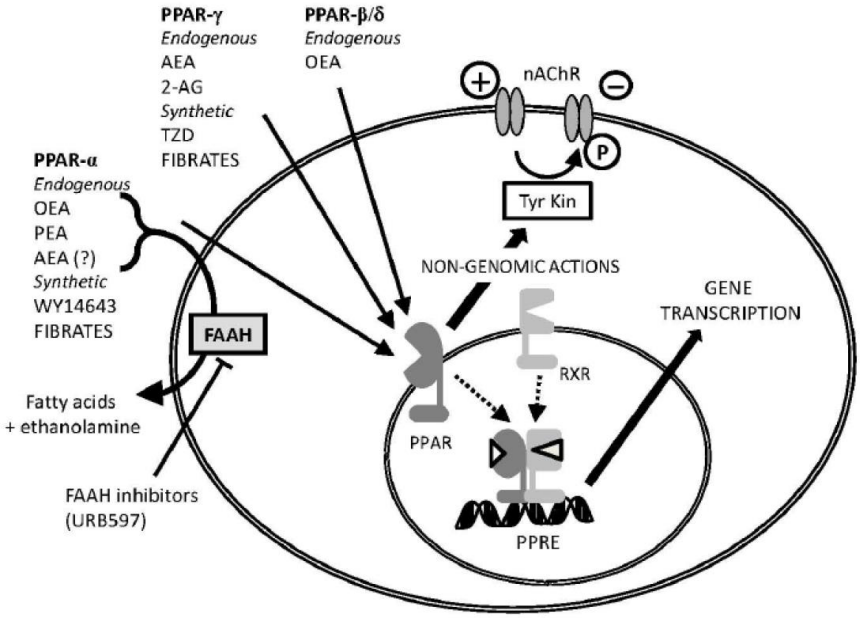

Figure 4.2. Schematic diagram of the mechanism of PPARa activation by OEA leading to non-genomic (rapid) and genomic (slow) effects. Figure adapted with permission from Pistis & Melis[242]. FAAH = fatty acid amide hydrolase; Tyr Kin = tyrosine kinase; P = phosphate; nAChR = nicotinic acetylcholine receptor; PPAR = peroxisome proliferator-activated receptor; PPRE = peroxisome proliferator response element; RXR = retinoid X receptor; 2-AG = 2-arachidonoyl glycerol; TZD = thiazolidinediones; AEA = anandamide; OEA = oleoylethanolamide.

As a means to potentially overcome the challenge of hydrolysis, as well as provide a physiologically suitable aqueous vehicle for administration of poorly soluble OEA, Younus et al.[258] recently reported the incorporation of OEA into self-assembling liquid crystalline lipid nanoparticles called cubosomes (with an encapsulation efficiency of >99%) which will be utilised as a delivery system for OEA in this **Chapter**. The structure of a cubosome can be described as a continuous negatively-curved lipid bilayer twisted around two non-intersecting water channels to form a structure with cubic symmetry (Figure 4.3)[259]. A cubosome has a very large surface area for its size and contains both hydrophilic and lipophilic regions, permitting the encapsulation of hydrophilic, amphiphilic or lipophilic additives. A surface stabiliser is necessary to prevent aggregation between the particles[260,261]. Cubosomes can be classified according to the three periodic minimal surfaces shown in Figure 4.3C[262]. In general, the *Ia3d* structure has been proposed to form at low hydration levels, transitioning to the *Pn3m* and then *Im3m* structure with increasing hydration and lessening negative curvature of the bilayer. The third structure, *Im3m*, also tends to form as a result of structural disruption by the incorporation

of other molecules above a certain concentration[261,263-264] and exhibits a larger lattice spacing[263]. It is this form which the OEA cubosomes used in this **Chapter** assume upon production[258].

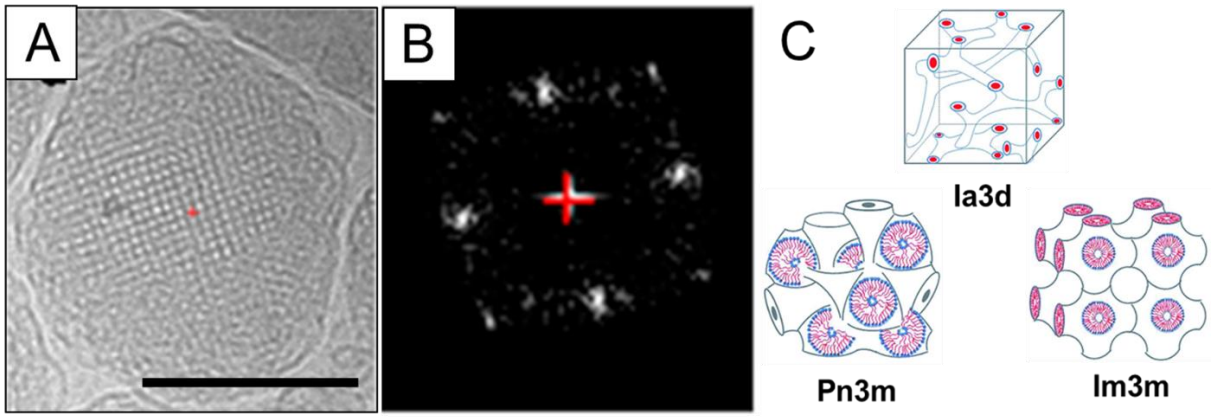

Figure 4.3. The internal structure of cubosomes. (A) Cryogenic transmission electron microscopy (Cryo-TEM) image of an OEA cubosome (scale bar = 200 nm), (B) Fast Fourier Transform of the image in A to reveal the internal cubic symmetry of the particle and (C) Schematic diagrams of the three possible internal structures of cubosomes: primitive (Ia3d), gyroid (Im3m) and diamond (Pn3m). Panels and B adapted with permission from Younus et al.[258] Copyright American Chemical Society. Panel C adapted from Chen et al.[265] with permission.

The self-assembly and maintenance of the cubosome structure is a factor of the geometric properties of the component molecules and their surrounding environment; particularly features such as solvent concentration and temperature, the modification of which may lead to dynamic changes in the internal structure to form alternative self-assembled lipid structures such as hexosomes or liposomes[260] (Figure 4.4). A critical, but so far infrequently studied, implication of this is the effect of complex biological media on cubosomes, which must inevitably be elucidated if systemic administration is to be an end application. Of particular note, a previous study has reported the transformation of basic phytantriol cubosomes to hexosomes on exposure to blood plasma[266], which it was speculated may have implications for systemic delivery of OEA cubosomes in this Chapter.

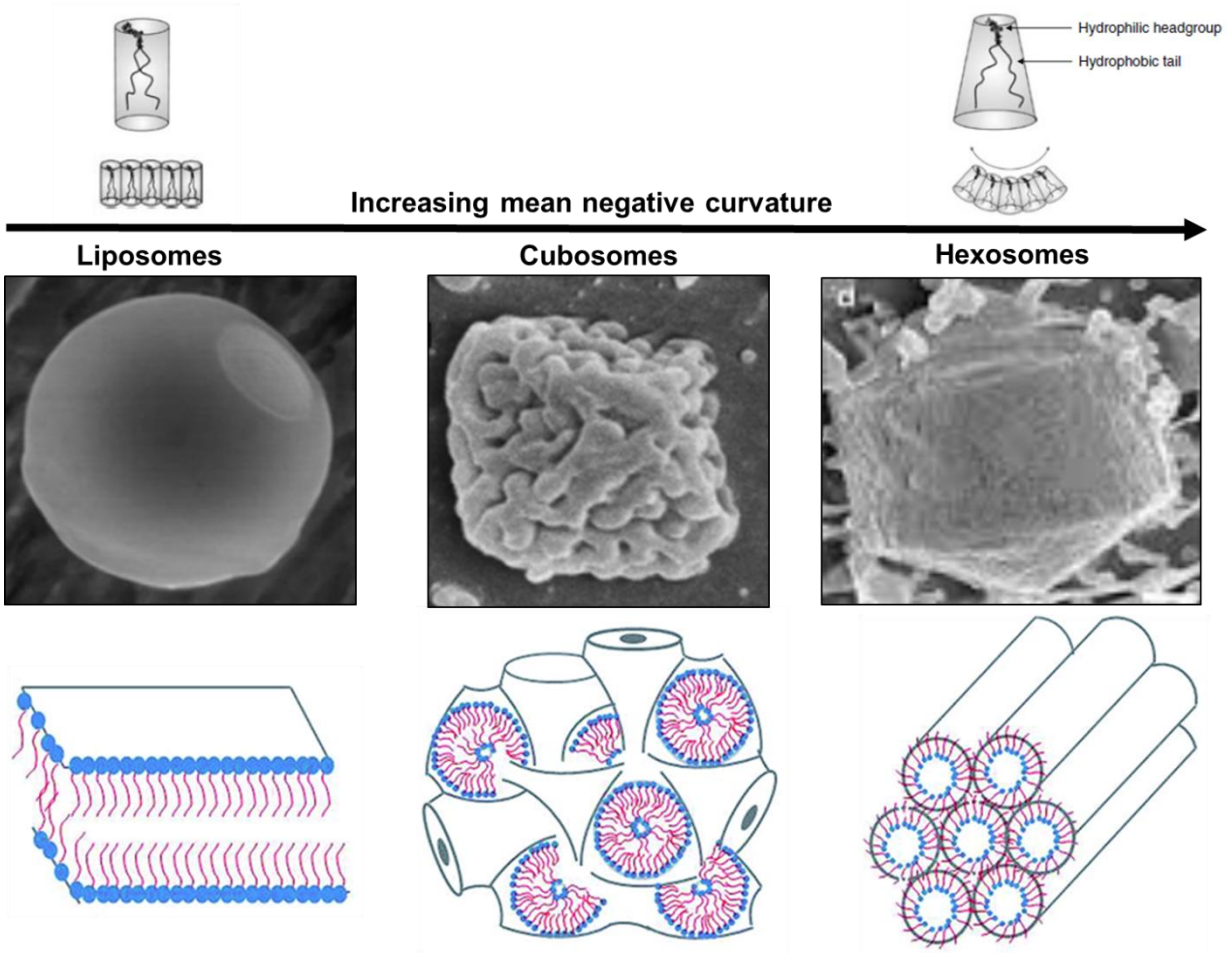

Figure 4.4. Relationship between cubosomes and other commonly studied self-assembling lyotropic liquid crystalline structures, liposomes and hexosomes. Adapted with permission from Huang and Gui[267](published by the Royal Society of Chemistry), Rizwan and Boyd[260], Rizwan et al.[268], Boyd et al.[269] (Copyright American Chemical Society) and Bibi et al.[270]

The premise of this approach is that OEA is co-formulated into the cubosome with a non-hydrolysable lipid, phytantriol, based on the hypothesis that both the tortuous structure and the presence of this second lipid will aid in shielding OEA from degradation and allowing it to reach its target site in the brain. Younus et al.[271] showed an *in vitro* resistance of the particulate OEA to FAAH hydrolysis but *in vivo* stability and brain delivery has not yet been studied. It is hypothesised that OEA will remain in a particulate form as it travels through the plasma or via the nose to the brain, allowing protection of OEA *in vivo*. This could perhaps be augmented by the adsorption of a protein corona to cover the surface of the nanoparticles, as has been described for similar drug delivery systems elsewhere[272–274] and supported by the present author's own unpublished extracurricular studies.

This Chapter sets out to evaluate whether administering OEA through the nose (and potentially avoiding the systemic circulation) could deliver it via this direct route to the brain and elicit an anti-seizure response. Given the unproven effects of OEA on seizures, however, it starts by investigating the systemic (intravenous) administration of cubosomal OEA. This permits exploration of the effect of the OEA cubosomes on seizures in two key ways. Firstly, in the absence of potentially confounding anaesthetic (an unavoidable limitation to intranasal studies) and secondly, after administration via a route which guarantees the OEA enters the blood circulation at a dose which could be expected to show an anti-seizure effect in the absence of rapid hydrolysis and following successful brain delivery. To complement this, the Chapter also investigates the pharmacokinetics of 13-Carbon-labelled OEA (^{13}C-OEA) delivered intravenously in cubosomes through the development of an LC-MS analytical method and studies the time-resolved *in vitro* structural stability of OEA cubosomes in plasma utilising small angle X-ray scattering (SAXS). To conclude the Chapter, the effects of intranasal OEA cubosomes on MEST seizure threshold and nasal epithelial integrity are determined.

4.2 Aims

The overall aim of this Chapter was to use the seizure model developed in **Chapter Two** and **Chapter Three** to investigate a potential anti-seizure effect of the endogenous endocannabinoid-like molecule, OEA, using cubosomes as a drug delivery platform. To achieve this, the following objectives were set:

- Determine if OEA (in cubosome form) has an effect on seizure threshold after systemic (intravenous) administration.
- Develop and validate an LC-MS method to detect ^{13}C-labelled OEA in rat plasma, brain and liver tissue.
- Determine the plasma, brain and liver tissue levels of ^{13}C-OEA after systemic administration as cubosomes to determine whether any pharmacodynamic effect seen (or not seen) could be attributable to chemical stability (or instability) of OEA.
- Evaluate the *in vitro* structural stability of OEA cubosomes in rat plasma to determine whether any pharmacodynamic effect seen (or not seen) and any chemical stability (or instability) might be attributable to structural stability (or instability) of OEA cubosomes.
- Evaluate the acute histological impact of OEA cubosomes on the rat nasal epithelium and determine a suitable dose for administration via the nose.
- Determine if OEA (in cubosome form) has an effect on seizure threshold after intranasal administration.
- Evaluate the histological impact of OEA cubosomes on the rat nasal epithelium in seizure test subjects after a three day period.

4.3 Hypotheses

- OEA will have an anti-seizure effect in the MEST seizure test after systemic (intravenous) administration, as reported for structurally similar NAEs in the related MES model.
- ^{13}C-OEA will exhibit a longer plasma half-life/resistance to degradation in plasma when administered as cubosomes compared with a ^{13}C-OEA control solution.
- OEA cubosomes will distribute and accumulate to some extent in the liver, given their size and previous reports on lipid nanoparticles accumulating there due to the presence of fenestrated blood vessels.
- OEA cubosomes will undergo structural changes on exposure to blood plasma which could play a role in their ability to protect OEA from hydrolysis and deliver it to the brain.
- OEA cubosomes can be intranasally administered without disrupting the integrity of the olfactory epithelium.
- OEA will elicit an anti-seizure effect after intranasal administration in cubosomes. The nose may offer a more direct route to the brain for OEA, thereby allowing a more rapid onset of effects and decreasing pre-target degradation in the systemic circulation allowing dose reduction.

4.4 Materials & Methods

4.4.1 Materials

Oleoylethanolamide (OEA) was purchased from Toronto Research Chemicals (Canada). Deuterated oleoylethanolamide (d_4-OEA) was purchased from Cayman Chemical (USA). ^{13}C-Oleoylethanolamide (^{13}C-OEA) was kindly synthesised and provided by Callaghan Innovation, New Zealand. Phytantriol (3,7,11,15-Tetramethyl-1,2,3-hexadecanetriol) was purchased from A & E Connock (England). Dimethyl sulfoxide (DMSO) (≥99.5%, plant cell culture tested), Polysorbate 80 (Tween 80®), propylene glycol (PG), formic acid (for mass spectrometry, ~98%) and phosphate-buffered saline sachets (pH 7.4) were purchased from Sigma Aldrich (New Zealand). EMSURE® Chloroform for analysis was purchased from Merck (Germany). Acetonitrile (ACN) (LiChrosolv®), Methanol (MeOH) (LiChrosolv®), tert-Butyl Methyl Ether (TBME) (LiChrosolv®) and Ethanol (EMSURE®) were purchased from Lab Supply (New Zealand). All of these solvents were liquid chromatography grade. Male Wistar rat plasma, brain and liver tissue for LC-MS method validation and standard preparation was obtained in-house from control rats administered saline treatments. Male Wistar rat plasma for SAXS experiments was kindly provided by Monash Institute of Pharmaceutical Sciences, Victoria, Australia. All water used in this study was ion exchanged, distilled and passed through a Milli-Q water purification system (Millipore, USA).

4.4.2 Animals

All procedures involving animals were approved by the University of Otago Animal Ethics Committee pursuant to Animal Use Protocols 08/16, 65/16 and 130/18. Male Wistar rats sourced from the Hercus Taieri Resource Unit were used in all experiments. Specific weights and ages of animals over the course of the experiments can be found in **Appendix B and N**. Animals were housed under laboratory conditions in the Hercus Taieri Resource Unit for the duration of the experiment.

4.4.3 Preparation of OEA Treatments

4.4.3.1 Preparation of OEA Cubosomes, Dispersion and Solution

Cubosomes for intranasal histopathology and pharmacodynamic MEST experiments were prepared with 30% OEA (stabilised with Polysorbate 80®) as described previously by Younus et al.[271] OEA was added to a 20 mL glass vial along with phytantriol so that it constituted 30%

w/w of the total lipid. In addition, propylene glycol (sufficient to achieve 5% w/v in the final dispersion) and a surface stabiliser (Polysorbate 80®) (sufficient to achieve 0.3% w/v in the final dispersion) were added and the mixture was dissolved in excess chloroform. The chloroform was evaporated fully from the vial using a Buchi Rotavapor R-210 (Buchi, USA) at a pressure of 300 kPa (generated by a Buchi V-850 vacuum controller with V-700 vacuum pump) in a 45 ºC water bath (Buchi B-491). Subsequently, Milli-Q® water, pre-heated to 45ºC, was added to the vial (in sufficient volume to give a final total lipid concentration of 20 mg/mL (2% w/v)), followed by a monolayer of 4 mm diameter soda lime glass beads. The vial was immediately vortexed for 10 minutes at 35 Hz. A free OEA suspension for use in the intranasal histopathology experiments was produced using the same method, but without the addition of the cubosome-forming lipid, phytantriol.

For the intravenous pharmacokinetic experiment, the same method was followed, but with ^{13}C-OEA (kindly synthesised and provided by Callaghan Innovation, New Zealand) replacing OEA and the OEA content of the cubosomes being reduced to 10% w/w of total lipid due to limited availability of the carbon-labelled compound. ^{13}C-OEA control solution was prepared by dissolving ^{13}C-OEA in DMSO and ethanol, then diluting this mixture with Milli-Q water to give a final composition of 10% DMSO, 40% ethanol and 50% water. The concentration of ^{13}C-OEA in both the control solution and the cubosome dispersion was 2 mg/mL.

For the SAXS experiments, cubosome dispersions were prepared at a concentration of 20 mg/mL lipid with 0% (phytantriol only), 10% and 30% OEA content (w/w total lipid) using the same method described above.

4.4.3.2 Dynamic Light Scattering (DLS)

Particle size and polydispersity index (PDI) of cubosome dispersions was measured using a Malvern ZetaSizer Nano® (ATA Scientific, Australia) in order to validate that the formulations to be used were comparable to those previously reported (published[258] and unpublished data). A sample of cubosome dispersion was diluted to a concentration of approximately 0.2 mg/mL (10 µL of dispersion added to 1 mL of water) total lipid in Milli-Q water and placed in a disposable cuvette to measure size (Z-average) and polydispersity index. Three sets of size measurements, each comprising 10 runs, were performed for each formulation at 25 °C and a scattering angle of 173 º.

4.4.4 Drug Administration

For the intravenous pharmacodynamic MEST study with OEA, rats were injected with a 7.5 mg/kg dose of OEA cubosomes through a lateral tail vein using a 0.3 mL or 0.5 mL insulin Lo-dose syringe (BD Biosciences, New Zealand) at a pre-determined time point before MEST stimulation. Isoflurane anaesthesia was not performed prior to drug administration in this experiment as, unlike intranasal administration, intravenous administration was able to be performed on conscious animals, therefore allowing the removal of the anaesthesia as a potential confounding variable from this experiment.

For the intravenous pharmacokinetic study with ^{13}C-OEA, rats were injected with a 1 mg/kg dose of ^{13}C-OEA in cubosomes or solution through a lateral tail vein using a 0.3 mL insulin Lo-dose syringe (BD biosciences) at a pre-determined time point before euthanasia.

For the intranasal studies, OEA cubosomes and OEA suspension were administered using the Rat Intranasal Catheter Device following isoflurane anaesthesia as described in **Chapter Three**. For initial dose screening studies, the concentration of each was equivalent to 6 mg/mL OEA. For the subsequent MEST experiments, the cubosome dispersion was diluted to a concentration of 1.5 mg/mL OEA (5 mg/mL w/v total lipid). The volume administered was kept constant at 20 µL.

4.4.5 Behavioural Analysis in Intranasal Dose Determination Studies

Behaviour was monitored for 60 minutes after administration of the OEA cubosomes and suspension for any potential signs of nasal irritation such as frequent sneezing, noisy breathing, red (porphyrin) discharge, nose-rubbing or general signs of pain/discomfort (with reference to the Rat Grimace Scale[275]).

4.4.6 Tissue Collection and Histological Processing

In ^{13}C-OEA pharmacokinetic studies, rats were euthanised after one of four time points (15, 30, 60 or 90 minutes) following the injection. Trunk blood was collected in a 6 mL blood tube coated with sodium heparin (BD Biosciences, New Zealand) at the time of euthanasia and centrifuged immediately for 10 minutes at 2000 G (Sigma 1-6 compact centrifuge, Sigma, Germany) to obtain plasma, then aliquoted and frozen immediately on dry ice before transfer to a -80 °C freezer. The brain and liver were immediately dissected, rinsed in PBS (pH 7.4), blotted on filter paper, weighed, and then frozen on dry ice.

In intranasal studies, nasal tissues were collected at 60 minutes after drug administration in the initial dose screening experiments and at either 60 minutes or three days after administration to determine effects of the formulation on the nasal epithelium of rats in the pharmacodynamic MEST experiments. As described in **Chapter Three**, rats were euthanased by guillotine decapitation and after removal of the brain, eyes, lower jaw and excess skin and tissue around the nasal passage were removed from the skull. A blunt needle was inserted 0.5 cm into the posterior nasopharyngeal duct and used to flush the nasal passage with 10 mL of 10% neutral buffered formalin. Subsequently, the nasal passage was fixed in 50 mL of NBF for 48-72 hours. The fixed nasal passage was then decalcified in 10% EDTA (pH 7.2) for two to three weeks, sliced coronally into blocks, as per published methods[83,150] and embedded in paraffin wax. A microtome (Leica Jung RM 2025, Leica Biosystems, Australia) was used to cut 5 µm sections from region III which were subsequently deparaffinised, stained with haemotoxylin and eosin, and cover-slipped with DPX mounting medium. Sections were imaged on an Aperio ScanScope (Leica Biosystems, Australia). Images were analysed using Aperio ImageScope v12.2.2.5015 software (Leica Biosystems, Australia).

4.4.7 Maximal Electroshock Stimulation Threshold Test

The MEST experiments were performed in accordance with the stimulation procedure outlined in **Chapter Two**. Intranasal studies followed the cross-over study design used in **Chapters Two and Three**, while the study design for the intravenous experiments was modified to allow screening at multiple time points after drug administration in a single batch of rats (Figure 4.5). It was hypothesised that the dose and systemic route of delivery of OEA should be sufficient to demonstrate an effect in a smaller group than in intranasal studies, if one was to be seen. The modified design also allowed the exclusion of potential confounding that might exist if washout of cubosomes and their respective components from the body after intravenous administration was inadequate, as no information is currently available on their clearance or effects on seizure threshold.

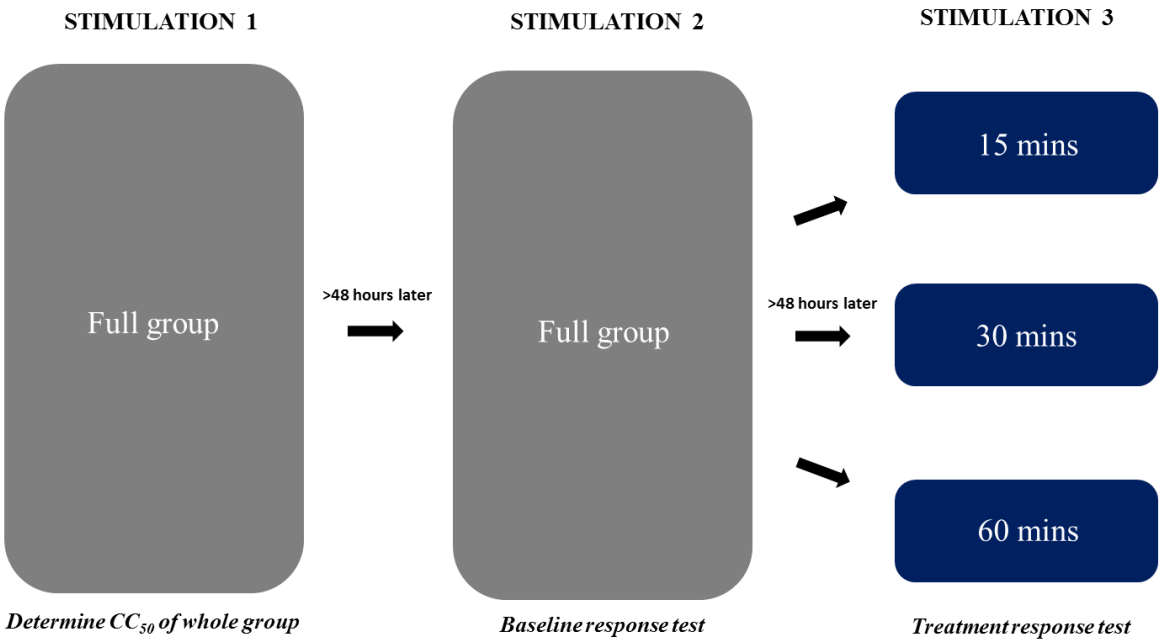

Figure 4.5. Study design for intravenous OEA cubosome experiments.

As in the cross-over design, a total of three stimulations were delivered to each rat, no less than 48 hours apart. For the first stimulation, the "up and down" method was used to estimate the CC_{50} for HLE in the group, as described in **Chapter Two**. For the second stimulation, all rats were stimulated at the calculated CC_{50} without any prior treatment and their baseline response recorded. Prior to the third stimulation, rats were randomly divided into three groups, each consisting of a 50% proportion of rats that had shown HLE at the CC_{50}. Each group was assigned a time point (15, 30 or 60 minutes), then OEA cubosomes were intravenously administered and each rat was stimulated at the CC_{50} at their assigned time point after drug treatment to determine their response. Statistical comparisons were made between responses using the sign test.

4.4.8 Small-Angle X-ray Scattering

SAXS is a technique used to elucidate the internal structure of liquid crystalline nanoparticles in a sample, allowing the predominant mesophase to be elucidated[260]. It was used in this Chapter to study the *in vitro* time-resolved stability of the internal structure of OEA cubosomes upon incubation with rat plasma to simulate stability after the intravenous administration that was performed in the pharmacokinetic and pharmacodynamic experiments. Experiments were conducted on the small-angle X-ray scattering/wide-angle X-ray scattering (SAXS/WAXS) beamline at the Australian Synchrotron (Victoria, Australia) during beamtime granted for

Proposal 13722. Samples were prepared in a clear 96-well plate and mounted vertically in a temperature-controlled holder maintained at 25 ºC or 37 ºC in the beam path. Measurements were taken with a photon energy of 13 kilo electron volts (keV). The detector was a Pilatus 1 M (170 mm × 170 mm). A sample-to-detector distance of 1.6 m and a scattering vector (q) range of 0.0126 to 0.62 were used.

The cubosome samples measured primarily included OEA-phytantriol cubosomes stabilised with Polysorbate 80 and containing OEA proportions of 10% and 30% w/w of total lipid, as well as phytantriol only cubosomes as a control to examine how OEA affected the outcome. Other cubosome formulations of indirect relevance to this Chapter were simultaneously studied and data from selected samples is provided in **Appendix O** of this thesis in order to supplement the experimental discussion of this Chapter. Initial measurements of cubosome dispersions were taken at 25 ºC to validate that the expected cubic mesophase existed in the samples before any temperature change or exposure to rat plasma. To determine the time-resolved stability of cubosomes upon incubation in rat plasma the procedure was as follows. Cubosomes or Milli Q water (control) in 100 µL aliquots were added to the wells. An aliquot of 100 µL of rat plasma or Milli Q water (control) was then added to each well and triturated gently using a multi-channel pipette. The plate was then loaded into the holder in the beam path. Measurements were taken from 30 minutes after mixing to allow temperature equilibration in the holder, then at 10 minute intervals from 30-60 minutes, 15 minute intervals from 60-180 minutes and 30 minute intervals thereafter over the course of seven hours. The two-dimensional diffraction patterns recorded on the Pilatus detector were reduced to one-dimensional intensity versus q profiles using Scatterbrain software provided by the Australian Synchrotron. The data was analysed by indexing Bragg peaks for known liquid crystalline structures[276] and lattice parameter dimensions calculated over time using known relationships from the d-spacings.

4.4.9 Liquid Chromatography Mass Spectrometry (LC-MS) Method for Analysis of ^{13}C-OEA in Plasma, Brain and Liver

4.4.9.1 Extraction and Sample Preparation

Frozen brains and livers were homogenised after adding 2 mL/g (based on wet weight determined after washing in PBS and blotting with filter paper at the time of dissection) of ice cold Milli Q water and allowing to sit on ice for 5 minutes prior to homogenisation on ice with a tip sonicator (UP50H Ultrasonic Processor, hielscher Ultrasound Technology, Germany) (1 cycle, 100% amplitude). The homogenate was aliquoted into 1.7 mL ultra clear microtubes

(Axygen, USA) and frozen at -80 °C again. Aliquots of 100 µL were made in quadruplicate at this stage and the rest were around 1 mL. Plasma was thawed on ice and prepared without dilution, except for four samples, which were diluted with blank plasma in order to be quantifiable within the standard range.

The 100 µL aliquot was taken out of the freezer and 5 µL of the internal standard (d_4-OEA), and 5 µL of methanol (solvent) added as it thawed. Once possible, this was vortexed, then 200 µL chilled ACN was added. This mixture was sonicated briefly, then 800 µL chilled TBME was added and it was sonicated briefly again, then vortexed briefly. It was then centrifuged at 17,200 G for 20 minutes at 4 °C (Prism™ R Microcentrifuge, Labnet International, Inc., USA).

The samples were taken into a precooled tray, then 800 µL of the supernatant was taken and transferred to a new tube. These tubes containing the supernatant were then evaporated to dryness in a centrifugal evaporator (Thermo Savant Speed Vac®, Thermo Fisher Scientific, New Zealand) until dry (4-10 hours, depending on the tissue type). A 200 µL volume of methanol was then added to each tube and it was briefly sonicated and vortexed to reconstitute. A brief centrifugation (10,000 revolutions per minute (rpm) for 1 second) followed to ensure all liquid was moved to the bottom of each tube. Samples were then pipetted into the top of a 1 mL syringe (BD Biosciences, New Zealand) and filtered through a 13 mm Nylon 0.22 µm syringe filter (Microanalytix, New Zealand) into a 250 µL or 100 µL insert (PP BM insert with bottom spring case (Phenomenex, USA)) in a 2 mL clear glass vial (Thermo Fisher Scientific, New Zealand). Samples were stored at 4 °C until analysis.

4.4.9.2 Standard Preparation

The stock solution for ^{13}C-OEA standard preparation was produced by dissolving ^{13}C-OEA powder in methanol at a concentration of 1 mg/mL. The stock solution for d_4-OEA was provided as a 1 mg/mL solution in ethanol. Serial dilution of these solutions in methanol was performed to achieve the desired standard concentrations. To prepare standard samples for analysis, aliquots of standard solutions (5 µL) were mixed with blank plasma, brain or liver homogenate aliquots (100 µL) in place of the 5 µL of blank methanol added to the unknown samples, as described above. The extraction procedure was the same from that point forward. Standards covered a range of 0.39 to 25 ng/mL for plasma and 1.17 to 75 ng/g for brain and liver tissue. Quality control samples were prepared alongside standards at concentrations within the relevant ranges.

4.4.9.3 LC-MS Analysis

Samples were analysed using an Agilent 1290 HPLC system (G4226A autosampler, LC binary SL pump, TCC SL (Agilent, USA)) connected to an AB Sciex QTRAP 5500 mass spectrometer with Turbo Spray ion source (Sciex, USA). Parameters were optimised to detect the compounds of interest as shown in Table 4.1.

Table 4.1. Optimised parameters for compound analysis.

Entrance potential (V)	10
Curtain gas (psi)	10
Collision gas	Medium
Ionspray voltage (V)	5500
Temperature (°C)	600
Ion source gas 1 (psi)	40
Ion source gas 2 (psi)	40

Figure 4.6 shows the molecular structures and molecular masses of the compounds analysed as well as the expected fragmentation in positive ion mode.

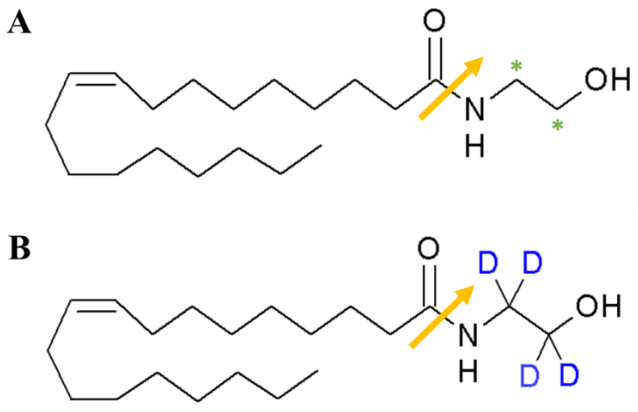

Figure 4.6. Molecular structures of (A) OEA (M_w = 325.3 g/mol) and (B) OEA-d4 (M_w = 329.3 g/mol). The asterisks in (A) indicate possible sites of the single ^{13}C carbon on each molecule of ^{13}C-OEA (M_w = 327.3 g/mol). The expected predominant fragmentation point in positive ion mode to produce the $[M+H]^+$ ethanolamine ion is shown by yellow arrows.

The following ions were monitored in MRM mode (positive ionisation) using the optimised parameters shown in Table 4.2.

Table 4.2. MRM optimised parameters for ions monitored.

Q1	Q3	Time (msec)	ID	DP (volts)	CE (volts)	CXP (volts)
326.206	62.000	150.0	OEA	166	23	12
330.255	66.000	150.0	OEA-d_4	71	21	18
327.201	63.000	150.0	^{13}C-OEA	111	21	10

Mobile phase A consisted of 0.1% formic acid in Milli Q water. Mobile B was 0.1% formic acid in 2:1 Acetonitrile:Methanol. Analysis was performed at a flow rate of 0.6 mL/min by injecting 5 µL of sample into a Kinetex EVO 5 µ 100 Å C18 (150 x 2.1 mm) column (fitted with a 4 x 2.0 Gemini-NX C18 SecurityGuard Cartridge) (Phenomenex, USA) in gradient mode, maintained at 40 °C. Starting pressure was approximately 2530 psi. The gradient was started at 20% A, 80% B and increased to 5% A, 95% B over 1.67 minutes, held there until 10 minutes for cleaning, then returned to 20% A, 80% B at 10.7 minutes and allowed to re-equilibrate until 12 minutes. Eluent was allowed to flow to the MS detector for the first 2.0 minutes for compound elution, then was diverted to waste until 3.7 minutes, then allowed to flow to the detector again until 12.0 minutes to re-equilibrate. 90% methanol in Milli Q water was used for needle cleaning between samples (10 seconds). Draw speed and eject speed were 200 µL /min. All three compounds eluted simultaneously at 1.64 minutes. The auto-sampler was kept at a temperature of 4 °C during analysis.

4.4.9.4 Data analysis

Data was collected in Analyst® software (Sciex, USA) and analyte/internal standard ratio was used to construct calibration curves and analyse the data in Microsoft Excel (Microsoft, USA). Standard curves were plotted in GraphPad Prism® (GraphPad, USA) for presentation in this thesis. The use of ^{13}C-OEAwas intended to clearly differentiate the exogenously administered compound from the endogenous 12-Carbon oleoylethanolamide (^{12}C-OEA). However, the ^{12}C-OEA was found to produce an ion pair with the same mass to charge ratio (m/z) as the ^{13}C-OEA (327/63), which was attributed to the formation of an $[M+2H]^{2+}$ ion (327/63) by ^{12}C-OEA. This pseudo background signal was found to occur as a consistent proportion of the ^{12}C-OEA signal (4-6%) and was therefore able to be corrected for using Equation 4.1 and the Analyte/IS ratio subsequently calculated using Equation 4.2. Data was compared statistically with t-tests and one-way analysis of variance (ANOVA) (with post-hoc Tukey's test) as appropriate, with $p < 0.05$ considered statistically significant.

Equation 4.1. Calculation of corrected ^{13}C-OEA intensity.

$$\text{Corrected } ^{13}\text{C-OEA intensity (sample or standard)} = {}^{13}\text{C-OEA intensity (sample or standard)} - \left(\frac{\text{Average } ^{13}\text{C-OEA intensity (blanks)}}{\text{Average } ^{12}\text{C-OEA intensity (blanks)}} \times {}^{12}\text{C-OEA intensity (sample)} \right)$$

Equation 4.2. Calculation of corrected analyte/IS ratio.

$$\textbf{Ratio (Analyte/IS)} = \frac{\textbf{Corrected } ^{13}\textbf{C-OEA intensity}}{\textbf{OEA-d}_4\textbf{ intensity}}$$

4.5 Results

4.5.1 Pharmacodynamic Evaluation of Intravenous OEA cubosomes

The first study in this Chapter used the MEST model to determine whether OEA cubosomes had an effect on seizure threshold after intravenous administration. The design was modified slightly from that used in the intranasal studies, as described in the *Methods* section, as a more pronounced effect was hypothesised to occur after intravenous administration, so less sensitivity was required. As shown in Figure 4.7, the CC_{50} of the group was found to be 63 mA (95% CI: 38-105 mA) (Figure 4.7A). Upon subsequent stimulation at this current after no treatment, only 43 % of the rats displayed HLE (Figure 4.7B). This suggested a slight underestimation of the true CC_{50}, however, this was able to be corrected prior to the drug treatment test with this study design by dividing the rats into three time point sub-groups in which 50% of rats in each group had shown HLE at the CC_{50} (Figure 4.7C). FLE was seen in 100% of rats at the CC_{50} in all groups.

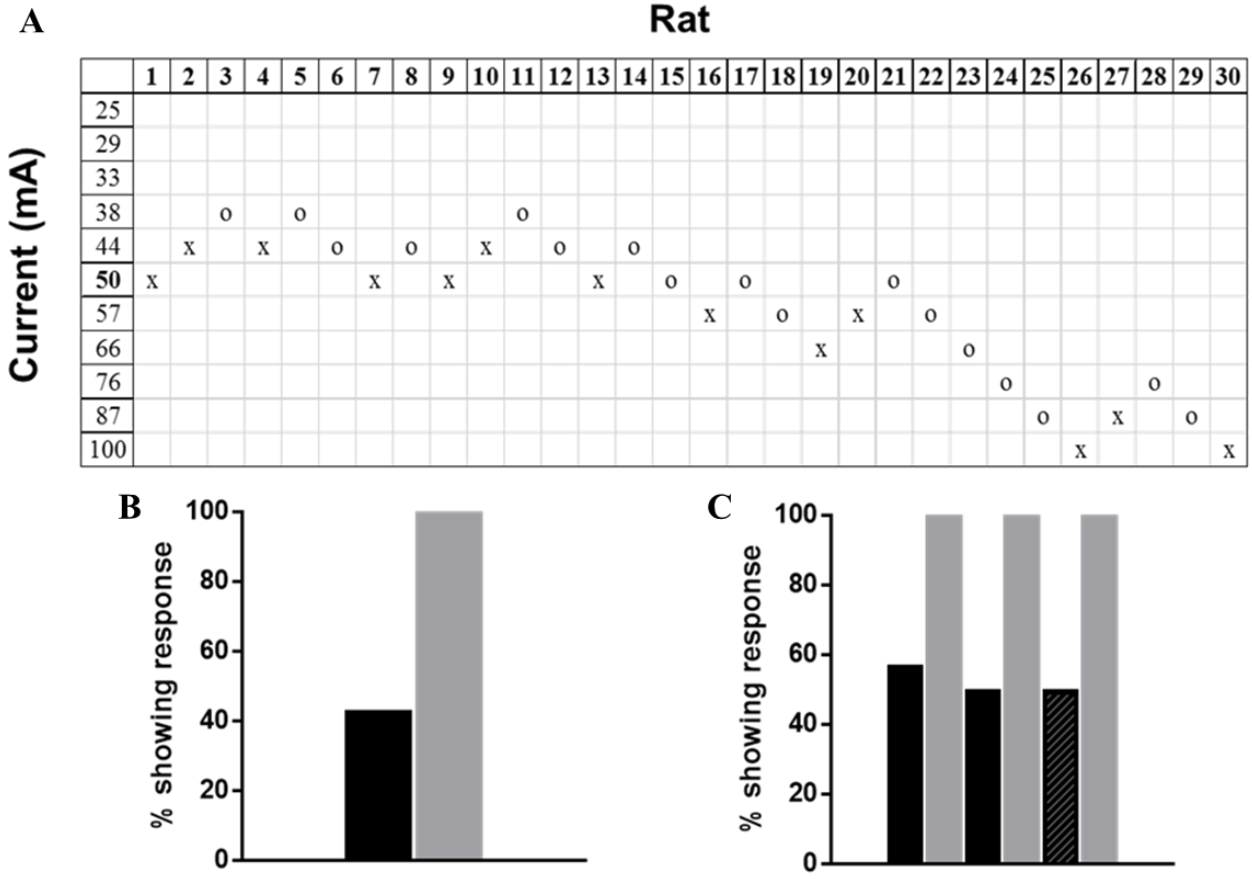

Figure 4.7. CC_{50} calculation (A) and baseline (B and C) data for the intravenous OEA cubosome MEST experiment. Responses after no treatment are shown for the full group (B) and the sub-groups that were used to test at different time points (C).

As shown in Figure 4.8, no statistically significant anti-seizure effect (or pro-seizure effect) was observed in the MEST test after intravenous administration of a single dose of OEA cubosomes (7.5 mg/kg OEA). Furthermore, there was no trend to suggest an underlying effect, as there was in **Chapter Three**. At 15 minutes, a 25 % reduction in the incidence of HLE occurred, while at 30 minutes, a 40 % reduction in incidence occurred, but so did a 20 % increase in rats which had not displayed it in the baseline study. Finally, at 60 minutes, a 25 % increase in the incidence of HLE was observed. No change in the incidence of FLE was seen.

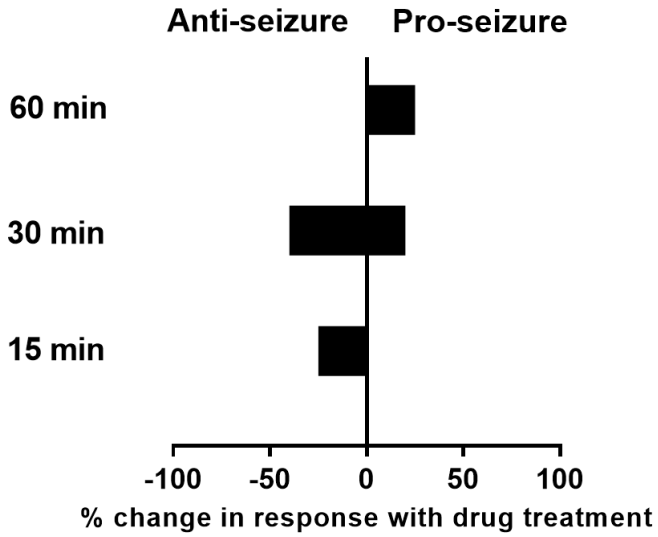

Figure 4.8. Effect of intravenous OEA cubosomes (7.5 mg/kg OEA) on HLE (black) and FLE (grey) at the group CC_{50} current 15 minutes (n=4 and 8 respectively; p = 0.32), 30 minutes (n=5 and 10 respectively; p = 0.56) and 60 minutes (n=4 and 7 respectively; p = 0.32) after treatment administration. Data is presented as percent change in response with respect to no treatment in the same rats. Animal numbers and the method used to calculate the percentage difference are shown in Appendix C. Note that FLE is not visible in the above Figure as no change was found in this experiment.

4.5.2 Validation of an LC-MS Method for Measuring Tissue ^{13}C-OEA Concentrations in Plasma, Brain and Liver Tissue

4.5.2.1 Specificity

As described above, the use of ^{13}C-OEA to study the pharmacokinetics of the exogenously administered OEA was intended to clearly differentiate it from background endogenous levels of OEA, however, a background signal at the same m/z ratio as the ^{13}C-OEA ion pair complicated the determination of specificity. Preliminary studies attributed this signal to the formation of an $[M+2H]^{2+}$ ion and determined that it was a consistent proportion (4-6%) of the OEA signal and could therefore be corrected for using blank samples run within each assay (Figure 4.9).

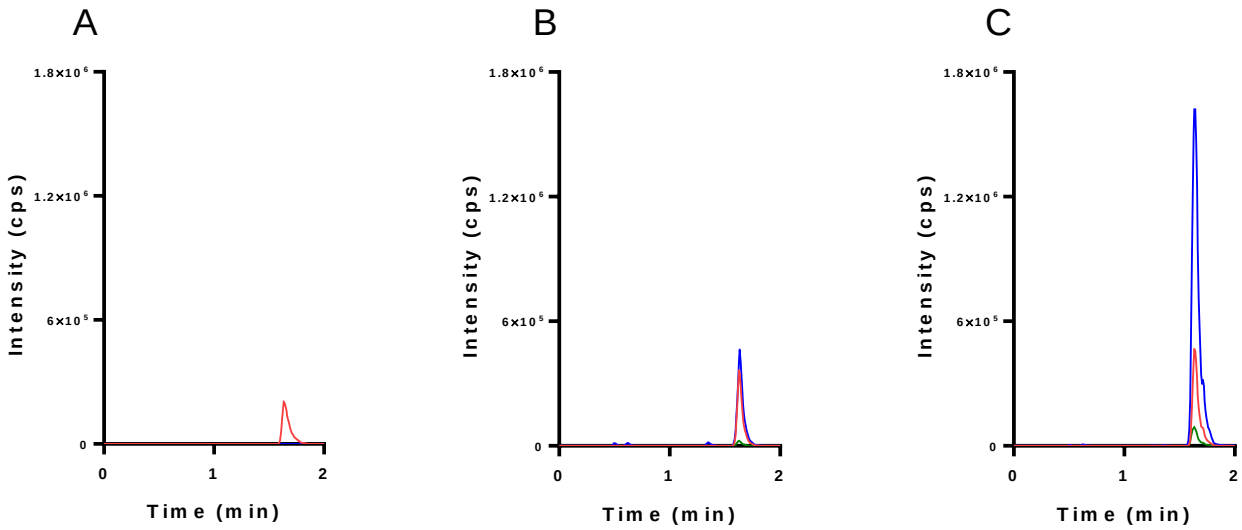

Figure 4.9. Blank tissue samples of rat plasma (A), liver homogenate (B) and brain homogenate (C) spiked with the same concentration of internal standard (d4-OEA) (red). Background endogenous OEA signal (blue) is shown along with the proportionately increasing pseudo-background ^{13}C-OEA signal (green).

The optimised method parameters allowed resolution of clear peaks representing the analyte ^{13}C-OEA and internal standard OEA-d_4 (Figure 4.10), as well as background OEA (Figure 4.9) so that the correction to the background ^{13}C-OEA signal could be made. The compounds eluted consistently at 1.64 minutes in all matrices.

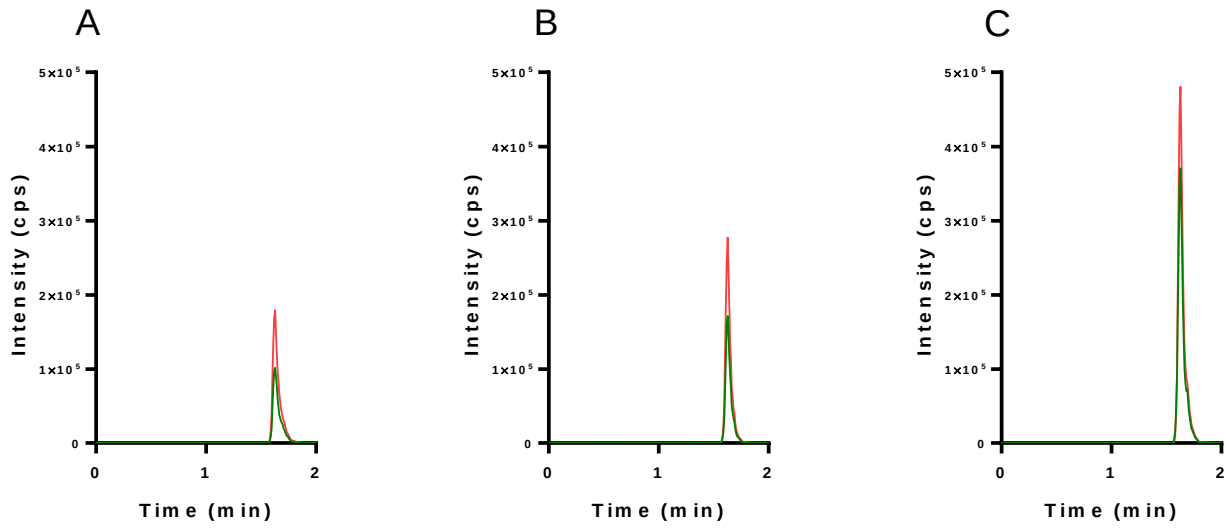

Figure 4.10. Representative chromatograms of ^{13}C-OEA (green) and OEA-d_4 (red) in rat plasma (A), rat liver homogenate (B) and rat brain homogenate (C). Note that original chromatogram data has been re-plotted using GraphPad Prism® to enhance clarity. The ^{13}C-OEA concentration in these chromatograms is 6.25 ng/mL for plasma and 18.8 ng/mL for brain and liver tissue due to dilution of the latter two, however all represent the same concentration in the actual sample. Accordingly, the internal standard (OEA-d_4) concentration is 12.5 ng/mL for plasma and 37.5 ng/g for brain and liver tissue.

4.5.2.2 Sensitivity

To determine the sensitivity of the assay, standard curves were produced by plotting mean analyte/internal standard ratio values against concentration and fitting to second order polynomial (quadratic) equations. The standard curve was validated in triplicate on three separate days (Figure 4.11). Accuracy and precision for all concentration values was found to be within the acceptable range of ± 15% and the fit of the curve maintained an R^2 value of ≥0.9998 (**Appendix P**).

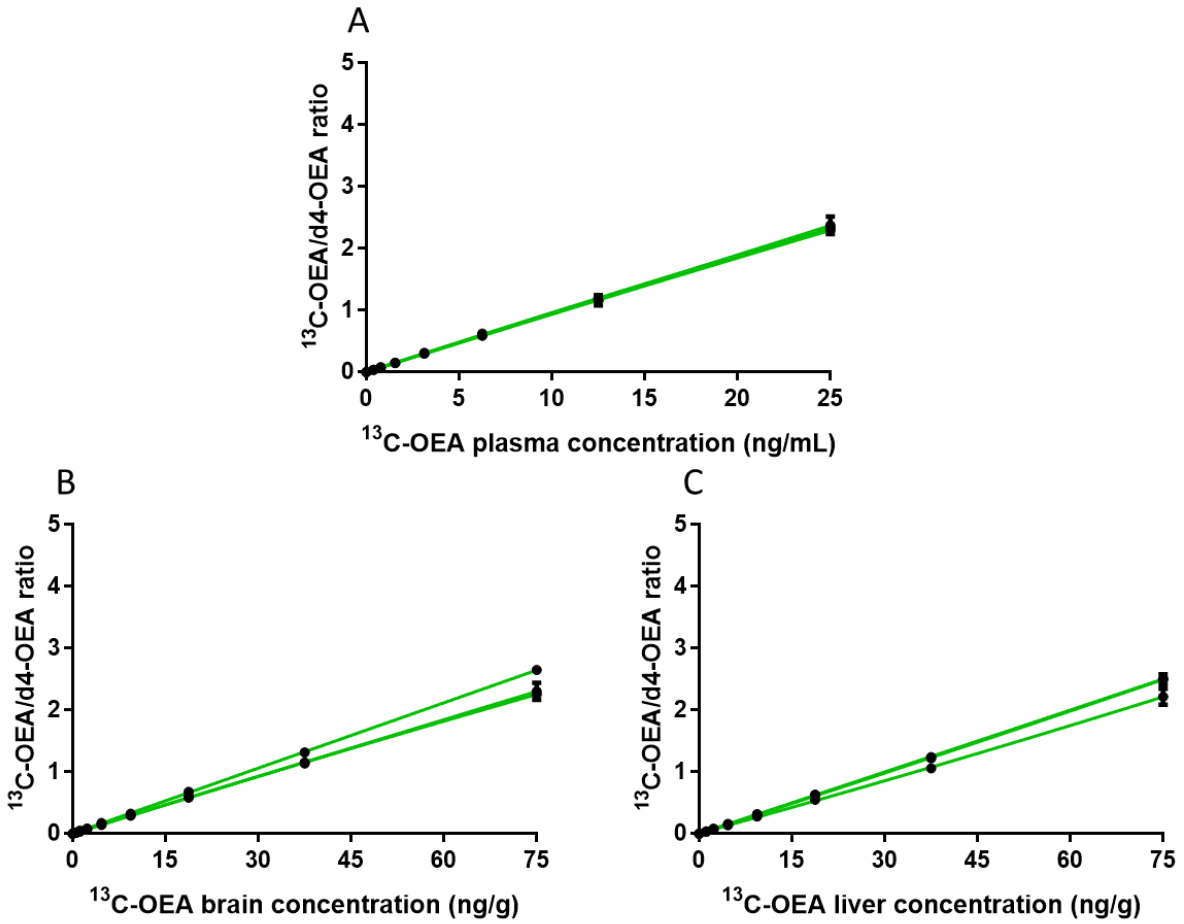

Figure 4.11. Standard curves of ^{13}C-OEA in rat plasma (A), brain homogenate (B) and liver homogenate (C). Data shown are the mean values (± SD) of the standards prepared and measured in triplicate on three different days. The relationship between analyte concentration and analyte/internal standard ratio was best modelled by fitting second order polynomial (quadratic) curves to the data as shown on the graphs.

4.5.2.3 Accuracy and Precision

The inter-day and intra-day accuracy and precision of the assays, based on quality control samples, are shown in Table 4.3 and Table 4.4. Variability was within the acceptable range of ± 15% for all assays.

Table 4.3. Inter-day accuracy and precision of ^{13}C-OEA quantification in rat plasma, brain and liver tissue based on quality control samples.

Matrix	Nominal conc (ng/mL or ng/g)	Inter-day (n=3)		
		Mean (ng/mL)	Accuracy (%)	Precision (CV%)
Plasma	0.78	0.72	92.3	3.7
	7.5	7.29	97.2	2.6
	20	20.1	100.7	1.4
Brain	2.34	2.27	97.2	2.3
	11.3	10.8	95.3	5.1
	30	29.1	97	4.2
	60	63.5	105.8	3.1
Liver	2.34	2.09	89.2	4.7
	11.3	10.0	88.8	4.1
	30	27.4	91.2	5.7
	60	56.5	94.2	3.8

Table 4.4. Intra-day accuracy and precision of ^{13}C-OEA quantification in rat plasma, brain and liver tissue based on quality control samples.

Analyte	Nominal conc (ng/mL or ng/g)	Intra-day 1 (n=3)			Intra-day 2 (n=3)			Intra-day 3 (n=3)		
		Mean (ng/mL)	Accuracy (%)	Precision (%CV)	Mean (ng/mL)	Accuracy (%)	Precision (%CV)	Mean (ng/mL)	Accuracy (%)	Precision (%CV)
Plasma	0.78	0.71	90.3	2.2	0.70	89.0	6.5	0.75	95.6	3.7
	7.5	7.30	97.3	2.4	7.10	94.7	5.2	7.48	99.8	3.0
	20	20.3	101.4	3.2	19.8	98.7	3.5	20.3	101.5	3.6
Brain	2.34	2.23	95.3	3.9	2.33	99.5	4.8	2.26	96.5	4.0
	11.3	10.5	92.9	2.1	11.4	101.1	3.3	10.4	92.1	6.4
	30	28.4	94.7	3.8	30.5	101.6	4.0	29.1	94.6	2.5
	60	63.8	106.4	2.6	65.3	108.9	3.5	63.5	102.3	3.2
Liver	2.34	2.04	87.1	2.8	2.02	86.0	5.4	2.20	93.7	4.5
	11.3	10.5	93.0	2.3	9.73	86.5	3.3	9.88	87.8	3.9
	30	28.9	96.2	4.1	27.4	91.3	7.8	25.8	85.8	6.6
	60	58.7	97.8	2.8	54.4	90.7	2.5	56.4	94.0	2.1

4.5.3 Pharmacokinetic Evaluation of OEA Biodistribution and *In Vivo* Stability

Cubosomes formulated with ^{13}C-OEA were used to determine biodistribution and biological stability of ^{13}C-OEA after intravenous administration.

4.5.3.1 ^{13}C-OEA Cubosome Dispersion Characterisation

Dynamic-light scattering was used to determine the average size and polydispersity of the cubosome dispersion used for the *in vivo* experiments (Table 4.5). These parameters were found to be comparable to those reported previously[258] suggesting that the ^{13}C-OEA formulation was representative of cubosome dispersions formulated with ^{12}C-OEA. The ^{13}C-OEA stock available was very limited, so more intensive characterisation (e.g. with SAXS) was not possible.

Table 4.5. Particle characteristics of the cubosomes dispersion used for the experiments (10% ^{13}C-OEA-phytantriol cubosomes stabilised with Tween 80). Data shown is the average ± standard deviation of triplicate measurements taken from the duplicate samples that were able to be taken from the stock dispersion at the end of the in vivo experiment.

	Zeta average (d.nm)	**PDI**
10% ^{13}C-OEA-phytantriol cubosomes-Tween 80	133 ± 2	0.216 ± 0.013

4.5.3.2 Pharmacokinetic Analysis

The plasma, brain and liver tissue concentrations of ^{13}C-OEA after intravenous administration as cubosomes or control solution, along with the respective brain/plasma and liver/plasma ratios are shown in Figure 4.12. Variability within some groups was quite significant, making interpretation of trends difficult. Despite not being statistically significant, average plasma ^{13}C-OEA concentrations (Figure 4.12A) trended towards decreasing over time after administration of control solution, as was to be expected following intravenous administration. Concentrations following cubosomes trended towards fluctuating a bit more. Interestingly, the concentration of ^{13}C-OEA did not fall below the LLOQ at any point up to 90 minutes suggesting a persistence of low levels of the molecule in the plasma after administration of either formulation. With respect to differences between cubosomes and control solution at each time point, the only statistically significant difference was found at 90 minutes after administration, with cubosome

^{13}C-OEA concentrations being lower than those after control solution, contrary to what was hypothesised. This same difference is suggested by the trends at earlier time points as well and the decreasing p values suggest it became gradually more significant over time.

Brain concentrations (Figure 4.12B) showed a similar trend, although many values were below the LLOQ in these samples and were zeroed for analysis in the Figure. The data including the values below the LLOQ is shown in **Appendix Q** for transparency and a general agreement with the plasma trends supports the credibility of the measurements, despite them not being able to be quantified within the specified limits of the LC-MS assay. As could be expected, the average brain/plasma ratios (Figure 4.12D) showed a similar trend towards a slightly higher ratio of ^{13}C-OEA in the brain after control solution compared with cubosomes, however all ratios were below 0.2 indicating that neither exogenous formulation led to a particularly good accumulation of ^{13}C-OEA in the brain compared with plasma.

Liver concentrations (Figure 4.12C) showed a similar trend, but no significant differences were found between cubosomes and control at any time point in this data set. This was also true for the liver/plasma ratio (Figure 4.12E), however, the trend over time was more interesting here in that the average ratio increased at 60 minutes after administration of cubosomes, but not control solution, to produce the only statistically significant difference within a formulation type over time in any of the data. Hence, the distribution of cubosomal ^{13}C-OEA to the liver was greater than to the brain, the former exhibiting a significant elevation at 60 minutes which persisted until 90 minutes, although it never exceeded 1.0.

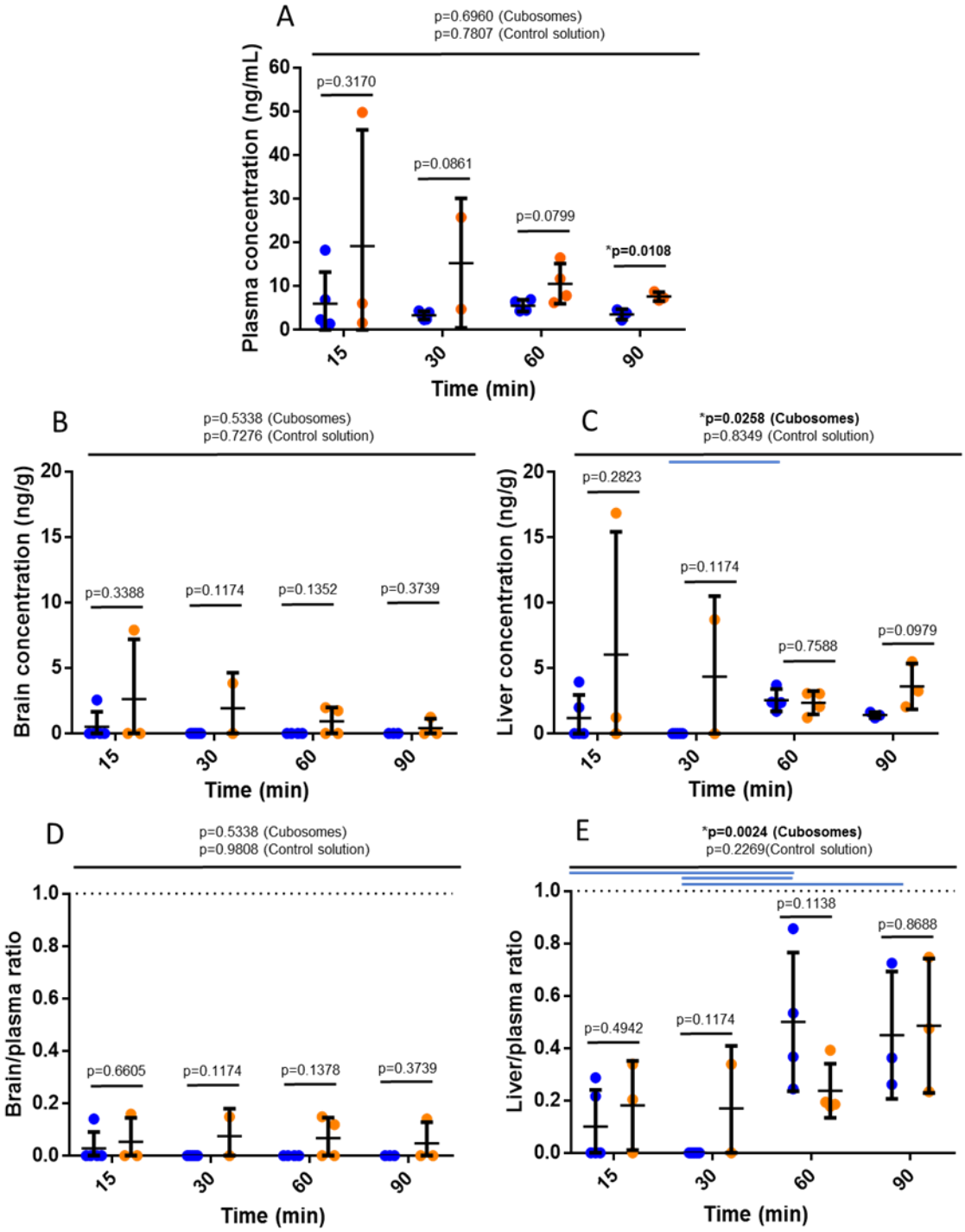

Figure 4.12. Pharmacokinetics of ^{13}C-OEA in rats up to 90 minutes after intravenous administration of cubosomes (^{13}C-OEA 10% w/w with phytantriol) (blue) or control solution (orange) at a concentration of 2 mg/mL. (A) Plasma concentration, (B) Brain concentration, (C) Liver concentration, (D) Brain to plasma ratio, (E) Liver to plasma ratio. Values represent means and error bars represent standard deviation. Values below the LLOQ of the assay are presented and analysed as zeroes. P-values are shown for comparison between cubosomes and control solution at a given time point (two-tailed t-test) and between each of the formulations over the different time points (one-way ANOVA). With respect to the latter, coloured bars (matched to the symbol colour) represent statistically significant differences determined by post-hoc analysis (Tukey's).

4.5.4 Small Angle X-ray Scattering (SAXS) Evaluation of Structural Kinetics in Plasma

SAXS was used to evaluate the *in vitro* structural stability of OEA cubosomes upon incubation in rat plasma at 37 ºC to supplement the pharmacokinetic and pharmacodynamic studies. Control measurements in the absence of plasma are presented in Figure 4.13. These were taken to confirm the initial cubosome structure of the nanoparticles prior to the experiment as well as to ascertain any potentially confounding effect of the raised temperature on them, as previous reports have presented data at ambient temperature only[258,277]. The consistent Bragg peak ratio[276] of $\sqrt{2}:\sqrt{4}:\sqrt{6}$ shows that the *Im3m* structure of the cubosomes was unaffected, however, the lattice parameters all decreased slightly over the course of the experiment from 102.5, 105.8 and 125.8 Å to 99.2, 105.2 and 119.4 Å for phytantriol, OEA 10% and OEA 30% cubosomes, respectively (Panels B to D).

The effect of plasma incubation on the OEA cubosomes (0%, 10% and 30% OEA) is presented in Figure 4.14. All of the cubosomes (Panels B to D), regardless of OEA content, rapidly transformed into hexosomes after *in vitro* incubation in plasma, as indicated by the appearance of Bragg peaks with a spacing ratio of $1:\sqrt{3}:\sqrt{4}$. An initial disappearance of the cubic phase was seen at the first measurement in all samples which can be interpreted as a reduction in the intensity of the cubic phase below the background signal, while the intensity of the hexagonal phase subsequently increased towards exceeding the background signal as a result of the relative change in the concentration of each particle type. Further evidence of this is provided in **Appendix R** which shows the effect of incubating cubosomes at different plasma concentrations in order to effectively slow the transition to a rate at which it could be observed. The emergence of the hexagonal peaks appeared to take slightly longer (75 minutes compared to 50 minutes) in the 30% OEA formulation (Panel D), suggesting that a greater proportion of OEA was associated with a delayed transformation. Also interesting was that the lattice parameters of the hexosomes at 420 minutes (at which the samples were deemed to have equilibrated) were different for each formulation (58.8, 60.0 and 64.3 Å), increasing with the proportion of OEA, as was the case for the original cubosome formulations mentioned earlier. This suggested that OEA remained associated with the particles during the transition rather than the possibility of it being exchanged for other plasma lipids. The control data of water mixed with plasma (Panel A) confirms that no other liquid crystalline structures were present in plasma in the absence of the added dispersion that could have contributed to the result.

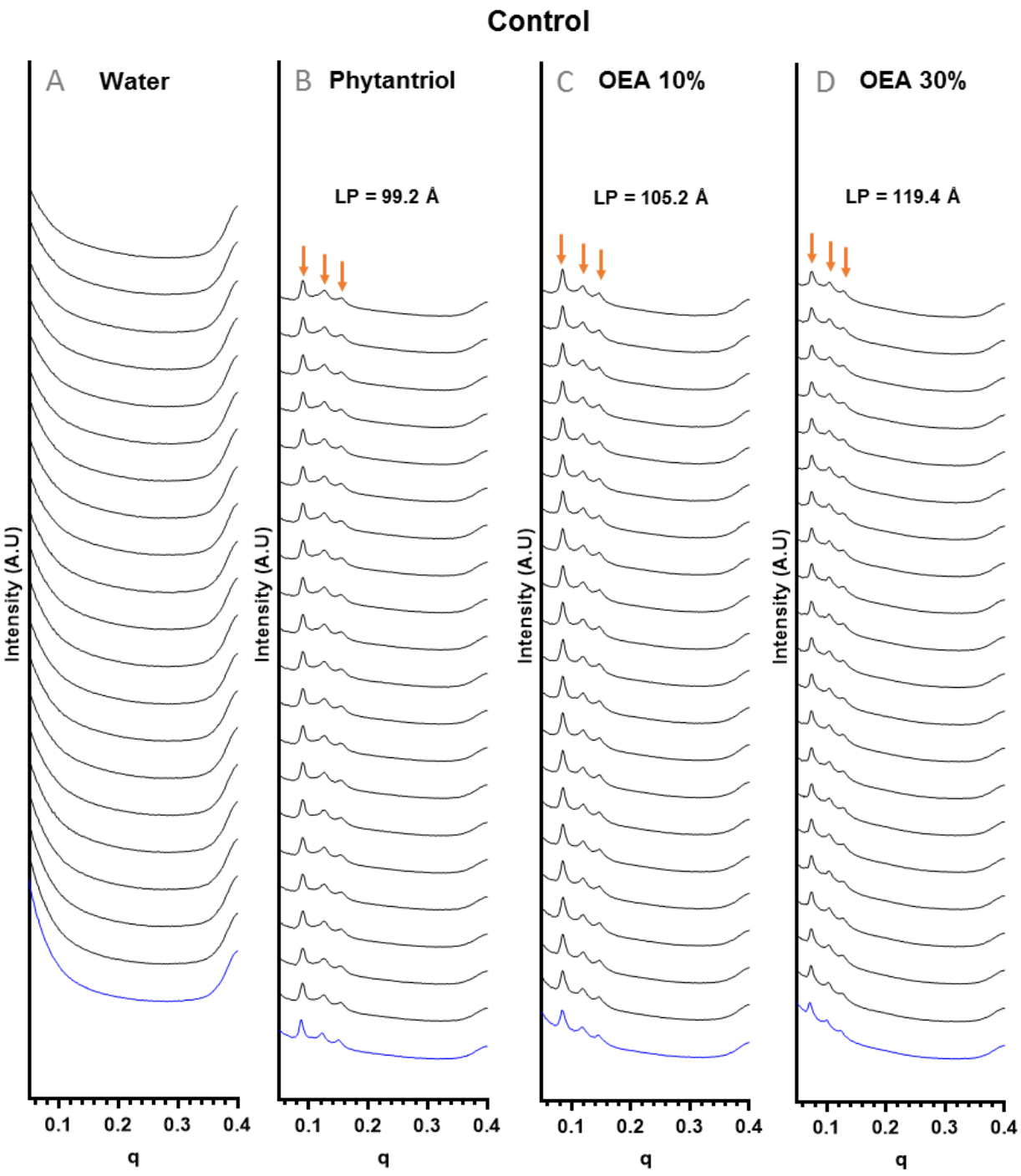

Figure 4.13. SAXS studies of OEA cubosomes in 50% Milli Q water incubated at 37 ºC for 420 minutes. Plots from left to right show data for Milli Q water, Phytantriol-Tween 80 cubosomes, 10% OEA-Phytantriol-Tween 80 cubosomes and 30% OEA-Phytantriol-Tween 80 cubosomes. The blue plots represent the initial measurement for each sample at ambient temperature. Subsequent measurements start at 30 minutes after mixing for consistency with plasma samples (10 minutes after placing in the temperature-controlled holder) and were taken at 10 minute intervals from 30-60 minutes, 15 minute intervals from 60-180 minutes and 30 minute intervals from 180-420 minutes. LP = lattice parameter.

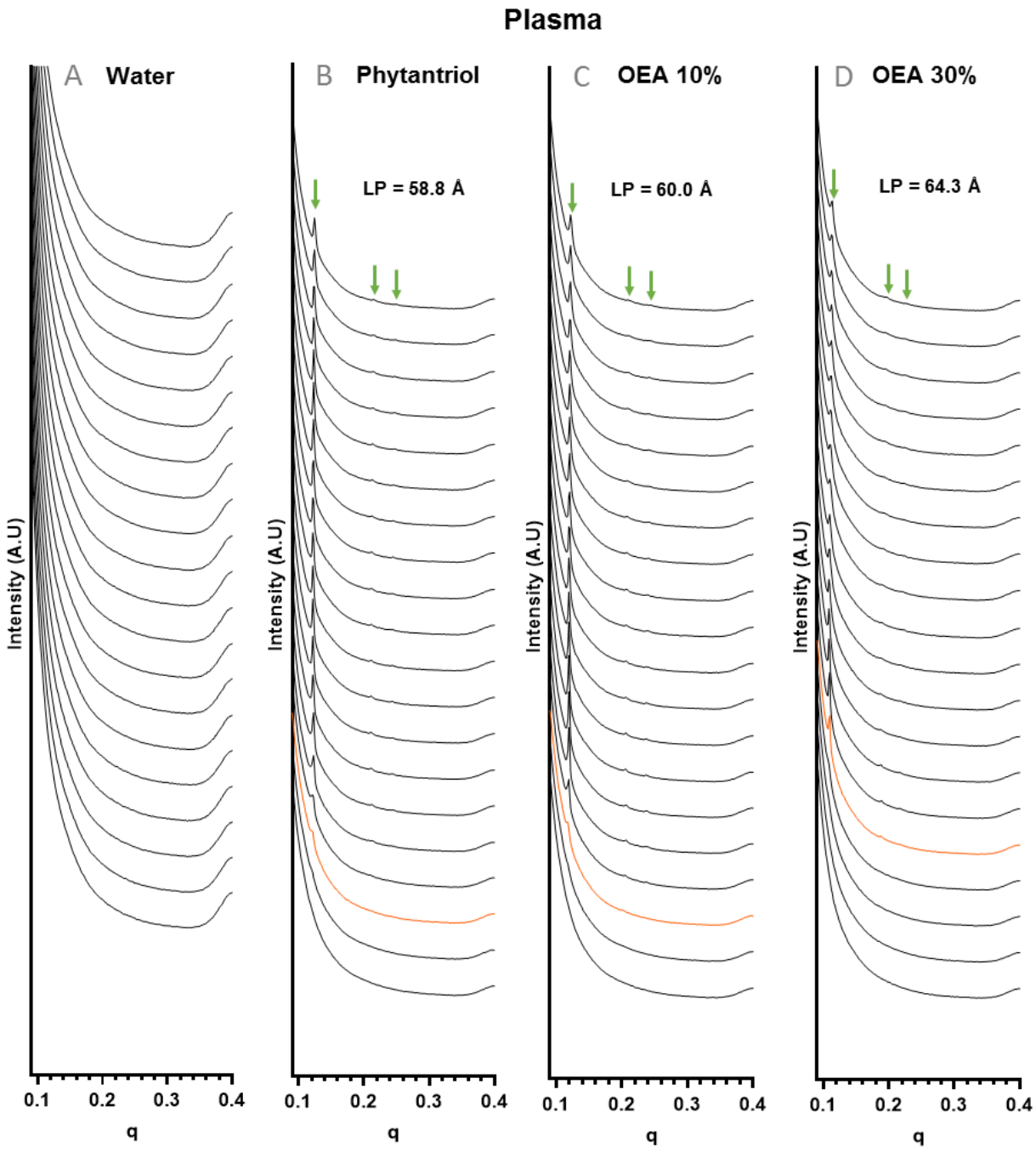

Figure 4.14. SAXS studies of OEA cubosomes in 50% rat plasma incubated at 37 ºC for 420 minutes. Plots from left to right show data for Milli Q water, Phytantriol-Tween 80 cubosomes, 10% OEA-Phytantriol-Tween 80 cubosomes and 30% OEA-Phytantriol-Tween 80 cubosomes. The orange plots represent the appearance of the hexagonal phase. Measurements start at 30 minutes after mixing and were taken at 10 minute intervals from 30-60 minutes, 15 minute intervals from 60-180 minutes and 30 minute intervals from 180-420 minutes. LP = lattice parameter.

4.5.5 Cubosome Nasal Toxicity Evaluation: Preliminary Histological Screening

The intention of the second part of this chapter was to investigate whether the nasal route offered any advantage to the delivery of OEA to the brain by offering a potential direct route avoiding the complex barriers of the systemic circulation, as were demonstrated in the results above. The first step towards achieving this aim was to study the effect of OEA cubosomes on the nasal epithelium in order to select an appropriate dose for testing. Representative images of the effects of OEA cubosomes on the olfactory epithelium at its maximum concentration 60 minutes after administration are shown in Figure 4.15. In the cubosome trial, there is clear damage to the integrity of the epithelium at the maximum dose of cubosomes, as indicated by degeneration, loss of apparently anuclear, necrotic cells and accumulation of debris and exudate in the lumen (Panel E). Free drug suspension (at an equivalent concentration of OEA) was also tested to elucidate the potential cause of the damage from the cubosomes, the images of which are also shown in Figure 4.15, Panels C and F. In comparison to the control nostril (Panel C), blood vessels appear to be dilated in the lamina propria suggesting inflammatory irritation and the epithelium appears uneven with some minor cell exfoliation (Panel F), but this is not on the scale seen with the cubosomes. This suggests the damage was primarily attributable to the presence of the cubosomes or the cubosome-forming lipid, phytantriol, rather than any other formulation component.

Behaviour after intranasal administration was recorded to supplement histological data. The most significant behaviour noted after administration of the highest dose (20 mg/mL dispersion) was a frequent narrowing of the eye on the side the nostril the formulation was administered to, likely due to the discomfort of the liquid in the upper nasal passage. This was not seen after saline administration or the control dispersion, however, suggesting it was not purely related to the presence of liquid and that the cubosome dispersion at this concentration was indeed irritant. Note that the powder in **Chapter Three** also did not have this effect. A small amount of porphyrin discharge was noted coming out of the treated nostril about 15 minutes after administration of the cubosomes, along with some sneezing and nose twitching further supporting that this dose was unsuitable for intranasal administration.

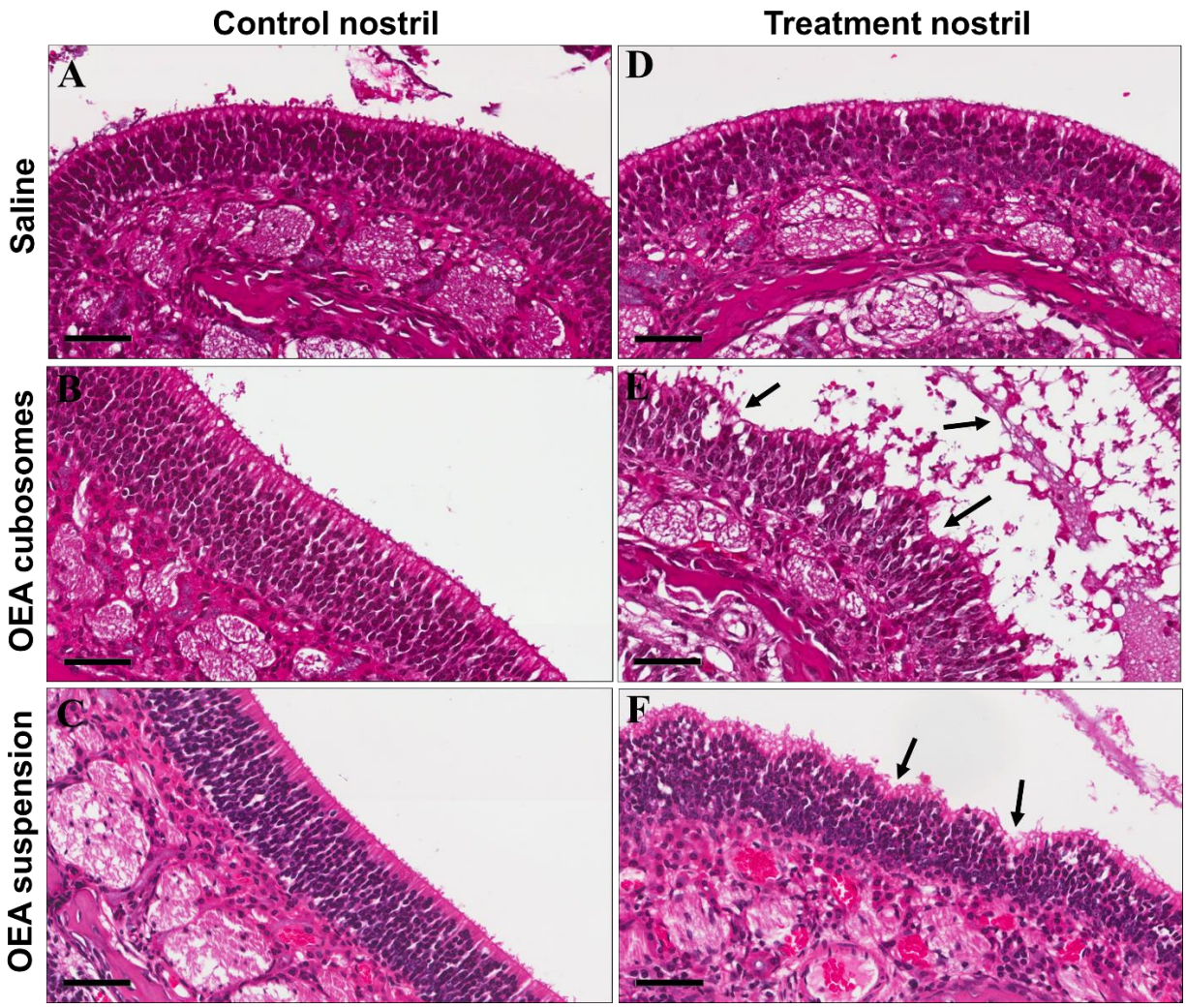

Figure 4.15. Representative histological images of the olfactory epithelium of rats 60 minutes after intranasal administration saline (D), OEA cubosome dispersion at the maximum concentration of 20 mg/mL total lipid (E), or equivalent concentration of free OEA suspension (F). The corresponding panels on the left (A-C) show the control (untreated) nostril of each rat. Scale bars = 50 µm. Arrows in panel E indicate degeneration, loss of anuclear, necrotic cells and accumulation of debris and exudate in the lumen. Arrows in panel F indicate uneven areas of the epithelium and some minor cell exfoliation.

In order to determine a dose that was suitable, two further concentrations were tested; 10 mg/mL and 5 mg/mL (Figure 4.16). A disruption of the epithelium compared with control was still evident at 10 mg/mL (Panels A and C), albeit lesser, but not at 5 mg/mL (Panels B and D). Observation of subject behaviour after administration was consistent with this finding, so the latter dose was selected for use in subsequent studies.

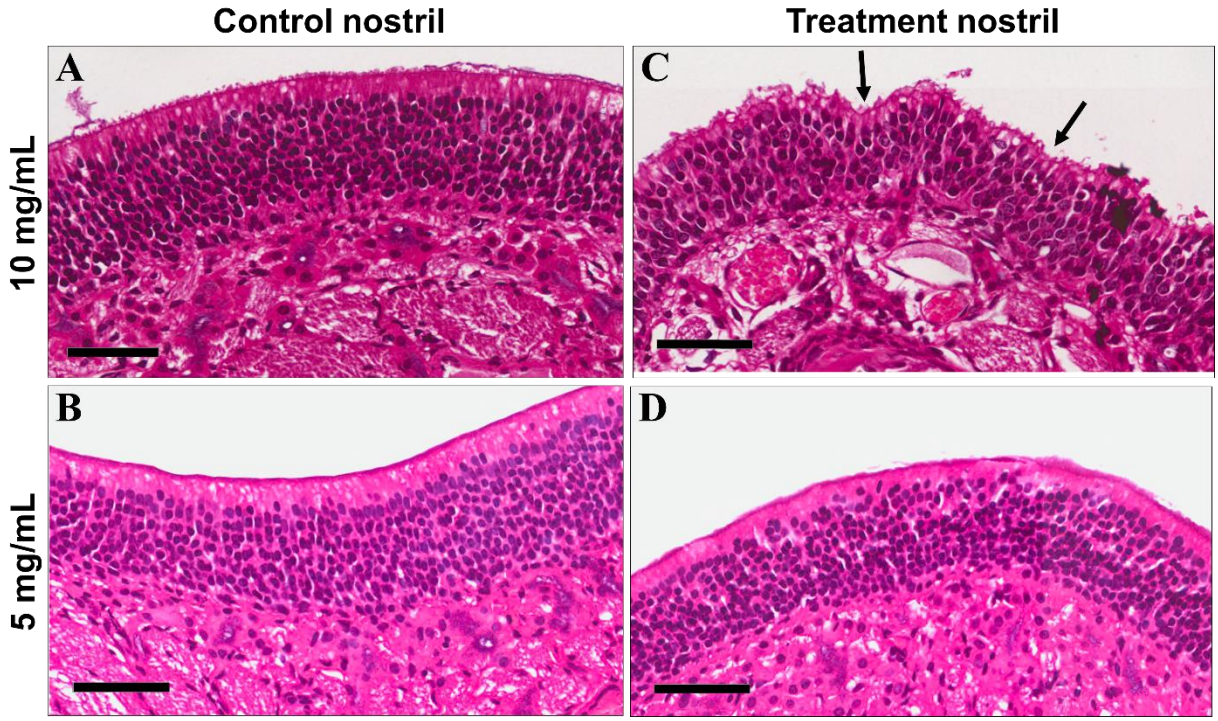

Figure 4.16. Representative histological images of the olfactory epithelium of rats 60 minutes after intranasal administration of OEA cubosome dispersions at concentrations of 10 mg/mL and 5 mg/mL total lipid. Panels A and B show the untreated epithelium in the control nostril and panels C and D show the epithelium in the nostril exposed to the cubosome dispersion. Scale bars = 50 µm.

4.5.6 Evaluation of Pharmacodynamics of OEA Cubosomes After Intranasal Administration

To determine whether OEA cubosomes had an effect on seizure threshold after intranasal administration, MEST trials were conducted with the aim of testing three time points; 15, 30 and 60 minutes after administration. The earlier time points were investigated as the *in vivo* time scale of protection of OEA from hydrolysis in cubosomes after intranasal administration was uncertain, but hypothesised to fall within this range.

The CC_{50} and control responses to stimulation for these studies are shown in Figure 4.17. The rats in the 60 minutes group had a calculated CC_{50} of 66 mA (18 – 240 mA) (Figure 4.17A), which translated to 39 % of rats exhibiting HLE after intranasal saline administration in the experimental control data (Figure 4.17B). The determination of the CC_{50} at earlier time points presented a more complex situation as the residual effect of the isoflurane anaesthetic was found to be significant. This meant that at the 15 minute time point, a series of eight rats stimulated

from 50 mA up to 132 mA yielded no cases of HLE rendering the CC_{50} indeterminable (Figure 4.17C). The remaining nine rats in the group were therefore used to estimate the CC_{50} at the 30 minute time point instead (Figure 4.17D). While the influence of isoflurane was still evident at this time point, a CC_{50} of 76 mA (39 – 148 mA) was able to be calculated and used for subsequent studies, however only 12 % of saline-treated rats subsequently exhibited HLE (Figure 4.17E) which heavily supressed the resolution for detecting an anti-seizure effect of OEA. All saline-treated rats in both groups displayed FLE after all stimulations.

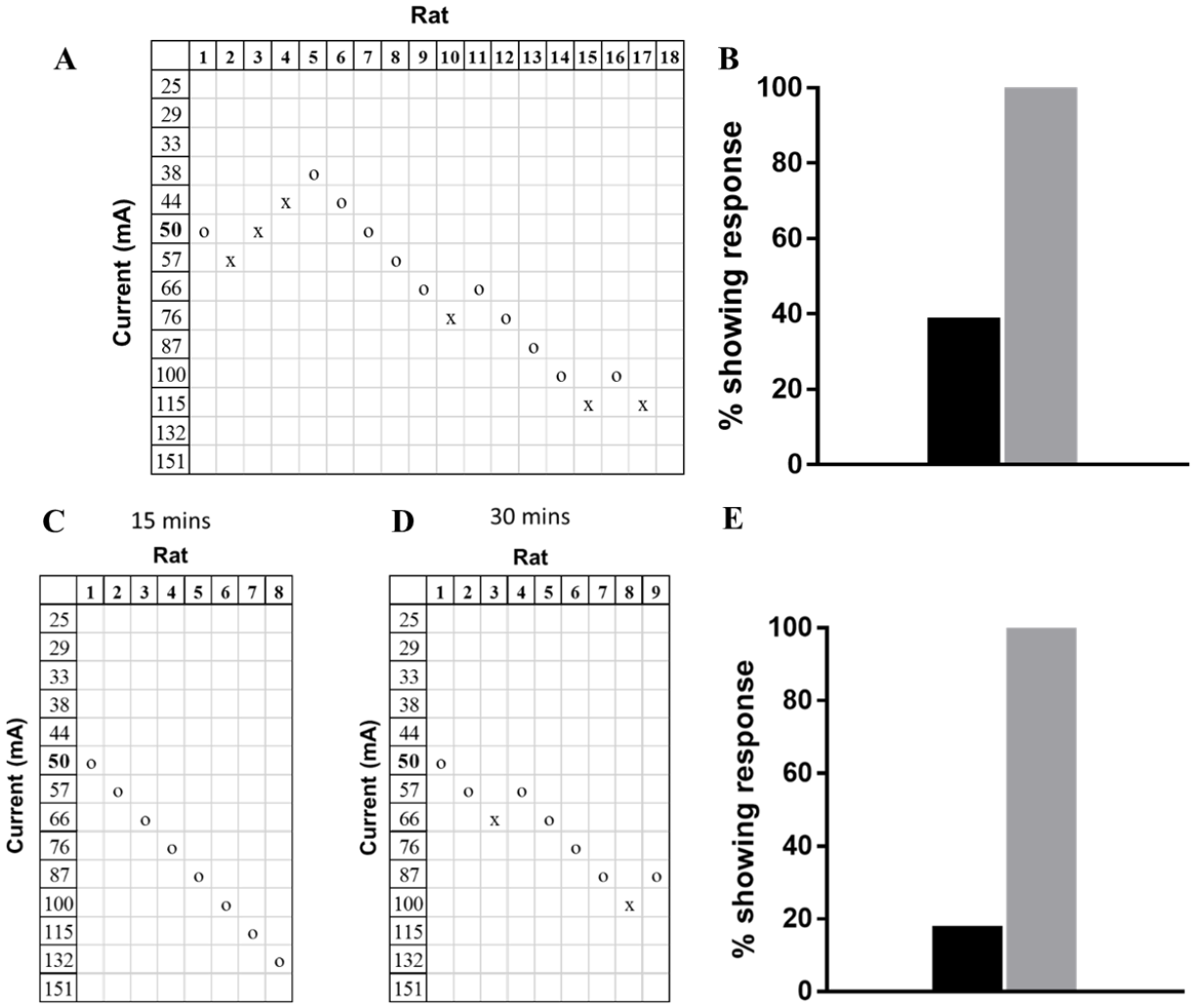

Figure 4.17. Determination of the CC_{50} and baseline response to stimulation at the CC_{50} in the batches of rats that participated in the study of intranasal OEA cubosomes (7.5 mg/mL OEA). Experimental data from the up and down method is shown for 60 minute (A), 15 minute (C) and 30 minute (D) time points, where "X" represents HLE and "O" represents no HLE. The CC_{50} was indeterminable at 15 minutes, so only the baseline responses of the rats when stimulated at the calculated CC_{50} 60 minutes (B) and 30 minutes (E) after intranasal saline administration are shown. The black bar represents the percentage of rats which exhibited HLE at the calculated CC_{50} and the grey bar represents those which exhibited FLE (with or without HLE).

As shown in Figure 4.18, no significant anti-seizure (or pro-seizure) effect was observed in the MEST test after intranasal administration of a single dose of OEA cubosomes at 30 minutes ($p = 1$) or 60 minutes ($p = 0.93$). At 60 minutes, a 29 % reduction in the incidence of HLE was observed, while at 30 minutes, a 33 % reduction was observed. These results were effectively nullified however, by an increase in the incidence of HLE (11% and 7% respectively) which was also observed at each time point. No change in the incidence of FLE was seen.

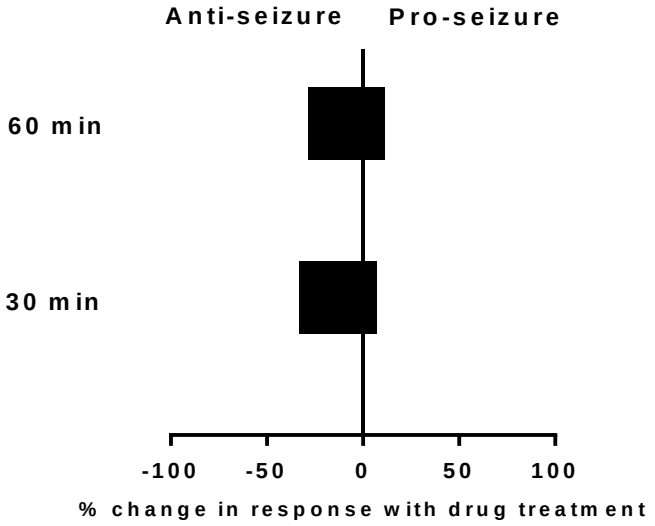

Figure 4.18. Effect of intranasal OEA cubosomes on HLE (black) and FLE (grey) at the group CC_{50} currents 30 minutes (n=4 and n=17 respectively) and 60 minutes (n=9 and n=17 respectively) after treatment administration. Data is presented as percent change in response with respect to intranasal saline treatment in the same rats. Animal numbers and the method used to calculate the percentage difference are shown in Appendix C. Note that FLE is not visible in the above Figure as no change was found in this experiment.

4.5.7 Evaluation of the Histological Effects of OEA Cubosomes on the Nasal Mucosa of Tested Animals

Nasal tissue from animals that participated in the seizure studies was histologically processed in order to examine the integrity of the olfactory epithelium throughout the experiment (Figure 4.19). Interestingly, a slight disruption to the epithelium was noted 60 minutes after administration of OEA cubosomes at 5 mg/mL (Panel B) which was not detected in the earlier dose optimisation studies. This was, however, minor and at three days after treatment (Panel D), it can be seen that the epithelium was once again comparable with that after saline

suggesting that no significant detrimental effects resulted from the intranasal administration of the formulation.

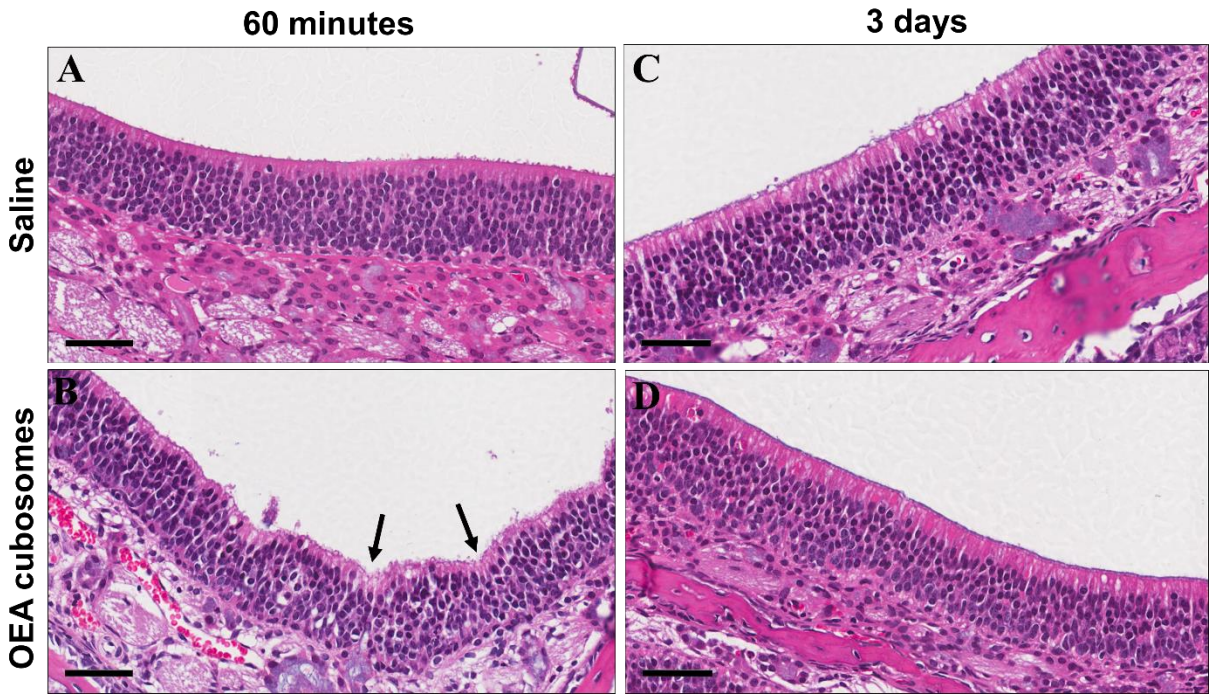

Figure 4.19. Representative histological images of the olfactory epithelium of rats that participated in the 60 minute MEST studies with OEA cubosomes. Images show short-term effects of the formulation on the olfactory epithelium in rats stimulated at 60 minutes after administration of saline (A) and OEA cubosomes (B) and longer-term effects at three days after administration of saline (C) and OEA cubosomes (D). Scale bars = 50 µm.

4.6 Discussion

Our lab group has previously reported formulation of OEA cubosomes with two different steric stabilisers; Poloxamer 407 and Polysorbate 80 (more commonly known by their respective trade names Pluronic F127® and Tween 80®). The latter were chosen for use in this Chapter as Polysorbate 80 has been suggested to enhance the delivery of cubosomes, as well as alternative nanoparticles, to the brain[258,277–280]. Azhari et al.[281] showed an increase in fluorescence in the zebrafish brain after administration of phytantriol cubosomes stabilised with Tween 80® compared with control and other stabilisers, while the present author's own extracurricular study of selachyl alcohol cubosomes stabilised with Tween 80® showed an enhanced *in vivo* delivery of drug to the brain compared with selachyl alcohol hexosomes stabilised with Pluronic F127® (unpublished data). Furthermore, Younus et al.[271] studied the *in vitro* hydrolysis of OEA cubosomes formulated with Tween 80® and Pluronic F127®, as mentioned earlier, and reported that both protected the OEA equally well from hydrolysis compared with control.

This Chapter began by investigating the pharmacodynamic effects of OEA cubosomes in the MEST seizure model after intravenous administration in order to determine if OEA had an effect on seizure threshold as hypothesised. The intravenous route was chosen as the OEA could be administered directly into the systemic circulation without ambiguity, at a dose that an ASD would be likely to show some effect[99]. The idea was that if an effect on seizures was seen, the data could act as a positive control for the effect of OEA, similar to the role played by the intravenous phenytoin trial in **Chapter Two**. In light of the discussion of anti-seizure effect screening in **Chapter One**, it was initially considered that our seizure model may not be able to detect the effects of OEA (being an untested molecule with an uncertain mechanism), but based on previous studies showing positive results of NAEs in the MES model[239,241], it was expected that an effect of OEA should be detected by the MEST model, assuming that the mechanism was similar. The result of this trial, however, was that no clear effect of OEA was seen.

The simplest conclusion from this would be that OEA does not have an effect on seizure threshold after intravenous administration. To be more specific, one might say that it does not have an *acute* effect on seizure threshold *after a single intravenous dose of 7.5 mg/kg in cubosome form*, which opens up a realm of possibilities. Firstly, it could be that the dose level tested (limited by the volume of injection and concentration of the cubosome dispersion) was inadequate to exert an anti-seizure effect. It is true that previous studies of NAEs have used

much higher doses (between 25 and 300 mg/kg), but they did not employ protective drug delivery systems to subvert hydrolysis like in this study. Nonetheless, given that this was a MEST test (which tested very close to the seizure threshold) rather than a supramaximal MES test (as was used in the previous NAE studies and is used in standard ASD screening), some noticeable effect on threshold would probably be expected if the molecule exhibited clinically relevant anti-seizure properties. Next, repeated dosing was not tested in this study and it could be that the effects of OEA might only be noticeable after chronic administration. This theory could be substantiated by the relatively slow genomic mechanisms proposed for OEA action[242] and the potential link to the ketogenic diet discussed earlier[254]. However, the trials of the other aforementioned NAEs suggested an acute effect was possible[239–241], which could lend more to dose being the major contributor to the lack of effect seen in this study.

The other major possibility, and a reason the dose might not have been adequate, was that the cubosomes may not have protected OEA from hydrolysis and/or delivered it to the brain, thereby depriving OEA of the chance to have an anti-seizure effect. As mentioned earlier, neither of these parameters had been investigated *in vivo* prior to this study. Given that this Chapter was, in essence, a study of a new drug delivery system, further studies were conducted to evaluate the likelihood that the inadequate delivery of OEA was the cause of the negative result. If this was the case, it might be something which could be improved upon (for example, by exploring a direct intranasal route to the brain to bypass the systemic circulation, as was planned for later in the Chapter) in contrast to the possibility that OEA simply had no pharmacological anti-seizure action which would make it useless for this application.

The first study performed looked at the pharmacokinetics of OEA administered in cubosomes. As OEA is an endogenous molecule, it is already present at varying levels in plasma and body tissues, so a carbon-labelled isotope of the molecule (^{13}C-OEA) formulated into cubosomes was used to track the exogenously administered compound. The concentration of ^{13}C-OEA was measured in the plasma into which it was injected, the brain to which it was targeted and finally the liver, which is thought to be a potential generic site of lipid nanoparticle accumulation[282,283]. A control solution was also tested to provide the baseline pharmacokinetics of exogenously administered ^{13}C-OEA for comparison.

As shown in Figure 4.12, the result was that ^{13}C-OEA appeared to be rapidly degraded in plasma, brain and liver by the time points tested, the first of which was 15 minutes, as in the pharmacodynamic study. At a glance this seems to strongly support the speculation above that

the reason no anti-seizure effect was seen was because the OEA was being rapidly degraded, despite the hypothesised protection afforded to it by the cubosome structure. In contrast to the *in vitro* assay of Younus et al.[271], the cubosomes were found to offer no additional protection against hydrolysis compared with the same control solution and there was even a suggestion that hydrolysis was increased by the cubosome formulation. The variability in the results however meant that this trend was generally not statistically significant. Despite not exhibiting superiority to control solution with regards to protection from hydrolysis, the cubosomes at least provided non-inferior ^{13}C-OEA concentrations in an aqueous formulation, unlike the heavily organic-solvent based control.

Out of all the body compartments studied, the highest concentrations of ^{13}C-OEA were found in the plasma at all time points. While this is perhaps not surprising given that the ^{13}C-OEA was administered intravenously, it suggested that accumulation in the brain (as desired) or the liver (as hypothesised, but not desired) was not significant. One must consider that it is possible the ^{13}C-OEA was rapidly delivered to either of these tissues, but was equally rapidly hydrolysed before the first time point of 15 minutes. In this respect, it would have been interesting to investigate levels of the labelled hydrolytic product of ^{13}C-OEA as well, namely ^{13}C-ethanolamine as deduced from the predominant m/z of the synthesised ^{13}C-OEA (Figure 4.6), but a labelled standard was unavailable. Detection with LC-MS would also likely have been a complex task, given the low molecular weight of ethanolamine and its potential to be rapidly conjugated to other lipid molecules in tissues. An alternative explanation for the results above could be preferential distribution to other tissues that were not analysed. This would, however, seem less likely in light of the abovementioned data indicating that Tween 80®-stabilised cubosomes are effective at delivering drug to the brain and other studies describing non-specific liver accumulation of lipid nanoparticles due to the enhanced permeability and retention (EPR) effect[282,283].

Overall, trends in the data were difficult to describe conclusively due to inter-subject variability. The design of this study necessitated the use of individual rats for each time point in order to obtain plasma, brain and liver for analysis at the designated time point after ^{13}C-OEA administration. This introduced potential for variability due to individual rat characteristics such as capacity to metabolise ^{13}C-OEA and the way the cubosomes would be processed *in vivo*. Also important is that each data point represented an individual tail vein injection (a technically difficult procedure), so the dose that was successfully injected into the circulation may have varied. To eliminate these variables, a suggestion for similar studies in the future

would be to attempt analysis at all time points (and additional earlier ones) in each animal for plasma and brain. For plasma, this would involve cannulation of the tail vein and blood sampling at the desired time points. Brain would represent a more complex set up, for instance involving microdialysis, which would require some expertise in the procedure. Such a method would also reduce the quantity of ^{13}C-OEA required, allowing higher doses of cubosomes to be explored, such as that equivalent to the dose used in the pharmacodynamic study which may also have an influence on the pharmacokinetics, as the current analysis is based on an assumption of linear pharmacokinetic behaviour between 1 mg/kg and 7.5 mg/kg doses.

The analytical method for measuring ^{13}C-OEA itself had some complexities. What should have been a straightforward LC-MS assay was slightly complicated by a background signal for the ^{13}C-OEA ion pair. This signal was found to be consistently proportional to the background OEA (i.e. ^{12}C-OEA) signal intensity which was present to varying degrees in all the tissues analysed (Figure 4.9). Preliminary experiments (data not shown) determined that the background signal was also found at the same proportion in a solution of commercially synthesised OEA (≥98% purity). Therefore, it was concluded that it was most likely to be due to production of the $[M+2H]^{2+}$ ion of OEA in the mass spectrometer, rather than a true background presence of ^{13}C-OEA. In further support of this, in order to give this m/z signal, background ^{13}C-OEA molecules would have to consistently constitute a ^{13}C atom on the ethanolamine portion of the molecule, as was determined to be the case for the synthesised compound. Furthermore, they would have to be present in a consistent proportion to OEA in all tissues and commercially synthesised product. All of this seems unlikely given the natural abundance of ^{13}C in the environment is estimated to be only 1%[284]. Nonetheless, it was impossible to prove in this study, as the blank tissues always contained background OEA.

Despite this complication, the consistent proportion of the signal allowed a correction to be applied to the data (Equation 4.1) which yielded a reproducible analytical method with satisfactory confidence limits down to the lowest concentration possible with this limitation (**Appendix P**). To produce a simpler method for any future studies that may occur, the recommendation of this author would be to explore firstly whether a different mass spectrometer would lead to different ionisation patterns and removal of the background signal and secondly whether ^{13}C-OEA could be synthesised with the ^{13}C label on the oleic acid portion of the molecule, rather than the ethanolamine portion which would be expected to produce an alternative ion pair (i.e. m/z = 327/62 rather than 327/63) that would not overlap with the $[M+2H]^{2+}$ ion of OEA. Furthermore, with reference to the discussion above, simultaneously

measuring the hydrolytic by-product ^{13}C-oleic acid might also be possible to further study the contribution of degradation.

The quantitative data discussed above had some limitations. Whether it was due to technical complexities, method limitations, hydrolysis or distribution, brain concentrations, and sometimes liver concentrations, were frequently below the lower limit of quantification of the method. The data to which this applies is treated as zeroes in Figure 4.12 as they could not be quantified within the limits of the assay, however, a presentation of the actual measured values is provided in **Appendix Q** for transparency to the reader.

It is worth considering how technical limitations may have contributed to the results of this experiment. At each time point there was an unavoidable delay between euthanasia of the animal and freezing of the tissue due to the need for dissection and centrifugation of plasma. This meant the tissues were somewhere between body and room temperature for up to 10 minutes post-mortem before being frozen with dry ice. In this time, hydrolytic enzyme activity may well have continued, reducing the concentration of ^{13}C-OEA in the tissues. The multiple time point experiment suggested above for future studies may provide an advantage in overcoming this, as it could allow more rapid freezing after sampling. Furthermore, sampling from a live animal would avoid the rapid increases in NAE concentrations reported after euthanasia[285] which could also have had an influence on the result and likely contributed to the high intensity background OEA signal found in the brain (Figure 4.9) as suggested by the wide range of endogenous OEA levels reported in post-mortem brains[286–288]. Another point where further enzymatic degradation may have occurred post-mortem was the necessary sample thawing during preparation for LC-MS analysis. Samples were kept on ice wherever possible during this process, however, so enzyme activity is less likely to have had a major influence at this point.

Finally, the characteristics of the cubosomes themselves must be considered. The nanoparticles have not been formulated with ^{13}C-OEA to date and while the isotope should have theoretically demonstrated the same physicochemical properties as regular OEA, it was possible that small differences in behaviour could have occurred, as has been reported for isotopic variants of other compounds[289,290]. To assess formulation characteristics, particle size and PDI were measured and found to be similar to that reported by Younus et al.[258], suggesting the formulation was representative of the previously reported OEA cubosome dispersion. The structure of the particles was unable to be verified by SAXS or Cryo-TEM due to very limited sample availability and the formidable cost of obtaining more of the compound, so the preservation of

particle structure remains unconfirmed when interpreting the results of this study. The second consideration regarding the particles is that due to the limited availability of the compound, the cubosomes tested in the pharmacokinetic study comprised only 10% OEA compared with the 30% OEA cubosomes used in the pharmacodynamic study, which one may argue could have affected their representation of the intravenous behaviour of the cubosomes in the latter. Considering that Younus et al.[271] reported greater *in vitro* protection of OEA from hydrolysis by 10% OEA cubosomes compared with 30% OEA cubosomes (unpublished data), the evidence so far would seem to suggest that the pharmacokinetic data would, if anything, provide an overestimation of the protective effect of the OEA cubosomes in the pharmacodynamic study. SAXS data from this Chapter which looked at the structural stability of both types of cubosomes during *in vitro* incubation with rat plasma suggested that their behaviour was comparable, as is discussed next.

SAXS data showed that both the 10% and 30% OEA cubosomes used in the abovementioned intravenous studies rapidly transform into hexosomes after *in vitro* incubation in rat plasma (Figure 4.14). Control studies (Figure 4.13) showed that this was not related to the increased incubation temperature, which only had the effect of slightly decreasing the average lattice parameter of the cubosomes, as has been reported elsewhere for phytantriol cubosomes stabilised with Pluronic F127® [290–295]. This raises the question of whether this structural transition might be at least in part the cause of the apparent poor delivery of OEA to the brain and protection from hydrolysis in the plasma. The hexagonal phase is typically associated with sustained drug release given that it is thought to be a 'closed' structure relative to the 'open' structure provided by cubosome water channels[268,296]. This would lead one to think that perhaps transformation to a hexagonal particle might be an aid to the protection of OEA, but the pharmacokinetic studies in this Chapter do not seem to agree with that.

The first consideration is whether the structural transition could be due to the OEA in the cubosome being accessed by enzymes and hydrolysed to oleic acid. Previous studies have shown that formulation of phytantriol cubosomes with >10% oleic acid induces a structural transition to hexosomes at neutral pH[297]. Pluronic F127® was the stabiliser used in the referenced study, but the phenomenon has been replicated in this author's own lab with Tween 80® stabilised cubosomes to show the same effect induced by the charged oleic acid increasing negative curvature of the phytantriol bilayer (unpublished data). While a reasonable theory, it is undermined by two other elements of the data – firstly, phytantriol cubosomes alone (in the absence of OEA) also undergo the same transition to hexosomes in plasma (Figure 4.14) and

secondly, 30% OEA cubosomes appear to undergo the transition at a slightly slower rate than 10% which is opposite to what might be expected due to the higher proportion of OEA.

The apparent decrease in the rate of cubosome transformation to hexosomes in plasma with increasing OEA composition could possibly be explained by the relative curvature of the cubosome bilayers. All structures exhibit an *Im3m* symmetry, which emanates from a less negatively curved lipid bilayer due to the insertion of the oleoyl chain of Tween 80® [277]. Upon addition of OEA, the lattice parameter of the cubosomes increases as the bilayer becomes even less negatively curved upon the incorporation of more oleoyl chains from more OEA molecules[258]. From this, it can be inferred that in order to transition to the state of high negative curvature that is the hexagonal phase, a greater change is needed in the less curved bilayer containing more OEA and hence more time. We can also infer another finding from the slower rate of transition with increased lattice parameter in support of the above paragraph in that the transition is likely not due to hydrolysis of OEA to oleic acid. This is because larger water channels would theoretically allow greater access to enzymes and a greater rate of hydrolysis and transition to the hexagonal phase (unless of course the emergence and relative effect on the bilayer of oleic acid was outweighed by the lesser negative curvature of the bilayer) as described by Younus et al. *in vitro*[271].

It should be noted that in order to achieve sufficient resolution of SAXS data, it was necessary to measure samples at a concentration of only 50% plasma relative to cubosome dispersion, as has been reported previously[266]. This means that while the data shows the relative structural kinetics of the different cubosomes, the actual time scale over which such transformations would occur would be much faster in 100% plasma *in vivo*[298,299] and could be expected to have taken place within the time range at which pharmacodynamic and pharmacokinetic testing took place. This concept is illustrated with supplementary data in **Appendix R** which was obtained with phytantriol Tween 80® cubosomes and shows the effect of changing plasma concentration on the rate of transformation, but not the actual outcome. Structural instability may therefore have played a role in the apparent ineffectiveness of OEA cubosomes at protecting OEA and delivering it to the brain in this study and further investigation into the causes of the structural instability and how it may be prevented would no doubt be an interesting avenue of future research.

As an entry point, a parallel study performed with OEA cubosomes stabilised with Pluronic F127® (the other OEA formulation characterised by Younus et al.[258]) is shown in **Appendix O**.

It also demonstrated a transition of cubosomes on incubation with plasma, however not to hexosomes, but a single broad peak which was not able to be unequivocally classified. Certainly though, the dispersion did not maintain the organised internal structure of cubosomes or hexosomes, suggesting that this stabiliser may be less effective compared with Tween 80® in maintaining the structural stability of intravenously administered liquid crystalline nanoparticles. It must be noted that the results are in contrast to previously reported data on phytantriol-Pluronic F127® cubosomes studied in human plasma which transformed into hexasomes[266]. While the source of plasma immediately appears as a potential explanation for the difference, it must also be considered that the phase homogeneity of the original cubosome formulation in the study was questionable. Whatever the case, these studies indicate that the appetite for discovering how to control the structural stability of liquid crystalline nanoparticles in biological media must continue to grow in an attempt to optimise and translate such delivery systems successfully in the future.

The second part of this Chapter investigated intranasal delivery of OEA cubosomes and ended up holding more weight than was hypothesised. It was initially thought that an anti-seizure effect of some degree would be observed after intravenous treatment with OEA cubosomes, but it was not, and the *in vivo* and *in vitro* studies into intravenous delivery of these nanoparticles unveiled a number of complexities. At the centre of these was the important question of whether inadequate protection or inadequate delivery (or both) was the cause of this failure. Hence, attention was shifted to the nose, as a potential method to deliver OEA to the brain while bypassing the route through the plasma and across the blood-brain barrier. Use of cubosomes as a delivery system was still important here due to the poor solubility of free OEA in aqueous vehicles and the constrictive volume limitations for intranasal dosing.

The results of the intranasal OEA cubosomes MEST studies, however, presented their own complexities. The initial study at 60 minutes after administration had a less than optimal, but still acceptable, 39 % of saline-treated rats displaying HLE at the statistically determined CC_{50}, however, the effect of drug treatment was inconclusive with small changes in the incidence of HLE in each direction, which were expectedly not statistically significant ($p = 0.93$). From this it could only be concluded that if there was an effect of OEA, it seemed to rapidly abate by 60 minutes. Subsequently, an attempt was made to check for a rapid onset effect from the OEA, but it was here that a major limitation was encountered in the form of confounding by the anaesthetic isoflurane. At 15 minutes after administration, a clear anti-seizure effect of the anaesthetic was evident, despite the rats having appeared to have regained function, so much so that it was not possible to determine the CC_{50} (Figure 4.17C). While a small number of rats

showed HLE at 30 minutes after administration, enabling a CC_{50} of 76 mA to be calculated (Figure 4.17D), this current was higher than that encountered in any other study in this thesis indicating that the effect of isoflurane was still significant. The results of the drug trial looked very similar to that at 60 minutes, and were likewise insignificant, but the particularly poor resolution due to the confounding meant that the outcome could not provide an adequate answer to the question at hand. As discussed in **Chapter One**, almost all studies report the use of anaesthesia of some sort in order to administer intranasal anti-seizure treatments to the olfactory region of the nasal cavity. Therefore, at this stage of science, it is difficult to see how such a procedure could be performed without it in order to credibly test rapid effects after intranasal delivery to the olfactory region in a simple screening model such as that used in this thesis. Nonetheless, it would be a very useful tool for future studies to investigate and should be addressed in order to increase the quality of the intranasal anti-seizure drug delivery literature.

The OEA cubosomes used in this Chapter were found to clearly disrupt the olfactory epithelium at the highest concentration (Figure 4.15E), meaning the dispersion had to be diluted to optimise it for nasal administration. Unfortunately, the volume limitation of the nasal cavity meant that dilution could not be compensated for by increasing volume, so total dose had to be reduced. The data once again support the argument raised in **Chapter One** and **Chapter Three** that the effect of any intranasal formulation or delivery system on the nasal epithelium should be histologically evaluated and raises the call to the field of pharmaceutical sciences to ensure quality data is presented alongside any pharmacokinetic or efficacy studies as a fundamental means of validation.

The intranasal histology study of this Chapter is also interesting from the perspective of cubosome toxicity to cells, which the current literature assesses heavily through the use of *in vitro* cell lines[293,300–303], but with little consideration as to how this translates *in vivo*. The closest studies found to those in this thesis are those which examine corneal histology of glyceryl monooleate (GMO) based cubosomes[304,305], but only a single concentration of cubosomes, much lower than those used in this Chapter, is tested (or at least selectively presented) in each, offering scarce room for comparisons to be made. The comparison to a control suspension containing all components but the essential cubosome-forming lipid phytantriol (Figure 4.15F) suggested that either the cubosomes themselves or the phytantriol were the major cause of epithelial disruption rather than the other components of the dispersion. This is supported by supplementary histological data from preliminary testing of phenytoin-loaded selachyl alcohol cubosomes presented in **Appendix I** for which the effect was similar. This data, based on

cubosomes formed from an alternative lipid along with *in vitro* cell toxicity studies of the free lipids, phytantriol and selachyl alcohol, by Younus et al.[271] suggest the cubosome structure itself to be the key cause of cell toxicity/epithelial disruption. The mechanism of this toxicity remains uncertain, but is likely due to a fusogenic mechanism of interaction between the negatively curved bilayers of the nanoparticles and the plasma membranes of the cells[306,307] which would obviously have a concentration limit above which it would be expected to become majorly disruptive. Tan et al.[303] have reviewed the subject in more detail and concluded that current literature suggests that greater negative curvature seems to reduce cell toxicity (i.e. toxicity would be expected to be in the order of hexagonal < *Pn3m* cubic < *Im3m* cubic) due to a lower degree of lipid mixing with the cell membrane. This would imply that perhaps *Pn3m* cubosomes (e.g. OEA-phytantriol cubosomes stabilised with Pluronic F127® [258] or hexasomes (e.g. phenytoin-loaded selachyl alcohol hexosomes stabilised with Pluronic F127®, as characterised by Younus et al.[271]) may be more suitable for delivering higher concentrations (and therefore higher doses) of the therapeutics intranasally. However, unpublished *in vitro* cell toxicity studies carried out by the present author and Younus et al.[271] have not found a difference between these formulations and the ones tested in this Chapter, so whether a difference would be seen *in vivo* remains questionable.

4.7 Conclusions

This Chapter applied the seizure model from the previous Chapters to the investigation of a formulated endogenous compound with untested anti-seizure activity, oleoylethanolamide. The primary findings suggest that OEA (at least in cubosome form) does not exhibit acute anti-seizure activity after intravenous administration at the dose tested. However, the subsequent chemical and structural stability studies of ^{13}C-OEA and OEA cubosomes respectively present ample evidence to suggest that the delivery of OEA cubosomes to the brain via the systemic circulation is complex. They support that it could have been subject to confounding from a range of different variables which it was not possible to tease out within the constraints of this Chapter. Intranasal delivery was therefore of particular interest as an alternative means to deliver OEA directly to the brain and bypass the systemic challenges altogether, however, these investigations were met with significant challenges of their own. Firstly, histology revealed that unlike the microparticles in the previous Chapter, the dose of cubosomes that could be administered to the nose was limited by concentration as well as volume. Secondly, testing for rapid effects on seizure threshold after intranasal administration (i.e. time points less than 60 minutes after administration) was impeded by the lingering anti-seizure effects of the isoflurane anaesthesia that was necessary to deliver the dose to the animals. This rendered the MEST study inconclusive and highlighted a need for development of new intranasal administration methods for pre-clinical testing of such hypotheses. To conclude, the evidence at hand suggests that OEA cubosomes are not likely to be a useful anti-seizure treatment, at least after acute administration, but further investigation into the complexities behind these results will confirm whether this judgement is justified. It will also confirm whether OEA cubosomes themselves can maintain the required stability to be useful for intravenous or intranasal treatment of other conditions.

Chapter Five

Summary & Future Directions

Epilepsy is the most common serious neurological disorder[3], affecting up to 50 million people worldwide[4]. Despite decades of international research towards developing new pharmacological treatments and the current availability of over 22 anti-seizure drugs (ASDs)[6], approximately 30% of patients are still classified as "drug-resistant"[7]. Investigation of new strategies to support the ability of ASDs to offer sustained seizure freedom and tolerability is critical to addressing this troubling statistic. This thesis aimed to explore delivery of ASDs through the nose, a somewhat alternative approach to ASD treatment which has been gaining a lot of traction in recent years, especially in light of proposed direct nose-to-brain delivery pathways that bypass the hurdles of the systemic circulation[33,82]. Due to the physical limitations of the nasal cavity[22,94], pharmaceutical formulation strategies are intimately relevant to the successful exploitation of this route of delivery and form the basis of the investigations in this thesis.

Chapter One introduced the topic of intranasal delivery of anti-seizure drugs from the link between the nose and seizures, to pathways to the brain, to current rudimentary formulations in clinical use. It then proceeded to a discussion of animal seizure models and their theoretical application to studying intranasal seizure treatments, following by a critical discussion of methodology and outcomes reported in the more exploratory ventures in the literature to date. Upon this foundation, the experimental component of the thesis aimed to develop a relatively simple screening model capable of detecting intranasal effects in **Chapter Two**. It aimed to

then use that to explore firstly, a drug delivery system carrying the pharmacokinetically troublesome anti-seizure drug phenytoin in **Chapter Three** and secondly, a delivery system carrying an endogenous molecule, oleoylethanolamide, with potential, but previously unstudied, anti-seizure action in **Chapter Four**.

Chapter Two proposed the development of a new cross-over study design based on the MEST test for assessing the effects of intranasal drug therapy on seizure threshold. As discussed in the preamble to that Chapter, the MEST test has been frequently used in the literature[15,98,99,101,172,174,308], but the template of two subsequent "up and down" stimulation trials left room for improvement with regards to achieving the aims of this study. The expectation that the effects of intranasally delivered drugs may be more localised and subtle than those seen after systemic administration meant that modifications were necessary to aim for the highest sensitivity and lowest variability possible while still maintaining a fairly simple screening procedure. The modified design clearly detected the anti-seizure effect of phenytoin after intravenous administration with respect to the two key outcomes, HLE and FLE, and this was supported by measurement of brain and plasma levels which were in line with other reports in the literature[175–177,187,188]. Importantly, isoflurane administration 60 minutes prior to stimulation did not appear to introduce any confounding effect between phenytoin and control that could have decreased the resolution for detecting anti-seizure effects. This was an important prerequisite for the following studies as anaesthetics are currently necessary to reliably and ethically perform intranasal administration to the olfactory region in rats, as discussed in **Chapter One**, so any effect of them on seizure tests must be minimised in order to obtain unambiguous results. A further important consideration for any seizure model is the impact on animal welfare. This was closely evaluated for this procedure and determined to be minimal, supporting the continued use of the model in the subsequent experiments.

Chapter Three proceeded to apply the seizure model to its intended purpose of evaluating an intranasal delivery system carrying phenytoin. The aim was both to evaluate the anti-seizure efficacy of tamarind polysaccharide-based phenytoin microparticles, an intranasal delivery system previously designed and characterised by Yarragudi et al.[204], as well as to test the capabilities and limitations of the model in detecting anti-seizure effects following the intranasal delivery of the known ASD phenytoin. With regards to evaluating the phenytoin microparticles as an intranasal anti-seizure drug delivery system, this study was particularly unique in that it is the first to the author's knowledge of an intranasal dry powder (anti-seizure) delivery system being administered and evaluated as a dry powder as opposed to being

suspended in a liquid before administration[146] to facilitate administration to animals, which no doubt affects the behaviour of the particulate delivery system. Furthermore, this study holistically addressed histological safety, pharmacokinetics and pharmacodynamics, as opposed to other *in vivo* studies of ASD delivery systems in the literature that encompassed only selected elements and carried avoidable limitations making them hard to draw conclusions from, as discussed in detail in **Chapter One**.

The modified MEST study design proved proficient at detecting intranasal anti-seizure effects, with a peak effect being identified at 120 minutes after administration which correlated with peak brain levels of phenytoin. As was seen in **Chapter One**, most studies of intranasal anti-seizure delivery systems aim to use the direct nose-to-brain route to achieve rapid effects for rescue therapy. The data in this Chapter, however, shows the microparticles to be a fairly slow-acting, but sustained anti-seizure drug delivery system more suitable for the potential application of regular dosing of phenytoin which presents the utility of the nose-to-brain route for the treatment of seizures from a different perspective. The implementation here would most likely be as a means to deliver the phenytoin effectively to keep seizures suppressed, while bypassing the pharmacokinetic pitfalls that mar its systemic use, thereby increasing tolerability and simplifying dosing.

A further area of interest is whether the direct intranasal delivery of phenytoin, which theoretically bypasses multi-drug transporters at the blood brain barrier, could be applied in cases of drug resistance attributed to multi-drug transporter overexpression. As discussed in **Chapter One** and **Chapter Three**, many studies have been performed to explore the multi-drug transporter hypothesis of resistance in the past two decades[9,122,133,174,201–203] and phenytoin, as a model drug, has been at the centre. The phenytoin-resistant kindled rat in particular was extensively characterised and presents an interesting future model in which the utility of the microparticles might be studied to ascertain whether the anti-seizure effect of phenytoin can be rekindled in animals which have developed resistance to the systemically administered drug. This is, however, a model of focal epilepsy, so preliminary studies would be recommended to investigate regional brain distribution to the focus (i.e. the amygdala).

In addition to the efficacy data, the results of this Chapter supported the previous claim by Yarragudi et al.[204] that delivery of phenytoin from the microparticles followed a direct route from the nasal passage to the brain. This was reflected in the relative plasma and brain concentrations of phenytoin, but also supplemented by going a step further and studying the

presence of its major metabolite, 4-HPPH, which was found to be elevated in the brain above the low percentage expected after systemic administration. The study of 4-HPPH also offered the suggestion that phenytoin was being partially metabolised by the nasal epithelium and the sustained release mechanism of the microparticles may therefore have facilitated direct transport to the brain through metabolite-induced inhibition of phenytoin metabolism[229]. This was an interesting incidental finding and suggested that future studies may be able to harness the approach to allow more in depth study into the delivery of ASDs via the nasal passage by also considering their metabolites.

Interestingly, in the studies of **Chapter Three**, the direct brain delivery of phenytoin did not appear to be primarily mediated through pathways associated with the olfactory bulbs. While previous studies have suggested intranasal trafficking of anti-seizure drugs through the olfactory bulbs[138,140,141], the data of this Chapter was to the contrary and in agreement with that presented by Yarragudi et al.[204] in that olfactory bulb concentrations were never higher relative to the main brain after microparticle administration (or for that matter, phenytoin control solution) and if anything, generally appeared to be lower. The present study, however, also studied brainstem concentrations of phenytoin and found an apparent elevation in this region. This finding, combined with the discussion of current literature in **Chapter One**, suggested a brainstem-associated bulk intranasal transport pathway (e.g. bulk flow peripheral to trigeminal neurons) to be the most likely mechanism which led to direct, but widespread brain delivery of phenytoin.

A final notable finding from **Chapter Three** concerns the importance of histological sampling as an essential component of intranasal drug delivery studies. **Chapter One** discussed the lack of regard for this in the current literature and the suggestion in a review by Kozlovskaya et al.[91] that fractions of drug reportedly delivered intranasally to the brain in many studies were so high that they implied a breach of physiological barriers due to formulation constituents. The credibility of this claim was seen experimentally in **Chapter Three** through the comparison of the biocompatible phenytoin microparticles with an evidently incompatible ethanol-containing phenytoin control solution which caused significant epithelial disruption and emphasised the need for quality histological studies to accompany all future investigations into intranasal drug delivery to ensure safety. The similarities between rodent and human nasal epithelia mean preclinical studies in rodents offer an ideal opportunity to screen histologically and optimise dosage and formulation at this early stage, while validating claims of direct intranasal delivery. Tissues can easily be obtained as a by-product from animals undergoing pharmacokinetic or efficacy experiments so future researchers should not be excused from having to present this

data. The data presented by Yarragudi et al.[204] and subsequently in **Chapter Three** supports the compatibility of phenytoin microparticles with the nasal epithelium and encourages future studies with this delivery system such as those mentioned earlier regarding seizure prevention in a more complex animal model, as well as tolerability of blank tamarind seed polysaccharide microparticles in human subjects.

Overall, the results of **Chapter Three** supported the use of the MEST seizure model as a screening tool to ascertain the effects of intranasally delivered anti-seizure drugs, so **Chapter Four** subsequently aimed to investigate a molecule with hypothesised, but previously untested activity. That molecule was oleoylethanolamide, an endogenous bioactive lipid of the N-acylethanolamide class with reported neuroprotective properties[236–238] that has recently been formulated into a nanoparticulate dispersion of cubosomes by Younus et al.[258] to improve solubility and stability. Other N-acylethanolamides have shown anti-seizure activity in MES studies in the literature[239,241], so it was hypothesised that OEA would too, simultaneously providing a demonstration of the proposed benefits of formulating it into cubosomes. This result, however, was not to be found.

The study began with an investigation of intravenously administered OEA cubosomes. This route was chosen to provide a positive control of the effects of OEA on seizures, such as that provided by intravenous phenytoin in **Chapter Two**, prior to intranasal studies. Unlike similar molecules (PEA and AEA) which have demonstrated an effect in the supramaximal MES test[239,241], OEA failed to show any significant effect (pro- or anti-seizure) in the submaximal threshold MEST test used in this study. It was therefore concluded that OEA, at least in cubosome form and at the dose tested, does not exhibit an acute effect on seizure threshold after intravenous administration. A couple of future directions immediately emerge upon stating this conclusion, namely whether the cubosome dispersion could be concentrated further or modified to increase the dose of OEA delivered or whether chronic administration of OEA cubosomes might be the key to uncovering anti-seizure effects of OEA, both of which were discussed in **Chapter Four**. Furthermore, the recent cubosome formulation of another NAE, linoleoylethanolamide (LEA), by Younus et al.[271] offers another avenue for MEST screening studies.

To provide a more wholesome foundation for directing such future studies, however, pharmacokinetic and structural stability analyses were subsequently conducted in **Chapter Four** to determine whether the lack of effect from OEA could be explained by the OEA

pharmacokinetic profile or a potential change in the environmentally malleable self-assembled cubosome structure. What was found opened up possibilities for a further range of future studies to tease out the complexities of the results. Pharmacokinetic studies with ^{13}C-OEA cubosomes suggested that the lack of effect may have been due to a lack of delivery of OEA to the brain after intravenous administration. However, it was unclear whether this was due to a rapid hydrolysis and a failure of the cubosomes to protect the OEA or a preferential distribution to other body compartments due to a failure of the cubosomes to target the brain. The former suggestion would be in disagreement with the *in vitro* findings of Younus et al.[271], while the latter would differ from the present author's extracurricular *in vivo* studies with phenytoin cubosomes which did suggest the cubosomes facilitated drug delivery to the brain. However, the delivery of intact cubosomes was not proven here and the different lipid used (i.e. selachyl alcohol) may have influenced its success (unpublished data). Methodological limitations may also have played a role, as was discussed in **Chapter Four** along with some suggested improvements. In particular, it is suggested that future studies be carried out which take samples of plasma (and brain if possible) concentrations in single animals over time, rather than the time point allocated groups in this study in order to eliminate intra-subject variability between time points in the pharmacokinetic profile and remove the effects of potential dosing errors and post-mortem NAE concentration changes. Also worth investigating would be the effect of stabiliser on the fate of OEA administered in cubosomes as Younus et al.[271] reported a slight (though statistically insignificant) increase in protection of OEA in Pluronic F127® cubosomes *in vitro* compared with Tween 80® when exposed to FAAH which could possibly have *in vivo* relevance.

To complicate matters further, *in vitro* SAXS studies indicated that the OEA cubosomes stabilised with Tween 80® rapidly transformed into a hexosomes upon contact with blood plasma which offered a further possible explanation for why the cubosomes seemed to be unsuccessful at delivering the OEA systemically. While hexosomes are not considered to be ineffective drug delivery systems[296,303,309], the change in structure raises questions about the stability and retention of OEA in the particles and the effect this may have on biological distribution as work to date has characterised these only with respect to cubosomes (unpublished data). As a starting point for further investigations, it is suggested that a study could be conducted whereby OEA cubosomes are incubated for a short time with plasma, then separated from it again using a size exclusion column, as in another of the present author's extracurricular studies investigating protein adsorption to cubosomes (unpublished data), and the retention of OEA in the nanoparticles measured. Furthermore, studies might then be

performed to compare the *in vitro* stability of the hexosomes against FAAH to that reported by Younus et al.[271] for the unexposed cubosomes. In light of the suggested pharmacokinetic studies with Pluronic F127®-stabilised OEA cubosomes above, similar studies might also be performed on the ambiguous-phased particles into which this type of cubosomes transformed, as was shown in **Appendix O**, to see how this alternative transformation influences the protection and delivery of OEA. As a more extensive continuation of this thread, studying what actually causes the transformation of cubosomes to hexosomes would be of great interest to the field of self-assembling lipid nanoparticles, not only with respect to OEA cubosomes, but also pure phytantriol cubosomes, as this could allow such mechanisms to be manipulated and exploited as has been the case for dispersions in gastrointestinal fluids[310].

In the context of this thesis, investigations then proceeded to explore if intranasal delivery could offer a means of delivering OEA directly to the brain and bypassing the systemic challenges altogether. The first obstacle in this study was presented by histology which showed that the dose of OEA dispersion that could be administered safely (i.e. without disrupting the olfactory epithelium) to the test animals was limited by concentration as well as volume and required dilution of the maximum possible with the presently characterised formulation. This was a setback compared with the powder formulation in **Chapter Three** for which the dose seemed to be limited only by how much powder could be administered from the insufflator. While powder would obviously reach a limit too, based on the safe volume of the nasal cavity it could occupy without impeding breathing, this delivery system was clearly more compatible than the cubosomes with the nasal epithelial cells. Further experiments confirmed that the cubosomes themselves appeared to be the cause of the disruption, rather than the individual components of the formulation. The testing of intranasal cubosomes has been reported before (though not for seizure treatment)[311], but the present study is the first to the author's knowledge to report a toxicity to the nasal epithelium independent of lipid type. This is somewhat surprising given the extensive attention given to the *in vitro* study of cubosome toxicity to various cell types as discussed in **Chapter Four** and stresses that quality histological data should be a fundamental means of validation of *in vivo* studies in the pharmaceutical sciences literature, especially with regards to direct nose-to-brain delivery for which it is intimately relevant. Furthermore, it offers an *in vivo* perspective on cubosome tolerability by cells which would do well to be expanded on in future studies and compared with *in vitro* dose-response findings to ascertain translatability of the data modelled in this setting and, if appropriate, use it to screen and optimise formulations further for interaction with the nasal epithelium. For instance, as discussed in **Chapter Four**, current literature suggests hexosomes might be more suitable for

higher dose nanoparticle administration[303], so modification of the phase of the OEA dispersion, perhaps by introducing a molecule to induce negative curvature (e.g. tocopheryl acetate[312]) could be explored and trialled *in vivo*.

Despite the above findings, dilution of the dispersion allowed a histologically safe dose of OEA cubosomes to be determined and this was used to test for an effect on seizure threshold. A reliable, but non-significant, result was only obtainable at 60 minutes after administration as it became evident that the effect of the anaesthetic isoflurane on seizures (which was necessary to allow deep intranasal administration) was significant at earlier time points of 15 and 30 minutes after administration and clouded the experimental outcome. This was not entirely unexpected given the discussion of the limitations posed by the need for anaesthetics in **Chapter One**, and though it was hoped the crossover study design and short duration of anaesthetic used in the present investigations may have offered some reprieve, this was not the case. It therefore remains an important issue for future pre-clinical studies to navigate should the study of rapid intranasal anti-seizure effects wish to progress. In the meantime, perhaps more attention should be given to administration of longer-acting anti-seizure drugs and delivery systems as regular dosing instruments, as in **Chapter Three**, or to testing compounds after chronic administration via the nose which could still be studied using the present methods and could be more relevant to the mechanism of action of OEA, as proposed earlier in discussion of intravenous studies. An intranasal pharmacokinetic study with ^{13}C-OEA may also shed some light on the timescale and pathway of the passage of OEA from the nose to the brain and be of use in guiding future work. Additionally, pharmacodynamic studies of OEA in other neurological conditions in which it is proposed to be effective (e.g. stroke and Parkinson's disease[236–238]), specifically those with measurable outcomes which are not so easily affected by anaesthetics, may provide a better initial evaluation of the potential of cubosomes to deliver OEA intranasally and whether investigations into its utility as a seizure treatment are worth pursuing. In light of the results obtained, **Chapter Four** had to conclude that OEA cubosomes appeared to be ineffective at influencing seizure threshold after acute administration by the intranasal route at the maximum non-disruptive dose. Whether this was due to a complete lack of efficacy of OEA, an inadequate maximum deliverable dose based on volume and concentration limitations, or the inability to see through the confounding of the anaesthetic remain questions to be investigated by the future studies discussed and provide a foundation for other studies investigating intranasal OEA.

Overall, this thesis has achieved its aim of establishing a model for testing intranasal ASD delivery and fundamentally evaluating the potential for delivery of ASDs through the nose to the brain using the selected particulate formulation strategies of microparticles and cubosomes. From the critique of the emerging intranasal field laid out in the opening review, to the practical implementation and challenges of the subsequently designed experiments, to the enticing follow-on questions summarised in this Chapter which are yet to be answered, the author hopes this text has stimulated critical thought and provided some sturdy groundwork on which future science can be built.

References

1. Fisher, R. S. *et al.* Epileptic Seizures and Epilepsy: Definitions Proposed by the International League Against Epilepsy (ILAE) and the International Bureau for Epilepsy (IBE). *Epilepsia* **46**, 470–472 (2005).
2. Huff, J. S. & Fountain, N. B. Pathophysiology and definitions of seizures and status epilepticus. *Emerg. Med. Clin. North Am.* **29**, 1–13 (2011).
3. Jacoby, A., Snape, D. & Baker, G. A. Epilepsy and social identity: the stigma of a chronic neurological disorder. *Lancet Neurol.* **4**, 171–178 (2005).
4. Ngugi, A. K., Bottomley, C., Kleinschmidt, I., Sander, J. W. & Newton, C. R. Estimation of the burden of active and life-time epilepsy: a meta-analytic approach. *Epilepsia* **51**, 883–90 (2010).
5. Sperling, M. R. The Consequences of Uncontrolled Epilepsy. *CNS Spectr.* **9**, 98–109 (2004).
6. Wilcox, K. S. *et al.* Issues related to development of new antiseizure treatments. *Epilepsia* **54**, 24–34 (2013).
7. Engel, J. Etiology as a risk factor for medically refractory epilepsy A case for early surgical intervention. *Neurology* **51**, 1243–1244 (1998).
8. Kwan, P. *et al.* Definition of drug resistant epilepsy: Consensus proposal by the ad hoc Task Force of the ILAE Commission on Therapeutic Strategies. *Epilepsia* **51**, 1069–1077 (2010).
9. Kwan, P., Schachter, S. C. & Brodie, M. J. Drug-Resistant Epilepsy. *N. Engl. J. Med.* **365**, 919–926 (2011).
10. Schmidt, D. & Löscher, W. Drug Resistance in Epilepsy: Putative Neurobiologic and Clinical Mechanisms. *Epilepsia* **46**, 858–877 (2005).

11. Walker, M. C. & Köhling, R. The problems facing epilepsy therapy. *Neuropharmacology* **69**, 1–2 (2013).
12. Gilliam, F. Optimizing health outcomes in active epilepsy. *Neurology* **58**, S9–S20 (2002).
13. Perucca, P. & Gilliam, F. G. Adverse effects of antiepileptic drugs. *Lancet Neurol.* **11**, 792–802 (2012).
14. Löscher, W. Critical review of current animal models of seizures and epilepsy used in the discovery and development of new antiepileptic drugs. *Seizure* **20**, 359–368 (2011).
15. Löscher, W. & Schmidt, D. Which animal models should be used in the search for new antiepileptic drugs? A proposal based on experimental and clinical considerations. *Epilepsy Res.* **2**, 145–181 (1988).
16. Kubek, M. J., Domb, A. J. & Veronesi, M. C. Attenuation of kindled seizures by intranasal delivery of neuropeptide-loaded nanoparticles. *Neurother. J. Am. Soc. Exp. Neurother.* **6**, 359–371 (2009).
17. Veronesi, M. C., Aldouby, Y., Domb, A. J. & Kubek, M. J. Thyrotropin-releasing hormone d,l polylactide nanoparticles (TRH-NPs) protect against glutamate toxicity in vitro and kindling development in vivo. *Brain Res.* **1303**, 151–160 (2009).
18. Fisher, R. S. & Ho, J. Potential new methods for antiepileptic drug delivery. *CNS Drugs* **16**, 579–593 (2002).
19. Bennewitz, M. F. & Saltzman, W. M. Nanotechnology for delivery of drugs to the brain for epilepsy. *Neurotherapeutics* **6**, 323–336 (2009).
20. Ruiz, M. E. & Castro, G. R. Nanoformulations of Antiepileptic Drugs: In Vitro and In Vivo Studies. in *Antiepileptic Drug Discovery* 299–326 (Humana Press, New York, NY, 2016). doi:10.1007/978-1-4939-6355-3_16.
21. Kapoor, M., Cloyd, J. C. & Siegel, R. A. A review of intranasal formulations for the treatment of seizure emergencies. *J. Controlled Release* **237**, 147–159 (2016).

22. Costantino, H. R., Illum, L., Brandt, G., Johnson, P. H. & Quay, S. C. Intranasal delivery: Physicochemical and therapeutic aspects. *Int. J. Pharm.* **337**, 1–24 (2007).

23. Jaseja, H. Scientific basis behind traditional practice of application of 'shoe-smell' in controlling epileptic seizures in the eastern countries. *Clin. Neurol. Neurosurg.* **110**, 535–538 (2008).

24. Betts, T. & Betts, H. John hall and his epileptic patients—epilepsy management in early 17th century england. *Seizure* **7**, 411–414 (1998).

25. Gowers, W. R. (William R. *Epilepsy and other chronic convulsive diseases : their causes, symptoms, & treatment*. (London : Churchill, 1881).

26. Efron, R. The effect of olfactory stimuli in arresting uncinate fits. *Brain* **79**, 267–281 (1956).

27. Efron, R. The conditioned inhibition of uncinate fits. *Brain* **80**, 251–262 (1957).

28. Betts, T. Use of aromatherapy (with or without hypnosis) in the treatment of intractable epilepsy—a two-year follow-up study. *Seizure* **12**, 534–538 (2003).

29. Dugan, P. *et al.* Auras in generalized epilepsy. *Neurology* **83**, 1444–1449 (2014).

30. Vaughan, D. N. & Jackson, G. D. The piriform cortex and human focal epilepsy. *Epilepsy* **5**, 259 (2014).

31. Blair, R. D. G. Temporal lobe epilepsy semiology. *Epilepsy Res. Treat.* **2012**, 751510 (2012).

32. Ache, B. W. & Young, J. M. Olfaction: Diverse Species, Conserved Principles. *Neuron* **48**, 417–430 (2005).

33. Lochhead, J. J. & Thorne, R. G. Intranasal delivery of biologics to the central nervous system. *Adv. Drug Deliv. Rev.* **64**, 614–628 (2012).

34. Bekkers, J. M. & Suzuki, N. Neurons and circuits for odor processing in the piriform cortex. *Trends Neurosci.* **36**, 429–438 (2013).

35. Courtiol, E. & Wilson, D. A. The olfactory thalamus: unanswered questions about the role of the mediodorsal thalamic nucleus in olfaction. *Front. Neural Circuits* **9**, (2015).

36. Nicola-Antoniu, I. Olfactory Dysfunctions in Alzheimer's Disease. in *The Clinical Spectrum of Alzheimer's Disease -The Charge Toward Comprehensive Diagnostic and Therapeutic Strategies* (2011).

37. Hummel, T. *et al.* Olfactory bulb volume in patients with temporal lobe epilepsy. *J. Neurol.* **260**, 1004–1008 (2013).

38. Pereira, P. M. G. *et al.* MR Volumetric Analysis of The Piriform Cortex and Cortical Amygdala in Drug-Refractory Temporal Lobe Epilepsy. *Am. J. Neuroradiol.* **26**, 319–332 (2005).

39. Bensafi, M., Sobel, N. & Khan, R. M. Hedonic-Specific Activity in Piriform Cortex During Odor Imagery Mimics That During Odor Perception. *J. Neurophysiol.* **98**, 3254–3262 (2007).

40. Ebert, U. & Löscher, W. Strong olfactory stimulation reduces seizure susceptibility in amygdala-kindled rats. *Neurosci. Lett.* **287**, 199–202 (2000).

41. Vismer, M. S., Forcelli, P. A., Skopin, M. D., Gale, K. & Koubeissi, M. Z. The piriform, perirhinal, and entorhinal cortex in seizure generation. *Front. Neural Circuits* **9**, (2015).

42. LÖSCHER, W. & EBERT, U. THE ROLE OF THE PIRIFORM CORTEX IN KINDLING. *Prog. Neurobiol.* **50**, 427–481 (1996).

43. Schwabe, K., Ebert, U. & Löscher, W. Bilateral lesions of the central but not anterior or posterior parts of the piriform cortex retard amygdala kindling in rats. *Neuroscience* **101**, 513–521 (2000).

44. Wahnschaffe, U., Ebert, U. & Löscher, W. The effects of lesions of the posterior piriform cortex on amygdala kindling in the rat. *Brain Res.* **615**, 295–303 (1993).

45. Lehmann, H., Ebert, U. & Löscher, W. Amygdala-kindling induces a lasting reduction of GABA-immunoreactive neurons in a discrete area of the ipsilateral piriform cortex. *Synapse* **29**, 299–309 (1998).

46. Acharya, V., Acharya, J. & Lüders, H. Olfactory epileptic auras. *Neurology* **51**, 56–61 (1998).

47. West, S. E. & Doty, R. L. Influence of epilepsy and temporal lobe resection on olfactory function. *Epilepsia* **36**, 531–542 (1995).

48. Laufs, H. *et al.* Converging PET and fMRI evidence for a common area involved in human focal epilepsies. *Neurology* **77**, 904–910 (2011).

49. Pires, A., Fortuna, A., Alves, G. & Falcão, A. Intranasal Drug Delivery: How, Why and What for? *J. Pharm. Pharm. Sci.* **12**, 288–311 (2009).

50. Kälviäinen, R. Intranasal therapies for acute seizures. *Epilepsy Behav.* **49**, 303–306 (2015).

51. Sutter, R., Kaplan, P. W. & Rüegg, S. Outcome predictors for status epilepticus—what really counts. *Nat. Rev. Neurol.* **9**, 525–534 (2013).

52. Chin, R. F. What are the best ways to deliver benzodiazepines in children/patients with prolonged convulsive seizures? *Epileptic. Disord.* **16**, S50–S58 (2014).

53. Wait, S. *et al.* The administration of rescue medication to children with prolonged acute convulsive seizures in the community: What happens in practice? *Eur. J. Paediatr. Neurol.* **17**, 14–23 (2013).

54. Spencer, D. Hope for new treatments for acute repetitive seizures. *Epilepsy Curr.* **14**, 147–149 (2014).

55. Connolly, A. M., Beavis, E., Mugica-Cox, B., Bye, A. M. & Lawson, J. A. Exploring carer perceptions of training in out-of-hospital use of buccal midazolam for emergency management of seizures (2008-2012): Buccal midazolam. *J. Paediatr. Child Health* **51**, 704–707 (2015).

56. Wolfe, T. R. & Macfarlane, T. C. Intranasal midazolam therapy for pediatric status epilepticus. *Am. J. Emerg. Med.* **24**, 343–346 (2006).

57. O'Regan, M. E., Brown, J. K. & Clarke, M. Nasal rather than rectal benzodiazepines in the management of acute childhood seizures? *Dev. Med. Child Neurol.* **38**, 1037–1045 (1996).

58. Jeannet, P.-Y. *et al.* Home and hospital treatment of acute seizures in children with nasal midazolam. *Eur. J. Paediatr. Neurol.* **3**, 73–77 (1999).

59. Kutlu, N. O., Yakinci, C., Dogrul, M. & Durmaz, Y. Intranasal midazolam for prolonged convulsive seizures. *Brain Dev.* **22**, 359–361 (2000).

60. Fişgin, T. *et al.* Nasal Midazolam Effects on Childhood Acute Seizures. *J. Child Neurol.* **15**, 833–835 (2000).

61. Harbord, M. G., Kyrkou, N. E., Kyrkou, M. R., Kay, D. & Coulthard, K. P. Use of intranasal midazolam to treat acute seizures in paediatric community settings. *J. Paediatr. Child Health* **40**, 556–558 (2004).

62. Wilson, M. T., Macleod, S. & O'Regan, M. E. Nasal/buccal midazolam use in the community. *Arch. Dis. Child.* **89**, 50–51 (2004).

63. Kanto, J. H. Midazolam: the first water-soluble benzodiazepine. Pharmacology, pharmacokinetics and efficacy in insomnia and anesthesia. *Pharmacotherapy* **5**, 138–155 (1985).

64. Pacifici, G. M. Clinical pharmacology of midazolam in neonates and children: effect of disease-a review. *Int. J. Pediatr.* **2014**, 309342 (2014).

65. Streisand, J. B. & Stanley, T. H. Newer drug delivery systems. *Curr. Anaesth. Crit. Care* **6**, 113–120 (1995).

66. Bhattacharyya, M., Kalra, V. & Gulati, S. Intranasal Midazolam vs Rectal Diazepam in Acute Childhood Seizures. *Pediatr. Neurol.* **34**, 355–359 (2006).

67. De Haan, G.-J., Van Der Geest, P., Doelman, G., Bertram, E. & Edelbroek, P. A comparison of midazolam nasal spray and diazepam rectal solution for the residential treatment of seizure exacerbations. *Epilepsia* **51**, 478–482 (2010).

68. Fişgin, T. *et al.* Effects of intranasal midazolam and rectal diazepam on acute convulsions in children: prospective randomized study. *J. Child Neurol.* **17**, 123–126 (2002).

69. Holsti, M. *et al.* Intranasal midazolam vs rectal diazepam for the home treatment of acute seizures in pediatric patients with epilepsy. *Arch. Pediatr. Adolesc. Med.* **164**, 747–753 (2010).

70. Lahat, E., Goldman, M., Barr, J., Bistritzer, T. & Berkovitch, M. Comparison of intranasal midazolam with intravenous diazepam for treating febrile seizures in children: prospective randomised study. *BMJ* **321**, 83–86 (2000).

71. Mahmoudian, T. & Mohammadi Zadeh, M. Comparison of intranasal midazolam with intravenous diazepam for treating acute seizures in children. *Epilepsy Behav.* **5**, 253–255 (2004).

72. Mittal, P., Manohar, R. & Rawat, A. K. Comparative study of intranasal midazolam and intravenous diazepam sedation for procedures and seizures. *Indian J. Pediatr.* **73**, 975–978 (2006).

73. Thakker, A. & Shanbag, P. A randomized controlled trial of intranasal-midazolam versus intravenous-diazepam for acute childhood seizures. *J. Neurol.* **260**, 470–474 (2013).

74. Sperling, M. R. *et al.* Dosing feasibility and tolerability of intranasal diazepam in adults with epilepsy. *Epilepsia* **55**, 1544–1550 (2014).

75. Ivaturi, V. *et al.* Bioavailability of Intranasal vs. Rectal Diazepam. *Epilepsy Res.* **103**, 254–261 (2013).

76. Wermeling, D. P. H., Miller, J. L., Archer, S. M., Manaligod, J. M. & Rudy, A. C. Bioavailability and pharmacokinetics of lorazepam after intranasal, intravenous, and intramuscular administration. *J. Clin. Pharmacol.* **41**, 1225–1231 (2001).

77. Anderson, M. *et al.* Pharmacokinetics of buccal and intranasal lorazepam in healthy adult volunteers. *Eur. J. Clin. Pharmacol.* **68**, 155–159 (2012).

78. Arya, R., Gulati, S., Kabra, M., Sahu, J. K. & Kalra, V. Intranasal versus intravenous lorazepam for control of acute seizures in children: A randomized open-label study. *Epilepsia* **52**, 788–793 (2011).

79. Harkema, J. R., Carey, S. A. & Wagner, J. G. The Nose Revisited: A Brief Review of the Comparative Structure, Function, and Toxicologic Pathology of the Nasal Epithelium. *Toxicol. Pathol.* **34**, 252–269 (2006).

80. Mistry, A., Stolnik, S. & Illum, L. Nanoparticles for direct nose-to-brain delivery of drugs. *Int. J. Pharm.* **379**, 146–157 (2009).

81. Illum, L. Transport of drugs from the nasal cavity to the central nervous system. *Eur. J. Pharm. Sci.* **11**, 1–18 (2000).

82. Dhuria, S. V., Hanson, L. R. & Frey, W. H. Intranasal delivery to the central nervous system: Mechanisms and experimental considerations. *J. Pharm. Sci.* **99**, 1654–1673 (2010).

83. Uraih, L. C. & Maronpot, R. R. Normal histology of the nasal cavity and application of special techniques. *Environ. Health Perspect.* **85**, 187–208 (1990).

84. Illum, L. Is nose-to-brain transport of drugs in man a reality? *J. Pharm. Pharmacol.* **56**, 3–17 (2004).

85. Thorne, R. G., Pronk, G. J., Padmanabhan, V. & Frey II, W. H. Delivery of insulin-like growth factor-I to the rat brain and spinal cord along olfactory and trigeminal pathways following intranasal administration. *Neuroscience* **127**, 481–496 (2004).

86. Lochhead, J. J., Wolak, D. J., Pizzo, M. E. & Thorne, R. G. Rapid transport within cerebral perivascular spaces underlies widespread tracer distribution in the brain after intranasal administration. *J. Cereb. Blood Flow Metab.* (2014).

87. van Riel, D., Verdijk, R. & Kuiken, T. The olfactory nerve: a shortcut for influenza and other viral diseases into the central nervous system. *J. Pathol.* **235**, 277–287 (2015).

88. Yang, Z., Huang, Y., Gan, G. & Sawchuk, R. J. Microdialysis evaluation of the brain distribution of stavudine following intranasal and intravenous administration to rats. *J. Pharm. Sci.* **94**, 1577–1588 (2005).

89. Luzzati, V., Benoit, E., Charpentier, G. & Vachette, P. X-ray scattering study of pike olfactory nerve: elastic, thermodynamic and physiological properties of the axonal membrane. *J. Mol. Biol.* **343**, 199–212 (2004).

90. Hadaczek, P. *et al.* The 'Perivascular Pump' Driven by Arterial Pulsation is a Powerful Mechanism for the Distribution of Therapeutic Molecules within the Brain. *Mol. Ther. J. Am. Soc. Gene Ther.* **14**, 69–78 (2006).

91. Kozlovskaya, L., Abou-Kaoud, M. & Stepensky, D. Quantitative analysis of drug delivery to the brain via nasal route. *J. Controlled Release* **189**, 133–140 (2014).

92. Illum, L. Nasal Delivery. The Use of Animal Models to Predict Performance in Man. *J. Drug Target.* **3**, 427–442 (1996).

93. McGann, J. P. Poor human olfaction is a 19th-century myth. *Science* **356**, eaam7263 (2017).

94. Djupesland, P. G., Mahmoud, R. A. & Messina, J. C. Accessing the brain: the nose may know the way. *J. Cereb. Blood Flow Metab.* **33**, 793–794 (2013).

95. Löscher, W. Fit for purpose application of currently existing animal models in the discovery of novel epilepsy therapies. *Epilepsy Res.* **126**, 157–184 (2016).

96. Putnam, T. J. & Merritt, H. H. EXPERIMENTAL DETERMINATION OF THE ANTICONVULSANT PROPERTIES OF SOME PHENYL DERIVATIVES. *Science* **85**, 525–526 (1937).

97. Peterson, S. L. & Albertson, T. E. *Neuropharmacology Methods in Epilepsy Research*. (CRC Press, 1998).

98. Browning, R. A. & Nelson, D. K. Variation in threshold and pattern of electroshock-induced seizures in rats depending on site of stimulation. *Life Sci.* **37**, 2205–2211 (1985).

99. Löscher, W., Fassbender, C. P. & Nolting, B. The role of technical, biological and pharmacological factors in the laboratory evaluation of anticonvulsant drugs. II. Maximal electroshock seizure models. *Epilepsy Res.* **8**, 79–94 (1991).

100. Kimball, A. W., Burnett, W. T., Jr. & Doherty, D. G. Chemical Protection against Ionizing Radiation: I. Sampling Methods for Screening Compounds in Radiation Protection Studies with Mice. *Radiat. Res.* **7**, 1–12 (1957).

101. Bankstahl, M., Bankstahl, J. P., Bloms-Funke, P. & Löscher, W. Striking differences in proconvulsant-induced alterations of seizure threshold in two rat models. *NeuroToxicology* **33**, 127–137 (2012).

102. Browning, R. A. & Nelson, D. K. Modification of electroshock and pentylenetetrazol seizure patterns in rats affer precollicular transections. *Exp. Neurol.* **93**, 546–556 (1986).

103. Poletaeva, I. I., Fedotova, I. B., Sourina, N. M. & Kostina, Z. A. Audiogenic Seizures - Biological Phenomenon and Experimental Model of Human Epilepsies. (2011) doi:10.5772/17229.

104. Piredda, S. G., Woodhead, J. H. & Swinyard, E. A. Effect of stimulus intensity on the profile of anticonvulsant activity of phenytoin, ethosuximide and valproate. *J. Pharmacol. Exp. Ther.* **232**, 741–745 (1985).

105. Löscher, W., Hönack, D., Fassbender, C. P. & Nolting, B. The role of technical, biological and pharmacological factors in the laboratory evaluation of anticonvulsant drugs. III. Pentylenetetrazole seizure models. *Epilepsy Res.* **8**, 171–189 (1991).

106. Brown, W. C., Schiffman, D. O., Swinyard, E. A. & Goodman, L. S. Comparative assay of an antiepileptic drugs by psychomotor seizure test and minimal electroshock threshold test. *J. Pharmacol. Exp. Ther.* **107**, 273–283 (1953).

107. Barton, M. E., Klein, B. D., Wolf, H. H. & Steve White, H. Pharmacological characterization of the 6 Hz psychomotor seizure model of partial epilepsy. *Epilepsy Res.* **47**, 217–227 (2001).

108. Barton, M. E., Peters, S. C. & Shannon, H. E. Comparison of the effect of glutamate receptor modulators in the 6 Hz and maximal electroshock seizure models. *Epilepsy Res.* **56**, 17–26 (2003).

109. Potschka, H. Animal models of drug-resistant epilepsy. *Epileptic. Disord.* **14**, 226–234 (2013).

110. American Epilepsy Society Proceedings. *Epilepsia* **37**, 1–214 (1996).

111. Löscher, W. & Hönack, D. Profile of ucb L059, a novel anticonvulsant drug, in models of partial and generalized epilepsy in mice and rats. *Eur. J. Pharmacol.* **232**, 147–158 (1993).

112. Klitgaard, H., Matagne, A., Gobert, J. & Wülfert, E. Evidence for a unique profile of levetiracetam in rodent models of seizures and epilepsy. *Eur. J. Pharmacol.* **353**, 191–206 (1998).

113. Metcalf, C. S. *et al.* Development and pharmacologic characterization of the rat 6 Hz model of partial seizures. *Epilepsia* (2017) doi:10.1111/epi.13764.

114. Purpura, D. P. *Experimental Models of Epilepsy--a Manual for the Laboratory Worker*. (Raven Press, 1972).

115. Löscher, W., Hönack, D. & Rundfeldt, C. Antiepileptogenic Effects of the Novel Anticonvulsant Levetiracetam (ucb L059) in the Kindling Model of Temporal Lobe Epilepsy. *J. Pharmacol. Exp. Ther.* **284**, 474–479 (1998).

116. Peterchev, A. V., Rosa, M. A., Deng, Z.-D., Prudic, J. & Lisanby, S. H. Electroconvulsive Therapy Stimulus Parameters: Rethinking Dosage. *J. ECT* **26**, 159–174 (2010).

117. Leclercq, K. & Kaminski, R. M. Genetic background of mice strongly influences treatment resistance in the 6 Hz seizure model. *Epilepsia* **56**, 310–318 (2015).

118. Löscher, W., Klitgaard, H., Twyman, R. E. & Schmidt, D. New avenues for anti-epileptic drug discovery and development. *Nat. Rev. Drug Discov.* **12**, 757–776 (2013).

119. Töllner, K., Wolf, S., Löscher, W. & Gernert, M. The Anticonvulsant Response to Valproate in Kindled Rats Is Correlated with Its Effect on Neuronal Firing in the Substantia Nigra Pars Reticulata: A New Mechanism of Pharmacoresistance. *J. Neurosci.* **31**, 16423–16434 (2011).

120. Racine, R. J. MODIFICATION OF SEIZURE ACTIVITY BY ELECTRICAL STIMULATION: II. MOTOR SEIZURE. *Electroenceph Clin Neurophysiol* 281–294 (1972).

121. Sato, M., Racine, R. J. & McIntyre, D. C. Kindling: basic mechanisms and clinical validity. *Electroencephalogr. Clin. Neurophysiol.* **76**, 459–472 (1990).

122. Ebert, U. & Löscher, W. Characterization of phenytoin-resistant kindled rats, a new model of drug-resistant partial epilepsy: influence of genetic factors. *Epilepsy Res.* **33**, 217–226 (1999).

123. Srivastava, A. K. & White, H. S. Carbamazepine, But Not Valproate, Displays Pharmacoresistance In Lamotrigine-Resistant Amygdala Kindled Rats. *Epilepsy Res.* **104**, 26–34 (2013).

124. Potschka, H., Volk, H. A. & Löscher, W. Pharmacoresistance and expression of multidrug transporter P-glycoprotein in kindled rats: *NeuroReport* **15**, 1657–1661 (2004).

125. *Mechanisms of Epileptogenesis - The Transition to Seizure | Marc Dichter | Springer*.

126. Araki, Y. & UEKI, S. Changes in sensitivity to convulsion in mice with olfactory bulb ablation. *Jpn. J. Pharmacol.* **22**, 447–456 (1972).

127. Alam, T. *et al.* Optimization of nanostructured lipid carriers of lamotrigine for brain delivery: in vitro characterization and in vivo efficacy in epilepsy. *Expert Opin. Drug Deliv.* **12**, 181–194 (2015).

128. Acharya, S. P., Pundarikakshudu, K., Upadhyay, P., Shelat, P. & Lalwani, A. Development of phenytoin intranasal microemulsion for treatment of epilepsy. *J. Pharm. Investig.* **45**, 375–384 (2015).

129. Acharya, S. P., Pundarikakshudu, K., Panchal, A. & Lalwani, A. Preparation and evaluation of transnasal microemulsion of carbamazepine. *Asian J. Pharm. Sci.* **8**, 64–70 (2013).

130. Löscher, W. Valproate: a reappraisal of its pharmacodynamic properties and mechanisms of action. *Prog. Neurobiol.* **58**, 31–59 (1999).

131. Houghton, G. W., Richens, A., Toseland, P. A., Davidson, S. & Falconer, M. A. Brain concentrations of phenytoin, phenobarbitone and primidone in epileptic patients. *Eur. J. Clin. Pharmacol.* **9**, 73–78 (1975).

132. Kwan, P. & Brodie, M. J. Potential Role of Drug Transporters in the Pathogenesis of Medically Intractable Epilepsy. *Epilepsia* **46**, 224–235 (2005).

133. Löscher, W. & Potschka, H. Drug resistance in brain diseases and the role of drug efflux transporters. *Nat. Rev. Neurosci.* **6**, 591–602 (2005).

134. Löscher, W., Nolting, B. & Fassbender, C. P. The role of technical, biological and pharmacological factors in the laboratory evaluation of anticonvulsant drugs. I. The influence of administration vehicles. *Epilepsy Res.* **7**, 173–181 (1990).

135. Ong, W.-Y., Shalini, S.-M. & Costantino, L. Nose-to-brain drug delivery by nanoparticles in the treatment of neurological disorders. *Curr. Med. Chem.* **21**, 4247–4256 (2014).

136. Ugwoke, M. I., Agu, R. U., Verbeke, N. & Kinget, R. Nasal mucoadhesive drug delivery: Background, applications, trends and future perspectives. *Adv. Drug Deliv. Rev.* **57**, 1640–1665 (2005).

137. Barakat, N. S., Omar, S. A. & Ahmed, A. a. E. Carbamazepine uptake into rat brain following intra-olfactory transport. *J. Pharm. Pharmacol.* **58**, 63–72 (2006).

138. Czapp, M., Bankstahl, J. P., Zibell, G. & Potschka, H. Brain penetration and anticonvulsant efficacy of intranasal phenobarbital in rats. *Epilepsia* **49**, 1142–1150 (2008).

139. Samia, O., Hanan, R. & Kamal, E. T. Carbamazepine mucoadhesive nanoemulgel (MNEG) as brain targeting delivery system via the olfactory mucosa. *Drug Deliv.* **19**, 58–67 (2012).

140. Serralheiro, A., Alves, G., Fortuna, A. & Falcão, A. Intranasal administration of carbamazepine to mice: A direct delivery pathway for brain targeting. *Eur. J. Pharm. Sci.* **60**, 32–39 (2014).

141. Serralheiro, A., Alves, G., Fortuna, A. & Falcão, A. Direct nose-to-brain delivery of lamotrigine following intranasal administration to mice. *Int. J. Pharm.* **490**, 39–46 (2015).

142. Patel, R. B., Patel, M. R., Bhatt, K. K. & Patel, B. G. Formulation consideration and characterization of microemulsion drug delivery system for transnasal administration of carbamazepine. *Bull. Fac. Pharm. Cairo Univ.* **51**, 243–253 (2013).

143. Patel, R. B., Patel, M. R., Bhatt, K. K., Patel, B. G. & Gaikwad, R. V. Microemulsion-based drug delivery system for transnasal delivery of Carbamazepine: preliminary brain-targeting study. *Drug Deliv.* **23**, 207–213 (2016).

144. Sharma, D. *et al.* Nose-To-Brain Delivery of PLGA-Diazepam Nanoparticles. *AAPS PharmSciTech* **16**, 1108–1121 (2015).

145. Eskandari, S., Varshosaz, J., Minaiyan, M. & Tabbakhian, M. Brain delivery of valproic acid via intranasal administration of nanostructured lipid carriers: in vivo pharmacodynamic studies using rat electroshock model. *Int. J. Nanomedicine* **6**, 363–371 (2011).

146. Taksande, J. B. Formulation and Pharmacodynamic Investigations of Lamotrigine Microspheres in Pentylenetetrazole-Induced Seizures in Mice. *Asian J. Pharm. AJP Free Full Text Artic. Asian J Pharm* **11**, (2017).

147. Mayor, S. H. & Illum, L. Investigation of the effect of anaesthesia on nasal absorption of insulin in rats. *Int. J. Pharm.* **149**, 123–129 (1997).

148. Illum, L. Nanoparticulate systems for nasal delivery of drugs: A real improvement over simple systems? *J. Pharm. Sci.* **96**, 473–483 (2007).

149. Renne, R. *et al.* Proliferative and Nonproliferative Lesions of the Rat and Mouse Respiratory Tract. *Toxicol. Pathol.* **37**, 5S–73S (2009).

150. Young, J. T. Histopathologic examination of the rat nasal cavity. *Fundam. Appl. Toxicol.* **1**, 309–312 (1981).

151. Löscher, W. The pharmacokinetics of antiepileptic drugs in rats: consequences for maintaining effective drug levels during prolonged drug administration in rat models of epilepsy. *Epilepsia* **48**, 1245–1258 (2007).

152. Kudriakova, T. B., Sirota, L. A., Rozova, G. I. & Gorkov, V. A. Autoinduction and steady-state pharmacokinetics of carbamazepine and its major metabolites. *Br. J. Clin. Pharmacol.* **33**, 611–615 (1992).

153. Greenspan, P. & Fowler, S. D. Spectrofluorometric studies of the lipid probe, nile red. *J. Lipid Res.* **26**, 781–789 (1985).

154. Manocha, A., Sharma, K. K. & Mediratta, P. K. Possible mechanism of anticonvulsant effect of ketamine in mice. *Indian J. Exp. Biol.* **39**, 1002–1008 (2001).

155. Synowiec, A. S. *et al.* Ketamine use in the treatment of refractory status epilepticus. *Epilepsy Res.* **105**, 183–188 (2013).

156. Borgeat, A. Propofol: pro- or anticonvulsant? *Eur. J. Anaesthesiol. Suppl.* **15**, 17–20 (1997).

157. Borowicz, K. K., Ł, J. & Czuczwar, S. J. Interactions between non-barbiturate injectable anesthetics and conventional antiepileptic drugs in the maximal electroshock test in mice—an isobolographic analysis. *Eur. Neuropsychopharmacol.* **14**, 163–172 (2004).

158. O'Connell, B. K., Gloss, D. & Devinsk, O. Cannabinoids in treatment-resistant epilepsy: A review. *Epilepsy Behav.* doi:10.1016/j.yebeh.2016.11.012.

159. Nasal delivery of cannabinoids to be developed in new agreement. *School of Pharmacy* https://pharmacy.uq.edu.au/article/2017/04/nasal-delivery-cannabinoids-be-developed-new-agreement (1493186400).

160. KAUFMAN, R. C. Lipid nanoparticle compositions and methods as carriers of cannabinoids in standardized precision-metered dosage forms. (2016).

161. Shende, A. J., Patil, R. R. & Devarajan, P. V. Microemulsion of lamotrigine for nasal delivery. *Indian J. Pharm. Sci.* **69**, 721 (2016).

162. Dave, K. & Purohit, S. Formulation and in vitro characterization of intranasal mucoadhesive microspheres of Lamotrigine using chitosan by gluteraldehyde cross linking. *Int J Pharm Bio Sci* **4**, 402–415 (2013).

163. Kawtikwar, P. S., Kulkarni, N. P., Yadav, S. & Sakarkar, D. M. Formulation and evaluation of an anti-epileptic drug-loaded microemulsion for nose to brain delivery. *Asian J. Pharm. AJP Free Full Text Artic. Asian J Pharm* **3**, (2014).

164. Chaudhari, S. Development of Valproic Acid Niosomal in situ Nasal Gel Formulation for Epilepsy. *Indian J. Pharm. Educ. Res.* **47**, 31–41 (2013).

165. Mandal, S. & Mandal, S. D. Design and development of carbamazepine mucoadhesive microemulsion for intranasal delivery: an ex-vivo study. *Int J Pharma Sci Rev Res* **3**, 56–60 (2010).

166. Desai, S., Vidyasagar, G., Shah, V. & Desai, D. Preparation and in vitro characterisation of mucoadhesive microspheres of midazolam: nose to brain administration. *Asian J Pharm Clin Res* **4**, 100–2 (2011).

167. Markowitz, G. J., Kadam, S. D., Boothe, D. M., Irving, N. D. & Comi, A. M. The pharmacokinetics of commonly used antiepileptic drugs in immature CD1 mice. *Neuroreport* **21**, 452–456 (2010).

168. Löscher, W. & Hönack, D. Intravenous Carbamazepine: Comparison of Different Parenteral Formulations in a Mouse Model of Convulsive Status Epilepticus. *Epilepsia* **38**, 106–113 (1997).

169. Miller, A. A., Wheatley, P., Sawyer, D. A., Baxter, M. G. & Roth, B. Pharmacological Studies on Lamotrigine, A Novel Potential Antiepileptic Drug. *Epilepsia* **27**, 483–489 (1986).

170. Löscher, W., Cramer, S. & Ebert, U. Limbic epileptogenesis alters the anticonvulsant efficacy of phenytoin in Sprague-Dawley rats. *Epilepsy Res.* **31**, 175–186 (1998).

171. Bialer, M. & White, H. S. Key factors in the discovery and development of new antiepileptic drugs. *Nat. Rev. Drug Discov.* **9**, 68–82 (2010).

172. Krupp, E. & Löscher, W. Anticonvulsant Drug Effects in the Direct Cortical Ramp-Stimulation Model in Rats: Comparison with Conventional Seizure Models. *J. Pharmacol. Exp. Ther.* **285**, 1137–1149 (1998).

173. Leppik, I. E. & Sherwin, A. L. Intravenous phenytoin and phenobarbital: anticonvulsant action, brain content, and plasma binding in rat. *Epilepsia* **20**, 201–207 (1979).

174. Löscher, W. & Rundfeldt, C. Kindling as a model of drug-resistant partial epilepsy: selection of phenytoin-resistant and nonresistant rats. *J. Pharmacol. Exp. Ther.* **258**, 483–489 (1991).

175. Ogiso, T., Iwaki, M., Tanino, T., Muraoka, O. & Tanabe, G. Pharmacokinetic analysis of phenytoin and its derivatives in plasma and brain in rats. *Biol. Pharm. Bull.* **16**, 1025–1030 (1993).

176. WANG, X. & PATSALOS, P. N. A comparison of central brain (cerebrospinal and extracellular fluids) and peripheral blood kinetics of phenytoin after intravenous phenytoin and fosphenytoin. *Seizure* **12**, 330–336 (2003).

177. Gerber, N. *et al.* Study of Dose-Dependent Metabolism of 5,5-Diphenylhydantion in the Rat Using New Methodology for Isolation and Quantitation of Metabolites in Vivo and in Vitro. *J. Pharmacol. Exp. Ther.* **178**, 567–579 (1971).

178. Hunter, J. C. *et al.* The effect of novel anti-epileptic drugs in rat experimental models of acute and chronic pain. *Eur. J. Pharmacol.* **324**, 153–160 (1997).

179. Castel-Branco, M. M., Falcão, A. C., Figueiredo, I. V. & Caramona, M. M. Lamotrigine pharmacokinetic/pharmacodynamic modelling in rats. *Fundam. Clin. Pharmacol.* **19**, 669–675 (2005).

180. Prescott, R. J. The Comparison of Success Rates in Cross-Over Trials in the Presence of an Order Effect. *J. R. Stat. Soc. Ser. C Appl. Stat.* **30**, 9–15 (1981).

181. Garg, U., Peat, J., Frazee, C., Nguyen, T. & Ferguson, A. M. A simple isotope dilution electrospray ionization tandem mass spectrometry method for the determination of free phenytoin. *Ther. Drug Monit.* **35**, 831–835 (2013).

182. Velíšek, L. MODELS | Models of Generalized Seizures in Freely Moving Animals. in *Encyclopedia of Basic Epilepsy Research* (ed. Schwartzkroin, P. A.) 775–780 (Academic Press, 2009). doi:10.1016/B978-012373961-2.00358-1.

183. Maguire, J. & Salpekar, J. A. Stress, Seizures, and Hypothalamic-Pituitary-Adrenal Axis Targets for the Treatment of Epilepsy. *Epilepsy Behav. EB* **26**, (2013).

184. Veronesi, M. C., Kubek, D. J. & Kubek, M. J. Isoflurane exacerbates electrically evoked seizures in amygdala-kindled rats during recovery. *Epilepsy Res.* **82**, 15–20 (2008).

185. Eger, E. I. I. & Johnson, B. H. M. Rates of Awakening from Anesthesia with I-653, Halothane, Isoflurane, and Sevoflurane: A Test of the Effect of Anesthetic Concentration and Duration in Rats. *Anesth. Analg.* **66**, 977–982 (1987).

186. Walton, N. Y., Uthman, B. M., Yafi, K. E., Kim, J. M. & Treiman, D. M. Phenytoin Penetration into Brain After Administration of Phenytoin or Fosphenytoin. *Epilepsia* **40**, 153–156 (1999).

187. Kim, Y. G. *et al.* Effects of cysteine on the pharmacokinetics of intravenous phenytoin in rats with protein-calorie malnutrition. *Int. J. Pharm.* **229**, 45–55 (2001).

188. Kim, Y. C., Kang, H. E. & Lee, M. G. Pharmacokinetics of phenytoin and its metabolite, 4′-HPPH, after intravenous and oral administration of phenytoin to diabetic rats induced by alloxan or streptozotocin. *Biopharm. Drug Dispos.* **29**, 51–61 (2008).

189. DeVane, C. L., Simpkins, J. W. & Stout, S. A. Distribution of Phenobarbital and Phenytoin in Pregnant Rats and Their Fetuses. *Epilepsia* **32**, 250–256 (1991).

190. Chou, R. C. & Levy, G. Effect of pregnancy on the pharmacokinetics of phenytoin in rats. *J. Pharmacol. Exp. Ther.* **229**, 351–358 (1984).

191. Brodie, M. J. Antiepileptic drug therapy the story so far. *Seizure* **19**, 650–655 (2010).

192. Kutt, H. & Harden, C. L. Phenytoin and Congeners. in *Antiepileptic Drugs: Pharmacology and Therapeutics* (eds. Eadie, M. J. & Vajda, F. J. E.) 229–265 (Springer Berlin Heidelberg, 1999). doi:10.1007/978-3-642-60072-2_9.

193. Yaari, Y., Selzer, M. E. & Pincus, J. H. Phenytoin: Mechanisms of its anticonvulsant action. *Ann. Neurol.* **20**, 171–184 (1986).

194. Nevitt, S. J., Sudell, M., Weston, J., Tudur Smith, C. & Marson, A. G. Antiepileptic drug monotherapy for epilepsy: a network meta-analysis of individual participant data. *Cochrane Database Syst. Rev.* **6**, CD011412 (2017).

195. Brigo, F. Phenytoin is dead, long live phenytoin? *Epilepsy Behav.* **24**, 152 (2012).

196. Nevitt, S. J., Marson, A. G. & Smith, C. T. Carbamazepine versus phenytoin monotherapy for epilepsy: an individual participant data review. *Cochrane Database Syst. Rev.* (2019) doi:10.1002/14651858.CD001911.pub4.

197. Nevitt, S. J., Marson, A. G., Weston, J. & Smith, C. T. Sodium valproate versus phenytoin monotherapy for epilepsy: an individual participant data review. *Cochrane Database Syst. Rev.* (2018) doi:10.1002/14651858.CD001769.pub4.

198. Browne, T. & LeDuc, B. Phenytoin and other hydantoins. Chemistry and biotransformation. in *Antiepileptic drugs* (eds. Levy, R., Mattson, R., Meldrum, B. & Perucca, E.) (Lippincott Williams & Wilkins).

199. Richens, A. & Dunlop, A. Serum-phenytoin levels in management of epilepsy. *Lancet Lond. Engl.* **2**, 247–248 (1975).

200. Potschka, H. & Löscher, W. In Vivo Evidence for P-Glycoprotein–Mediated Transport of Phenytoin at the Blood–Brain Barrier of Rats. *Epilepsia* **42**, 1231–1240 (2001).

201. Löscher, W. & Potschka, H. Role of Multidrug Transporters in Pharmacoresistance to Antiepileptic Drugs. *J. Pharmacol. Exp. Ther.* **301**, 7–14 (2002).

202. Sisodiya, S. M. Mechanisms of antiepileptic drug resistance. *Curr. Opin. Neurol.* **16**, 197–201 (2003).

203. Löscher, W., Rundfeldt, C. & Hönack, D. Pharmacological characterization of phenytoin-resistant amygdala-kindled rats, a new model of drug-resistant partial epilepsy. *Epilepsy Res.* **15**, 207–219 (1993).

204. Yarragudi, S. B. Formulation Strategies to Enhance Nose-to-Brain Delivery of Drugs (Thesis, Doctor of Philosophy). (University of Otago, 2018).

205. Cekić, N. D. *et al.* Preparation and characterisation of phenytoin-loaded alginate and alginate-chitosan microparticles. *Drug Deliv.* **14**, 483–490 (2007).

206. Li, Z. *et al.* Formulation of spray-dried phenytoin loaded poly(epsilon-caprolactone) microcarrier intended for brain delivery to treat epilepsy. *J. Pharm. Sci.* **96**, 1018–1030 (2007).

207. Yarragudi, S. B. *et al.* Formulation of olfactory-targeted microparticles with tamarind seed polysaccharide to improve nose-to-brain transport of drugs. *Carbohydr. Polym.* **163**, 216–226 (2017).

208. Everitt, J. I. & Gross, E. A. Chapter 20 - Euthanasia and Necropsy. in *The Laboratory Rat (Second Edition)* (eds. Suckow, M. A., Weisbroth, S. H. & Franklin, C. L.) 665–678 (Academic Press, 2006). doi:10.1016/B978-012074903-4/50023-6.

209. Fischer, W. Influence of ethanol on the threshold for electroshock-induced seizures and electrically-evoked hippocampal afterdischarges. *J. Neural Transm. Vienna Austria 1996* **112**, 1149–1163 (2005).

210. Clarke, H. B. & Gabrielsen, T. O. Seizure Induced Disruption of Blood-Brain Barrier Demonstrated by CT. *J. Comput. Assist. Tomogr.* **13**, 889–892 (1989).

211. Marchi, N. *et al.* Blood–brain barrier damage and brain penetration of antiepileptic drugs: Role of serum proteins and brain edema. *Epilepsia* **50**, 664–677 (2009).

212. van Vliet, E. A. *et al.* Blood–brain barrier leakage may lead to progression of temporal lobe epilepsy. *Brain* **130**, 521–534 (2007).

213. van Vliet, E. A. *et al.* Region-specific overexpression of P-glycoprotein at the blood-brain barrier affects brain uptake of phenytoin in epileptic rats. *J. Pharmacol. Exp. Ther.* **322**, 141–147 (2007).

214. Rüber, T. *et al.* Evidence for peri-ictal blood-brain barrier dysfunction in patients with epilepsy. *Brain J. Neurol.* **141**, 2952–2965 (2018).

215. Öztas, B., Kaya, M. & Camurcu, S. Age related changes in the effect of electroconvulsive shock on the blood brain barrier permeability in rats. *Mech. Ageing Dev.* **51**, 149–155 (1990).

216. Tiwari, G. & Tiwari, R. Bioanalytical method validation: An updated review. *Pharm. Methods* **1**, 25–38 (2010).

217. Henney III, H. R., Sperling, M. R., Rabinowicz, A. L., Bream, G. & Carrazana, E. J. Assessment of pharmacokinetics and tolerability of intranasal diazepam relative to rectal gel in healthy adults. *Epilepsy Res.* **108**, 1204–1211 (2014).

218. Friden, M., Ljungqvist, H., Middleton, B., Bredberg, U. & Hammarlund-Udenaes, M. Improved measurement of drug exposure in the brain using drug-specific correction for residual blood. *J. Cereb. Blood Flow Metab.* **30**, 150–161 (2010).

219. Amtorp, O. Estimation of capillary permeability of inulin, sucrose and mannitol in rat brain cortex. *Acta Physiol. Scand.* **110**, 337–342 (1980).

220. Bickel, U. How to measure drug transport across the blood-brain barrier. *NeuroRx* **2**, 15–26 (2005).

221. Chou, R. C. & Levy, G. Effect of heparin or salicylate infusion on serum protein binding and on concentrations of phenytoin in serum, brain and cerebrospinal fluid of rats. *J. Pharmacol. Exp. Ther.* **219**, 42–48 (1981).

222. Heydel, J.-M., Faure, P. & Neiers, F. Nasal odorant metabolism: enzymes, activity and function in olfaction. *Drug Metab. Rev.* **51**, 224–245 (2019).

223. Dhamankar, V. S. Cytochrome P450-mediated drug metabolizing activity in the nasal mucosa (Thesis, Doctor of Philosophy). (University of Iowa, 2013).

224. Thorn, C. F., Whirl-Carrillo, M., Leeder, J. S., Klein, T. E. & Altman, R. B. PharmGKB summary: phenytoin pathway. *Pharmacogenet. Genomics* **22**, 466–470 (2012).

225. Antunes Viegas, D. *et al.* Development and application of an ex vivo fosphenytoin nasal bioconversion/permeability evaluation method. *Eur. J. Pharm. Sci.* **89**, 61–72 (2016).

226. Yamazaki, H. *et al.* Decreases in phenytoin hydroxylation activities catalyzed by liver microsomal cytochrome P450 enzymes in phenytoin-treated rats. *Drug Metab. Dispos. Biol. Fate Chem.* **29**, 427–434 (2001).

227. Kinobe, R. T., Parkinson, O. T., Mitchell, D. J. & Gillam, E. M. J. P450 2C18 Catalyzes the Metabolic Bioactivation of Phenytoin. *Chem. Res. Toxicol.* **18**, 1868–1875 (2005).

228. Zanger, U. M. & Schwab, M. Cytochrome P450 enzymes in drug metabolism: Regulation of gene expression, enzyme activities, and impact of genetic variation. *Pharmacol. Ther.* **138**, 103–141 (2013).

229. Rundfeldt, C. & Löscher, W. Anticonvulsant efficacy and adverse effects of phenytoin during chronic treatment in amygdala-kindled rats. *J. Pharmacol. Exp. Ther.* **266**, 216–223 (1993).

230. Perucca, E., Makki, K. & Richens, A. Is phenytoin metabolism dose-dependent by enzyme saturation or by feedback inhibition? *Clin. Pharmacol. Ther.* **24**, 46–51 (1978).

231. Behl, C. R., Pimplaskar, H. K., Sileno, A. P., deMeireles, J. & Romeo, V. D. Effects of physicochemical properties and other factors on systemic nasal drug delivery. *Adv. Drug Deliv. Rev.* **29**, 89–116 (1998).

232. McMartin, C., Hutchinson, L. E. F., Hyde, R. & Peters, G. E. Analysis of Structural Requirements for the Absorption of Drugs and Macromolecules from the Nasal Cavity. *J. Pharm. Sci.* **76**, 535–540 (1987).

233. Ozsoy, Y., Gungor, S. & Cevher, E. Nasal delivery of high molecular weight drugs. *Mol. Basel Switz.* **14**, 3754–3779 (2009).

234. Cullingford, T. The vagus nerve—a common route for epilepsy therapies? *Lancet Neurol.* **3**, 518 (2004).

235. Astarita, G. *et al.* Pharmacological Characterization of Hydrolysis-Resistant Analogs of Oleoylethanolamide with Potent Anorexiant Properties. *J. Pharmacol. Exp. Ther.* **318**, 563–570 (2006).

236. Sun, Y. *et al.* Cannabinoid activation of PPARα; a novel neuroprotective mechanism. *Br. J. Pharmacol.* **152**, 734–743 (2007).

237. Zhou, Y. *et al.* Orally administered oleoylethanolamide protects mice from focal cerebral ischemic injury by activating peroxisome proliferator-activated receptor α. *Neuropharmacology* **63**, 242–249 (2012).

238. Gonzalez-Aparicio, R. *et al.* The systemic administration of oleoylethanolamide exerts neuroprotection of the nigrostriatal system in experimental Parkinsonism. *Int. J. Neuropsychopharmacol.* **17**, 455–468 (2014).

239. Lambert, D. M., Vandevoorde, S., Diependaele, G., Govaerts, S. J. & Robert, A. R. Anticonvulsant Activity of N-Palmitoylethanolamide, a Putative Endocannabinoid, in Mice. *Epilepsia* **42**, 321–327 (2001).

240. Sheerin, A. H., Zhang, X., Saucier, D. M. & Corcoran, M. E. Selective Antiepileptic Effects of N-Palmitoylethanolamide, a Putative Endocannabinoid. *Epilepsia* **45**, 1184–1188 (2004).

241. Wallace, M. J., Martin, B. R. & DeLorenzo, R. J. Evidence for a physiological role of endocannabinoids in the modulation of seizure threshold and severity. *Eur. J. Pharmacol.* **452**, 295–301 (2002).

242. Pistis, M. & Melis, M. From surface to nuclear receptors: the endocannabinoid family extends its assets. *Curr. Med. Chem.* **17**, 1450–1467 (2010).

243. Battista, N., Di Tommaso, M., Bari, M. & Maccarrone, M. The endocannabinoid system: an overview. *Front. Behav. Neurosci.* **6**, (2012).

244. Ueda, N., Puffenbarger, R. A., Yamamoto, S. & Deutsch, D. G. The fatty acid amide hydrolase (FAAH). *Chem. Phys. Lipids* **108**, 107–121 (2000).

245. Hansen, H. S. Palmitoylethanolamide and other anandamide congeners. Proposed role in the diseased brain. *Exp. Neurol.* **224**, 48–55 (2010).

246. Porta, N. *et al.* Fenofibrate, a peroxisome proliferator–activated receptor-α agonist, exerts anticonvulsive properties. *Epilepsia* **50**, 943–948 (2009).

247. Payandemehr, B. *et al.* Involvement of PPAR receptors in the anticonvulsant effects of a cannabinoid agonist, WIN 55,212-2. *Prog. Neuropsychopharmacol. Biol. Psychiatry* **57**, 140–145 (2015).

248. Puligheddu, M. *et al.* PPAR-Alpha Agonists as Novel Antiepileptic Drugs: Preclinical Findings. *PLoS ONE* **8**, e64541 (2013).

249. Cullingford, T. E. The ketogenic diet; fatty acids, fatty acid-activated receptors and neurological disorders. *Prostaglandins Leukot. Essent. Fatty Acids* **70**, 253–264 (2004).

250. Cullingford, T. E., Dolphin, C. T. & Sato, H. The peroxisome proliferator-activated receptor α-selective activator ciprofibrate upregulates expression of genes encoding fatty acid oxidation and ketogenesis enzymes in rat brain. *Neuropharmacology* **42**, 724–730 (2002).

251. Tamura, K., Ono, A., Miyagishima, T., Nagao, T. & Urushidani, T. Profiling of Gene Expression in Rat Liver and Rat Primary Cultured Hepatocytes Treated with Peroxisome Proliferators. *J. Toxicol. Sci.* **31**, 471–490 (2006).

252. Punapart, M. *et al.* Effect of Chronic Valproic Acid Treatment on Hepatic Gene Expression Profile in Wfs1 Knockout Mouse. *PPAR Research* https://www.hindawi.com/journals/ppar/2014/349525/ (2014) doi:10.1155/2014/349525.

253. Szalowska, E., Burg, B. van der, Man, H.-Y., Hendriksen, P. J. M. & Peijnenburg, A. A. C. M. Model Steatogenic Compounds (Amiodarone, Valproic Acid, and Tetracycline) Alter Lipid Metabolism by Different Mechanisms in Mouse Liver Slices. *PLOS ONE* **9**, e86795 (2014).

254. Bough, K. J. & Rho, J. M. Anticonvulsant Mechanisms of the Ketogenic Diet. *Epilepsia* **48**, 43–58 (2007).

255. Plaza-Zabala, A. *et al.* Effects of the endogenous PPAR-Î± agonist, oleoylethanolamide on MDMA-induced cognitive deficits in mice. *Synapse* **64**, 379–389 (2010).

256. Melis, M. *et al.* Endogenous fatty acid ethanolamides suppress nicotine-induced activation of mesolimbic dopamine neurons through nuclear receptors. *J. Neurosci. Off. J. Soc. Neurosci.* **28**, 13985–13994 (2008).

257. Raggenbass, M. & Bertrand, D. Nicotinic receptors in circuit excitability and epilepsy. *J. Neurobiol.* **53**, 580–589 (2002).

258. Younus, M., Prentice, R. N., Clarkson, A. N., Boyd, B. J. & Rizwan, S. B. Incorporation of an Endogenous Neuromodulatory Lipid, Oleoylethanolamide, into Cubosomes: Nanostructural Characterization. *Langmuir* **32**, 8942–8950 (2016).

259. Spicer, P. T. Dekker Encyclopedia of Nanoscience and Nanotechnology. (2004).

260. Rizwan, S. B. & Boyd, B. J. Cubosomes: Structure, Preparation and Use as an Antigen Delivery System. in *Subunit Vaccine Delivery* (eds. Foged, C., Rades, T., Perrie, Y. & Hook, S.) 125–140 (Springer New York, 2015).

261. Chong, J. Y. T., Mulet, X., Waddington, L. J., Boyd, B. J. & Drummond, C. J. Steric stabilisation of self-assembled cubic lyotropic liquid crystalline nanoparticles: high throughput evaluation of triblock polyethylene oxide-polypropylene oxide-polyethylene oxide copolymers. *Soft Matter* **7**, 4768–4777 (2011).

262. Seddon, J. M. *et al.* Pressure-jump X-ray studies of liquid crystal transitions in lipids. *Philos. Trans. R. Soc. Math. Phys. Eng. Sci.* **364**, 2635–2655 (2006).

263. Sagalowicz, L. *et al.* Crystallography of dispersed liquid crystalline phases studied by cryo-transmission electron microscopy. *J. Microsc.* **221**, 110–121 (2006).

264. Yaghmur, A. & Glatter, O. Characterization and potential applications of nanostructured aqueous dispersions. *Adv. Colloid Interface Sci.* **147**–**148**, 333–342 (2009).

265. Chen, Y., Ma, P. & Gui, S. Cubic and Hexagonal Liquid Crystals as Drug Delivery Systems. *BioMed Res. Int.* **2014**, e815981 (2014).

266. Mat Azmi, I. D. *et al.* Modulatory Effect of Human Plasma on the Internal Nanostructure and Size Characteristics of Liquid-Crystalline Nanocarriers. *Langmuir* **31**, 5042–5049 (2015).

267. Huang, Y. & Gui, S. Factors affecting the structure of lyotropic liquid crystals and the correlation between structure and drug diffusion. *RSC Adv.* **8**, 6978–6987 (2018).

268. Rizwan, S. B., Dong, Y.-D., Boyd, B. J., Rades, T. & Hook, S. Characterisation of bicontinuous cubic liquid crystalline systems of phytantriol and water using cryo field emission scanning electron microscopy (cryo FESEM). *Micron* **38**, 478–485 (2007).

269. Boyd, B. J., Rizwan, S. B., Dong, Y.-D., Hook, S. & Rades, T. Self-Assembled Geometric Liquid-Crystalline Nanoparticles Imaged in Three Dimensions: Hexosomes Are Not Necessarily Flat Hexagonal Prisms. *Langmuir* **23**, 12461–12464 (2007).

270. Bibi, S. *et al.* Microscopy imaging of liposomes: From coverslips to environmental SEM. *Int. J. Pharm.* **417**, 138–150 (2011).

271. Younus, M. Non-Lamellar Liquid Crystalline Nanoparticles for Targeted Delivery of Endogenous Lipids to the Brain (Thesis, Doctor of Philosophy). (University of Otago, 2019).

272. Göppert, T. M. & Müller, R. H. Plasma protein adsorption of Tween 80- and poloxamer 188-stabilized solid lipid nanoparticles. *J. Drug Target.* **11**, 225–231 (2003).

273. Diederichs, J. E. Plasma protein adsorption patterns on liposomes: establishment of analytical procedure. *Electrophoresis* **17**, 607–611 (1996).

274. Caracciolo, G. Liposome–protein corona in a physiological environment: Challenges and opportunities for targeted delivery of nanomedicines. *Nanomedicine Nanotechnol. Biol. Med.* **11**, 543–557 (2015).

275. Sotocinal, S. G. *et al.* The Rat Grimace Scale: A partially automated method for quantifying pain in the laboratory rat via facial expressions. *Mol. Pain* **7**, 55 (2011).

276. Hyde, S. *Identification of Lyotropic Liquid Crystalline Mesophases*. vol. Handbook of Applied Surface and Colloid Chemistry-Chapter 16 (John Wiley & Sons Ltd, 2001).

277. Azhari, H., Strauss, M., Hook, S., Boyd, B. J. & Rizwan, S. B. Stabilising cubosomes with Tween 80 as a step towards targeting lipid nanocarriers to the blood–brain barrier. *Eur. J. Pharm. Biopharm.* **104**, 148–155 (2016).

278. Younus, M., Hawley, A., Boyd, B. J. & Rizwan, S. B. Bulk and dispersed aqueous behaviour of an endogenous lipid, selachyl alcohol: Effect of Tween 80 and Pluronic F127 on nanostructure. *Colloids Surf. B Biointerfaces* **169**, 135–142 (2018).

279. Kreuter, J. *et al.* Direct evidence that polysorbate-80-coated poly(butylcyanoacrylate) nanoparticles deliver drugs to the CNS via specific mechanisms requiring prior binding of drug to the nanoparticles. *Pharm. Res.* **20**, 409–416 (2003).

280. Alyaudtin, R. N. *et al.* Interaction of poly(butylcyanoacrylate) nanoparticles with the blood-brain barrier in vivo and in vitro. *J. Drug Target.* **9**, 209–221 (2001).

281. Azhari, H. Surface modified cubosomes for drug delivery across the blood-brain barrier (Thesis, Doctor of Philosophy). (University of Otago, 2018).

282. Van Haute, D. & Berlin, J. M. Challenges in realizing selectivity for nanoparticle biodistribution and clearance: lessons from gold nanoparticles. *Ther. Deliv.* **8**, 763–774 (2017).

283. Lorenzer, C., Dirin, M., Winkler, A.-M., Baumann, V. & Winkler, J. Going beyond the liver: Progress and challenges of targeted delivery of siRNA therapeutics. *J. Controlled Release* **203**, 1–15 (2015).

284. Smith, B. N. Natural Abundance of the Stable Isotopes of Carbon in Biological Systems. *BioScience* **22**, 226–231 (1972).

285. Giuffrida, A., Rodríguez de Fonseca, F. & Piomelli, D. Quantification of bioactive acylethanolamides in rat plasma by electrospray mass spectrometry. *Anal. Biochem.* **280**, 87–93 (2000).

286. Bystrowska, B., Smaga, I., Tyszka-Czochara, M. & Filip, M. Troubleshooting in LC-MS/MS method for determining endocannabinoid and endocannabinoid-like molecules in rat brain structures applied to assessing the brain endocannabinoid/endovanilloid system significance. *Toxicol. Mech. Methods* **24**, 315–322 (2014).

287. Richardson, D., Ortori, C. A., Chapman, V., Kendall, D. A. & Barrett, D. A. Quantitative profiling of endocannabinoids and related compounds in rat brain using liquid chromatography–tandem electrospray ionization mass spectrometry. *Anal. Biochem.* **360**, 216–226 (2007).

288. Liput, D. J. *et al.* Quantification of anandamide, oleoylethanolamide and palmitoylethanolamide in rodent brain tissue using high performance liquid chromatography–electrospray mass spectroscopy. *J. Pharm. Anal.* **4**, 234–241 (2014).

289. Guard-Friar, D., Chen, C. H. & Engle, A. S. Deuterium isotope effect on the stability of molecules: phospholipids. *J. Phys. Chem.* **89**, 1810–1813 (1985).

290. Yepuri, N. R. *et al.* Deuterated phytantriol – A versatile compound for probing material distribution in liquid crystalline lipid phases using neutron scattering. *J. Colloid Interface Sci.* **534**, 399–407 (2019).

291. Dong, Y.-D. *et al.* Impurities in Commercial Phytantriol Significantly Alter Its Lyotropic Liquid-Crystalline Phase Behavior. *Langmuir* **24**, 6998–7003 (2008).

292. Fong, W.-K. *et al.* Controlling the Nanostructure of Gold Nanorod–Lyotropic Liquid-Crystalline Hybrid Materials Using Near-Infrared Laser Irradiation. *Langmuir* **28**, 14450–14460 (2012).

293. Zhai, J. *et al.* Lipid–PEG Conjugates Sterically Stabilize and Reduce the Toxicity of Phytantriol-Based Lyotropic Liquid Crystalline Nanoparticles. *Langmuir* **31**, 10871–10880 (2015).

294. Nguyen, T.-H., Hanley, T., Porter, C. J. H., Larson, I. & Boyd, B. J. Phytantriol and glyceryl monooleate cubic liquid crystalline phases as sustained-release oral drug delivery systems for poorly water soluble drugs I. Phase behaviour in physiologically-relevant media: Phytantriol and glyceryl monooleate cubic liquid crystalline phases. *J. Pharm. Pharmacol.* **62**, 844–855 (2010).

295. Warren, D. B., Anby, M. U., Hawley, A. & Boyd, B. J. Real Time Evolution of Liquid Crystalline Nanostructure during the Digestion of Formulation Lipids Using Synchrotron Small-Angle X-ray Scattering. *Langmuir* **27**, 9528–9534 (2011).

296. Nguyen, T.-H., Hanley, T., Porter, C. J. H. & Boyd, B. J. Nanostructured reverse hexagonal liquid crystals sustain plasma concentrations for a poorly water-soluble drug after oral administration. *Drug Deliv. Transl. Res.* **1**, 429–438 (2011).

297. Du, J. D., Liu, Q., Salentinig, S., Nguyen, T.-H. & Boyd, B. J. A novel approach to enhance the mucoadhesion of lipid drug nanocarriers for improved drug delivery to the buccal mucosa. *Int. J. Pharm.* **471**, 358–365 (2014).

298. Göppert, T. M. & Müller, R. H. Adsorption kinetics of plasma proteins on solid lipid nanoparticles for drug targeting. *Int. J. Pharm.* **302**, 172–186 (2005).

299. Harnisch, S. & Müller, R. H. Adsorption kinetics of plasma proteins on oil-in-water emulsions for parenteral nutrition. *Eur. J. Pharm. Biopharm.* **49**, 41–46 (2000).

300. Hinton, T. M. *et al.* Bicontinuous cubic phase nanoparticle lipid chemistry affects toxicity in cultured cells. *Toxicol. Res.* **3**, 11–22 (2013).

301. Shen, H.-H. *et al.* The influence of dipalmitoyl phosphatidylserine on phase behaviour of and cellular response to lyotropic liquid crystalline dispersions. *Biomaterials* **31**, 9473–9481 (2010).

302. Murgia, S. *et al.* Nanoparticles from lipid-based liquid crystals: emulsifier influence on morphology and cytotoxicity. *J. Phys. Chem. B* **114**, 3518–3525 (2010).

303. Tan, A., Hong, L., Du, J. D. & Boyd, B. J. Self-Assembled Nanostructured Lipid Systems: Is There a Link between Structure and Cytotoxicity? *Adv. Sci.* **6**, 1801223 (2019).

304. Han, S. *et al.* Novel vehicle based on cubosomes for ophthalmic delivery of flurbiprofen with low irritancy and high bioavailability. *Acta Pharmacol. Sin.* **31**, 990–998 (2010).

305. Ali, Z., Sharma, P. K. & Warsi, M. H. Fabrication and Evaluation of Ketorolac Loaded Cubosome for Ocular Drug Delivery -. *J. Appl. Pharm. Sci.* **6**, 204–208 (2016).

306. Rodrigues, L. *et al.* Cellular uptake of self-assembled phytantriol-based hexosomes is independent of major endocytic machineries. *J. Colloid Interface Sci.* **553**, 820–833 (2019).

307. Shen, H.-H. *et al.* The interaction of cubosomes with supported phospholipid bilayers using neutron reflectometry and QCM-D. *Soft Matter* **7**, 8041 (2011).

308. Erker, T. *et al.* The bumetanide prodrug BUM5, but not bumetanide, potentiates the antiseizure effect of phenobarbital in adult epileptic mice. *Epilepsia* **57**, 698–705 (2016).

309. Jain, S., Bhankur, N., Swarnakar, N. K. & Thanki, K. Phytantriol Based 'Stealth' Lyotropic Liquid Crystalline Nanoparticles for Improved Antitumor Efficacy and Reduced Toxicity of Docetaxel. *Pharm. Res.* **32**, 3282–3292 (2015).

310. Fong, W. K. *et al.* Generation of Geometrically Ordered Lipid-Based Liquid-Crystalline Nanoparticles Using Biologically Relevant Enzymatic Processing. *Langmuir* **30**, 5373–5377 (2014).

311. Wu, H. *et al.* A novel small Odorranalectin-bearing cubosomes: Preparation, brain delivery and pharmacodynamic study on amyloid-β25–35-treated rats following intranasal administration. *Eur. J. Pharm. Biopharm.* **80**, 368–378 (2012).

312. Dong, Y.-D., Larson, I., Hanley, T. & Boyd, B. J. Bulk and dispersed aqueous phase behavior of phytantriol: effect of vitamin E acetate and F127 polymer on liquid crystal nanostructure. *Langmuir ACS J. Surf. Colloids* **22**, 9512–9518 (2006).

Appendix A: Weight progression of rats over the course of all seizure studies in Chapter Three. Days of stimulation are indicated by red arrows.

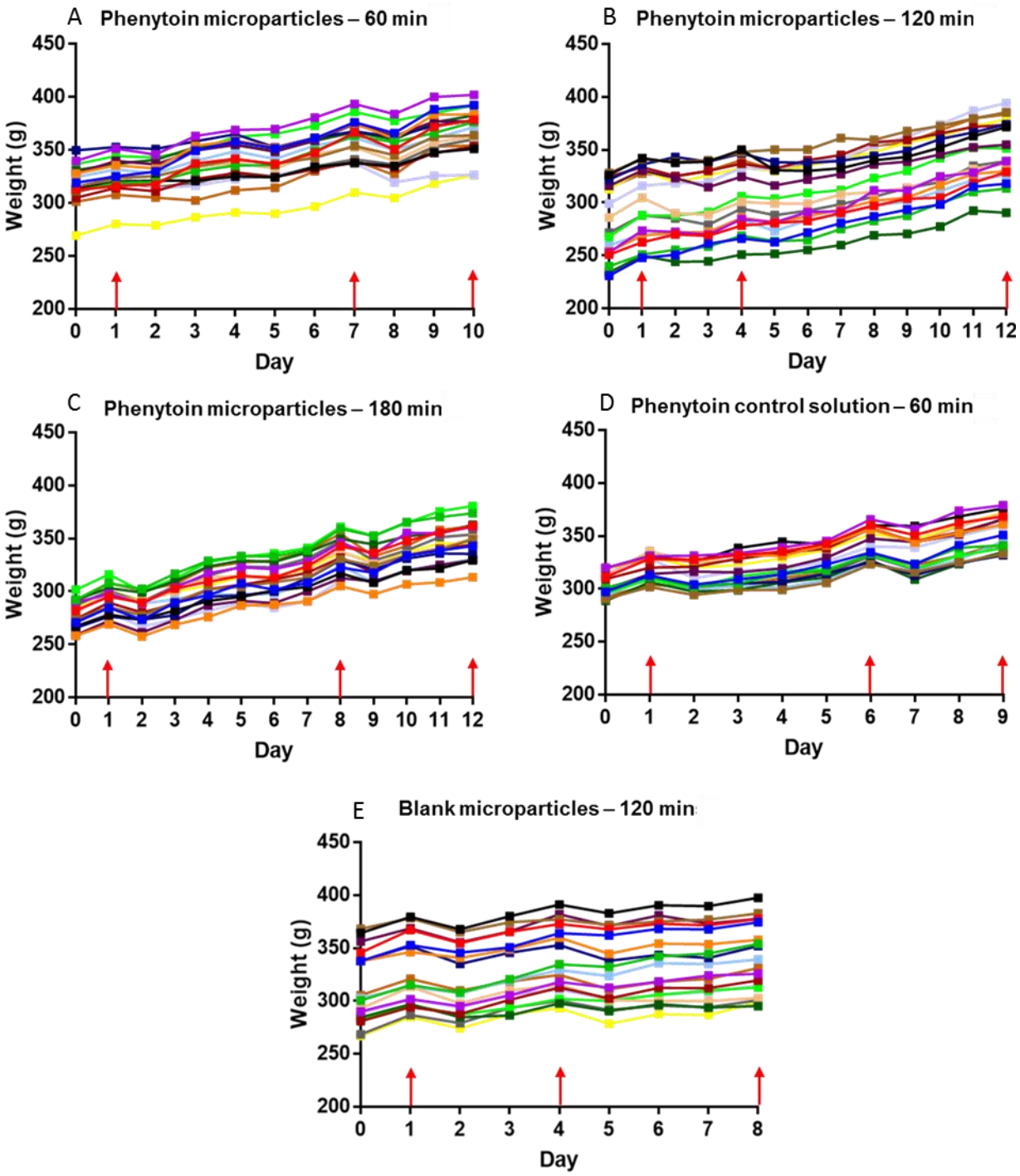

Appendix B: Average age (±SD) of rats over the course of each of the seizure experiments.

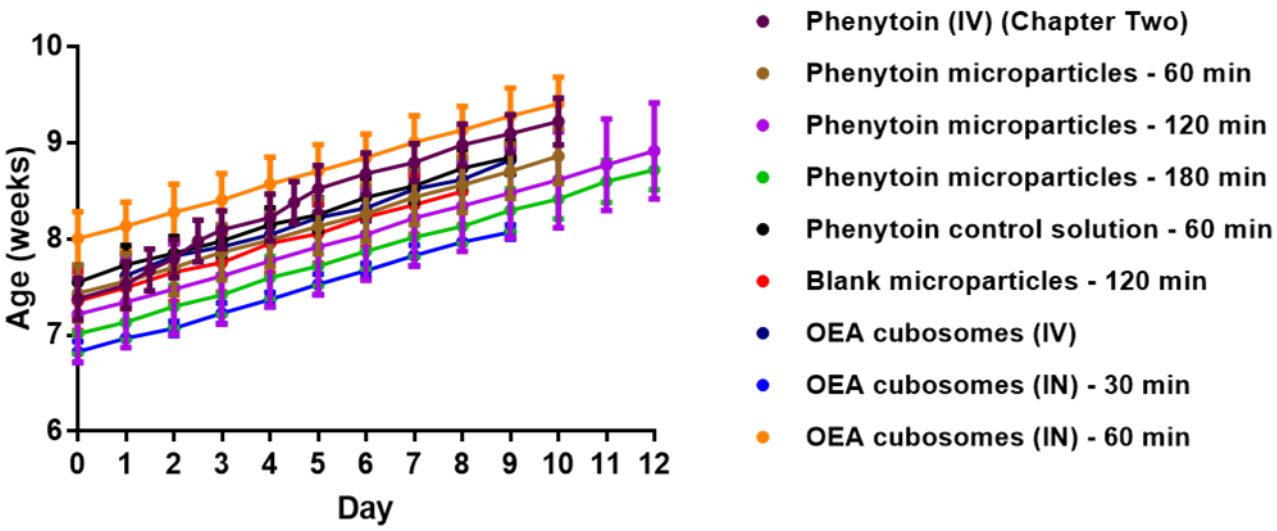

Appendix C: Results of all MEST experiments presented in terms of the number of rats displaying a result. Black bars represent a change in HLE response, while grey bars represent no change in HLE response between trials. Details of the calculation method for the percentage differences presented in the Chapters are also given.

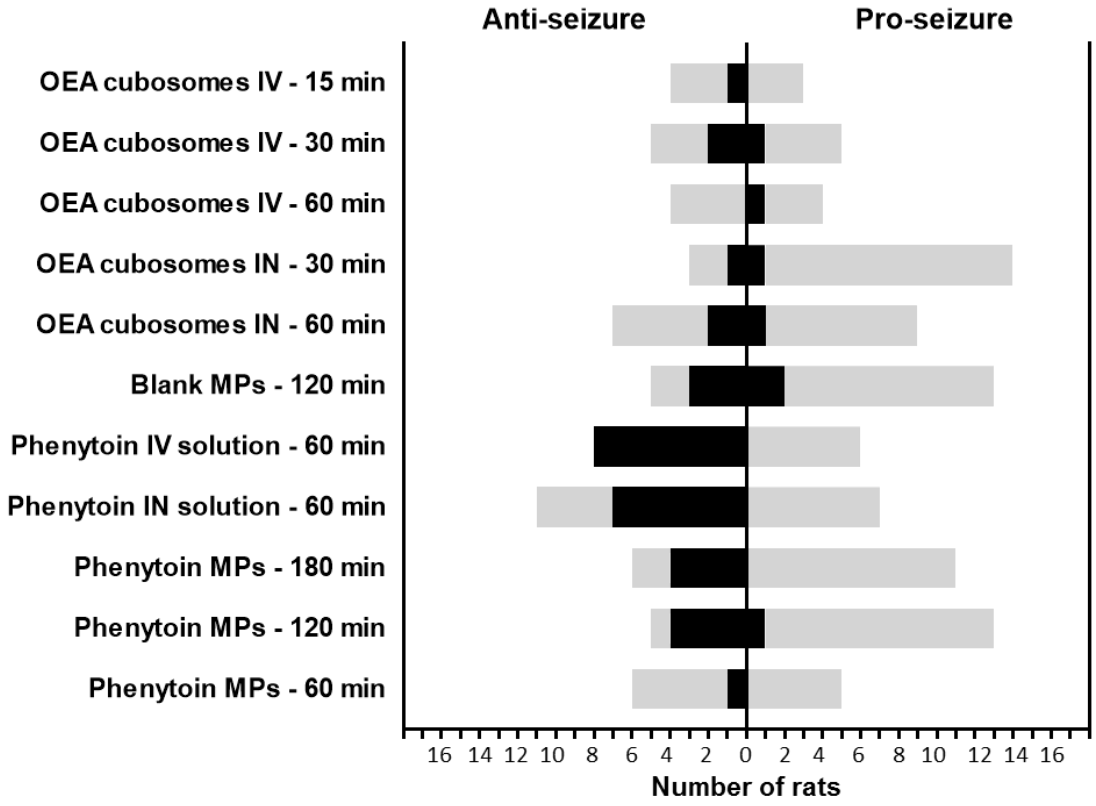

Anti-seizure effect was determined by the ability of the treatment to prevent HLE:

Anti-seizure effect (%) = Cases of drug preventing HLE (i.e. saline = HLE, drug = no HLE) (black) / (all cases of HLE both times (no anti-seizure effect) (grey) + cases of drug preventing HLE (i.e. saline = HLE, drug = no HLE) (black)) x 100

Pro-seizure effect was determined by ability of the treatment to cause HLE:

Pro-seizure effect (%) = Cases of drug causing HLE (i.e. saline = no HLE, drug = HLE) (black) / (all cases of no HLE (i.e. no pro-seizure effect) (grey) + cases of drug causing HLE (i.e. saline = no HLE, drug = HLE) (black) x 100

Appendix D: Chromatograms from the validation of the specificity of the phenytoin and 4-HPPH LC-MS Method. A = solvent (methanol), B = Plasma blank, C = Plasma LLOQ concentration, D = Brain blank, E = Brain LLOQ concentration.

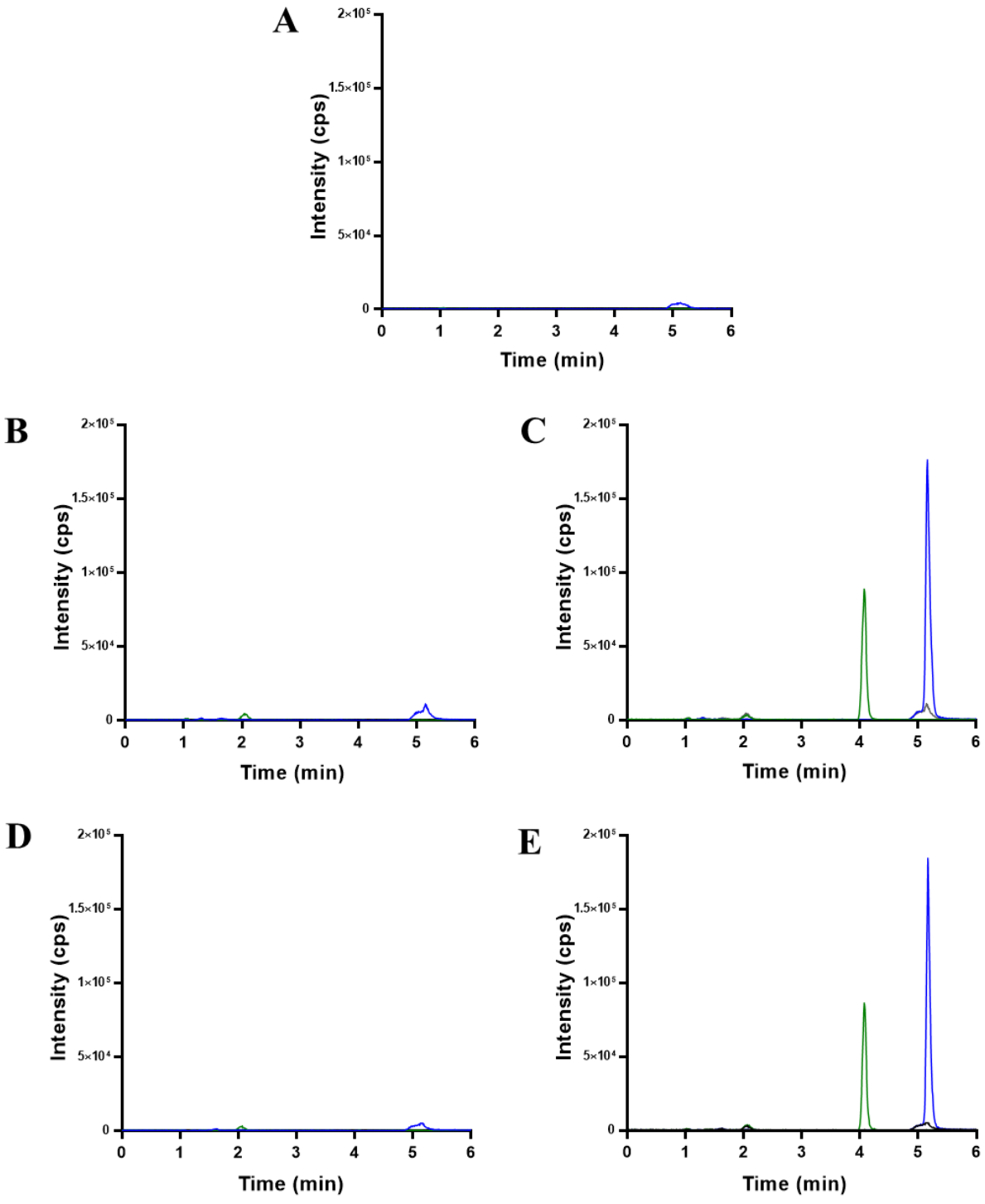

Appendix E: Intraday variability in phenytoin and 4-HPPH standard curves.

Analyte	Nominal conc (ng/mL)	Intraday 1 (n=3)				Intraday 2 (n=3)				Intraday 3 (n=3)			
		R^2	Mean (ng/mL)	Accuracy (%)	Precision (%CV)	R^2	Mean (ng/mL)	Accuracy (%)	Precision (%CV)	R^2	Mean (ng/mL)	Accuracy (%)	Precision (%CV)
Plasma													
Phenytoin	7.81	0.9999	7.3	93.6	4.0	0.9998	6.8	87.3	4.8	0.9999	7.4	94.9	3.5
	15.6		15.0	95.8	3.2		14.7	94.2	6.4		16.0	102.3	1.3
	31.3		32.1	102.6	2.2		32.5	104.1	9.4		29.6	94.7	3.1
	62.5		61.6	98.6	3.7		64.3	102.8	7.0		64.0	102.5	0.5
	125		126	100.8	1.4		124	98.9	7.6		129	103.3	4.7
	250		251	100.3	2.6		251	100.3	2.9		271	108.3	0.6
4-HPPH	7.81	0.9999	7.5	95.6	5.3	0.9992	8.3	106.7	0.9	0.9996	8.1	103.9	6.6
	15.6		16.2	103.4	1.7		15.1	96.9	3.4		15.1	96.4	4.7
	31.3		31.8	101.7	5.1		27.0	86.5	5.9		30.4	97.1	3.9
	62.5		60.9	97.4	0.6		62.4	99.9	3.0		60.5	96.7	5.5
	125		126	100.8	4.1		126	100.5	4.2		129	102.9	2.6
	250		252	100.8	2.3		242	96.9	3.9		253	101.3	0.7
Brain													
Phenytoin	23.4	0.9998	24.2	103.1	5.0	0.9996	22.8	97.1	4.0	0.9999	22.1	94.5	4.8
	46.9		48.1	102.6	4.9		48.4	103.2	4.6		47.1	100.6	4.6
	93.8		93.2	99.4	5.7		90.1	96.1	3.1		98.5	105.1	10.7
	188		181	96.5	4.7		197	105.3	2.0		185	98.8	4.6
	375		378	100.9	4.0		367	97.9	1.8		371	99.0	3.1
	750		745	99.3	2.5		739	98.6	0.8		742	98.9	1.0
4-HPPH	23.4	1	23.4	99.7	5.1	0.9998	22.5	96.1	3.0	0.9999	21.9	93.4	2.6
	46.9		48.9	104.4	4.8		48.9	104.2	3.3		48.4	103.3	2.4
	93.8		94.6	100.9	3.6		93.3	99.6	2.0		100.7	107.4	5.6
	188		185	98.9	4.5		197	104.9	3.2		190	101.3	0.6
	375		380	101.3	2.5		374	99.7	1.8		377	100.4	2.7
	750		755	100.7	3.2		759	101.2	2.5		759	101.2	0.9

Appendix F: Phenytoin concentrations matched to individual response of each phenytoin-treated rat in the second treatment trial of the validation experiment in Chapter Two.

Rat	Phenytoin Concentration		Response		
	Plasma (µg/mL)	Brain (µg/g)	HLE	FLE	Other
1*	2.1	3.4	No	Yes	Clonus
2	5.0	6.1	No	No	Audiogenic-like
3	6.0	6.5	No	No	Audiogenic-like
4*	5.5	6.2	No	No	Short clonus
5	7.3	9.3	No	No	Audiogenic-like
6	7.8	7.3	No	No	Audiogenic-like
7	7.2	7.7	No	No	Very short clonus
8	7.5	8.4	No	No	Very short clonus
9	7.9	7.8	No	No	Audiogenic-like

*Invalid response in one MEST trial, so this animal was excluded from the pharmacodynamic data analysis. Note: The rat which displayed FLE as presented in the pharmacodynamic data did so in the second stage of the experiment (i.e. the first treatment trial), so plasma and brain phenytoin concentrations were not taken and are therefore not presented in the above table.

Appendix G: Average mass of phenytoin (or equivalent of TSP) delivered from intranasal insufflator in microparticle experiments.

Experiment	Average phenytoin (or phenytoin equivalent mass) delivered (±SD) (mg)
PHT MPs 60 min	1.7 (±0.4)
PHT MPs 120 min	1.6 (±0.6)
PHT MPs 180 min	1.5 (±0.5)
Blank MPs 120 min	1.5 (±0.3)

Appendix H: Brainstem and olfactory bulb intra-day standard curve accuracy and precision for quantification of phenytoin and 4-HPPH.

		Brainstem		
Analyte	**Nominal conc (ng/g)**	**Intraday (n=3)**		
		Mean (ng/g)	**Accuracy (%)**	**Precision (CV%)**
Phenytoin	23.4	22.1	94.1	2.7
	46.9	47.5	101.1	3.1
	93.8	95.4	101.8	4.7
	187.5	187.5	100.0	0.5
	375	371	99.0	1.9
	750	744	99.2	1.2
4-HPPH	23.4	21.1	90.0	2.2
	46.9	47.9	102.1	1.8
	93.8	97.3	103.8	2.1
	187.5	192.0	102.4	3.6
	375	369	98.4	4.0
	750	747	99.6	5.9
		Olfactory bulbs		
Analyte	**Nominal conc (ng/mL)**	**Intraday (n=3)**		
		Mean (ng/g)	**Accuracy (%)**	**Precision (CV%)**
Phenytoin	23.4	23.7	101.3	4.1
	46.9	48.0	102.4	2.4
	93.8	93.8	100.0	3.8
	187.5	182.5	97.3	2.5
	375	380	101.2	3.5
	750	744	99.2	0.2
4-HPPH	23.4	23.6	100.8	0.8
	46.9	46.7	99.7	0.9
	93.8	93.8	100.1	4.4
	187.5	184	98.3	1.8
	375	378	100.9	3.2
	750	754	100.5	3.0

Appendix I: Histological effect of selachyl alcohol-based phenytoin cubosomes 50 mg/mL (w/w lipid) or equivalent phenytoin suspension on the olfactory mucosa of rats. Dispersions consisted of 0.5 mg/mL phenytoin, 0.75% w/v Polysorbate 80 and 12.5% w/v propylene glycol with or without 5% w/v selachyl alcohol. Control nostril (A, B, C) and treatment nostril (D, E, F) are shown for saline, phenytoin cubosomes and phenytoin free drug suspension respectively.

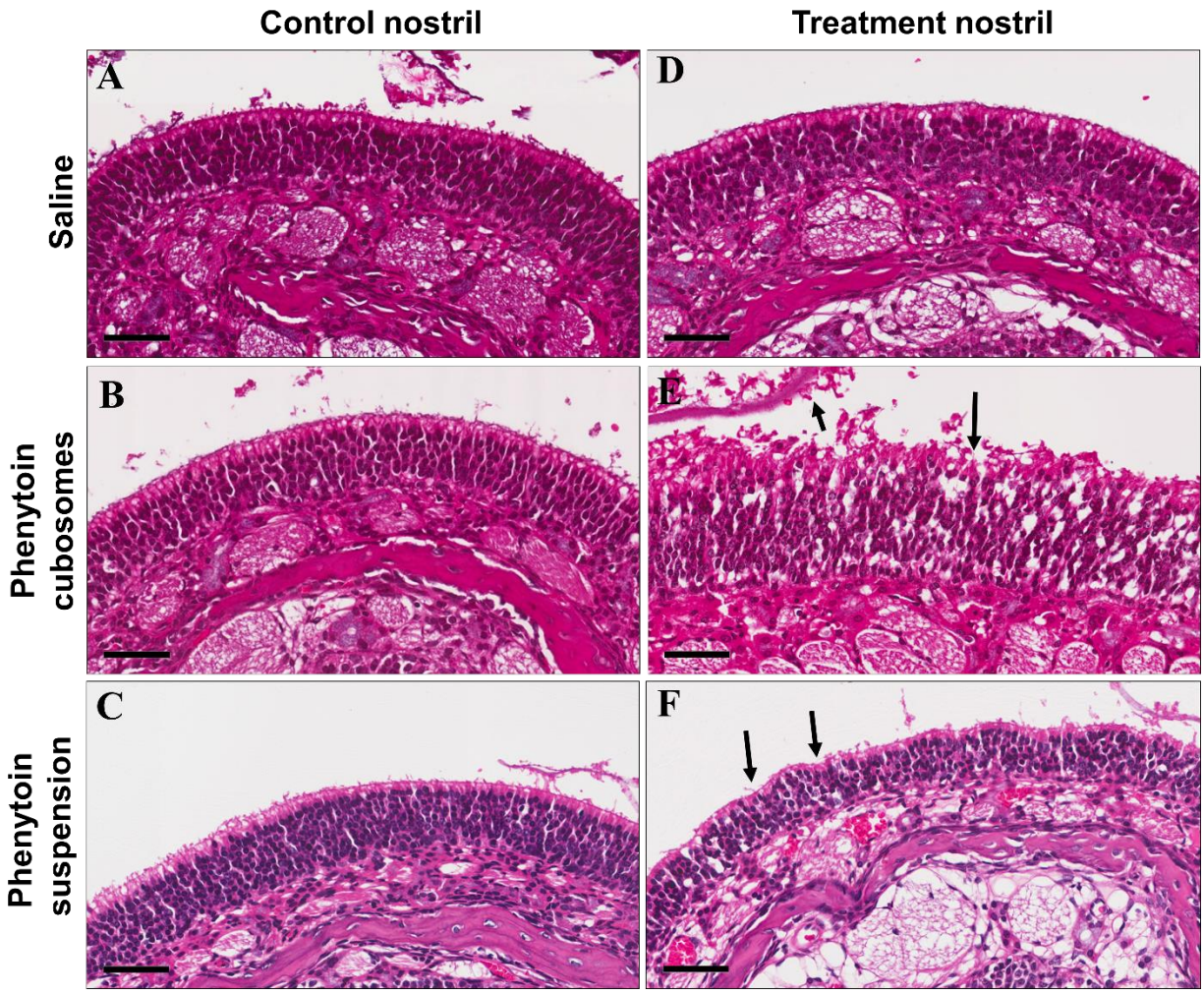

Appendix J: Calculation procedure used to prepare stock solutions for phenytoin and 4-HPPH standards for LC-MS.

To make standards in plasma and brain using 5 µL aliquots of stock solution:

Plasma:

Concentration of standard stock solution (ng/mL) =
Desired standard concentration in plasma (ng/mL) x (100 µL/1000 µL) x (1000 µL/5 µL aliquot of stock solution)

e.g. Desired 50 ng/mL standard conc in plasma x 0.1 mL plasma aliquot x (1000 µL/5 µL aliquot of stock solution) = 1000 ng/mL stock solution

Brain:

Concentration of standard stock solution (ng/mL) =
Desired standard concentration in brain (ng/g) x (1 g/3 mL homogenate) x (100 µL/1000 µL) x (1000 µL/5 µL aliquot of stock solution)

e.g. Desired 150 ng/g standard conc in brain x (1g/3mL homogenate) x 0.1 mL brain homogenate aliquot x (1000 µL/5 µL aliquot of stock solution) = 1000 ng/mL stock solution

Appendix K: Percentage of HLE and FLE in individual MEST treatment groups.

Experiment	%HLE after saline	%HLE after drug treatment
Phenytoin 25mg/kg IV (60 min)	57	0
Phenytoin microparticles (60 min)	55	46
Phenytoin microparticles (120 min)	28	11
Phenytoin microparticles (180 min)	35	12
Blank microparticles (120 min)	28	22
Phenytoin control solution IN (60 min)	61	22
OEA cubosomes IV (15 min)	57	43
OEA cubosomes IV (30 min)	50	40
OEA cubosomes IV (60 min)	50	62.5
OEA cubosomes IN (30 min)	13	18
OEA cubosomes IN (60 min)	39	28

Appendix L: Prescott's test tables with two-tailed p-values for all MEST experiments.

Phenytoin microparticles (60 minutes); p=0.8				
Sequence	**HLE 1st time only**	**HLE or No HLE both times**	**HLE 2nd time only**	**Total**
Saline → Drug	**1**	**3**	**0**	**4**
Drug → Saline	**0**	**6**	**0**	**6**
Total	**1**	**9**	**0**	**10**

Phenytoin microparticles (120 minutes); p=0.3647				
Sequence	**HLE 1st time only**	**HLE or No HLE both times**	**HLE 2nd time only**	**Total**
Saline → Drug	**3**	**6**	**0**	**9**
Drug → Saline	**1**	**7**	**1**	**9**
Total	**4**	**13**	**1**	**18**

Phenytoin microparticles (180 minutes); p=0.1412				
Sequence	**HLE 1st time only**	**HLE or No HLE both times**	**HLE 2nd time only**	**Total**
Saline → Drug	**2**	**6**	**0**	**8**
Drug → Saline	**0**	**7**	**2**	**9**
Total	**2**	**13**	**2**	**17**

Pooled phenytoin microparticles (60, 120, 180 minutes); p=0.016				
Sequence	**HLE 1st time only**	**HLE or No HLE both times**	**HLE 2nd time only**	**Total**
Saline → Drug	**6**	**15**	**0**	**21**
Drug → Saline	**1**	**20**	**3**	**24**
Total	**7**	**35**	**3**	**45**

Blank microparticles (120 minutes); p=1				
Sequence	**HLE 1st time only**	**HLE or No HLE both times**	**HLE 2nd time only**	**Total**
Saline → Drug	**1**	**7**	**1**	**9**
Drug → Saline	**1**	**6**	**2**	**9**
Total	**2**	**13**	**3**	**18**

Intranasal phenytoin control solution (60 minutes) – HLE; p=0.0136				
Sequence	**HLE 1st time only**	**HLE or No HLE both times**	**HLE 2nd time only**	**Total**
Saline → Drug	**2**	**7**	**0**	**9**
Drug → Saline	**0**	**4**	**5**	**9**
Total	**2**	**13**	**5**	**18**

Intranasal phenytoin control solution (60 minutes) – FLE; p=1				
Sequence	**HLE 1st time only**	**HLE or No HLE both times**	**HLE 2nd time only**	**Total**
Saline → Drug	**1**	**8**	**0**	**9**
Drug → Saline	**0**	**9**	**0**	**9**
Total	**1**	**17**	**0**	**18**

Intravenous phenytoin 25 mg/kg (60 minutes) – HLE; p=0.0035				
Sequence	**HLE 1st time only**	**HLE or No HLE both times**	**HLE 2nd time only**	**Total**
Saline → Drug	**6**	**1**	**0**	**7**
Drug → Saline	**0**	**5**	**2**	**7**
Total	**6**	**6**	**2**	**14**

Intravenous phenytoin 25 mg/kg (60 minutes) – FLE; p=0.0006				
Sequence	**HLE 1st time only**	**HLE or No HLE both times**	**HLE 2nd time only**	**Total**
Saline → Drug	**7**	**0**	**0**	**7**
Drug → Saline	**0**	**1**	**6**	**7**
Total	**7**	**1**	**6**	**14**

OEA cubosomes (i.n.) (30 minutes); p=1				
Sequence	**HLE 1st time only**	**HLE or No HLE both times**	**HLE 2nd time only**	**Total**
Saline → Drug	**0**	**8**	**0**	**8**
Drug → Saline	**1**	**7**	**0**	**8**
Total	**1**	**15**	**0**	**16**

OEA cubosomes (i.n.) (60 minutes); p=0.93				
Sequence	**HLE 1st time only**	**HLE or No HLE both times**	**HLE 2nd time only**	**Total**
Saline → Drug	**0**	**8**	**0**	**8**
Drug → Saline	**0**	**6**	**1**	**7**
Total	**0**	**14**	**1**	**15**

Appendix M: Comparison of baseline log CC_{50} values (±SD) between MEST experiments.

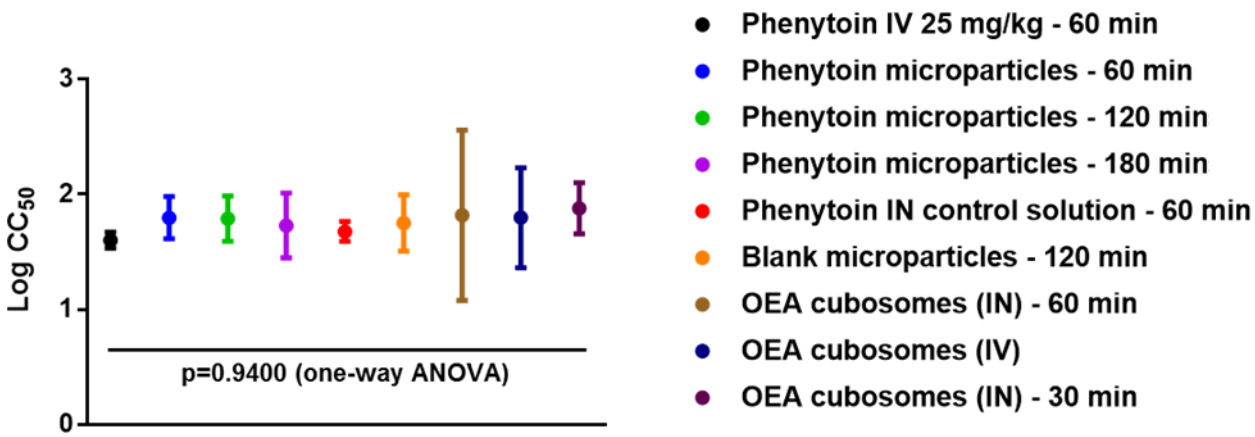

Appendix N: Weight progression of rats over the course of all seizure studies in Chapter Four. Days of stimulation are indicated by red arrows.

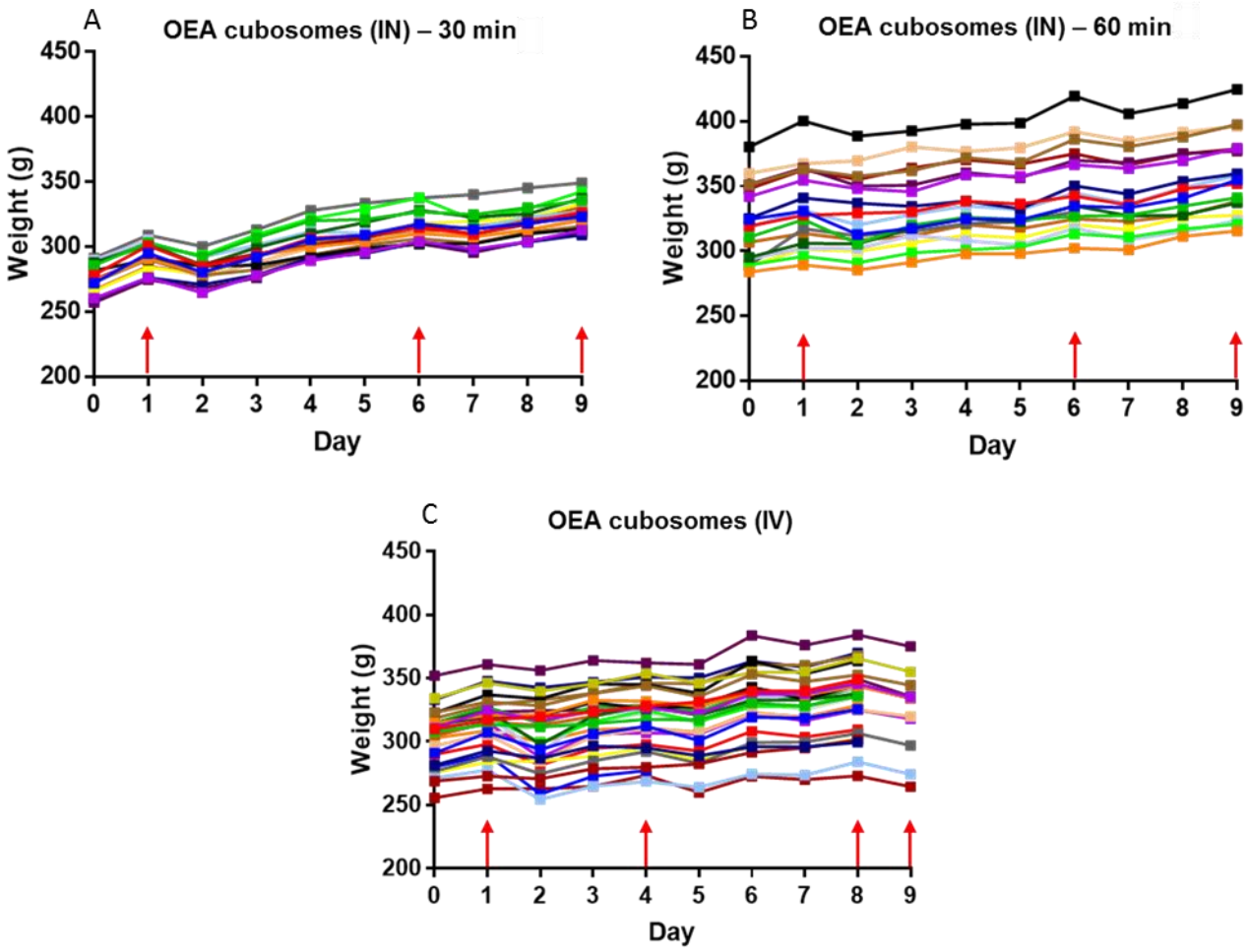

Appendix O: Control and rat plasma SAXS studies of OEA cubosomes stabilised with Pluronic F127®. Arrows show the relative peak positions of the *Pn3m* cubic phase. For the plasma data, the phase was not able to be identified.

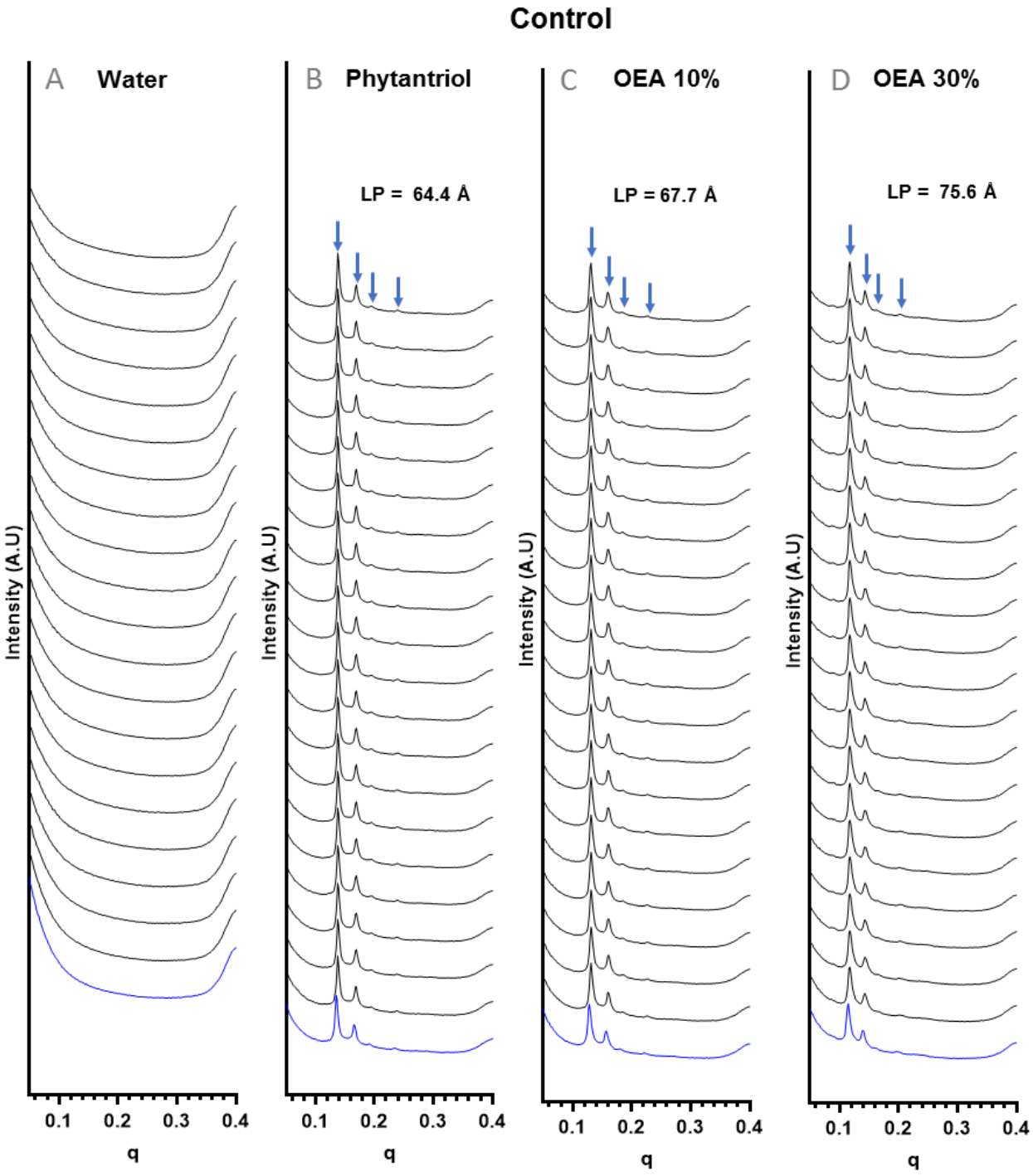

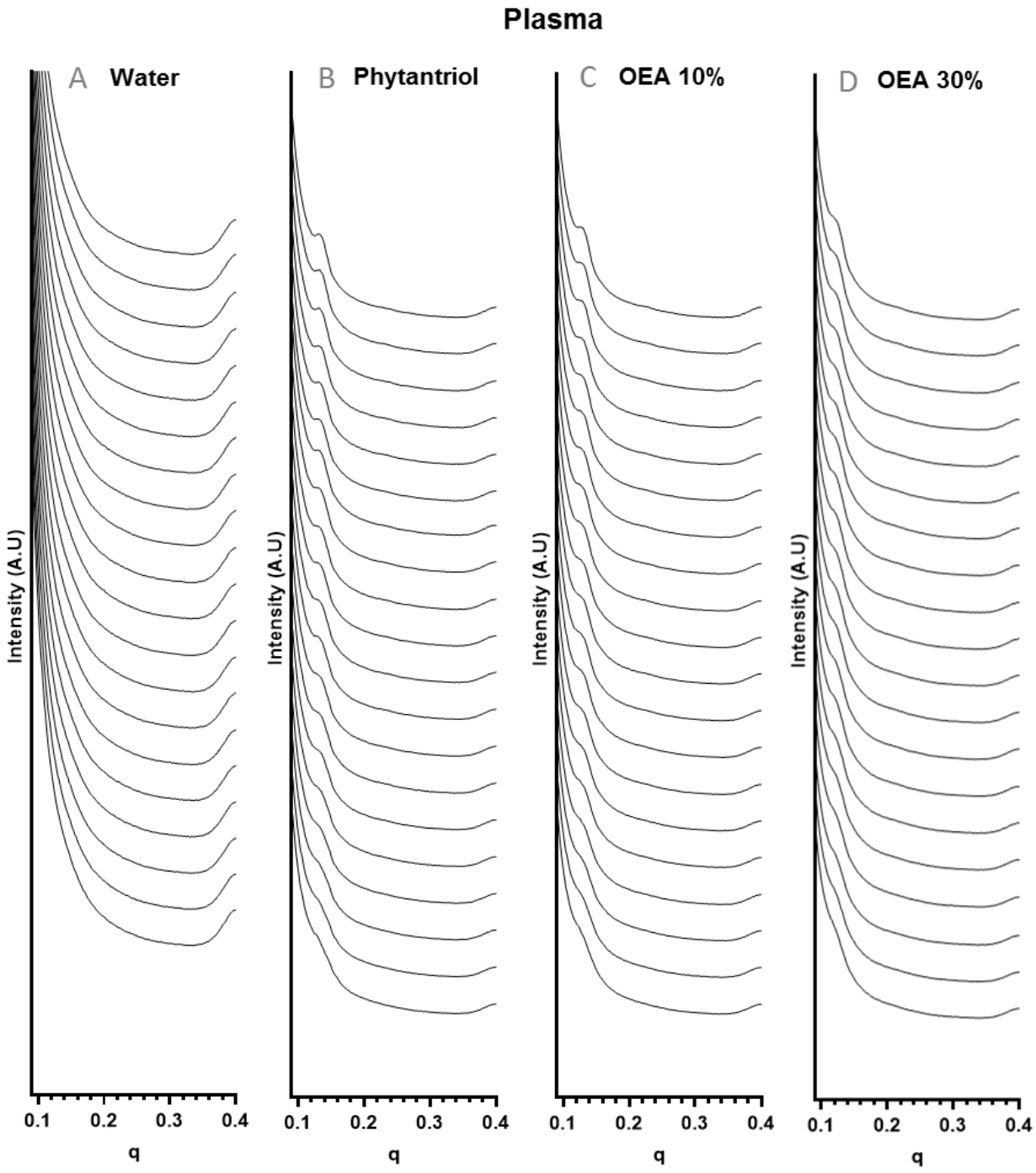
Plasma
A Water
B Phytantriol
C OEA 10%
D OEA 30%
Intensity (A.U)
Intensity (A.U)
Intensity (A.U)
Intensity (A.U)
0.1
0.2
0.3
0.4
q
q
q
q

Appendix P: Intraday variability in ^{13}C-OEA standard curves from LC-MS method validation.

Analyte	Nominal conc (ng/mL)	Intraday 1 (n=3)				Intraday 2 (n=3)				Intraday 3 (n=3)			
		R^2	Mean (ng/mL)	Accuracy (%)	Precision (%CV)	R^2	Mean (ng/mL)	Accuracy (%)	Precision (%CV)	R^2	Mean (ng/mL)	Accuracy (%)	Precision (%CV)
Plasma													
^{13}C-OEA	0.39	1	0.40	102	1.2	1	0.39	99.1	1.8	0.9997	0.35	90.1	6.1
	0.78		0.78	99.3	1.4		0.78	99.3	0.9		0.76	97.9	5.7
	1.56		1.52	97.4	5.3		1.55	99.1	4.0		1.55	99.4	4.7
	3.13		3.16	101.3	0.6		3.19	102.1	1.3		3.14	100.4	6.1
	6.25		6.25	100.0	1.3		6.18	98.9	4.2		6.59	105.4	3.3
	12.5		12.4	99.3	1.2		12.5	99.9	0.8		12.3	98.0	6.0
	25		24.8	99.1	0.4		24.9	99.5	1.3		25.0	100.2	5.0
Brain													
^{13}C-OEA	1.17	1	1.18	101.1	9.8	0.9998	1.11	95.0	8.9	0.9999	1.21	103.5	1.3
	2.34		2.40	102.4	1.2		2.27	96.9	5.3		2.35	100.4	8.9
	4.69		4.63	98.8	6.4		4.82	102.8	7.8		4.79	102.1	2.2
	9.38		9.26	98.8	1.4		9.43	100.5	4.7		9.13	97.4	1.4
	18.8		18.8	100.0	2.9		19.5	104.1	6.2		19.2	102.2	5.8
	37.5		37.5	99.9	2.3		37.0	98.6	1.8		37.3	99.5	2.6
	75		74.8	99.7	0.7		75.2	100.3	4.9		75.1	100.2	2.3
Liver													
^{13}C-OEA	1.17	0.9998	1.00	85.1	7.5	1	1.09	93.1	8.0	1	1.13	96.7	5.5
	2.34		2.29	97.7	4.3		2.35	100.3	2.0		2.31	98.4	1.5
	4.69		4.73	100.9	3.6		4.68	99.8	2.0		4.74	101.1	1.2
	9.38		9.74	103.9	0.9		9.54	101.8	3.0		9.47	101.1	3.9
	18.8		19.4	103.7	1.5		19.1	102.0	2.8		19.0	101.1	4.6
	37.5		37.0	98.7	1.0		37.4	99.7	0.9		37.3	99.4	1.5
	75		75.6	100.9	4.8		75.7	100.9	2.5		75.0	100.0	0.2

Appendix Q: Pharmacokinetic analysis of ^{13}C-OEA (Figure 4.12) including values below the lower limit of quantification of the LC-MS assay (unfilled symbols), as measured and calculated by extrapolation of the model.

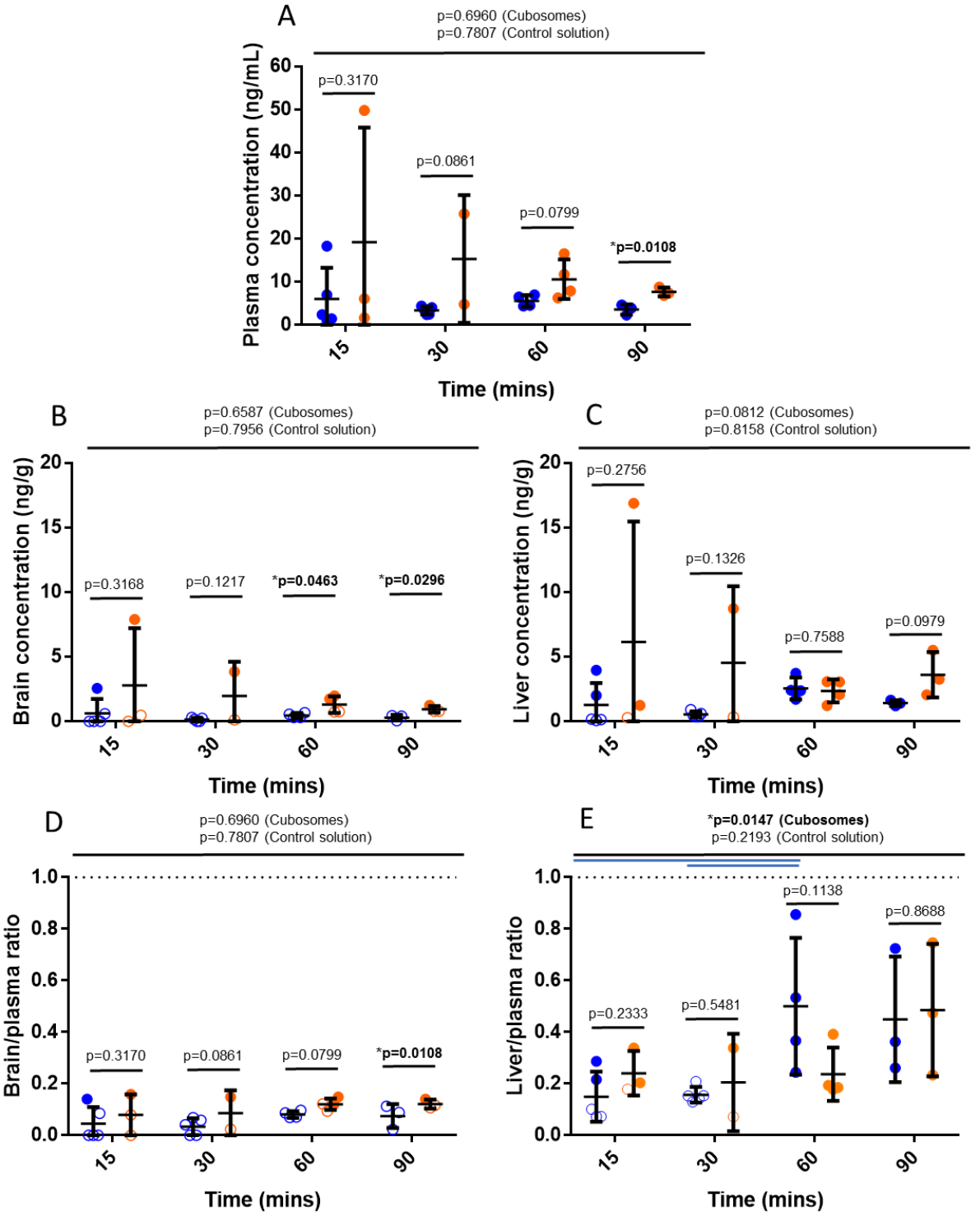

Appendix R: SAXS studies of phytantriol-Tween 80® cubosomes incubated at 37 ºC in different concentrations of plasma at 5 min (A) and 60 min (B) to allow observation of the *Im3m* cubosome to hexasome transformation. A 100 µL aliquot of cubosome dispersion was added to 100 µL of rat plasma pre-diluted with phosphate buffered saline (PBS) pH 7.4 to between 1 and 8 times its original concentration. For the control, rat plasma was replaced with PBS alone. Emergence of the hexasome peaks are indicated by arrows.